Leukocyte trafficking and vascular integrity

Heemskerk, N.

[Link to publication](#)

Leukocyte trafficking and vascular integrity

Niels Heemskerk

LEUKOCYTE TRAFFICKING
AND
VASCULAR INTEGRITY

Leukocyte trafficking and vascular integrity

The research described in this thesis was conducted at the department of Molecular Cell Biology at Sanquin Research and the Landsteiner Laboratory, Academic Medical Center, University of Amsterdam, Amsterdam, The Netherlands.

LEUKOCYTE TRAFFICKING
AND
VASCULAR INTEGRITY

ACADEMISCH PROEFSCHRIFT

ter verkrijging van de graad van doctor

aan de Universiteit van Amsterdam

op gezag van de Rector Magnificus

prof.dr.ir. K.I.J. Maex

ten overstaan van een door het College voor Promoties

ingestelde commissie, in het openbaar te verdedigen

in de Agnietenkapel

op vrijdag 10 februari 2017 om 14.00 uur

door

Niels Heemskerk

geboren te Haarlem

Promotiecommissie

Promotor: prof.dr. P.L. Hordijk   Universiteit van Amsterdam
Copromotor: dr. J.D. van Buul   Sanquin Research

Overige leden:
       prof.dr. T.W.J. Gadella Jr.   Universiteit van Amsterdam
       prof.dr. K. Jalink   Universiteit van Amsterdam
       prof.dr. C. J.M. de Vries   Universiteit van Amsterdam
       dr. J. de Rooij   Universitair Medisch Centrum Utrecht
       prof.dr. A. Sonnenberg   Leiden Academic Centre for Drugs
                                     Research

Faculteit der Natuurwetenschappen, Wiskunde en Informatica

TABLE OF CONTENTS

1

GENERAL INTRODUCTION

General introduction

The cardiovascular system is a complex network formed by numerous connected blood vessels that are embedded in tissue throughout the human body. Removing all tissues leaving only the vascular system intact fully outlines the shape of the human body showing the high density of blood vessels in our tissues and organs. Proper function of this high density network is essential for human health, since it provides our body with nutrients, oxygen, hormones and regulates homeostasis by controlling temperature and pH. In addition, the vascular system provides guidance to traveling and stationary immune cells and thereby supports protective immune functions that keep our body free of pathogens, cancer and foreign material [1,2]. For example, macrophages lining the endothelial cells (EC) in the sinusoids of the liver catch and kill bacteria, that entered through the intestines, or kill circulating tumor cells, thus averting bacteremia, septic shock and liver metastasis [3]. Moreover, during inflammation, ECs expose a variety of adhesion molecules at their surface that slow down and arrest travelling immune cells in the blood circulation. These adhesive molecules are thought to inform immune cells where and when to breach the blood vessel wall through a multi-step process known as transendothelial migration (TEM) or diapedesis [4].

Transendothelial migration 'hotspots'

The regulation of immune cell trafficking is complex and goes far beyond our current understanding. Although much is yet to discover, intensive research over the past decade has revealed several fundamental principles that regulate cell migration in a variety of immune cell related responses such as hematopoiesis, immune surveillance and innate and adaptive immunity. The current paradigm of transendothelial migration is a refined version of the multi-step model that was first proposed by Butcher and Springer [5,6]. The prevailing multistep paradigm comprises: leukocyte rolling, arrest, crawling, firm adhesion and transmigration. The latter occurs either through the endothelial junctions (paracellular route) [7,8] or through the endothelial cell body (transcellular route) [9-11]. Interestingly, leukocyte diapedesis appears to occur at predefined places in the endothelium. Some locations even favor the migration of multiple immune cells that breach the endothelial lining in rapid succession. This raises some important questions, such as what factors determine these so called 'hotspots for transmigration', why do two routes exist and what defines the use of one over the other? So far, several key principles

have been established. First of all, immune cells are attracted towards an optimal concentration of chemokines (chemotaxis), density of adhesion molecules (haptotaxis) or cellular stiffness (durotaxis). Secondly, migration into a tissue or organ is believed to follow the path of least resistance (tenertaxis). In addition, other factors such as shear forces, vessel type and composition of the glycocalyx play an important regulatory role in dictating suitable exit sites (Fig. 1). I will briefly delineate each principle starting with chemotaxis. Chemokines (chemotactic cytokines) are of key importance for leukocyte TEM not only because of their involvement in chemotaxis but also because of their role in integrin activation inducing leukocyte arrest. There are some indications that oligomeric chemokine-forms activate leukocyte-integrins directing leukocyte arrest and firm adhesion whereas monomeric-forms activate integrin subsets on the leukocyte that govern cell movement [12,13]. Chemokines are immobilized by heparan sulfate (HS) glycosaminoglycans (GAGs) that are part of a 50-100 nm thick, negatively charged network on the apical surface of EC called the glycocalyx [14]. Transcytosis of chemokines, transport from the extracellular space to the luminal side of the vasculature, is considered as an important process to mark the site of inflammation. Macrophages are a major source for the production of chemokines. Recently, it has been shown that perivascular macrophages locally secrete chemokines that form local "hotspots" for neutrophil diapedesis *in vivo* [15]. Thus, chemokines presented at the apical side of EC provide chemotactic cytokine gradients that direct traveling immune cells to a particular site in the body enabling them to fulfill their immune functions. In addition to that, an optimal amount and/or distribution of leukocyte-integrin ligands at the luminal surface of EC, has also been proposed to regulate leukocyte directional migration through so-called *haptotaxis*. High surface levels of ICAM-1 creating a homogeneous ICAM-1 distribution induces a transition from paracellular to robust transcellular migration, while intermediate levels favor the paracellular route, possibly because of the high junctional ICAM-1 distribution under these circumstances [16]. Furthermore, migrating cells are thought to be attracted to an optimal surface stiffness also referred to as stiffness sensing or *durotaxis*. Migrating leukocytes sense their physical surroundings and respond accordingly. For example, neutrophils migrate slower on 4 kPa and 13 kPa fibronectin-coated surfaces whereas optimal crawling speeds were reached on 7 kPa. Interestingly, fibronectin density also affected the outcome of migration speed. Using FN concentrations of 100 µg/ml, the optimal stiffness for migration is 4 kPa while on 10 µg/ml the optimal stiffness for maximal migration is increased to 7 kPa [17]. This suggests that leukocyte TEM *in vivo* depends on the combination between matrix rigidity (durotaxis) and the amount and distribution of locally

available surface ligands (haptotaxis). Another phenomenon that is often observed when an endothelial barrier is very tight, is the predominant use of the transcellular route. This is in contrast to a situation of weak endothelial junctional integrity, which shows high association with paracellular diapedesis [18]. To find these spots of low junctional resistance, lymphocytes dynamically probe the underlying endothelium by extending invadosome-like protrusions into its surface that deform the plasma membrane, depolymerize F-actin filaments at the membrane cortex and ultimately breach the barrier [18,19]. These authors suggest that leukocyte
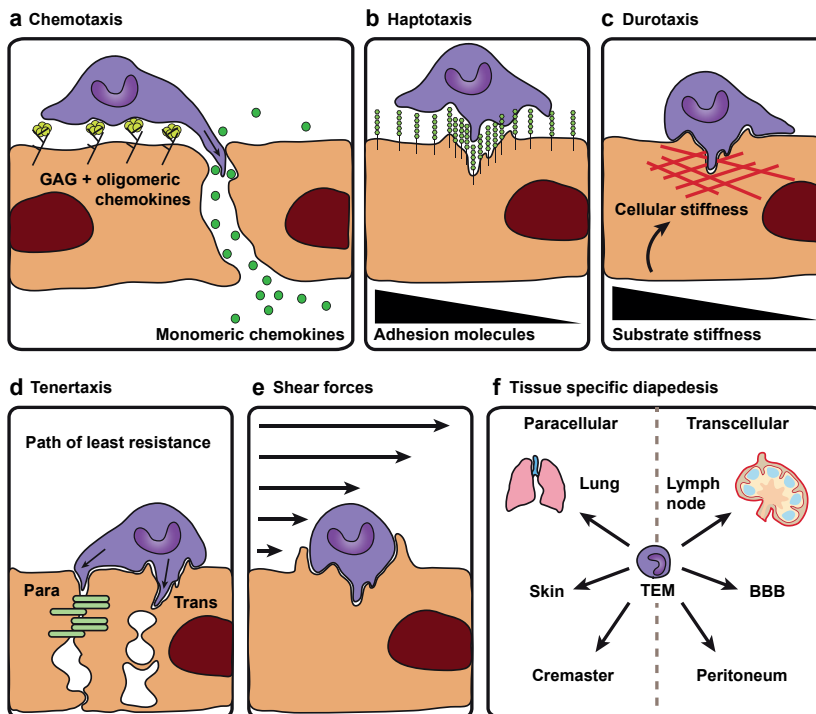
Figure 1. Factors that determine ´hotspots´ for transendothelial migration. Several key principles are thought to govern leukocyte diapedesis at predefined places in the vasculature. In the first place leukocytes are attracted towards an optimal; (**a**) concentration of chemokines (chemotaxis), (**b**) density of adhesion molecules (haptotaxis) or (**c**) cellular stiffness (durotaxis). Oligomeric chemokine-forms bound to glycosaminoglycans (GAGs) are thought to direct leukocyte firm adhesion and arrest whereas monomeric chemokine-forms govern directional cell movement. (**d**) Secondly, migration into a tissue or organ is believed to follow the path of least resistance (tenertaxis). Tenertaxis may affect the decision making to go trans or paracellular. Additional factors such as (**e**) shear forces and (**f**) vessel type play an important regulatory role in dictating suitable exit sites. The major route of transmigration into lung, skin and cremaster is believed to be the paracellular route whereas the transcellular route is recognized as the dominant route to enter the lymph node, blood brain barrier (BBB) or the peritoneum.

transmigration is guided by a common principle namely 'the path of least resistance' named *tenertaxis* [18]. Moreover, the impact of shear forces on leukocyte behavior has been established by several research groups. For instance, transmigration kinetics during neutrophil diapedesis was significantly faster under shear stress than under static conditions [20], and applying shear stress on adherent lymphocytes promoted leukocyte transmigration across chemokine-bearing ECs [21]. Of note, most leukocyte adhesion and diapedesis is observed in areas with low venous shear stress. However, during some pathological conditions such as atherosclerosis, monocytes adhere and transmigrate through the endothelial lining of the arterial wall where shear stress is much higher. Mechanistically, it has been shown that leukocytes tether to and roll on platelet-decorated ultra-large von Willebrand factor (ULVWF) string-like structures, but not directly on ECs. Using platelets as intermediate substrates, monocytes are able to transmigrate under high shear stresses varying between 20 and 40 dyne/cm^2 in a P-selectin dependent manner [22]. Enhanced and prolonged inflammatory responses alter the balance in: leukocyte recruitment, platelet activation and endothelial activation, which is now generally accepted to be contribute to the progression of atherosclerosis [23,24].

Finally, leukocyte diapedesis across the blood brain barrier, the peritoneum or into the lungs is differentially regulated. For instance, neutrophil diapedesis in ICAM-1/P-selectin null mice is normal in the lungs but totally abrogated in the peritoneum [25]. In another study, it has been shown that locking the endothelial junctions using a VE-cadherin-α-catenin fusion protein prevented leukocyte diapedesis, but not in all tissues. Diapedesis into lung, skin and cremaster muscle was severely reduced establishing the paracellular route as the dominant route in these tissues. However, the migration of naïve lymphocytes into lymph nodes and emigration of neutrophils into the peritoneum was not affected by junctional locking [26].

THE DOCKING STRUCTURE

A widely observed phenomenon associated with leukocyte TEM is the formation of endothelial membrane protrusions rich in Filamentous (F)-actin that surround transmigrating leukocytes. These endothelial structures were first described by Barreiro and colleagues who defined them as docking structures [27]. Other researchers found similar endothelial structures but proposed different names, e.g. transmigratory cups, apical cups, dome structures, ICAM-1-enriched contact areas, actin dynamic structures [10,28–32]. The names where based on the hypothesized function

or morphology of these structures. Inspiring work of Carman and co-workers showed that these structures, that are formed both during para- and transcellular diapedesis, were more frequently associated with leukocytes in the process of crossing the endothelial barrier than with firm adhesion prior to diapedesis [10]. Many of these F-actin structures comprise vertical microvilli-like projections. These projections have been suggested to anchor endothelial adhesion receptors, such as ICAM-1 and VCAM-1. As such they may serve as migration-supporting platforms or adhesion substrates to assist leukocyte transmigration [33-37]. It has been shown that assembly of F-actin, the major component and driving force to induce such apical projections, requires the activation of several small GTPases that include RhoG and Rac1 but not RhoA GTPase activity [28,38]. Currently, the major proposed function of the docking structure is thought to provide guidance for transmigrating leukocytes [39].

PARACELLULAR AND TRANSCELLULAR MIGRATION

Breaching of the endothelial barrier by immune cells occurs either between the junctions, involving multiple ECs (paracellular route), or through the cell body of an individual endothelial cell (transcellular route). Each route has its own distinct mechanisms of endothelial barrier opening (Fig. 2).

Paracellular migration is the main route taken by neutrophils to enter lung, skin and cremasteric tissue [8,26]. Currently, two hypotheses to open EC junctions dominate the field of leukocyte diapedesis. The first is based on research conducted on GPCR signaling in ECs, such as thrombin-induced junctional opening [40] and postulates that leukocytes induce actomyosin contraction in ECs triggering junctional opening [41-43]. The second hypothesis anticipates that EC junctions are locally destabilized to allow migrating cells to squeeze through the transient gap in the junction. Recent evidence supporting the latter hypothesis shows that leukocytes trigger rapid dephosphorylation of Tyr731 via the tyrosine phosphatase SHP-2, which allowed the adaptin AP-2 to bind and initiate endocytosis of VE-cadherin. This destabilizes VE-cadherin-based junctions, allowing junctional opening and paracellular migration of leukocytes [44].

Transcellular migration is the major transmigration route used by neutrophils to enter the peritoneum and for lymphocytes to enter lymph nodes [26]. The initiation of a transcellular passageway is thought to occur through fusion of ICAM-1 bearing endocytic vesicles forcing a transcellular pore that allows transcellular migration to occur [45]. Several studies showed that transcellular migration, for instance in the peritoneum, is ICAM-1
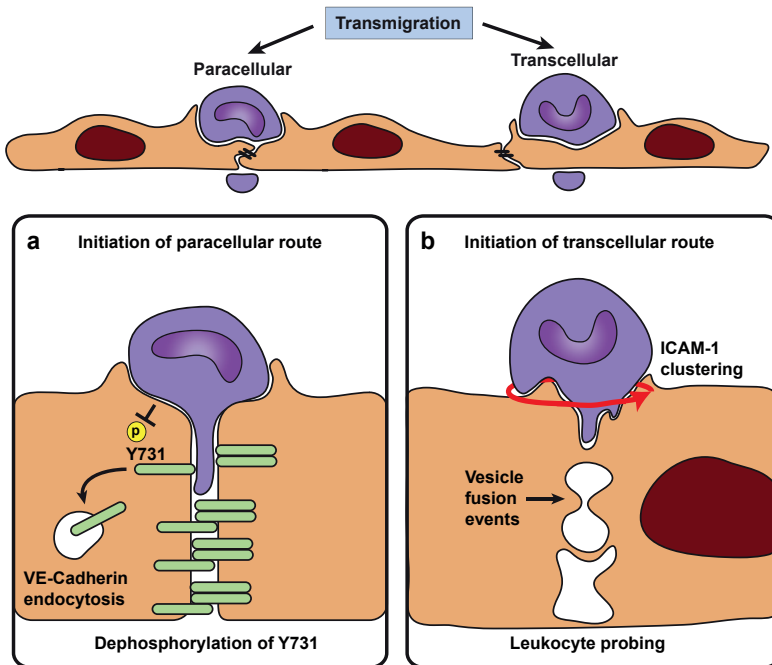
Figure 2. Leukocyte diapedesis through or between endothelial cells. (**a**) The initiation of paracellular and transcellular transmigration is believed to involve distinct molecular mechanisms that allow transient endothelial permeability to leukocytes. Destabilization of VE-cadherin based cell-cell contacts is recognized as the major mechanisms that initiates the opening of the paracellular pathway. It is thought that leukocytes trigger rapid dephosphorylation of Tyr731 via the tyrosine phosphatase SHP-2 allowing the adaptin AP-2 to bind and initiate endocytosis of VE-cadherin and thereby destabilize VE-cadherin based junctions. (**b**) The initiation of a transcellular passageway is thought to occur through fusion of ICAM-1 bearing endocytic vesicles forcing a transcellular pore allowing transcellular migration to occur. For both transmigration routes, endothelial pore opening is in part mediated by mechanical forces that are generated by migrating leukocytes. Polarized actin polymerization in the leukocyte elicits pulling and pushing forces that supports their movement through the confined endothelial pore**.**

dependent [16,25,26,45]. The role of ICAM-1 in leukocyte TEM is proposed to make endocytic vesicle fusions happening through transient lymphocyte induced ICAM-1 clustering. If this occurs in areas with a high density of caveolae and actin stress fibers, ICAM-1 may associate with, and induce fusion of caveolae resulting in the formation of a transcellular pore. Lymphocytes search for sites where they can transmigrate by forming protrusions that constantly probe the endothelial surface for the perfect exit spot [45]. In agreement with a role for endocytic vesicle fusion, chemotaxis during transcellular migration of lymphocytes was shown to be mediated by intraendothelial vesicle stores rather than by extracellular chemokine

depots [46]. Endocytic vesicle fusion supports a simultaneous release of chemokines and initiation of a transcellular passageway. In addition to ICAM-1 driven endocytic vesicle fusion events, local depolymerization of F-actin at the endothelial cell cortex turns out to make the endothelial cell less rigid in a confined region underneath the adherent leukocyte causing endothelial membrane to bend inwards until a transcellular pore has been formed [19,47].

In conclusion, leukocyte transendothelial migration occurs paracellular and transcellular and is dependent on the microenvironment and tissue type. Each mode is distinctly regulated, transcellular diapedesis in particular involves vesicle fusion events whereas destabilization of VE-cadherin has an essential role in junctional opening during paracellular diapedesis.

REGULATION OF RHO GTPASES ACTIVITY

Leukocyte transendothelial migration requires proper Rho GTPase function in leukocytes as well as in the endothelium. Timed Rho GTPase activation and deactivation is therefore important for proper regulation of the diapedesis process. To understand how this is regulated I will now introduce the regulators of the regulators. Guanine-nucleotide exchange factors (GEFs) and GTPase activating proteins (GAPs) are the master regulators of Rho-family GTPases. In EC GEFs and GAPs regulate numerous cellular responses such as maintenance of stable endothelial cell-cell junctions or directional migration of leukocytes. Endothelial cells express over 22 Rho GTPases and more than 69 GEFs and a similar number of GAPs [53]. The number of exchange factors is far greater than the number of Rho GTPases, indicating that the GEFs and GAPs determine signal specificity. GEF and GAP function is required to regulate the rate, location and timing of GTPase activity. This is probably why cells express a higher variety of GEFs and GAPs compared to the number of GTPases, to fine-tune complex cellular processes. Rho proteins cycle between GDP- and GTP-bound states. GEFs exchange the transition between Rho-GDP (inactive) to a Rho-GTP (active) loaded state. Whereas GAPs enhance the relatively slow intrinsic GTPase activity of Rho proteins. A general domain found in RhoGEFs is the DH (Dbl-Homology) domain, which catalyzes the exchange of GDP for GTP, thus activating Rho GTPases. Another domain found in many GEFs is the PH (Pleckstrin Homology) domain. PH domains have been reported to target the GEF to the plasma membrane [54] or to facilitate binding to the GTPase. For instance the leukemia associated Rho GEF (LARG) binds directly to RhoA through its PH domain [55]. Interestingly,

PH domains not only bind to phospholipids or GTPases but also to other proteins within the cell, as is the case for the first PH-DH domain of TRIO, which directly interacts with the actin cross linker filamin [56].

Depending on their subcellular localization, RhoGEFs can globally and locally change equilibrium of the Rho-GDP/GTP bound states. Local Rho GTPase activation can be achieved by subcellular sequestration of the GEF. For instance, the GEF NET1 resides inactive in the nucleus but after translocation to the plasma membrane it activates RhoA [57]. Similarly, Ect2 is normally localized in the nucleus during interphase but exits the nucleus during cell division to activate RhoA to regulate the cleavage furrow that separates the two cells during cell division [58]. Another example is GEF-H1 which directly interacts with microtubules, inhibiting its exchange potential towards RhoA. Tubulin depolymerization breaks this interaction resulting in local RhoA activation [59].

In addition, GEFs and GAPs can also function as signal integrators, independent of their intrinsic GEF activity, supporting larger protein complexes up- or downstream of RhoGTPases. For instance to drive chemotaxis in neutrophils, alpha-Pix acts as a scaffold to integrate activating signals for Cdc42 that arise from upstream GPCRs. Moreover, the pathway that regulates production of reactive oxygen species (ROS) important to kill pathogenic bacteria involves the GEF beta-Pix that tethers NADPH oxidase-1 for activation by Rac1 [60] showing the same principle of GEFs functioning as signal integrators. To dissect the spatiotemporal activation of GEFs and GAPs during GTPase activation, FRET-based biosensors have become the instrumental device of choice. Currently, the dimerization optimized reporters for activation (DORA) sensors for RhoA, RhoB, RhoC, Rac1 and Cdc42 are published and available for general scientific use [61–65].

LEUKOCYTE EXTRAVASATION AND VASCULAR PERMEABILITY COUPLED OR UNCOUPLED?

Inflammation is characterized by increased vasodilation, microvascular leakage and leukocyte recruitment. However, whether the transmigration of leukocytes directly causes increased microvascular permeability has been debated for decades. Some studies propose leukocyte adhesion and transmigration to be acute events leading to tissue damage and organ failure during inflammation and ischemia-reperfusion [66,67]. A strong argument that supports this hypothesis are the neutrophil depletion or CD11/CD18 blocking experiments that have been shown to attenuate vascular injury under these conditions [67–70]. However, when microvascular
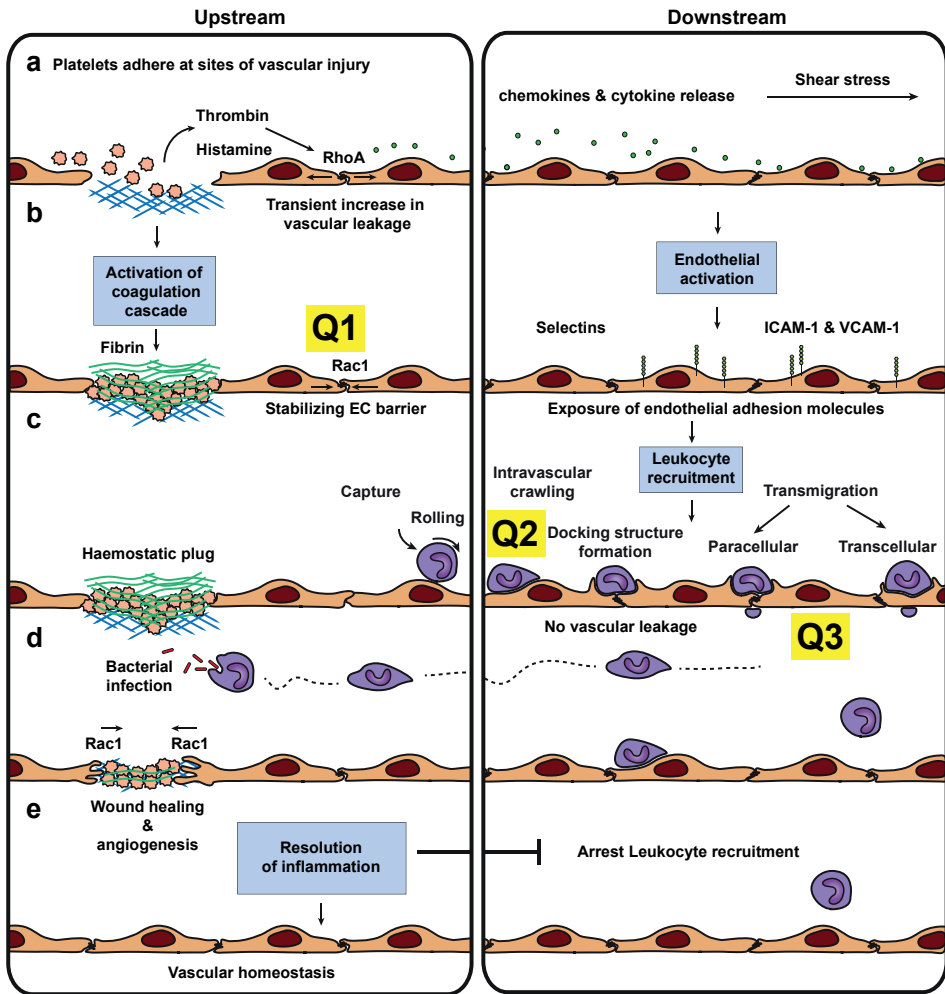
Figure 3. Schematic overview of research investigated in this thesis. Vascular injury in the skin is resolved by various sequential processes that initiate tissue repair and the clearance of pathogens and dirt to restore vascular homeostasis. (**a**) The first phase of repair is associated with increased vascular leakage, during this stage platelets adhere to exposed collagen forming a haemostatic plug of fibrin that arrests blood leakage (**a-c**). Activated platelets produce thrombin, a compound that activates the coagulation cascade to produce the haemostatic plug. Thrombin released by activated platelets and histamine released by tissue basophils and mast cells are thought to initiate endothelial activation, a transient increase in endothelial permeability provoked by RhoA-mediated actomyosin contractility, and local enhancement of blood flow. This results in chemokine and cytokine release by various cell types followed by inflammation close to the site of injury. (**b**) Downstream of vascular injury endothelial cells get activated and in turn expose a variety of adhesion molecules at their surface. Upstream local endothelial Rac1 activation induces membrane protrusions that help to restore junctional integrity and barrier function, counterbalancing the transient permeability increase. However, which exchange factors specifically regulate local Rac1 activity during junctional stabilization

permeability was measured simultaneously with leukocyte-endothelial interactions, local plasma leakage sites were often distinct from those of leukocyte adhesion or transmigration [71-76]. Plasma leakage was observed upstream of the sites where leukocytes entered the tissue. During inflammation in the respiratory tract of rats, plasma protein leakage is predominantly observed in the postcapillary venules whereas capillaries and arterioles did not leak. Under these inflammatory conditions most leukocyte diapedesis, in particular that of neutrophils, occurs in the collecting venules downstream of the leaky postcapillary venules [72]. Moreover, several studies have shown that the timing of leukocyte adhesion and transmigration is not well correlated with the evoked permeability change during acute inflammation [77-80]. Recently, molecular evidence for the uncoupling between leukocyte TEM and vascular permeability has been presented by Wessel and colleagues. They mechanistically uncoupled leukocyte extravasation and vascular permeability by showing that opening of endothelial junctions in those distinct processes are controlled by different tyrosine residues of VE-cadherin *in vivo* [36,44]. Thus, during a well-regulated and balanced inflammatory response, plasma protein leakage and leukocyte recruitment are two distinct events that can occur side by side, but are not necessarily caused by the direct movement of immune cells between the ECs.

However, in several diseases, such as thrombocytopenia, ischemia and rheumatoid arthritis, accumulation of immune cells evokes serious collateral damage resulting in tissue damage, vascular leakage and edema formation. In case of thrombocytopenia we know that the physical movement of immune cells through the endothelial barrier elicits hemorrhages [81]. This bleeding disorder is partly caused by the incapability of ECs to maintain a tight barrier during the physical movement of immune cells through the EC layer. For that reason, blocking immune cell

requires further research (Q1). (**c**) The local increase in vascular permeability does also enhance the recruitment of immune cells to the damaged site since chemotactic stimuli released by bacteria and tissue macrophages are easily transported and released in the circulation through the permeable endothelial junctions. Endothelial activation results in the upregulation of luminal exposed adhesion molecules such as ICAM-1 and VCAM-1 which mediate leukocyte diapedesis. ICAM-1 has been described to be involved in every step within the multi-step paradigm. The distribution of ICAM-1 in specialized membrane domains could explain these multi-functional roles of ICAM-1. However, what proteins regulate ICAM-1 distribution within the endothelial membrane are not well understood (Q2). Moreover, recruitment of innate immune cells occurs through transient openings in the endothelium without plasma leakage [26,44,77]. However, how the endothelium maintains a tight barrier during leukocyte transendothelial migration is poorly understood (Q 3). (**d**) Infiltrating leukocytes scan and clear pathogens and dirt from the site of infection. Rac1-mediated wound healing and angiogenesis repair damaged tissue and vessels. (**e**) Finally, tissue macrophages secrete chemokines that resolve inflammation arresting leukocyte recruitment to restore vascular homeostasis.

adhesion molecules may prevent TEM and consequently reduce patient's symptoms. Over the past decades much effort has been devoted to the development of blocking antibodies targeting leukocyte integrins or integrin ligands that are exposed at the endothelial surface. However, two clinical trials that tried to interfere with ICAM-1 and CD18 evoked serious side effects and aggravated the patients conditions, since the murine IgG2a monoclonal antibody enlimomab targeting human ICAM-1 and the humanized IgG1 antibody directed at human CD18 activated the immune cells rather than blocking adhesion [82]. Patients that received the treatment developed fever, cutaneous reactions, and neurological disability and showed a trend towards excess mortality compared to patients that got the placebo. The antibodies caused unwanted cellular activation and repeated administration of the antibody evoked allergic reactions since the enlimomab was of murine origin. We must learn from studies like the enlimomab trial in order to improve treatments for inflammatory and immune cell related diseases. Thus it is required that we increase our general understanding about the signaling pathways that regulate leukocyte TEM, both at the cellular and molecular level. In this thesis, I focus on the mechanisms that underlie endothelial junctional remodeling and ICAM-1 mediated adhesion during leukocyte diapedesis (Fig. 3).

SCOPE OF THE THESIS

The precise mechanisms by which the vasculature maintains its integrity to cope with daily stressors such as leukocyte diapedesis, temperature, shear stress and inflammatory mediators are not yet fully understood. In chapter 2 we reviewed the role of RhoGTPases in transendothelial migration (TEM) from an endothelial point of view. This review puts forward the importance of the β2 integrin-ligand ICAM-1 in activation of endothelial RhoGTPases during TEM. ICAM-1 is believed to be involved in all the steps of the paradigm for leukocyte diapedesis. However, how ICAM-1 can specifically mediate all these distinct step remains elusive. In chapter 3 we show that this is in part regulated by the spatial distribution of ICAM-1 in microdomains within the plasma membrane. We identified a regulatory role for the calcium effector protein annexin A2 which mediates an ICAM-1 transition from ezrin to caveolin-1-rich microdomains after ICAM-1 clustering. The redistribution of ICAM-1 into these caveolin-1-rich microdomains negatively affects neutrophil transmigration and adhesion. On a daily basis billions of leukocytes traverse the endothelial barrier without damaging the vascular bed or underlying tissue. The precise mechanisms by which the endothelium maintains a tight barrier during

leukocyte transendothelial migration is currently poorly understood. In chapter 4 we show that local RhoA-mediated F-actin rings contribute to endothelial pore confinement that locally maintain endothelial barrier integrity preventing vascular leakage during leukocyte diapedesis. We show that the endothelial small GTPase RhoA is required to maintain a tight EC barrier during leukocyte diapedesis. Depletion in vitro or inhibition of endothelial RhoA in vivo increased vascular leakage, provoked by neutrophil transmigration, but did not alter neutrophil adhesion or transmigration. Using a novel RhoA FRET biosensor, we found that endothelial RhoA was transiently activated around transmigrating neutrophils. At this stage, ECs assemble RhoA-controlled contractile F-actin structures around endothelial pores that prevent vascular leakage during leukocyte extravasation. Next, in the contexts of inflammation, the exact mechanisms by which EC dynamically remodel cell-cell junctions to stabilize the endothelial barrier after exposure to inflammatory mediators such as thrombin are not yet fully understood. In chapter 5 we identify a key role for the Rho-GEF Trio in stabilizing VE-cadherin-based junctions after thrombin treatment. Moreover, the work presented in chapter 4 demonstrates that vascular permeability and inflammation-driven leukocyte recruitment are independent events. We developed a screening method to study the involvement of GEFs and GAPs during junctional regulation in each of these mechanistically independent processes. In chapter 6 we described the methodology to screen for new endothelial proteins that regulate vascular integrity during leukocyte diapedesis. Chapter 7 describes a brief summary of the research presented in this thesis. In addition a short outlook is presented to give the reader an impression of future research directions.

REFERENCES

1. Grivennikov, S. I., Greten, F. R. & Karin, M. Immunity, inflammation, and cancer. *Cell* **140,** 883–99 (2010).
2. Nourshargh, S., Hordijk, P. L. & Sixt, M. Breaching multiple barriers: leukocyte motility through venular walls and the interstitium. *Nat. Rev. Mol. Cell Biol.* **11,** 366–78 (2010).
3. Gül, N. *et al.* Macrophages eliminate circulating tumor cells after monoclonal antibody therapy. *J. Clin. Invest.* (2014). doi:10.1172/JCI66776
4. Heemskerk, N., Van Rijssel, J. & Van Buul, J. D. Rho-GTPase signaling in leukocyte extravasation: An endothelial point of view. *Cell Adhesion and Migration* **8,** 67–75 (2014).
5. Butcher, E. C. Leukocyte-endothelial cell recognition: three (or more) steps to specificity and diversity. *Cell* **67,** 1033–6 (1991).
6. Springer, T. A. Traffic signals for lymphocyte recirculation and leukocyte emigration: the multistep paradigm. *Cell* **76,** 301–14 (1994).
7. Kroon, J., Daniel, A. E., Hoogenboezem, M. & van Buul, J. D. Real-time imaging of endothelial cell-cell junctions during neutrophil transmigration under physiological flow. *J. Vis. Exp.* e51766 (2014). doi:10.3791/51766
8. Schulte, D. *et al.* Stabilizing the VE-cadherin–catenin complex blocks leukocyte extravasation and vascular permeability. *EMBO J.* **30,** 4157–4170 (2011).
9. Carman, C. V. Mechanisms for transcellular diapedesis: probing and pathfinding by 'invadosome-like protrusions'. *J. Cell Sci.* **122,** 3025–3035 (2009).
10. Carman, C. V. & Springer, T. A. A transmigratory cup in leukocyte diapedesis both through individual vascular endothelial cells and between them. *J. Cell Biol.* **167,** 377–388 (2004).
11. Feng, D., Nagy, J. A., Pyne, K., Dvorak, H. F. & Dvorak, A. M. Neutrophils emigrate from venules by a transendothelial cell pathway in response to FMLP. *J. Exp. Med.* **187,** 903–15 (1998).
12. Salanga, C. L. & Handel, T. M. Chemokine oligomerization and interactions with receptors and glycosaminoglycans: The role of structural dynamics in function. *Exp. Cell Res.* **317,** 590–601 (2011).
13. Shulman, Z. *et al.* Lymphocyte Crawling and Transendothelial Migration Require Chemokine Triggering of High-Affinity LFA-1 Integrin. *Immunity* **30,** 384–396 (2009).
14. Bao, X. *et al.* Endothelial heparan sulfate controls chemokine presentation in recruitment of lymphocytes and dendritic cells to lymph nodes. *Immunity* **33,** 817–829 (2010).
15. Abtin, A. *et al.* Perivascular macrophages mediate neutrophil recruitment during bacterial skin infection. *Nat. Immunol.* **15,** 45–53 (2013).
16. Abadier, M. *et al.* Cell surface levels of endothelial ICAM-1 influence the transcellular or paracellular T-cell diapedesis across the blood-brain barrier. *Eur. J. Immunol.* **45,** 1043–58 (2015).
17. Stroka, K. M. & Aranda-Espinoza, H. Neutrophils display biphasic relationship between migration and substrate stiffness. *Cell Motil. Cytoskeleton* **66,** 328–341 (2009).
18. Martinelli, R. *et al.* Probing the biomechanical contribution of the endothelium to lymphocyte migration: diapedesis by the path of least resistance. *J. Cell Sci.* **127,** 3720–3734 (2014).
19. Isac, L., Thoelking, G., Schwab, A., Oberleithner, H. & Riethmuller, C. Endothelial f-actin depolymerization enables leukocyte transmigration. *Anal. Bioanal. Chem.* **399,** 2351–2358 (2011).
20. Kitayama, J., Hidemura, a, Saito, H. & Nagawa, H. Shear stress affects migration behavior of polymorphonuclear cells arrested on endothelium. *Cell. Immunol.* **203,** 39–46 (2000).
21. Cinamon, G., Shinder, V. & Alon, R. Shear forces promote lymphocyte migration across vascular endothelium bearing apical chemokines. *Nat. Immunol.* **2,** 515–22 (2001).
22. Bernardo, a. *et al.* Platelets adhered to endothelial cell-bound ultra-large von Willebrand factor strings support leukocyte tethering and rolling under high shear stress. *J. Thromb. Haemost.* **3,** 562–570 (2005).
23. Kapoor, J. R. Platelet activation and atherothrombosis. *N. Engl. J. Med.* **358,** 1638; author reply 1638–1639 (2008).
24. Langer, H. F. & Gawaz, M. Platelet-vessel wall interactions in atherosclerotic disease. *Thromb. Haemost.* **99,** 480–6 (2008).
25. Bullard, D. C. *et al.* P-selectin/ICAM-1 double mutant mice: Acute emigration of neutrophils into the peritoneum is completely absent but is normal into pulmonary alveoli. *J. Clin. Invest.* **95,** 1782–1788 (1995).

26. Küppers, V., Vestweber, D. & Schulte, D. Locking endothelial junctions blocks leukocyte extravasation, but not in all tissues. *Tissue barriers* **1,** e23805 (2013).

27. Barreiro, O. *et al.* Dynamic interaction of VCAM-1 and ICAM-1 with moesin and ezrin in a novel endothelial docking structure for adherent leukocytes. *J. Cell Biol.* **157,** 1233–1245 (2002).

28. Van Buul, J. D. *et al.* RhoG regulates endothelial apical cup assembly downstream from ICAM1 engagement and is involved in leukocyte trans-endothelial migration. *J. Cell Biol.* **178,** 1279–1293 (2007).

29. Phillipson, M., Kaur, J., Colarusso, P., Ballantyne, C. M. & Kubes, P. Endothelial domes encapsulate adherent neutrophils and minimize increases in vascular permeability in paracellular and transcellular emigration. *PLoS One* **3,** e1649 (2008).

30. Kaur, J. *et al.* Endothelial LSP1 is involved in endothelial dome formation , minimizing vascular permeability changes during neutrophil transmigration in vivo. **117,** 942–953 (2014).

31. Vestweber, D., Zeuschner, D., Rottner, K. & Schnoor, M. and ICAM-1 clustering in endothelium Implications for the formation of docking structures. 1–5 (2013).

32. Mooren, O. L., Li, J., Nawas, J. & Cooper, J. A. Endothelial cells use dynamic actin to facilitate lymphocyte transendothelial migration and maintain the monolayer barrier. *Mol. Biol. Cell* **25,** 4115–29 (2014).

33. Ley, K., Laudanna, C., Cybulsky, M. I. & Nourshargh, S. Getting to the site of inflammation: the leukocyte adhesion cascade updated. *Nat. Rev. Immunol.* **7,** 678–89 (2007).

34. Luissint, A. C., Nusrat, A. & Parkos, C. A. JAM-related proteins in mucosal homeostasis and inflammation. *Seminars in Immunopathology* **36,** 211–226 (2014).

35. Sullivan, D. P. & Muller, W. A. Neutrophil and monocyte recruitment by PECAM, CD99, and other molecules via the LBRC. *Semin. Immunopathol.* **36,** 193–209 (2014).

36. Vestweber, D., Wessel, F. & Nottebaum, A. F. Similarities and differences in the regulation of leukocyte extravasation and vascular permeability. *Seminars in Immunopathology* **36,** 177–192 (2014).

37. Barreiro, O. *et al.* Endothelial adhesion receptors are recruited to adherent leukocytes by inclusion in preformed tetraspanin nanoplatforms. *J. Cell Biol.* **183,** 527–542 (2008).

38. van Rijssel, J. *et al.* The Rho-guanine nucleotide exchange factor Trio controls leukocyte transendothelial migration by promoting docking structure formation. *Mol. Biol. Cell* **23,** 2831–2844 (2012).

39. Vestweber, D. How leukocytes cross the vascular endothelium. *Nat. Rev. Immunol.* **15,** 692–704 (2015).

40. Amerongen, G. P. v. N., Delft, S. v., Vermeer, M. A., Collard, J. G. & van Hinsbergh, V. W. M. Activation of RhoA by Thrombin in Endothelial Hyperpermeability : Role of Rho Kinase and Protein Tyrosine Kinases. *Circ. Res.* **87,** 335–340 (2000).

41. Hixenbaugh, E. A. *et al.* Stimulated neutrophils induce myosin light chain phosphorylation and isometric tension in endothelial cells. *Am J Physiol Hear. Circ Physiol* **273,** H981–988 (1997).

42. Huang, a J. *et al.* Endothelial cell cytosolic free calcium regulatesneutrophil migration across monolayers of endothelial cells. *J.Cell Biol.* **120,** 1371–1380 (1993).

43. Saito, H., Minamiya, Y., Saito, S. & Ogawa, J. Endothelial Rho and Rho kinase regulate neutrophil migration via endothelial myosin light chain phosphorylation. *J. Leukoc. Biol.* **72,** 829–36 (2002).

44. Wessel, F. *et al.* Leukocyte extravasation and vascular permeability are each controlled in vivo by different tyrosine residues of VE-cadherin. *Nat. Immunol.* **15,** 223–30 (2014).

45. Millán, J. *et al.* Lymphocyte transcellular migration occurs through recruitment of endothelial ICAM-1 to caveola- and F-actin-rich domains. *Nat. Cell Biol.* **8,** 113–123 (2006).

46. Shulman, Z. *et al.* Transendothelial migration of lymphocytes mediated by intraendothelial vesicle stores rather than by extracellular chemokine depots. *Nat. Immunol.* **13,** 67–76 (2011).

47. Lemichez, E., Gonzalez-Rodriguez, D., Bassereau, P. & Brochard-Wyart, F. Transcellular tunnel dynamics: Control of cellular dewetting by actomyosin contractility and I-BAR proteins. *Biol. Cell* **105,** 109–117 (2013).

48. Thompson, P. W., Randi, A. M. & Ridley, A. J. Intercellular adhesion molecule (ICAM)-1, but not ICAM-2, activates RhoA and stimulates c-fos and rhoA transcription in endothelial cells. *J. Immunol.* **169,** 1007–1013 (2002).

49. Greenwood, J. *et al.* Intracellular domain of brain endothelial intercellular adhesion molecule-1 is essential for T lymphocyte-mediated signaling and migration. *J. Immunol.* **171,** 2099–2108 (2003).

50. Toyjanova, J., Flores-Cortez, E., Reichner, J. S. & Franck, C. Matrix Confinement Plays a Pivotal Role in Regulating Neutrophil-generated Tractions, Speed and Integrin Utilization. *J. Biol. Chem.* **290,** jbc.M114.619643 (2014).
51. Rabodzey, A., Alcaide, P., Luscinskas, F. W. & Ladoux, B. Mechanical forces induced by the transendothelial migration of human neutrophils. *Biophys. J.* **95,** 1428–1438 (2008).
52. Jannat, R. a., Dembo, M. & Hammer, D. a. Traction forces of neutrophils migrating on compliant substrates. *Biophys. J.* **101,** 575–584 (2011).
53. Van Buul, J. D., Geerts, D. & Huveneers, S. Rho GAPs and GEFs: Controling switches in endothelial cell adhesion. *Cell Adhes. Migr.* **8,** 108–124 (2014).
54. Ferguson, K. M., Lemmon, M. A., Schlessinger, J. & Sigler, P. B. Structure of the high affinity complex of inositol trisphosphate with a phospholipase C pleckstrin homology domain. *Cell* **83,** 1037–1046 (1995).
55. Kristelly, R., Gao, G. & Tesmer, J. J. G. Structural determinants of RhoA binding and nucleotide exchange in leukemia-associated Rho guanine-nucleotide exchange factor. *J. Biol. Chem.* **279,** 47352–47362 (2004).
56. Bellanger, J. M. *et al.* The Rac1- and RhoG-specific GEF domain of Trio targets filamin to remodel cytoskeletal actin. *Nat. Cell Biol.* **2,** 888–92 (2000).
57. Schmidt, A. & Hall, A. The Rho exchange factor Net1 is regulated by nuclear sequestration. *J. Biol. Chem.* **277,** 14581–14588 (2002).
58. Tatsumoto, T., Xie, X., Blumenthal, R., Okamoto, I. & Miki, T. Human ECT2 is an exchange factor for Rho GTPases, phosphorylated in G2/M phases, and involved in cytokinesis. *J. Cell Biol.* **147,** 921–8 (1999).
59. Krendel, M., Zenke, F. T. & Bokoch, G. M. Nucleotide exchange factor GEF-H1 mediates cross-talk between microtubules and the actin cytoskeleton. *Nat. Cell Biol.* **4,** 294–301 (2002).
60. Park, H. S. *et al.* Sequential activation of phosphatidylinositol 3-kinase, beta Pix, Rac1, and Nox1 in growth factor-induced production of H2O2. *Mol. Cell. Biol.* **24,** 4384–94 (2004).
61. Kedziora, K. M. *et al.* Rapid remodeling of invadosomes by Gi-coupled receptors: dissecting the role of Rho GTPases. *J. Biol. Chem.* jbc.M115.695940 (2016). doi:10.1074/jbc.M115.695940
62. van Unen, J., Reinhard, N.R., Yin, T., Wu, Y.I., Postma, M., Gadella Jr., T.W., Goedhart, J. Plasma membrane restricted RhoGEF activity is sufficient for RhoA-mediated actin polymerization. *Sci. Rep.* (2015).
63. Timmerman, I. *et al.* A local VE-cadherin / Trio-based signaling complex stabilizes endothelial junctions through Rac1 Journal of Cell Science Accepted manuscript. (2015).
64. Lin, B., Yin, T., Wu, Y. I., Inoue, T. & Levchenko, A. Interplay between chemotaxis and contact inhibition of locomotion determines exploratory cell migration. *Nat. Commun.* **6,** 6619 (2015).
65. Reinhard, N. R. *et al.* Spatiotemporal analysis of RhoA/B/C activation in primary human endothelial cells. *Sci. Rep.* **6,** 25502 (2016).
66. Oliver, M. G., Specian, R. D., Perry, M. A. & Granger, D. N. Morphologic assessment of leukocyte-endothelial cell interactions in mesenteric venules subjected to ischemia and reperfusion. *Inflammation* **15,** 331–346 (1991).
67. Hernandez, L. a *et al.* Role of neutrophils in ischemia-reperfusion-induced microvascular injury. *Am. J. Physiol.* **253,** H699–H703 (1987).
68. Kubes, P., Suzuki, M. & Granger, D. N. Modulation of PAF-induced leukocyte adherence and increased microvascular permeability. *Am. J. Physiol.* **259,** G859–G864 (1990).
69. Sumagin, R., Lomakina, E. & Sarelius, I. H. Leukocyte-endothelial cell interactions are linked to vascular permeability via ICAM-1-mediated signaling. *Am. J. Physiol. Heart Circ. Physiol.* **295,** H969–H977 (2008).
70. Carden, D. L., Smith, J. K. & Korthuis, R. J. Neutrophil-mediated microvascular dysfunction in postischemic canine skeletal muscle. Role of granulocyte adherence. *Circ. Res.* **66,** 1436–1444 (1990).
71. McDonald, D. M., Thurston, G. & Baluk, P. Endothelial gaps as sites for plasma leakage in inflammation. *Microcirculation* **6,** 7–22 (1999).
72. Baluk, P., Bolton, P., Hirata, A., Thurston, G. & McDonald, D. M. Endothelial gaps and adherent leukocytes in allergen-induced early- and late-phase plasma leakage in rat airways. *Am. J. Pathol.* **152,** 1463–76 (1998).
73. McDonald, D. M. Endothelial gaps and permeability of venules in rat tracheas exposed to inflammatory stimuli. *Am. J. Physiol.* **266,** L61–L83 (1994).
74. Baluk, P., Bertrand, C., Geppetti, P., McDonald, D. M. & Nadel, J. A. NK1 receptors mediate leukocyte adhesion in neurogenic inflammation in the rat trachea. *Am. J. Physiol.* **268,**

L263–L269 (1995).

75. Gawlowski, D. M., Benoit, J. N. & Granger, H. J. Microvascular pressure and albumin extravasation after leukocyte activation in hamster cheek pouch. *Am. J. Physiol.* **264,** H541–6 (1993).

76. Rosengren, S., Ley, K. & Arfors, K. E. Dextran sulfate prevents LTB4-induced permeability increase, but not neutrophil emigration, in the hamster cheek pouch. *Microvasc. Res.* **38,** 243–254 (1989).

77. Valeski, J. E. & Baldwin, a L. Effect of early transient adherent leukocytes on venular permeability and endothelial actin cytoskeleton. *Am. J. Physiol.* **277,** H569–H575 (1999).

78. Kim, M.-H., Curry, F.-R. E. & Simon, S. I. Dynamics of neutrophil extravasation and vascular permeability are uncoupled during aseptic cutaneous wounding. *Am. J. Physiol. Cell Physiol.* **296,** C848–56 (2009).

79. Lewis, R. E. & Granger, H. J. Diapedesis and the permeability of venous microvessels to protein macromolecules: the impact of leukotriene B4 (LTB4). *Microvasc. Res.* **35,** 27–47 (1988).

80. Lewis, R. E., Miller, R. A. & Granger, H. J. Acute microvascular effects of the chemotactic peptide N-formyl-methionyl-leucyl-phenylalanine: Comparisons with leukotriene B4. *Microvasc. Res.* **37,** 53–69 (1989).

81. Hillgruber, C. *et al.* Blocking neutrophil diapedesis prevents hemorrhage during thrombocytopenia. *J. Exp. Med.* (2015). doi:10.1084/jem.20142076

82. Becker, K. J. Anti-leukocyte antibodies: LeukArrest (Hu23F2G) and Enlimomab (R6.5) in acute stroke. *Curr. Med. Res. Opin.* **18 Suppl 2,** s18–s22 (2002).

1

2

Rho-GTPase signaling in leukocyte extravasation
An endothelial point of view

Niels Heemskerk, Jos van Rijssel, and Jaap D van Buul*

Department of Molecular Cell Biology; Sanquin Research and Landsteiner Laboratory; Academic Medical Center; University of Amsterdam; Amsterdam, the Netherlands

ABSTRACT

Leukocyte transendothelial migration (TEM) is one of the crucial steps during inflammation. A better understanding of the key molecules that regulate leukocyte extravasation aids to the development of novel therapeutics for treatment of inflammation-based diseases, such as atherosclerosis and rheumatoid arthritis. The adhesion molecules ICAM-1 and VCAM-1 are known as central mediators of TEM. Clustering of these molecules by their leukocytic integrins initiates the activation of several signaling pathways within the endothelium, including a rise in intracellular Ca^{2+}, activation of several kinase cascades, and the activation of Rho-GTPases. Activation of Rho-GTPases has been shown to control adhesion molecule clustering and the formation of apical membrane protrusions that embrace adherent leukocytes during TEM. Here, we discuss the potential regulatory mechanisms of leukocyte extravasation from an endothelial point of view, with specific focus on the role of the Rho-GTPases.

INTRODUCTION

Efficient and tightly controlled leukocyte transendothelial migration (TEM) is of key importance in physiological processes such as immune surveillance and acute inflammation. Uncontrolled and excessive TEM is characteristic for various disorders such as chronic inflammatory diseases (e.g., rheumatoid arthritis, atherosclerosis, asthma) and tumor cell metastasis (Muller, 2009; Dietmar Vestweber, 2012a). In order to specifically interfere with excessive leukocyte or tumor cell TEM, a detailed understanding of endothelial signaling that regulates TEM is required. It is believed that the TEM process occurs through different steps. Butcher and Springer proposed in timeless reviews the multi-step model for the process of TEM (Butcher, 1991; Springer, 1994). Currently, the basis of this model is still accurate and some additional steps have been included (Fig. 1). Importantly, the active contribution of endothelial signaling in TEM has been recognized. The group of Alon described the need for the presence of immobilized chemokines on the surface of the endothelium (Guy Cinamon, Shinder, Shamri, & Alon, 2004). Recently, they showed that the endothelium itself generates chemokines and presents those at the apical surface to promote TEM (Shulman et al., 2011). The same group also put forward the importance of shear flow during TEM (G Cinamon, Shinder, & Alon, 2001). Barreiro and colleagues, together with Carman and co-workers, showed the contribution of cup-like membrane structures created by the endothelium that surround adherent leukocytes in order to facilitate directional transmigration (Barreiro et al., 2002; Carman & Springer, 2004; Carman, Jun, Salas, & Springer, 2003). Nevertheless, the main steps of TEM, namely rolling, adhesion, and transmigration, as proposed by Butcher and Springer more than 20 years ago, still constitute the central processes that drive leukocyte extravasation (Fig. 1) (Butcher, 1991; Springer, 1994). In this review, we discuss the regulatory mechanisms that control the different steps of leukocyte extravasation (Fig. 1) from an endothelial point of view, with specific focus on the role of the Rho-GTPases and their activators guanine-nucleotide exchange factors (GEFs).

STEP 1: CAPTURE AND ROLLING

Initially, transient leukocyte–endothelial cell interactions are mediated by the endothelial adhesion molecules E- and P-selectin with their leukocyte counterparts L-selectin and PSGL-1. These interactions comprise the so-called "rolling step;" slowing down the leukocytes on the endothelial

cell surface (Fig. 1, step 1). P-selectin, also known as CD62P, is present in Weibel-Palade bodies and can be quickly released and presented at the luminal side of the endothelium upon activation with histamine/ thrombin or with pharmacological compounds such as Ca^{2+} ionophores or phorbol esters (Bonfanti, Furie, Furie, & Wagner, 1989; R P McEver, Beckstead, Moore, Marshall-Carlson, & Bainton, 1989; Rodger P McEver, 2002; D Vestweber et al., 1999). Maximal expression of P-selectin on the endothelial surface is seen after 10 min of activation, after which (30–60 min) the protein is being downregulated, either by internalization or shedding. CD63 was found to be an essential co-factor for P-selectin, since endothelial cells deficient for CD63 showed a loss of P-selectin-mediated adhesion function (Doyle et al., 2011). E-selectin (CD62E) is not found in Weibel-Palade bodies (Bevilacqua, Pober, Mendrick, Cotran, & Gimbrone, 1987), but is rapidly upregulated by inflammatory stimuli, such as TNF-α and IL-1β. As for P-selectin, the upregulation involves the small Rho-GTPases RhoA, RhoB, and Rac1 (Cernuda-Morollón & Ridley, 2006). Maximum expression for E-selectin is reached after approximately 3–4 h of stimulation. Interestingly, clustering of E- and also P-selectin, using crosslinking of antibodies, induced intracellular signals into the endothelium, including a remodeling of actin stress fibers (Lorenzon et al., 1998). The authors also reported that initial leukocyte adhesion to the endothelium induced an immediate increase in calcium concentrations in the endothelium, in line with the role of selectins, mediating initial interaction of the leukocytes with the endothelium. Additionally, clustering of E-selectin has been shown to redistribute E-selectin to caveolin-rich membrane domains and promote its interaction with and activation of phospholipase Cγ (Kiely, Hu, Garcia-Cardena, & Gimbrone, 2003).
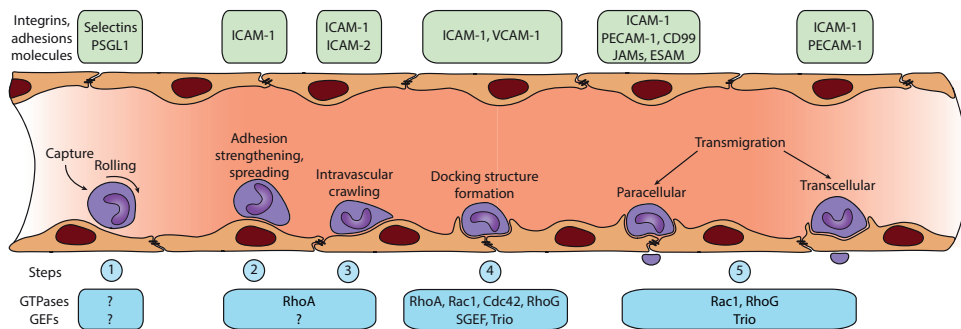
Figure 1. The multistep process of leukocyte transendothelial migration, divided in five consecutive steps. Step 1 represents the rolling and tethering phase; step 2 shows the initial adhesion of the leukocytes to the endothelium. Step 3 is the firm adhesion and crawling part. In step 4, the cup-like structures are formed, resulting in step 5; actual transmigration, either para- or transcellular.

Moreover, E-selectin clustering also triggers the activation of Erk1/2 and expression of c-fos (Y Hu, Kiely, Szente, Rosenzweig, & Gimbrone, 2000; Yenya Hu, Szente, Kiely, & Gimbrone, 2001), as well as changes in the endothelial cell morphology and F-actin distribution, in line with the work by Lorenzon and colleagues (Lorenzon et al., 1998). In fact, clustering of E-selectin induced by monocytes was dependent on upstream RhoA activation (Wójciak-Stothard, Williams, & Ridley, 1999). Additionally, E-selectin clustering induced a linkage to the actin cytoskeleton through its intracellular tail (Kaplanski et al., 1994; Wójciak-Stothard et al., 1999; Yoshida et al., n.d.). Yoshida and co-workers showed the presence of actin-associated proteins α-actinin, vinculin, filamin, FAK, and paxillin, but not talin, in E-selectin-clustering precipitation assays (Yoshida et al., n.d.). In addition, blocking actin polymerization reduced the adhesive capacity of E-selectin. This was measured by applying mechanical stress to the endothelial cells using anti-E-selectin antibody-coated ferromagnetic beads with a magnetical twisting cytometer. These data suggested that actin remodeling is instrumental for proper E-selectin function and strongly suggests a prominent role for small Rho-GTPases. And although Rho-GTPases have been implicated upstream from P- and E-selectin, so far no role for Rho-GTPase signaling downstream from either P- or E-selectin during step 1 of TEM has been reported. In the next section, we will discuss the endothelial signaling during step 2 and 3 in more detail.

STEP 2 AND 3: ADHESION, STRENGTHENING, SPREADING, AND INTRAVASCULAR CRAWLING

Firm adhesion of leukocytes is initiated upon binding of activated integrins to their endothelial ligands Intercellular Adhesion Molecule 1 (ICAM-1) and Vascular Cell Adhesion Molecule (VCAM-1). To demonstrate the importance of ICAM-1 in firm adhesion and TEM, Chinese Hamster Ovary (CHO), or HeLa cells that expressed no or very little endogenous ICAM-1 were artificially transfected with ICAM-1. This was sufficient to recapitulate the entire process of neutrophil adhesion and migration across these cells (Celli, Ryckewaert, Delachanal, & Duperray, 2006) (van Buul JD, data not shown). The group of Silverstein showed that leukocyte adhesion to endothelial cells induced the release of intracellular calcium in endothelial cells although the upstream signals, i.e., selectin- or CAM-mediated, were unknown at that time (Huang et al., 1993). Nevertheless, they were the first to show the importance of intracellular signaling in endothelial cells during the adhesion step of leukocyte TEM. Clustering of the adhesion molecules ICAM-1 and VCAM-1 is crucial to induce endothelial signaling.

This is both a passive and an active event. ICAM-1 and VCAM-1 reside in preformed membrane nanodomains (also termed endothelial adhesive platforms) that are controlled by several members of the tetraspanin family of integral membrane proteins (Barreiro et al., 2008). Leukocyte binding to the endothelium through the engagement of integrins induces these nanodomains to coalesce into higher order clusters, leading to the activation of several signaling pathways in endothelial cells. It is now well recognized that this signaling, in turn, activates positive feedback loops, promoting additional clustering of Ig-CAMs like ICAM-1 and VCAM-1 into ringlike structures around adherent leukocytes, which subsequently amplifies signaling through a positive feedback loop (Alcaide, Auerbach, & Luscinskas, 2009; Carman et al., 2003; Jaap D van Buul, van Rijssel, van Alphen, Hoogenboezem, et al., 2010; Jaap D van Buul, van Rijssel, van Alphen, van Stalborch, et al., 2010; J. van Rijssel et al., 2012). The carboxyl (C)-terminal intracellular domain of ICAM-1 is relatively small (28 amino acids) compared with its extracellular region (481 aa). Nevertheless, signaling by ICAM-1 was shown to be dependent on this small intracellular domain (Greenwood et al., 2003; Lyck et al., 2003; Jaap D. Van Buul et al., 2007; J. van Rijssel et al., 2012). Also, VCAM-1 shows a relatively small C-terminal intracellular domain compared with its extracellular domain (19 vs. 699 aa, respectively). Since the C-terminal domains of these proteins do not contain any apparent signaling motifs, signaling is likely relayed via adaptor proteins. Several adaptor proteins have been reported to interact with the intracellular domains of ICAM-1 and VCAM-1, including α-actinin, cortactin, filamin, and members of the ERM protein family (Barreiro et al., 2002; Celli et al., 2006; Kanters et al., 2008; Oh et al., 2007; Romero, Amos, Greenwood, & Adamson, 2002; Schnoor et al., 2011). Besides acting as scaffolding proteins, these adapters are also able to bind actin, and can therefore anchor ICAM-1 and VCAM-1 physically to the actin cytoskeleton (Bretscher, Edwards, & Fehon, 2002; Kirkbride, Sung, Sinha, & Weaver, n.d.; Stossel et al., 2001; Jaap D van Buul & Hordijk, 2009). Early studies showed that leukocyte adhesion and clustering of ICAM-1 promote an increase in intracellular Ca^{2+} levels (Huang et al., 1993). Others followed up on this crucial finding and showed that the change in calcium concentration leads to activation of the tyrosine kinase Src by protein kinase C (PKC) (Etienne-Manneville et al., 2000). In turn, Src induces tyrosine phosphorylation of focal adhesion proteins, such as paxillin, cortactin, and FAK. The group of Luscinskas underscored the importance of endothelial Src-mediated phosphorylation of cortactin in leukocyte TEM. They showed that a non-phosphorylatable mutant of cortactin, expressed in endothelial cells, blocked leukocyte TEM (Yang et al., 2006). In addition, ICAM-1 clustering leads to the activation

of the small GTPase RhoA, which stimulates the formation of F-actin stress fibers (Etienne et al., 1998; Thompson, Randi, & Ridley, 2002). Moreover, RhoA activity was also demonstrated to be required for efficient ICAM-1 recruitment around adherent monocytes, suggesting an upstream role for RhoA within the ICAM-1-induced signaling cascade (Wójciak-Stothard et al., 1999). Interestingly, others have shown that thrombin-induced RhoA activation, resulting in increased stress fibers, showed loss of cell–cell contacts and increased gap formation in endothelial cells (Amerongen, Delft, Vermeer, Collard, & van Hinsbergh, 2000). However, high RhoA activity and increased stress fibers downstream from ICAM-1 clustering did not necessarily result in endothelial gap formation (Thompson et al., 2002; Jaap D van Buul et al., 2002). This indicates that the consequences of the intracellular signals that lead from RhoA activation to cell–cell junctions in endothelial cells specifically depend on the extracellular stimulus. Although guanine–nucleotide exchange factors (GEFs) are likely candidates to activate RhoA downstream from ICAM-1 engagement, no direct RhoA–GEF interaction has been identified so far. Etienne and colleagues showed that the Rap1–GEF C3G binds to Cas upon antibody-induced clustering of ICAM-1 (Etienne et al., 1998). They additionally indicated no role for the Ras- and Rac1-GEF SOS-1 downstream from ICAM-1 in their model system. Interestingly, RhoA can also be directly activated in a GEF-independent manner by reactive oxygen species (ROS) (Amir Aghajanian, Wittchen, Campbell, & Burridge, 2009). Aghajanian and co-workers demonstrated that ROS can directly target two critical cysteine residues that are located in a unique redox-sensitive motif within the phosphoryl binding loop of RhoA, resulting in RhoA-GTP loading (Amir Aghajanian et al., 2009). Clustering of VCAM-1 was shown to promote activation of the GTPase Rac1, leading to the production of ROS (Cook-Mills et al., 2004; van Wetering et al., 2002). VCAM-1-dependent ROS production was demonstrated to regulate the activation of matrix metalloproteases, which may contribute to the local breakdown of the endothelial adherens junctions (Deem & Cook-Mills, 2004). In addition, VCAM-1 clustering was shown to regulate lymphocyte TEM by activation of the kinase PKCα and the tyrosine phosphatase PTP1B in a ROS-dependent manner (Deem, Abdala-Valencia, & Cook-Mills, 2007). More recently, it was shown by the group of Vestweber that VCAM-1-induced Rac1 activation and subsequent ROS production was also involved in the dissociation of the endothelial receptor phosphatase VE-PTP from the junctional adhesion molecule VE-cadherin, which is an obligatory event during leukocyte TEM (Vockel & Vestweber, 2013). More recent advances in confocal microscopy have allowed detailed analysis of leukocyte–endothelium interactions in three dimensions. This revealed that upon

clustering, both ICAM-1 and VCAM-1 were recruited to cup-like, F-actin-rich membrane protrusions that surround adherent leukocytes (step 4) (Barreiro et al., 2002; Carman & Springer, 2004; Carman et al., 2003). In the next section, we will discuss the signaling and function that underlies the formation of these structures.
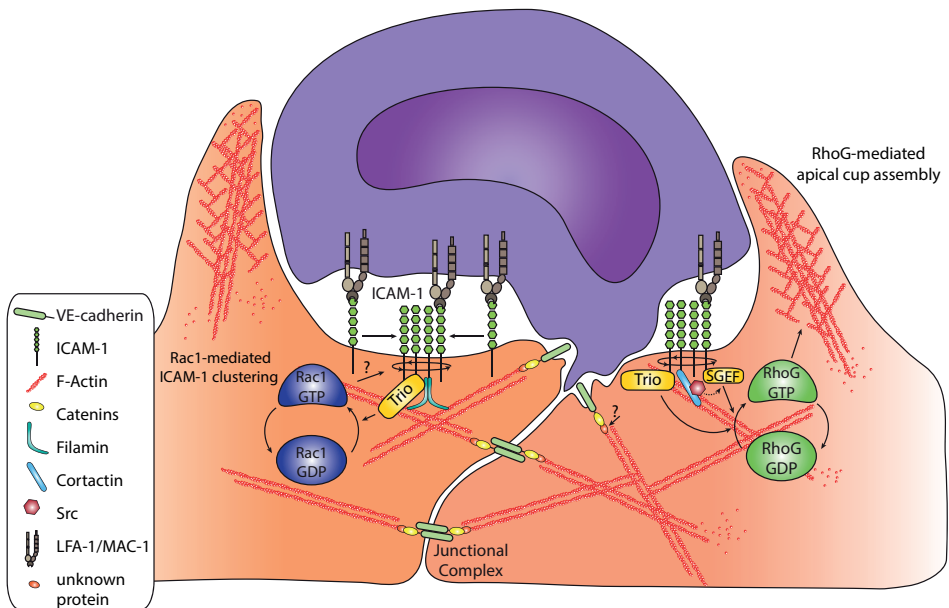
Step 4: Cup-Like Structures

Barreiro and co-workers were the first to report on the induction of these F-actin rich "cups." (Barreiro et al., 2002). Using live-cell imaging, they showed that adhesion and spreading of lymphoblasts on the endothelial cell surface induced the recruitment of VCAM-1 and the ERM-family member moesin, whereas ICAM-1 and moesin recruitment were primarily observed during TEM. In addition, adhesion of K562 cells that were stably transfected with α4 integrin (4M7 cells) resulted in an actin-rich endothelial cup structure embracing the 4M7 cells, and contained ICAM-1, VCAM-1, moesin, ezrin, α-actinin, vinculin, and VASP. Phospho-inositides and the Rho-ROCK-pathway were involved in the generation and maintenance of these so-called docking structures (Barreiro et al., 2002). Initially, Barreiro and colleagues proposed that thestructures are essential during the docking or adhesion phase and may protect leukocytes from detachment by shear flow, hence the term "docking structures." (Barreiro et al., 2002; Barreiro, Vicente-Manzanares, Urzainqui, Yáñez-Mó, & Sánchez-Madrid, 2004). This was underscored by Samson et al., who demonstrated using in vivo studies that removal of one of the crucial players involved in docking structure formation reduced leukocyte adhesion (Samson et al., 2013). However, although docking structures are formed around adhering leukocytes, it is still under debate whether or not these structures function in strengthening the adhesion of the leukocyte to the endothelium. Several reports have shown that inhibition of ICAM-1 signaling, and thus, preventing docking structure formation in vitro, affects leukocyte TEM, but not adhesion (Greenwood et al., 2003; Lyck et al., 2003; J. van Rijssel et al., 2012). In fact, Carman and colleagues revealed that the endothelium pro-actively generates microfilament, microtubule, and calcium-dependent ICAM-1-enriched cup-like structures within minutes of binding to LFA-1-bearing leukocytes (Carman et al., 2003). Interestingly, disruption of endothelial projections by blocking actin polymerization (cytochalasin D) or microtubule polymerization (colchicine), or by chelating calcium (BAPTA) did not affect firm adhesion of leukocytes. Thus, from this work, these structures appear not to function in adhesion strengthening, but may in fact play a more direct

role in the final diapedesis step. To assess the role of Rho-GTPases in the formation of these endothelial actin-rich projections, Carman and colleagues treated the endothelial cells with Clostridium diffucile toxin-B to inhibit Rho, Rac1, and Cdc42 (Carman et al., 2003). Toxin-B treatment was associated with a 2-fold reduction in total projections and TEM. In contrast to the docking structures proposed by Barreiro and co-workers, blocking Rho by C3 transferase had no effect on either projections or TEM. These data suggest an active role for the Rho-GTPases Rac1 and Cdc42 in projection formation and provide correlative support for a functional role of projections in leukocyte diapedesis. A year later, the Carman lab demonstrated a cup-like structure that is formed around transmigrating leukocytes in both the paracellular and transcellular migration pathway (Carman & Springer, 2004). Disruption of these projections was highly correlated with inhibition of transmigration. Again, blocking Rho-kinase (by Y27632) or Rho (by C3) did not prevent cup formation downstream from ICAM-1 engagement. The structure contained high ICAM-1 and VCAM-1 and was enriched for vertical microvilli-like structures. Leukocyte integrins were redistributed into linear tracks oriented in parallel to the direction of diapedesis. Carman and co-workers proposed that docking structures may promote diapedesis by providing additional membrane surface to provide directional guidance to leukocytes for transmigration, and hence, proposed the term "transmigratory cups." (Carman & Springer, 2004, 2008). Alternatively, the group of Kubes demonstrated in vivo that during neutrophil TEM, docking structures develop into domelike structures, which completely encapsulate the neutrophil (Kaur et al., 2014; Phillipson, Kaur, Colarusso, Ballantyne, & Kubes, 2008). They additionally showed that when dome formation was inhibited by silencing the expression of the F-actin-binding protein Lsp1, vascular leakage during neutrophil diapedesis was increased (Kaur et al., 2014). They therefore proposed that endothelial domes may function to seal off the transmigrating leukocyte in order to minimize vascular leakage during extravasation. It is interesting to note that several molecular players in the formation of endothelial cup structures, such as Rac1, cortactin, and filamin, were also reported to be important for maintaining endothelial monolayer integrity (Romero et al., 2002; Singleton, Dudek, Chiang, & Garcia, 2005; Jos Van Rijssel et al., 2013). It is therefore possible that activation or recruitment of these molecules during leukocyte TEM may have a dual purpose by promoting diapedesis, and at the same time maintaining endothelial barrier integrity, although proof for this hypothesis is currently lacking. The formation of the endothelial cup-like structure shows several similarities with the formation of the so-called phagocytic cup. Also, the role of the Rho-GTPase RhoG in the phagocytosis

of apoptotic cells (deBakker et al., 2004) and its specific exchange factor SH3- containing GEF (SGEF) in micropinocytosis (Ellerbroek et al., 2004) show similar functions in both processes. This was the rationale to examine if RhoG and SGEF may contribute to the formation of endothelial cups and participate in TEM. Our group showed that ICAM-1 binds SGEF through its intracellular tail (Jaap D. Van Buul et al., 2007). Subsequently, this results in Src-dependent activation of RhoG, leading to the formation of apical cup assembly. Specifically, SGEF binds to ICAM-1 via its SH3 domain and silencing of endothelial SGEF or RhoG decreased cup formation and inhibited leukocyte TEM, but did not affect leukocyte adhesion. Recently, Schnoor and co-workers showed that ICAM-1-induced activation of RhoG required cortactin (Schnoor et al., 2011). Interestingly, the ICAM-1/SGEF interaction was independent of ICAM-1 clustering. However, using nucleotide-free GST mutants of RhoG to measure GEF activity (García-Mata et al., 2006), we found that ICAM-1 clustering did activate SGEF (JDvB, data not shown). Using a SGEF-deficient mouse line, Samson and colleagues showed that SGEF deficiency resulted in reduced on-set of atherosclerosis, most likely by the inability of the vasculature to form proper cup-like structures and prevent leukocyte TEM (Samson et al., 2013). These data suggest that the RhoG/SGEF signaling axis is one of the central mediators of cup-structure formation. The work by Carman and colleagues suggested a role for the small GTPase Rac1 downstream from leukocyte adhesion. When measuring Rac1 activation downstream from ICAM-1 clustering, in parallel with RhoG activation, it became clear that Rac1 activity preceded RhoG activation (J. van Rijssel et al., 2012). This indicated that, next to SGEF, which activates RhoG, another GEF is activated downstream from ICAM-1 clustering. Our initial data showed that ICAM-1, when clustered, interacted with the actinadaptor protein filamin (Kanters et al., 2008). Interestingly, the exchange factor Trio was shown to recruit filamin (Bellanger et al., 2000). Also, deBakker and colleagues showed that Trio activates RhoG to allow phagocytosis of apoptotic cells (deBakker et al., 2004). Moreover, next to RhoG, this GEF was also able to activate Rac1 and RhoA (J. D. van Buul & Hordijk, 2004), two GTPases known to be involved in downstream ICAM-1 signaling (Adamson, Etienne, Couraud, Calder, & Greenwood, 1999; Etienne et al., 1998; Thompson et al., 2002; J. van Rijssel et al., 2012). Additional data from our laboratory showed that depletion of Rac1 or RhoG reduced TEM of primary neutrophils (J. van Rijssel et al., 2012). Rac1 depletion showed defects in actual ICAM-1 clustering, and RhoG depletion impaired the induction of cup structures (J. van Rijssel et al., 2012). These data implicate that Rac1 and RhoG have separate functions to induce endothelial cup structures upon leukocyte binding (Fig. 2). Additionally, Trio binds to the intracellular tail of ICAM-1

2

via regions located in the N-terminal GEF domain. Surprisingly, the binding of Trio to ICAM-1 is independent of filamin. However, reduced filamin expression in endothelial cells did prevent ICAM-1-induced Rac1 and RhoG activation (J. van Rijssel et al., 2012). Moreover, also ICAM-1-induced Trio activation, measured through its binding to the nucleotide-free GTPase mutants (Rac1-G15A/RhoGG15A), was impaired in filamin-deficient cells. So, although filamin did not regulate the binding of Trio to ICAM-1, it did control downstream GTPase activity, probably through other signaling molecules such as Src-family kinases (Stossel et al., 2001). One of the drawbacks of the above-described study is the use of artificial anti-ICAM-1 antibody-coated beads to cluster ICAM-1. It is therefore good to note that the kinetics of ICAM-1 clustering in these experiments may differ from ICAM-1 signaling during leukocyte diapedesis. In fact, from the timepoint of firm adhesion, neutrophils take approximately 100 s to cross the endothelium (Woodfin et al., 2011). Thus, the real-time temporal and also spatial activation of Rac1 and RhoG during neutrophil TEM remains an open question. As mentioned above, the different steps in the formation of endothelial cup-like structures are reminiscent of the process

Figure 2. The cup-like structure. Signaling routes that are initiated by clustering of ICAM-1 and result in the remodeling of the actin cytoskeleton and the formation of cup-like structures. Signaling includes the activation of the small GTPases Rac1 and RhoG downstream from ICAM-1 clustering and involvement of at least two GEFs, Trio and SGEF. Additionally, Rac1 activation may result in a positive feedback loop, increasing the clustering of ICAM-1.

of phagocytic cup formation by phagocytic cells (Swanson, 2008). Formation of a phagocytic cup is initiated by a local coalescence of F-actin in a ring-like structure, followed by membrane protrusion around the opsonized cell or particle (Rougerie, Miskolci, & Cox, 2013). Finally, actomyosin contractility forces ingestion and membrane fusion completes the process (Bellanger et al., 2000; García-Mata et al., 2006). Although we never observed complete closure and fusion of membrane protrusions during docking structure formation in vitro, others have reported in vivo docking structures advancing into dome-like structures, completely covering the transmigrating leukocyte (Phillipson et al., 2008). Interestingly, similar molecular players, including the GTPases RhoG, Rac1/2, Ccd42, RhoA and GEFs Trio, and SGEF were reported to regulate phagocytosis or related processes such as macropinocytosis, suggesting that cells use analogous signaling pathways (deBakker et al., 2004; Ellerbroek et al., 2004; Sayedyahossein & Dagnino, 2013). Using FRET-based biosensors for Rac1, Rac2, and Cdc42, these GTPases were shown to have different spatial activation patterns within the phagocytic cup (Hoppe & Swanson, 2004). It is therefore tempting to speculate that also within a docking structure RhoG, Rac1, and RhoA are distinctly spatially activated, with RhoA activation at the base of the cup, followed by Rac1 at the base and leading edge of the cup, and RhoG within the membrane protrusions. Previous work to delineate the role of GTPase signaling in leukocyte TEM was primarily based on inhibitor studies, knockdown studies, or biochemical assays such as classical GTPase pull-down or pull-down assays using nucleotide-free GTPase mutants. To date, genetically encoded FRET-based biosensors of Rho-GTPases would be the best tool to delineate the fast and local kinetics of Rho-GTPase activation in endothelial cells during leukocyte TEM (Welch, Elliott, Danuser, & Hahn, 2011). Overall, it is evident that endothelial signaling is essential to initiate the final step of the TEM process: transmigration.

Step 5: Transmigration

To breech the endothelial barrier, leukocytes can take two different routes: (1) paracellular, i.e., through the endothelial cell–cell junctions or (2) transcellular, i.e., through the endothelial cell body (Fig. 1, step 5) (Carman & Springer, 2008; Carman, 2009; Sage & Carman, 2009). However, what signal determines to finally transmigrate across the endothelium and by which pathway? First, shear stress has been suggested to be an important initiator of diapedesis (G Cinamon, Shinder, et al., 2001). Although shear clearly plays an important role in TEM and triggers

diapedesis, robust diapedesis is also observed in the absence of shear. For more information on the role of shear stress on TEM, the reader is referred to reviews, listed here (Alcaide et al., 2009; G Cinamon, Grabovsky, et al., 2001; Stroka & Aranda-Espinoza, 2010). Second, central-to-peripheral expression gradients of adhesion molecules, such as PECAM-1, CD99, and JAMs, have been proposed to direct leukocytes to those sides to provide the required traction to drive diapedesis at these locations (Jim Middleton et al., 2002; C. Weber, Fraemohs, & Dejana, 2007; K. S. Weber, von Hundelshausen, Clark-Lewis, Weber, & Weber, 1999). In addition, chemokines presented at the luminal surface of the endothelium may also drive diapedesis through cell–cell junctions by using similar gradients as the adhesion molecules. For instance, IL-8 and RANTES have been shown to be distributed apically on endothelial microvilli in vivo (James Middleton et al., 1997; Jim Middleton et al., 2002; Whittall et al., 2013). Recently, it has been shown that perivascular macrophages, lining pericytes that cover blood vessels, locally secrete chemokines that cause local "hotspots" for neutrophil diapedesis in vivo (Abtin et al., 2013). Third, the spatial and temporal recruitment of adhesion molecules upon leukocyte binding, followed by their interactions with cytoskeletal components, induce signals in the endothelium, resulting in actin-rich structures that embrace adherent leukocyte, i.e., cup-like structures (step 4), and may provide directional guidance to leukocytes for diapedesis (Carman & Springer, 2008). The dynamic distribution of endothelial and leukocytic adhesion molecules with the actin cytoskeleton during TEM was first studied by Martin Sandig and co-workers (Sandig, Negrou, & Rogers, 1997). They identified a circular structure in endothelial cell–cell contact regions that facilitates leukocyte diapedesis. Additionally, they noticed that leukocytes induced LFA-1-containing pseudopodia that penetrated in between endothelial cells. At sites of diapedesis, high levels of LFA-1 and F-actin were found, suggesting a major role for these molecules in TEM. This work was supported by work from the Luscinskas lab (Shaw et al., 2004). They showed that upon transmigration, LFA-1 was rapidly redistributed in a ring-like structure together with ICAM-1. The redistribution and co-clustering of ICAM-1 and LFA-1 was also demonstrated by the group of Carman (Carman et al., 2007, 2003). In fact, they showed that invasive podosomes from leukocytes initiate transcellular migration, i.e., through the endothelial cell body. Sandig and co-workers furthermore showed that endothelial adherence junction proteins were locally redistributed at sites of leukocyte diapedesis, but the VE-cadherin complex, judged by VE-cadherin and α-catenin co-localization, remained intact during diapedesis (Sandig et al., 1997). Our previous work underscored that junctional proteins like VE-cadherin are locally dispersed upon passage

of leukocytes (Jaap D van Buul et al., 2002). Additionally, Su and co-workers demonstrated differential movement of VE-cadherin and PECAM-1 upon leukocyte passage. Whereas these authors underscored the local redistribution of VE-cadherin, they additionally showed that PECAM-1 forms a ring-like structure upon diapedesis (Su, Chen, & Jen, 2002). These data show that, next to endothelial cell adhesion molecules, junctional proteins can be differently regulated during the final TEM step, and therefore, may be involved in the final decision when and where leukocytes cross.

Forces during TEM

Remarkable little vascular leakage occurs when leukocytes cross the endothelium through the cell–cell junctions (He, 2010; Dietmar Vestweber, 2012b). However, under certain patho-physiological conditions such as chronic inflammation, leakage is increased (Chavez, Smith, & Mehta, 2011). To be able to interfere with this effect, it is important to understand how junctions are restored after leukocyte passage. Recently, Martinelli and
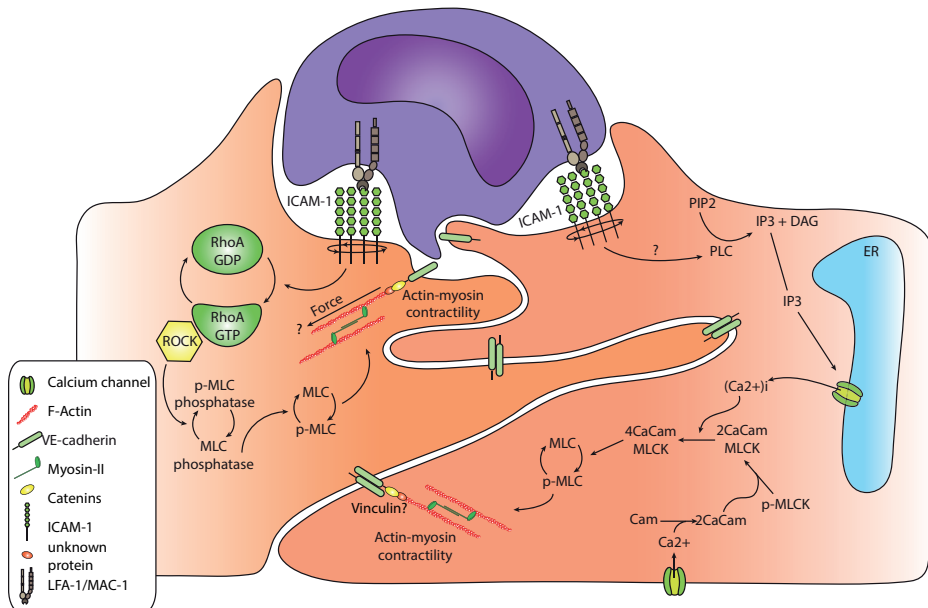
Figure 3. Leukocyte adhesion-induced endothelial tension. Leukocyte adhesion results in the induction of actin-myosin contractility, as depicted in the figure, through the Rho-ROCK pathway or calcium signaling, resulting in MLC phosphorylation. This may finally result in the opening of cell–cell junctions, and thus, be involved in facilitating leukocyte TEM.

co-workers provide a mechanism by which endothelial cells maintain their barrier function during leukocyte transendothelial migration (Martinelli et al., 2013). In response to μm-scale disruptions induced by transmigrating leukocytes, endothelial cells generate unique ventral lamellipodia that close these small gaps in the endothelium. These ventral lamellipodia were enriched in Rac1 effectors cortactin, IQGAP, and p47phox. They propose that barrier disruptions are detected as local release of isometric tension and unloading of force, which is directly coupled to ROS-dependent self-restorative membrane protrusions (Martinelli et al., 2013). Closing the gap after leukocyte passage is one thing, opening the junctions to allow crossing is another. Although several papers have described the importance of ICAM-1-induced phosphorylation of VE-cadherin, possibly through Src-like kinases, leading to the opening of VE-cadherin-mediatedcell–cell junctions, and thereby, facilitating TEM (reviewed in refs. (A Aghajanian, Wittchen, Allingham, Garrett, & Burridge, 2008; D Vestweber, 2007; Dietmar Vestweber et al., 2009; Wittchen, 2009)), we focused in this section on the potential role of endothelial tension in the final step of TEM. Hixenbaugh and colleagues showed that fMLP-stimulated neutrophils induced phosphorylation of endothelial myosin light chain (MLC) on T18/S19 that was mediated by the calcium/calmodulin-regulated enzyme MLC-kinase (Hixenbaugh et al., 1997). In turn, MLCkinase facilitated the interaction of myosin with the actin cytoskeleton, leading to the actomyosin–contractile responses and increased tension in endothelial cells. They proposed that increased endothelial contraction and generation of isometric tension may function as a mechanism by which endothelial cells open their intercellular junctions, thereby facilitating leukocyte TEM (Fig. 3). Adherent neutrophils measured under static conditions induce cytoskeletal rearrangements in the form of stress fibers and increase pMLC after 30 min (H Saito et al., 1998). Inhibition of the calcium–calmodulin-regulated enzyme MLC-kinase (by KT-5926 or ML-9) or treatment with the calmodulin antagonist Trifluoperazine reduced PMN transendothelial migration toward a leukotriene B4 chemotactic gradient, indicating that the cytoskeletal rearrangements were depending on calcium signaling. When endothelial cells were treated with calyculin, a myosin-phosphatase inhibitor, increasing MLC phosphorylation, this resulted in increased endothelial cell contraction, paracellular gap formation, and enhanced neutrophil TEM (Garcia, Verin, Herenyiova, & English, 1998). In addition, inhibition of the endothelial Rho/ROCK pathway, using C3 or Y-27632, significantly reduced actin polymerization, myosin II filament formation, MLC phosphorylation, and neutrophil TEM, suggesting that Rho/ROCK regulate TEM through the control of MLC activity (Hajime Saito, Minamiya, Saito, & Ogawa, 2002). However, one should take in account that these

assays were all done under static conditions. Also, the initial trigger to induce MLC phosphorylation downstream from leukocyte adhesion is not known. Recently, the group of Chen showed that monocytes induced traction force onto the endothelial cells (Liu, Sniadecki, & Chen, 2010). Interestingly, the forces were measured in the endothelial cell to which a single monocyte was adhering to. Moreover, the direction of these forces aligned centripetally to the migrating monocytes. The increased endothelial traction force was measured in the sub-cellular zone of monocytes adhesion. Thus, the above-discussed results suggest that leukocytes can directly induce signals into a single endothelial cell that in turn induce actin-mediated forces. In fact, Liu and colleagues used beads that were coated with anti-ICAM-1 and anti-VCAM-1 antibodies. Using these beads they noticed similar traction forces, indicating that these signals are indeed submitted through ICAM-1 and VCAM-1 and induced by clustering. Potentially, this process can be involved in opening endothelial cell–cell junctions, and thus, in facilitating leukocyte TEM.

Conclusion

From the above-discussed data, it is clear that endothelial Rho-GTPases play an essential role in the process of transendothelial migration by remodeling the actin cytoskeleton. In particular in step 2 to 5, Rho-GTPase signaling is critical to remodel the actin cytoskeleton to induce membrane protrusions, i.e., cup-like structures and support leukocyte-induced tension force in order to open or close the cell–cell junctions or gaps through which leukocytes have crossed. Future challenges remain to investigate the spatial and temporal activation of the Rho-GTPases during the different steps of TEM, and which GEFs are locally activating these GTPases.

References

Abtin, A., Jain, R., Mitchell, A. J., Roediger, B., Brzoska, A. J., Tikoo, S., … Weninger, W. (2013). Perivascular macrophages mediate neutrophil recruitment during bacterial skin infection. *Nature Immunology*, *15*(1), 45–53. http://doi.org/10.1038/ni.2769

Adamson, P., Etienne, S., Couraud, P. O., Calder, V., & Greenwood, J. (1999). Lymphocyte migration through brain endothelial cell monolayers involves signaling through endothelial ICAM-1 via a rho-dependent pathway. *Journal of Immunology (Baltimore, Md. : 1950)*, *162*(5), 2964–73. Retrieved from http://www.ncbi.nlm.nih.gov/pubmed/10072547

Aghajanian, A., Wittchen, E. S., Allingham, M. J., Garrett, T. A., & Burridge, K. (2008). Endothelial cell junctions and the regulation of vascular permeability and leukocyte transmigration. *Journal of Thrombosis and Haemostasis : JTH*, *6*(9), 1453–60. http://doi.org/10.1111/j.1538-7836.2008.03087.x

Aghajanian, A., Wittchen, E. S., Campbell, S. L., & Burridge, K. (2009). Direct activation of RhoA by reactive oxygen species requires a redox-sensitive motif. *PloS One*, *4*(11), e8045. http://doi.org/10.1371/journal.pone.0008045

Alcaide, P., Auerbach, S., & Luscinskas, F. W. (2009). Neutrophil recruitment under shear flow: it's all about endothelial cell rings and gaps. *Microcirculation (New York, N.Y. : 1994)*, *16*(1), 43–57. http://doi.org/10.1080/10739680802273892

Amerongen, G. P. v. N., Delft, S. v., Vermeer, M. A., Collard, J. G., & van Hinsbergh, V. W. M. (2000). Activation of RhoA by Thrombin in Endothelial Hyperpermeability : Role of Rho Kinase and Protein Tyrosine Kinases. *Circulation Research*, *87*(4), 335–340. http://doi.org/10.1161/01.RES.87.4.335

Barreiro, O., Vicente-Manzanares, M., Urzainqui, A., Yáñez-Mó, M., & Sánchez-Madrid, F. (2004). Interactive protrusive structures during leukocyte adhesion and transendothelial migration. *Frontiers in Bioscience : A Journal and Virtual Library*, *9*, 1849–63. Retrieved from http://www.ncbi.nlm.nih.gov/pubmed/14977592

Barreiro, O., Yáñez-Mó, M., Serrador, J. M., Montoya, M. C., Vicente-Manzanares, M., Tejedor, R., … Sánchez-Madrid, F. (2002). Dynamic interaction of VCAM-1 and ICAM-1 with moesin and ezrin in a novel endothelial docking structure for adherent leukocytes. *Journal of Cell Biology*, *157*, 1233–1245. http://doi.org/10.1083/jcb.200112126

Barreiro, O., Zamai, M., Yáñez-Mó, M., Tejera, E., López-Romero, P., Monk, P. N., … Sánchez-Madrid, F. (2008). Endothelial adhesion receptors are recruited to adherent leukocytes by inclusion in preformed tetraspanin nanoplatforms. *Journal of Cell Biology*, *183*(3), 527–542. http://doi.org/10.1083/jcb.200805076

Bellanger, J. M., Astier, C., Sardet, C., Ohta, Y., Stossel, T. P., & Debant, A. (2000). The Rac1- and RhoG-specific GEF domain of Trio targets filamin to remodel cytoskeletal actin. *Nature Cell Biology*, *2*(12), 888–92. http://doi.org/10.1038/35046533

Bevilacqua, M. P., Pober, J. S., Mendrick, D. L., Cotran, R. S., & Gimbrone, M. A. (1987). Identification of an inducible endothelial-leukocyte adhesion molecule. *Proceedings of the National Academy of Sciences of the United States of America*, *84*(24), 9238–42. Retrieved from http://www.ncbi.nlm.nih.gov/pubmed/2827173

Bonfanti, R., Furie, B. C., Furie, B., & Wagner, D. D. (1989). PADGEM (GMP140) is a component of Weibel-Palade bodies of human endothelial cells. *Blood*, *73*(5), 1109–12. Retrieved from http://www.ncbi.nlm.nih.gov/pubmed/2467701

Bretscher, A., Edwards, K., & Fehon, R. G. (2002). ERM proteins and merlin: integrators at the cell cortex. *Nature Reviews. Molecular Cell Biology*, *3*(8), 586–99. http://doi.org/10.1038/nrm882

Butcher, E. C. (1991). Leukocyte-endothelial cell recognition: three (or more) steps to specificity and diversity. *Cell*, *67*, 1033–6. http://doi.org/10.1016/0092-8674(91)90279-8

Carman, C. V., & Springer, T. a. (2004). A transmigratory cup in leukocyte diapedesis both through individual vascular endothelial cells and between them. *Journal of Cell Biology*, *167*(2), 377–388. http://doi.org/10.1083/jcb.200404129

Carman, C. V. (2009). Mechanisms for transcellular diapedesis: probing and pathfinding by "invadosome-like protrusions". *Journal of Cell Science*, *122*, 3025–3035. http://doi.org/10.1242/jcs.047522

Carman, C. V, Jun, C.-D., Salas, A., & Springer, T. a. (2003). Endothelial cells proactively form microvilli-like membrane projections upon intercellular adhesion molecule 1 engagement of leukocyte LFA-1. *Journal of Immunology (Baltimore, Md. : 1950)*, *171*, 6135–6144. http://doi.org/10.4049/jimmunol.171.11.6135

Carman, C. V, Sage, P. T., Sciuto, T. E., de la Fuente, M. A., Geha, R. S., Ochs, H. D., …

Springer, T. A. (2007). Transcellular diapedesis is initiated by invasive podosomes. *Immunity*, *26*(6), 784–97. http://doi.org/10.1016/j.immuni.2007.04.015

Carman, C. V, & Springer, T. A. (2008). Trans-cellular migration: cell-cell contacts get intimate. *Current Opinion in Cell Biology*, *20*(5), 533–40. http://doi.org/10.1016/j.ceb.2008.05.007

Celli, L., Ryckewaert, J.-J., Delachanal, E., & Duperray, A. (2006). Evidence of a Functional Role for Interaction between ICAM-1 and Nonmuscle -Actinins in Leukocyte Diapedesis. *The Journal of Immunology*, *177*(6), 4113–4121. http://doi.org/10.4049/jimmunol.177.6.4113

Cernuda-Morollón, E., & Ridley, A. J. (2006). Rho GTPases and leukocyte adhesion receptor expression and function in endothelial cells. *Circulation Research*, *98*(6), 757–67. http://doi.org/10.1161/01.RES.0000210579.35304.d3

Chavez, A., Smith, M., & Mehta, D. (2011). Chapter six – New Insights into the Regulation of Vascular Permeability. In *International Review of Cell and Molecular Biology* (Vol. 290, pp. 205–248). http://doi.org/10.1016/B978-0-12-386037-8.00001-6

Cinamon, G., Grabovsky, V., Winter, E., Franitza, S., Feigelson, S., Shamri, R., … Alon, R. (2001). Novel chemokine functions in lymphocyte migration through vascular endothelium under shear flow. *Journal of Leukocyte Biology*, *69*(6), 860–6. Retrieved from http://www.ncbi.nlm.nih.gov/pubmed/11404368

Cinamon, G., Shinder, V., & Alon, R. (2001). Shear forces promote lymphocyte migration across vascular endothelium bearing apical chemokines. *Nature Immunology*, *2*(6), 515–22. http://doi.org/10.1038/88710

Cinamon, G., Shinder, V., Shamri, R., & Alon, R. (2004). Chemoattractant signals and beta 2 integrin occupancy at apical endothelial contacts combine with shear stress signals to promote transendothelial neutrophil migration. *Journal of Immunology (Baltimore, Md. : 1950)*, *173*(12), 7282–91. Retrieved from http://www.ncbi.nlm.nih.gov/pubmed/15585851

Cook-Mills, J. M., Johnson, J. D., Deem, T. L., Ochi, A., Wang, L., & Zheng, Y. (2004). Calcium mobilization and Rac1 activation are required for VCAM-1 (vascular cell adhesion molecule-1) stimulation of NADPH oxidase activity. *The Biochemical Journal*, *378*(Pt 2), 539–47. http://doi.org/10.1042/BJ20030794

deBakker, C. D., Haney, L. B., Kinchen, J. M., Grimsley, C., Lu, M., Klingele, D., … Xue, D. (2004). Phagocytosis of Apoptotic Cells Is Regulated by a UNC-73/TRIO-MIG-2/RhoG Signaling Module and Armadillo Repeats of CED-12/ELMO. *Current Biology*, *14*(24), 2208–2216. http://doi.org/10.1016/j.cub.2004.12.029

Deem, T. L., Abdala-Valencia, H., & Cook-Mills, J. M. (2007). VCAM-1 activation of endothelial cell protein tyrosine phosphatase 1B. *Journal of Immunology (Baltimore, Md. : 1950)*, *178*(6), 3865–73. Retrieved from http://www.ncbi.nlm.nih.gov/pubmed/17339486

Deem, T. L., & Cook-Mills, J. M. (2004). Vascular cell adhesion molecule 1 (VCAM-1) activation of endothelial cell matrix metalloproteinases: role of reactive oxygen species. *Blood*, *104*(8), 2385–93. http://doi.org/10.1182/blood-2004-02-0665

Doyle, E. L., Ridger, V., Ferraro, F., Turmaine, M., Saftig, P., & Cutler, D. F. (2011). CD63 is an essential cofactor to leukocyte recruitment by endothelial P-selectin. *Blood*, *118*(15), 4265–73. http://doi.org/10.1182/blood-2010-11-321489

Ellerbroek, S. M., Wennerberg, K., Arthur, W. T., Dunty, J. M., Bowman, D. R., DeMali, K. A., … Burridge, K. (2004). SGEF, a RhoG guanine nucleotide exchange factor that stimulates macropinocytosis. *Molecular Biology of the Cell*, *15*(7), 3309–19. http://doi.org/10.1091/mbc.E04-02-0146

Etienne, S., Adamson, P., Greenwood, J., Strosberg, A. D., Cazaubon, S., & Couraud, P. O. (1998). ICAM-1 signaling pathways associated with Rho activation in microvascular brain endothelial cells. *Journal of Immunology (Baltimore, Md. : 1950)*, *161*(10), 5755–61. Retrieved from http://www.ncbi.nlm.nih.gov/pubmed/9820557

Etienne-Manneville, S., Manneville, J.-B., Adamson, P., Wilbourn, B., Greenwood, J., & Couraud, P.-O. (2000). ICAM-1-Coupled Cytoskeletal Rearrangements and Transendothelial Lymphocyte Migration Involve Intracellular Calcium Signaling in Brain Endothelial Cell Lines. *The Journal of Immunology*, *165*(6), 3375–3383. http://doi.org/10.4049/jimmunol.165.6.3375

Garcia, J. G., Verin, A. D., Herenyiova, M., & English, D. (1998). Adherent neutrophils activate endothelial myosin light chain kinase: role in transendothelial migration. *Journal of Applied Physiology (Bethesda, Md. : 1985)*, *84*(5), 1817–21. Retrieved from http://www.ncbi.nlm.nih.gov/pubmed/9572834

García-Mata, R., Wennerberg, K., Arthur, W. T., Noren, N. K., Ellerbroek, S. M., & Burridge, K. (2006). Analysis of Activated GAPs and GEFs in Cell Lysates. *Methods in Enzymology*,

406, 425–437. http://doi.org/10.1016/S0076-6879(06)06031-9

Greenwood, J., Amos, C. L., Walters, C. E., Couraud, P.-O., Lyck, R., Engelhardt, B., & Adamson, P. (2003). Intracellular domain of brain endothelial intercellular adhesion molecule-1 is essential for T lymphocyte-mediated signaling and migration. *Journal of Immunology (Baltimore, Md. : 1950)*, *171*(4), 2099–2108.

He, P. (2010). Leucocyte/endothelium interactions and microvessel permeability: coupled or uncoupled? *Cardiovascular Research*, *87*(2), 281–90. http://doi.org/10.1093/cvr/cvq140

Hixenbaugh, E. A., Goeckeler, Z. M., Papaiya, N. N., Wysolmerski, R. B., Silverstein, S. C., & Huang, A. J. (1997). Stimulated neutrophils induce myosin light chain phosphorylation and isometric tension in endothelial cells. *Am J Physiol Heart Circ Physiol*, *273*(2), H981–988. Retrieved from http://ajpheart.physiology.org/content/273/2/H981

Hoppe, A. D., & Swanson, J. A. (2004). Cdc42, Rac1, and Rac2 display distinct patterns of activation during phagocytosis. *Molecular Biology of the Cell*, *15*(8), 3509–19. http://doi.org/10.1091/mbc.E03-11-0847

Hu, Y., Kiely, J. M., Szente, B. E., Rosenzweig, A., & Gimbrone, M. A. (2000). E-selectin-dependent signaling via the mitogen-activated protein kinase pathway in vascular endothelial cells. *Journal of Immunology (Baltimore, Md. : 1950)*, *165*(4), 2142–8. Retrieved from http://www.ncbi.nlm.nih.gov/pubmed/10925300

Hu, Y., Szente, B., Kiely, J.-M., & Gimbrone, M. A. (2001). Molecular Events in Transmembrane Signaling via E-selectin. *Journal of Biological Chemistry*, *276*(51), 48549–48553.

Huang, a J., Manning, J. E., Bandak, T. M., Ratau, M. C., Hanser, K. R., & Silverstein, S. C. (1993). Endothelial cell cytosolic free calcium regulatesneutrophil migration across monolayers of endothelial cells. *J.Cell Biol.*, *120*(6), 1371–1380.

Kanters, E., Van Rijssel, J., Hensbergen, P. J., Hondius, D., Mul, F. P. J., Deelder, A. M., … Hordijk, P. L. (2008). Filamin B mediates ICAM-1-driven leukocyte transendothelial migration. *Journal of Biological Chemistry*, *283*(46), 31830–31839. http://doi.org/10.1074/jbc.M804888200

Kaplanski, G., Farnarier, C., Benoliel, a M., Foa, C., Kaplanski, S., & Bongrand, P. (1994). A novel role for E- and P-selectins: shape control of endothelial cell monolayers. *Journal of Cell Science*, *107 (Pt 9*, 2449–57. Retrieved from http://www.ncbi.nlm.nih.gov/pubmed/7531200

Kaur, J., Long, E. M., Li, H., Parsons, S. A., Butz, S., Phillipson, M., … Kubes, P. (2014). Endothelial LSP1 is involved in endothelial dome formation , minimizing vascular permeability changes during neutrophil transmigration in vivo, *117*(3), 942–953. http://doi.org/10.1182/blood-2010-02-270561.The

Kiely, J.-M., Hu, Y., Garcia-Cardena, G., & Gimbrone, M. A. (2003). Lipid Raft Localization of Cell Surface E-Selectin Is Required for Ligation-Induced Activation of Phospholipase C. *The Journal of Immunology*, *171*(6), 3216–3224. http://doi.org/10.4049/jimmunol.171.6.3216

Kirkbride, K. C., Sung, B. H., Sinha, S., & Weaver, A. M. (n.d.). Cortactin: a multifunctional regulator of cellular invasiveness. *Cell Adhesion & Migration*, *5*(2), 187–98. Retrieved from http://www.ncbi.nlm.nih.gov/pubmed/21258212

Liu, Z., Sniadecki, N. J., & Chen, C. S. (2010). Mechanical Forces in Endothelial Cells during Firm Adhesion and Early Transmigration of Human Monocytes. *Cellular and Molecular Bioengineering*, *3*(1), 50–59. http://doi.org/10.1007/s12195-010-0105-3

Lorenzon, P., Vecile, E., Nardon, E., Ferrero, E., Harlan, J. M., Tedesco, F., & Dobrina, A. (1998). Endothelial cell E- and P-selectin and vascular cell adhesion molecule-1 function as signaling receptors. *The Journal of Cell Biology*, *142*(5), 1381–91. Retrieved from http://www.ncbi.nlm.nih.gov/pubmed/9732297

Lyck, R., Reiss, Y., Gerwin, N., Greenwood, J., Adamson, P., & Engelhardt, B. (2003). T-cell interaction with ICAM-1/ICAM-2 double-deficient brain endothelium in vitro: The cytoplasmic tail of endothelial ICAM-1 is necessary for transendothelial migration of T cells. *Blood*, *102*(10), 3675–3683. http://doi.org/10.1182/blood-2003-02-0358

Martinelli, R., Kamei, M., Sage, P. T., Massol, R., Varghese, L., Sciuto, T., … Carman, C. V. (2013). Release of cellular tension signals self-restorative ventral lamellipodia to heal barrier micro-wounds. *The Journal of Cell Biology*, *201*(3), 449–65. http://doi.org/10.1083/jcb.201209077

McEver, R. P. (2002). Selectins: lectins that initiate cell adhesion under flow. *Current Opinion in Cell Biology*, *14*(5), 581–586. http://doi.org/10.1016/S0955-0674(02)00367-8

McEver, R. P., Beckstead, J. H., Moore, K. L., Marshall-Carlson, L., & Bainton, D. F. (1989). GMP-140, a platelet alpha-granule membrane protein, is also synthesized by vascular endothelial cells and is localized in Weibel-Palade bodies. *The Journal of Clinical*

2

Investigation, *84*(1), 92–9. http://doi.org/10.1172/JCI114175

Middleton, J., Neil, S., Wintle, J., Clark-Lewis, I., Moore, H., Lam, C., … Rot, A. (1997). Transcytosis and Surface Presentation of IL-8 by Venular Endothelial Cells. *Cell*, *91*(3), 385–395. http://doi.org/10.1016/S0092-8674(00)80422-5

Middleton, J., Patterson, A. M., Gardner, L., Schmutz, C., Ashton, B. A., Rot, A., … Yoshie, O. (2002). Leukocyte extravasation: chemokine transport and presentation by the endothelium. *Blood*, *100*(12), 3853–60. http://doi.org/10.1182/blood.V100.12.3853

Muller, W. A. (2009). Mechanisms of transendothelial migration of leukocytes. *Circulation Research*. http://doi.org/10.1161/CIRCRESAHA.109.200717

Oh, H.-M., Lee, S., Na, B.-R., Wee, H., Kim, S.-H., Choi, S.-C., … Jun, C.-D. (2007). RKIKK motif in the intracellular domain is critical for spatial and dynamic organization of ICAM-1: functional implication for the leukocyte adhesion and transmigration. *Molecular Biology of the Cell*, *18*(6), 2322–35. http://doi.org/10.1091/mbc.E06-08-0744

Phillipson, M., Kaur, J., Colarusso, P., Ballantyne, C. M., & Kubes, P. (2008). Endothelial domes encapsulate adherent neutrophils and minimize increases in vascular permeability in paracellular and transcellular emigration. *PLoS ONE*, *3*(2), e1649. http://doi.org/10.1371/journal.pone.0001649

Romero, I. a., Amos, C. L., Greenwood, J., & Adamson, P. (2002). Ezrin and moesin co-localise with ICAM-1 in brain endothelial cells but are not directly associated. *Molecular Brain Research*, *105*, 47–59. http://doi.org/10.1016/S0169-328X(02)00392-3

Rougerie, P., Miskolci, V., & Cox, D. (2013). Generation of membrane structures during phagocytosis and chemotaxis of macrophages: role and regulation of the actin cytoskeleton. *Immunological Reviews*, *256*(1), 222–239. http://doi.org/10.1111/imr.12118

Sage, P. T., & Carman, C. V. (2009). Settings and mechanisms for trans-cellular diapedesis. *Frontiers in Bioscience (Landmark Edition)*, *14*, 5066–83. Retrieved from http://www.ncbi.nlm.nih.gov/pubmed/19482605

Saito, H., Minamiya, Y., Kitamura, M., Saito, S., Enomoto, K., Terada, K., & Ogawa, J. (1998). Endothelial myosin light chain kinase regulates neutrophil migration across human umbilical vein endothelial cell monolayer. *Journal of Immunology (Baltimore, Md. : 1950)*, *161*(3), 1533–40. Retrieved from http://www.ncbi.nlm.nih.gov/pubmed/9686621

Saito, H., Minamiya, Y., Saito, S., & Ogawa, J. (2002). Endothelial Rho and Rho kinase regulate neutrophil migration via endothelial myosin light chain phosphorylation. *Journal of Leukocyte Biology*, *72*(4), 829–36. Retrieved from http://www.ncbi.nlm.nih.gov/pubmed/12377953

Samson, T., van Buul, J. D., Kroon, J., Welch, C., Bakker, E. N., Matlung, H. L., … Burridge, K. (2013). The Guanine-Nucleotide Exchange Factor SGEF Plays a Crucial Role in the Formation of Atherosclerosis. *PLoS ONE*, *8*(1), e55202. http://doi.org/10.1371/journal.pone.0055202

Sandig, M., Negrou, E., & Rogers, K. A. (1997). Changes in the distribution of LFA-1, catenins, and F-actin during transendothelial migration of monocytes in culture. *Journal of Cell Science*, *110 (Pt 2*, 2807–2818.

Sayedyahossein, S., & Dagnino, L. (2013). Integrins and Small GTPases as Modulators of Phagocytosis (Vol. 302, pp. 321–354). http://doi.org/10.1016/B978-0-12-407699-0.00006-6

Schnoor, M., Lai, F. P. L., Zarbock, A., Kläver, R., Polaschegg, C., Schulte, D., … Vestweber, D. (2011). Cortactin deficiency is associated with reduced neutrophil recruitment but increased vascular permeability in vivo. *The Journal of Experimental Medicine*, *208*(8), 1721–35. http://doi.org/10.1084/jem.20101920

Shaw, S. K., Ma, S., Kim, M. B., Rao, R. M., Hartman, C. U., Froio, R. M., … Luscinskas, F. W. (2004). Coordinated redistribution of leukocyte LFA-1 and endothelial cell ICAM-1 accompany neutrophil transmigration. *The Journal of Experimental Medicine*, *200*(12), 1571–80. http://doi.org/10.1084/jem.20040965

Shulman, Z., Cohen, S. J., Roediger, B., Kalchenko, V., Jain, R., Grabovsky, V., … Alon, R. (2011). Transendothelial migration of lymphocytes mediated by intraendothelial vesicle stores rather than by extracellular chemokine depots. *Nature Immunology*, *13*(1), 67–76. http://doi.org/10.1038/ni.2173

Singleton, P. A., Dudek, S. M., Chiang, E. T., & Garcia, J. G. N. (2005). Regulation of sphingosine 1-phosphate-induced endothelial cytoskeletal rearrangement and barrier enhancement by S1P1 receptor, PI3 kinase, Tiam1/Rac1, and -actinin. *The FASEB Journal*, *19*(12), 1646–1656. http://doi.org/10.1096/fj.05-3928com

Springer, T. A. (1994). Traffic signals for lymphocyte recirculation and leukocyte emigration: the multistep paradigm. *Cell*, *76*(2), 301–14. Retrieved from http://www.ncbi.nlm.nih.

2

gov/pubmed/7507411

Stossel, T. P., Condeelis, J., Cooley, L., Hartwig, J. H., Noegel, A., Schleicher, M., & Shapiro, S. S. (2001). Filamins as integrators of cell mechanics and signalling. *Nature Reviews. Molecular Cell Biology*, *2*(2), 138–45. http://doi.org/10.1038/35052082

Stroka, K. M., & Aranda-Espinoza, H. (2010). A biophysical view of the interplay between mechanical forces and signaling pathways during transendothelial cell migration. *The FEBS Journal*, *277*(5), 1145–58. http://doi.org/10.1111/j.1742-4658.2009.07545.x

Su, W.-H., Chen, H., & Jen, C. J. (2002). Differential movements of VE-cadherin and PECAM-1 during transmigration of polymorphonuclear leukocytes through human umbilical vein endothelium. *Blood*, *100*(10), 3597–603. http://doi.org/10.1182/blood-2002-01-0303

Swanson, J. A. (2008). Shaping cups into phagosomes and macropinosomes. *Nature Reviews Molecular Cell Biology*, *9*(8), 639–649. http://doi.org/10.1038/nrm2447

Thompson, P. W., Randi, A. M., & Ridley, A. J. (2002). Intercellular adhesion molecule (ICAM)-1, but not ICAM-2, activates RhoA and stimulates c-fos and rhoA transcription in endothelial cells. *Journal of Immunology (Baltimore, Md. : 1950)*, *169*, 1007–1013. http://doi.org/10.4049/jimmunol.169.2.1007

Van Buul, J. D., Allingham, M. J., Samson, T., Meller, J., Boulter, E., García-Mata, R., & Burridge, K. (2007). RhoG regulates endothelial apical cup assembly downstream from ICAM1 engagement and is involved in leukocyte trans-endothelial migration. *Journal of Cell Biology*, *178*(7), 1279–1293. http://doi.org/10.1083/jcb.200612053

van Buul, J. D., & Hordijk, P. L. (2004). Signaling in Leukocyte Transendothelial Migration. *Arteriosclerosis, Thrombosis, and Vascular Biology*, *24*(5), 824–833. http://doi.org/10.1161/01.ATV.0000122854.76267.5c

van Buul, J. D., & Hordijk, P. L. (2009). Endothelial adapter proteins in leukocyte transmigration. *Thrombosis and Haemostasis*, *101*(4), 649–55. Retrieved from http://www.ncbi.nlm.nih.gov/pubmed/19350107

van Buul, J. D., van Rijssel, J., van Alphen, F. P. J., Hoogenboezem, M., Tol, S., Hoeben, K. A., … Hordijk, P. L. (2010). Inside-out regulation of ICAM-1 dynamics in TNF-alpha-activated endothelium. *PloS One*, *5*(6), e11336. http://doi.org/10.1371/journal.pone.0011336

van Buul, J. D., van Rijssel, J., van Alphen, F. P. J., van Stalborch, A.-M., Mul, E. P. J., Hordijk, P. L., … Hordijk, P. L. (2010). ICAM-1 clustering on endothelial cells recruits VCAM-1. *Journal of Biomedicine & Biotechnology*, *2010*, 120328. http://doi.org/10.1155/2010/120328

van Buul, J. D., Voermans, C., van den Berg, V., Anthony, E. C., Mul, F. P. J., van Wetering, S., … Hordijk, P. L. (2002). Migration of human hematopoietic progenitor cells across bone marrow endothelium is regulated by vascular endothelial cadherin. *Journal of Immunology (Baltimore, Md. : 1950)*, *168*(2), 588–96. Retrieved from http://www.ncbi.nlm.nih.gov/pubmed/11777950

van Rijssel, J., Kroon, J., Hoogenboezem, M., van Alphen, F. P. J., de Jong, R. J., Kostadinova, E., … van Buul, J. D. (2012). The Rho-guanine nucleotide exchange factor Trio controls leukocyte transendothelial migration by promoting docking structure formation. *Molecular Biology of the Cell*, *23*, 2831–2844. http://doi.org/10.1091/mbc.E11-11-0907

Van Rijssel, J., Timmerman, I., Van Alphen, F. P. J., Hoogenboezem, M., Korchynskyi, O., Geerts, D., … Ostrowski, M. C. (2013). The Rho-GEF Trio regulates a novel pro-inflammatory pathway through the transcription factor Ets2. *Biology Open*, *2*(6), 569–79. http://doi.org/10.1242/bio.20134382

van Wetering, S., van Buul, J. D., Quik, S., Mul, F. P., Anthony, E. C., ten Klooster, J. P., … Hordijk, P. L. (2002). Reactive oxygen species mediate Rac-induced loss of cell-cell adhesion in primary human endothelial cells. *J.Cell Sci.*, *115*(Pt 9), 1837–1846. Retrieved from http://jcs.biologists.org/content/115/9/1837.full.pdf

Vestweber, D. (2007). Molecular mechanisms that control leukocyte extravasation through endothelial cell contacts. *Ernst Schering Foundation Symposium Proceedings*, (3), 151–67. Retrieved from http://www.ncbi.nlm.nih.gov/pubmed/18512285

Vestweber, D. (2012a). Novel insights into leukocyte extravasation. *Current Opinion in Hematology*, *19*(3), 212–217. http://doi.org/10.1097/MOH.0b013e3283523e78

Vestweber, D. (2012b). Relevance of endothelial junctions in leukocyte extravasation and vascular permeability. *Annals of the New York Academy of Sciences*, *1257*, 184–92. http://doi.org/10.1111/j.1749-6632.2012.06558.x

Vestweber, D., Blanks, J. E., ABBASSI, O., KISHIMOTO, T. K., McINTIRE, L. V., ANDERSON, D. C., … OLWIN, B. B. (1999). Mechanisms that regulate the function of the selectins and their ligands. *Physiological Reviews*, *79*(1), 181–213. http://doi.org/10.1172/jci116889

Vestweber, D., Winderlich, M., Cagna, G., Nottebaum, A. F., Ley, K., al., et, … al., et. (2009). Cell adhesion dynamics at endothelial junctions: VE-cadherin as a major player. *Trends*

in Cell Biology, *19*(1), 8–15. http://doi.org/10.1016/j.tcb.2008.10.001

Vockel, M., & Vestweber, D. (2013). How T cells trigger the dissociation of the endothelial receptor phosphatase VE-PTP from VE-cadherin. *Blood*, *122*(14), 2512–22. http://doi.org/10.1182/blood-2013-04-499228

Weber, C., Fraemohs, L., & Dejana, E. (2007). The role of junctional adhesion molecules in vascular inflammation. *Nature Reviews Immunology*, *7*(6), 467–477. http://doi.org/10.1038/nri2096

Weber, K. S., von Hundelshausen, P., Clark-Lewis, I., Weber, P. C., & Weber, C. (1999). Differential immobilization and hierarchical involvement of chemokines in monocyte arrest and transmigration on inflamed endothelium in shear flow. *European Journal of Immunology*, *29*(2), 700–12. http://doi.org/10.1002/(SICI)1521-4141(199902)29:02<700::AID-IMMU700>3.0.CO;2-1

Welch, C. M., Elliott, H., Danuser, G., & Hahn, K. M. (2011). Imaging the coordination of multiple signalling activities in living cells. *Nature Reviews Molecular Cell Biology*, *12*(11), 749–756. http://doi.org/10.1038/nrm3212

Whittall, C., Kehoe, O., King, S., Rot, A., Patterson, A., & Middleton, J. (2013). A chemokine self-presentation mechanism involving formation of endothelial surface microstructures. *Journal of Immunology (Baltimore, Md. : 1950)*, *190*(4), 1725–36. http://doi.org/10.4049/jimmunol.1200867

Wittchen, E. S. (2009). Endothelial signaling in paracellular and transcellular leukocyte transmigration. *Frontiers in Bioscience (Landmark Edition)*, *14*, 2522–45. Retrieved from http://www.ncbi.nlm.nih.gov/pubmed/19273217

Wójciak-Stothard, B., Williams, L., & Ridley, A. J. (1999). Monocyte adhesion and spreading on human endothelial cells is dependent on Rho-regulated receptor clustering. *The Journal of Cell Biology*, *145*(6), 1293–307. Retrieved from http://www.pubmedcentral.nih.gov/articlerender.fcgi?artid=2133155&tool=pmcentrez&rendertype=abstract

Woodfin, A., Voisin, M.-B., Beyrau, M., Colom, B., Caille, D., Diapouli, F.-M., … Nourshargh, S. (2011). The junctional adhesion molecule JAM-C regulates polarized transendothelial migration of neutrophils in vivo. *Nature Immunology*, *12*(8), 761–9. http://doi.org/10.1038/ni.2062

Yang, L., Kowalski, J. R., Yacono, P., Bajmoczi, M., Shaw, S. K., Froio, R. M., … Luscinskas, F. W. (2006). Endothelial cell cortactin coordinates intercellular adhesion molecule-1 clustering and actin cytoskeleton remodeling during polymorphonuclear leukocyte adhesion and transmigration. *Journal of Immunology (Baltimore, Md. : 1950)*, *177*, 6440–6449. http://doi.org/10.4049/jimmunol.177.9.6440

Yoshida, M., Westlin, W. F., Wang, N., Ingber, D. E., Rosenzweig, A., Resnick, N., & Gimbrone, M. A. (n.d.). Leukocyte Adhesion to Vascular Endothelium Induces E-Selectin Linkage to the Actin Cytoskeleton.

3

Annexin A2 limits neutrophil transendothelial migration by organizing the spatial distribution of ICAM-1.

Niels Heemskerk, Mohammed Asimuddin, Chantal Oort, Jos van Rijssel and Jaap D. van Buul*

Department of Molecular Cell Biology, Sanquin Research and Landsteiner Laboratory, Academic Medical Center, University of Amsterdam, the Netherlands.

* To whom correspondence should be addressed: Jaap D. van Buul, Sanquin Research and Landsteiner Laboratory, Academic Medical Center, University of Amsterdam, Plesmanlaan 125, 1066 CX Amsterdam, the Netherlands. tel. +31-20-5121219; fax: +31-20-5123310; E-mail j.vanbuul@sanquin.nl

ABSTRACT

Intracellular adhesion molecule-1 (ICAM-1) is required for firm adhesion of leukocytes to the endothelium. However, how the spatial organization of endothelial ICAM-1 regulates leukocyte adhesion is not well understood. Here, we identified the calcium-effector protein annexin A2 as a novel binding partner for ICAM-1. ICAM-1 clustering promotes the ICAM-1-annexin A2 interaction and induces translocation of ICAM-1 into caveolin-1-rich membrane domains. Depletion of endothelial annexin A2 using RNA interference enhances ICAM-1 membrane mobility and prevents the translocation of ICAM-1 into caveolin-1-rich membrane domains. Surprisingly, this results in increased neutrophil adhesion and transendothelial migration under flow conditions and reduced crawling time, velocity and lateral migration distance of neutrophils on the endothelium. In conclusion, our data show that annexin A2 limits neutrophil transendothelial migration by organizing the spatial distribution of ICAM-1.

INTRODUCTION

ICAM-1 at the endothelial cell (EC) surface functions as an adhesive ligand for neutrophil β2-integrins supporting the rolling, arrest, crawling and transmigration of neutrophils *in vivo* (1-6). However, to what extend ICAM-1 is specifically involved and how ICAM-1 functionally facilitates each distinct step during neutrophil transmigration has been controversial. Depletion of the intracellular domain of ICAM-1 abolishes T-lymphocyte as well as neutrophil transmigration, but not adhesion (7-9). This work established the importance of the intracellular domain of ICAM-1 as signaling molecule in orchestrating leukocyte transmigration, but also showed the importance of the extracellular domain of ICAM-1 in leukocyte adhesion. Studies that used LFA-1 (α_Lβ2,CD11a/CD18) and MAC-1 (α_Mβ2,CD11b/CD18) deficient mice showed that neutrophil arrest depends mainly on LFA-1-ICAM-1 interactions whereas neutrophil crawling requires MAC-1-ICAM-1 interactions (2,3). Moreover, the binding site of ICAM-1 for MAC-1, but not LFA-1 is regulated by glycosylation which may provide a mechanistic explanation for sequential roles in ICAM-1-mediated arrest and crawling (10,11). In addition to LFA-1-ICAM-1 interactions in mediating neutrophil arrest, the LFA-1-ICAM-1 interaction has also been reported to be involved in neutrophil transmigration since it has been shown to be rapidly co-clustered into a ring-like-structure around transmigrating neutrophils (12,13). Since the intracellular tail of ICAM-1 contains no identified signaling domains, activation of intracellular signaling is thought to be mediated by receptor clustering (14,15).

Clustering of ICAM-1 using anti-ICAM-1 antibodies is commonly used to study leukocyte induced ICAM-1 signaling. It has been reported that antibody-induced clustering of ICAM-1 initiates a rise in intracellular calcium, activates small Rho GTPases, Protein kinase C, Src family protein kinases, eNOS and MAPK (7,15-18), and induces the recruitment of several membrane-actin binding proteins to the intracellular tail of ICAM-1 (14,19-22). Moreover, antibody-induced crosslinking of ICAM-1 has been shown to translocate ICAM-1 to F-actin- and caveolin-1-rich areas at the EC periphery (23). This translocation has been suggested to link the sequential steps of leukocyte adhesion and transcellular transmigration (23). Studies that examined ICAM-1 surface distribution showed that depletion or blockage of the intracellular tail of ICAM-1, using cell-penetratin-ICAM-1 peptides competitive for the RKIKK motif, induced a more homogeneous cell surface distribution and loss of ICAM-1-positive microvilli (24). ICAM-1 can form at least three different topologies on the cell surface through dimerization of domain 1 that does not interfere with LFA-1 or MAC-1 binding (25). Moreover, structural basis of ICAM-

1 dimerization on the cell surface provides the existence of preformed ICAM-1 cis dimers on the cell membrane (26).

In line with this, Barreiro and colleagues showed that adhesive molecules such as ICAM-1 are physically organized and compartmentalized in preformed tetraspanin nanoplatforms (27,28). Those studies suggest the existence of multiple ICAM-1 complexes with different protein content, spatial organization or subcellular localization. However, little is known about how the spatial organization of ICAM-1 affects its adhesive function and what proteins regulate the distribution of ICAM-1 at the EC surface.

Here, we investigated the spatial organization of ICAM-1 at the EC surface and found annexin A2 as novel binding partner for ICAM-1. Our data show that annexin A2 negatively regulates the adhesion, crawling and subsequent transmigration of neutrophils across the endothelium by controlling the spatial organization of ICAM-1.

Materials and Methods

DNA and RNA constructs

YCam3.6 in a mammalian expression vector, based on a clontech-styl pEGFP-C1 backbone and driving expression from a CMV promotor was provided by Joachim Goedhart (Swammerdam Institute for Life Sciences, Amsterdam, the Netherlands). Briefly, the single chain Ycam3.6 biosensor consist of an enhanced (E)CFP, calmodulin E104Q, the calmodulin-binding peptide M13p, and a circular permutated (cp)-Venus. Binding of calcium makes calmodulin wrap around the M13 domain, increasing the FRET between the flanking FPs (47). shRNA in pLKO.1 targeting annexin A2 (A9) (TRCN 56145), annexin A2 (G5) (TRCN 56144) were purchased from sigma Aldrich mission library. ICAM-1-GFP was a kind gift from Dr. F. Sanchez-Madrid (University of Madrid, Madrid, Spain). pE AnnexinA2-GFP (N3) was purchased from Addgene.

Antibodies

Polyclonal rabbit antibodies against ICAM-1 for WB were purchased from Santa Cruz Biotechnology (Cat #SC-7891). Polyclonal rabbit antibody against annexin A2 (H50)(SC-9061) and The Alexa Fluor 405 monoclonal mouse antibody against ICAM-1 CD54 (15.2)(Sc-107 AF405) were purchased from Santa Cruz (Bio-Connect). Monoclonal ICAM-1 CD54 (BBIG-I1 / IIC81) antibodies used for ICAM-1 clustering were purchased from R&D systems (Cat #BBA9). Polyclonal Goat anti-mouse Fcγ IgG was purchased from Jackson (Cat #115-005-071). Monoclonal antibody against annexin A2 was a kind gift from Dr. Gerke (Institute of Medical

Biochemistry ZMBE Center for Molecular Biology of Munich, Germany). Rabbit monoclonal annexin A2 (D11G2) was purchased from Cell Signaling (BIOKÉ) (8235). Monoclonal mouse antibody against Actin (AC-40) was purchased from Sigma (Cat# A3853). The Alexa Fluor 405 goat anti-rabbit IgG (Cat# A31556), Alexa Fluor 647 chicken anti-goat IgG (Cat# A21469), Alexa Fluor 488 chicken anti-rabbit IgG (Cat# A21441) and Texas red 568 Phalloidin (Cat #T7471) were purchased from Invitrogen. Alexa Fluor 405 Phalloidin was purchased from Promokine (Cat# PK-PF405-7-01). Polyclonal Rabbit antibody against caveolin-1 was purchased from BD Biosciences (Cat # 610059). Mouse monoclonal actin antibodies were purchased from Sigma-Aldrich (Cat #A3853). Mouse monoclonal human Ezrin (18) was purchased from Transduction Laboratories (BD) (Cat# 610602). Mouse monoclonal RhoGDI antibodies were purchased from Transduction Laboratories (Cat #610255), mouse monoclonal antibodies against VCAM-1 were purchased from R&D systems (Cat #2090), and mouse monoclonal Filamin A antibodies were purchased from Serotec (Cat #MCA464S). Secondary HRP-conjugated goat anti-mouse, swine anti-rabbit antibodies were purchased from Dako (Heverlee, Belgium). All antibodies were used according to manufacturer's protocol.

Cell cultures, treatment and transfections

Pooled Human umbilical vein ECs (HUVECs) purchased from Lonza (P938, Cat # C2519A), were cultured on fibronectin-coated dishes in EGM-2 medium, supplemented with singlequots (Lonza, Verviers, Belgium) HUVECs were cultured until passage 9. HEK-293T were maintained in Dulbecco's Modified Eagle Medium (DMEM) (Invitrogen, Breda, The Netherlands) containing 10% (v/v) heat-inactivated fetal calf serum (Invitrogen, Breda, The Netherlands), 300 mg/ml L-glutamine, 100 U/ml penicillin and streptomycin and 1x sodium pyruvate (Invitrogen, Breda, The Netherlands). Cells were cultured at 37°C and 5% CO_2. HUVECs were pre-treated with 10 ng/ml recombinant Tumor-Necrosis-Factor (TNF)-α (PeproTech, Rocky Hill, NJ) 24 hours before each leukocyte TEM experiment, pre-treated with 1 µM ionomycin (Invitrogen, I-24222) for periods as indicated. Cells were transfected with the expression vectors according to the manufacturer's protocol with Trans IT-LT1 (Myrus, Madison, WI, USA). Lentiviral constructs were packaged into lentivirus in Human embryonic kidney (HEK)-293T cells by means of third generation lentiviral packaging plasmids (Dull et al., 1998; Hope et al 1990). Lentivirus containing supernatant was harvested on day 2 and 3 after transfection. Lentivirus was concentrated by Lenti-X concentrator (Clontech, Cat# 631232). Transduced target cells were used for assays after 72 hours. ICAM-1-GFP was delivered into HUVECs by adenoviral transduction 48h before imaging.

PULL-DOWN ASSAY

A synthetic, biotinylated peptides encoding the intracellular domains of human ICAM-1 and VCAM-1 were used in pull-down assays as previously described (Kanters et al. 2008). The following sequences were used: ICAM-1: NH2-RQRKIKKYRLQQAQKGTPMKPNTQATPP-COOH; VCAM-1: IIYFARKANMKGSYSLVEAQKSKV-COOH.

PULL-OUT ASSAY AND IMMUNOPRECIPITATION

1.2 mg/ml dynabeads goat-x-ms IgG (Dynal, Invitrogen) per condition were washed ones with 1 ml buffer 1 containing PBS + 2 mM EDTA and 0.1% BSA (Millipore) using a magnetic holder. Dynabeads were coated with 1.6 µg α-ICAM-1 CD54 (BBIG-I1/IIC81, R&D systems (Cat #BBA9) antibodies per condition and incubated head-over-head at 4ºC for 45 min. The beads were washed twice using buffer 1 and resuspended in PBS++ containing 0.5 $MgCl_2$ and 1 mM $CaCl_2$. Overnight TNF-α treated (10 ng/ml) HUVEC (2-5 million cells) were pre-treated with 1 µM ionomycin (Invitrogen, I-24222) for 10 min. 1.2 mg/ml dynabeads per condition were used to cluster ICAM-1 for 10-30 minutes. Cells were washed once on ice using PBS++. Next, cells were lysed in 1 ml cold pH7.4 RIPA buffer containing 50 mM Tris, 100 mM NaCl, 10 mM $MgCl_2$, 1% NP40, 10% glycerol, 0.1% SDS, 1% DOC (Sigma-Aldrich), DNAse inhibitor and protease phosphatase inhibitor cocktail for 5 min. Cells were scraped together and lysates were transferred to a new tube. Then, ICAM-1 coated dynabeads were added to non-clustered-control cells. 50 µl whole cell lysate was taken from all conditions. Beads and cell-lysates were subsequently incubated head-over-head for 1-2h at 4º C. Next cells were washed twice with Ripa buffer and three times with NP-40 lysis buffer. Beads were resuspended in 30 µl 2x SDS-sample buffer and assessed by Western blotting.

WESTERN BLOTTING

Cells were washed twice with PBS, and lysed with 95°C SDS-sample buffer containing 4% β-mecapto-ethanol. Samples were boiled at 95°C for 4 minutes to denature proteins. Proteins were separated on 4–12% NuPAGE Novex Bis-Tris gels (Invitrogen), transferred to Immobilon-PVDF transfer membranes (Millipore Corp., Billerica, MA) and subsequently blocked with 2.5% (w/v) bovine serum albumin (BSA) in Tris-buffered saline with Tween 20 (TBST) for 60 minutes. The immunoblots were analyzed using primary antibodies incubated overnight at 4°C and secondary antibodies linked to horseradish peroxidase (HRP) (GE Healthcare, UK), after each step immunoblots were washed 6x with TBST. Signals were visualized by enhanced chemiluminescence and light sensitive films (GE Healthcare, UK).

FRET MEASUREMENTS: MICROSCOPY, IMAGE ACQUISITION, AND ANALYSES

We use a Zeiss Observer Z1 microscope with 40x NA 1.3 oil immersion objective, a HXP 120 V excitation light source, a Chroma 510 DCSP dichroic splitter, and two Hamamatsu ORCA-R2 digital CCD cameras for simultaneous monitoring of ECFP and Venus emissions. Image acquisition was performed using Zeiss Zen 2011 microscope software. The lowest achievable HXP excitation power, through a FRET filter cube (Exciter ET 436/20x, and 455 DCLP dichroic mirror (Chroma), the emission filter is removed) was used to excite the ECFP donor. The emission is directed to the left side port by a 100% mirror, to an attached dual camera adaptor (Zeiss) controlling a 510 DCSP dichroic mirror. Emission wavelengths between 455-510 nm are directed to an emission filter (ET 480/40, Chroma) and then captured by the 'straight' Hamamatsu ORCA-R2 camera resulting in ECFP image acquisition. The Emission wavelength 510 nm and higher are directed to a six positions LEP filter wheel (Ludl Electronic Products) placed in front of the second 'rear' Hamamatsu ORCA-R2 camera. Position 1 in the emission filter wheel is equipped with an ET 540/40m used for Venus image acquisition. Position 2 is left empty to allow mCherry image acquisition (EX BP 572/25, BS FT 590, EM BP 629/62, Zeiss). The LEP filter wheel is controlled by the MAC 6000 controller system (Ludl Electronic Products). Exposure time of DIC image was set to 76 ms and exposure time of simultaneous ECFP and Venus acquisition was set to +/-800 ms, images were subsequently recorded every 5 seconds by two 1344 (H) x 1024 (V) Hamamatsu ORCA-R2 digital CCD cameras (2x2 binning) for periods as indicated. Offline ratio analysis between ECFP and Venus images were processed utilizing the MBF ImageJ collection (Tony Collins). The raw ECFP and Venus image stacks were background (BG) corrected using the plug-in 'ROI, BG subtraction from ROI'. Then, the ECFP and Venus stacks were aligned using the registration plug-in 'Registration, MultiStackReg'. A smooth filter was applied to both image stacks to improve image quality by reducing the noise. Next, both image stacks were converted to a 32-bit image format, required for subsequent masking. A threshold was applied exclusively to the Venus image stack, converting the background pixels to 'not a number' (NaN). It allows elimination of artifacts in ratio image stemming from the background noise. Finally the Venus/ECFP ratio was calculated using the plug-in 'Ratio Plus', and a custom lookup table was applied to generate a color-coded image illustrating the high 'red' and low 'blue' activities. Note that some of the plug-ins, namely MultiStackReg, and Ratio Plus are not included in the basic MBF ImageJ collection and should be downloaded from the plug-in page in the ImageJ website (http://rsb.info.nih.gov/ij/plugins/index.html). Normalized intensity graphs; the intensity of an ROI of interest and

the BG of the raw ECFP and Venus image stacks were measured using the plug-in ROI, Multi Measure in ImageJ. The raw ECFP and Venus intensities were BG subtracted using equation ECFP = (ECFP raw - BG), subsequently Venus only was corrected for bleed through using the equation VenusC = (Venus)-(0.5748*(ECFP), and normalized using the equation ECFPNorm = ECFP/Average (ECFP 3-13), and finally the Venus/ECFP ratio was calculated using the equation Venus/ECFP = VenusNorm/ECFPNorm using Excel.

IMMUNOFLUORESCENCE STAINING

HUVECs were cultured on FN-coated glass bottom (14-30 mm) until confluency. After treatment, cells were washed with cold PBS, containing 1 mM $CaCl_2$ and 0.5 mM $MgCl_2$, and fixed in 4% (v/v) formaldehyde for 10 minutes. After fixation, cells were permeabilized in PBS supplemented with 0.5% (v/v) Triton X-100 for 10 minutes followed by a blocking step in PBS supplemented with 2.5% (w/v) BSA. Cells were incubated with primary and secondary antibodies and after each step washed with PBS and mounted on microscope glasses using Mowiol. Image acquisition was performed on a confocal laser scanning microscope (LSM510/Meta; Carl Zeiss Micro-Imaging) using a voxel size of 0.06x0.06x0.48 µm and a 63x NA 1.4 oil immersion objective. Line profile plots were generated in ImageJ using the plot profile plug-in.

DETERGENT-FREE MEMBRANE FRACTIONATION

HUVEC were transduced with control or annexin A2 shRNA and left for 72 hours. Anti-ICAM-1 antibodies were allowed to bind to 4h TNF-α-stimulated (10 ng/ml) HUVEC monolayer for 30 min. ICAM-1 was subsequently cross-linked using secondary goat anti-mouse IgG antibodies for another 30 min. Next procedures were all carried out on ice. Two ten cm^2 confluent HUVEC were washed and scraped into base buffer (20 mM Tris-HCL, pH 7.8, 250 mM sucrose) to which had been added 1mM $CaCl_2$ and 1 mM $MgCl_2$. Cells were pelleted by centrifugation for 2 min at 250 g and resuspended in 1 ml of base buffer containing 1 mM $CaCl_2$ and 1 mM $MgCl_2$ and protease inhibitors (Invitrogen). The cells were then lysed by passage through a 22 g x 3" needle 20x. Lysates were centrifuged at 1,000 xg for 10 min. The resulting post nuclear supernatant was collected and transferred to a separate tube. The pellet was again lysed by the addition of 1 ml base buffer, followed by sheering 20x through a needle and syringe. After centrifugation at 1,000 xg for 10 min, the second post nuclear supernatant was combined with the first. An equal volume (2 ml) of base buffer containing 50% OptiPrep (Sigma-Aldrich St. Louis, MO) was added to the combined post nuclear supernatants and placed in the bottom of a 12 ml centrifuge tube. An 8

ml gradient of 0% to 18% OptiPrep in base buffer was poured on top of the lysate, which was now 25% in OptiPrep. Gradients were centrifuged for 90 minutes at 52,000 xg using an SW-41 rotor in a Beckman ultracentrifuge. After centrifugation, gradients were fractionated into 0.8 ml fractions, and the distribution of various proteins was assessed by Western blotting. This method was developed by Macdonald and Pike (36).

ICAM-1 MOBILITY ASSAYS

Live-cell imaging was conducted with a ZEISS LSM510 confocal microscope (Carl Zeiss MicroImaging, USA) using ZEN 2007 (Carl Zeiss Micro Imaging) image acquisition software with appropriate filter settings. To assess the mobility of ICAM-1 on the plasma membrane we bleached a small fraction of ICAM-1-GFP positive plasma membrane and measured the fluorescent recovery of ICAM-1-GFP into this region for 200 seconds. Data was further analysed in ImageJ. Intensities were normalized with the following equation = (intensity-intensityAfterbleech)/(intensityPrebleech-intensityAfterbleech)*100. To examine ICAM-1 mobility TNF-α treated ECs were incubated with 10 µm size polystyrene beads (Polysciences, Inc) that were coated with a monoclonal antibody against ICAM-1 CD54 (BBIG-I1/IIC81, R&D systems (Cat #BBA9) for 30 minutes. Percentage ICAM-1-GFP positive rings were quantified as the number of ICAM-1-GFP positive rings divided by the number of beads per ECs.

NEUTROPHIL ISOLATION

Neutrophils were isolated from whole blood derived from healthy donors. Whole blood was diluted (1:1) with 5% (v/v) TNC in PBS. Diluted whole blood was pipetted carefully on 12.5 ml Percoll (room temperature) 1.076 g/ml. Tubes were centrifuged (Rotanta 96R) at 2000 rpm, slow start, low brake for 20 minutes. Ring fraction containing lymphocytes and monocytes was discarded. After erythrocyte lysis in an ice-cold isotonic lysis buffer (155 mM NH_4CL, 10 mM $KHCO_3$, 0.1 mM EDTA, pH7.4 in Milli-Q(Millipore), neutrophils were centrifuged at 1500 rpm for five minutes at 4°C, incubated once with lysis buffer for 5 minutes on ice, centrifuged again at 1500 rpm for five minutes at 4°C, washed once with PBS, centrifuged again at 1500 rpm for five minutes at 4°C and resuspended in HEPES medium (20 mM HEPES, 132 mM NaCl, 6 mM KCL, 1 mM $CaCL_2$, 1 mM $MgSO_4$, 1.2 mM K_2HPO_4, 5 mM glucose (all from Sigma-Aldrich), and 0.4 % (w/v) human serum albumin (Sanquin Reagents), pH7.4) and kept at room temperature for not longer than four hours until use. Neutrophil counts were determined by cell counter (Casey).

Neutrophil TEM under physiological flow

HUVECs were cultured to 70% confluence in FN-coated 6 well plate, and transduced with lentivirus containing shAnxA2 and shCtrl for 24h. HUVECs were cultured in a FN-coated ibidi µ-slide VI$^{0.4}$ (ibidi, Munich, Germany) the day before the experiment was executed and stimulated overnight with TNF-α (10 ng/ml). Freshly isolated neutrophils were resuspended at 1×10^6 cells per ml in HEPES medium and were incubated for 30 minutes at 37°C. Cultured HUVECs in ibidi flow chambers were connected to a perfusion system and exposed to 0.5 ml/minute HEPES shear flow for 10 minutes (0.8 dyne/cm^2). Neutrophils were subsequently injected into the perfusion system and real-time leukocyte-endothelial interactions were recorded for 20 minutes by a Zeiss Observer Z1 microscope using a 40x NA 1.3 oil immersion objective. All live imaging was performed at 37°C in the presence of 5% CO_2. Transmigrated neutrophils were distinguished from those adhering to the apical surface of the endothelium by their transition from bright to phase-dark morphology. Percentage adherent or transmigrated neutrophils were manually quantified using the ImageJ plug-in Cell Counter (type 1, adherent cells, type 2, transmigrated cells). Neutrophil rolling velocity, crawling Time, crawling velocity and crawling distance were quantified using the ImageJ plug-in manual tracking.

Statistics

Filamin and annexin A2 binding to anti-ICAM-1-coated beads was tested using a one-way ANOVA assuming no matching or pairing, comparing the mean of each column with the mean of every other column, that were corrected for multiple comparisons by Tukey multiple comparisons test, with a single pooled variance. The student T-test performed statistical comparison between experimental groups. A two-tailed p-value of < 0.05 was considered significant. Unless otherwise stated, a representative experiment out of at least three independent experiments is shown.

Results

The intracellular tail of ICAM-1 interacts with annexin A2

To identify new proteins involved in the regulation of ICAM-1-mediated leukocyte transendothelial migration (TEM), we performed a pull down assay using biotinylated peptides encoding the intracellular tail of ICAM-1. Peptide-bound proteins were subsequently separated by SDS-PAGE, visualized by silver staining and specific protein bands were analyzed by mass spectrometry. A protein band interacting with the ICAM-1 peptide that migrated at a molecular mass of 36 kDa was identified by mass

spectrometry as the calcium effector protein annexin A2. To corroborate the interaction of annexin A2 with the intracellular domain of ICAM-1, biochemical pull down assays from cell lysates using peptides were repeated, analyzed by Western blot and confirmed the binding of annexin A2 to the intracellular tail of ICAM-1, and not to the intracellular domain of VCAM-1 or streptavidin beads (Fig. 1a). Filamin A, previously reported to interact with the intracellular domain of ICAM-1 (14), was used as a positive control (Fig. 1a). To investigate the endogenous interaction between annexin A2 and ICAM-1, we immunoprecipitated endogenous ICAM-1 using magnetic beads coated with anti-ICAM-1 antibodies that induced the clustering of ICAM-1 (14). Anti-VCAM-1 or anti-IgG isotype control antibody-coated beads were used as controls. Using this method endogenous ICAM-1 and VCAM-1 were effectively precipitated from TNF-α-treated endothelial cells (Fig. 1b). Analysis of the binding of annexin A2 and Filamin A showed that these proteins interacted with ICAM-1 using anti-ICAM-1 antibody-coated beads (Fig. 1b). In contrast to annexin A2 that was only co-precipitated with anti-ICAM-1 antibody-coated beads, a low amount of Filamin A did also co-precipitate with anti-VCAM-1 antibody-
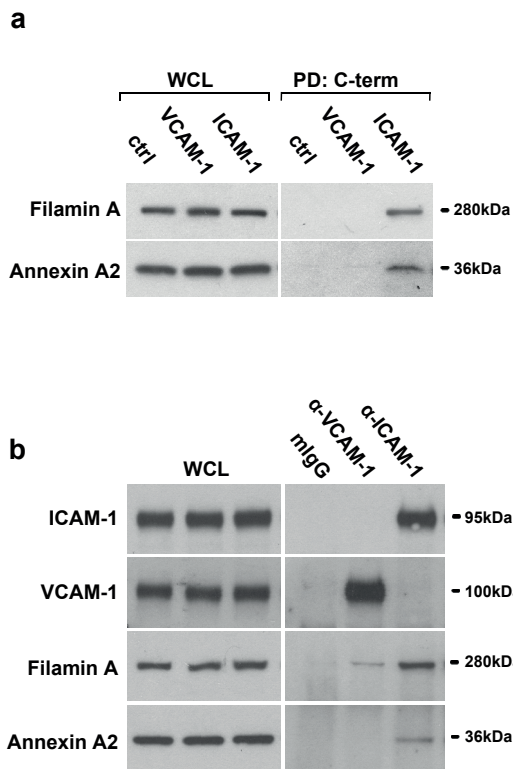
Figure 1. The intracellular tail of ICAM-1, but not VCAM-1 interacts with annexin A2. (**a**) Immunoblot analysis of protein extracts prepared from TNF-α-stimulated EC that were incubated with peptides encoding the intracellular tail (PD: C-term) of ICAM-1 or VCAM-1. Extracts were probed with antibodies directed against annexin A2 and filamin A. Streptavidin beads were used as a negative control. WCL: whole cell lysate. (**b**) Immunoprecipitation of ICAM-1 using magnetic beads coated with anti-ICAM-1 antibodies. Anti-VCAM-1 or anti-IgG isotype control antibody-coated beads were used as controls. Beads were incubated 30 minutes at the cell surface of TNF-α-stimulated EC before lysis. Extracts were probed with antibodies directed against ICAM-1, VCAM-1, filamin A and annexin A2. Data are from three experiments (**a, b**).
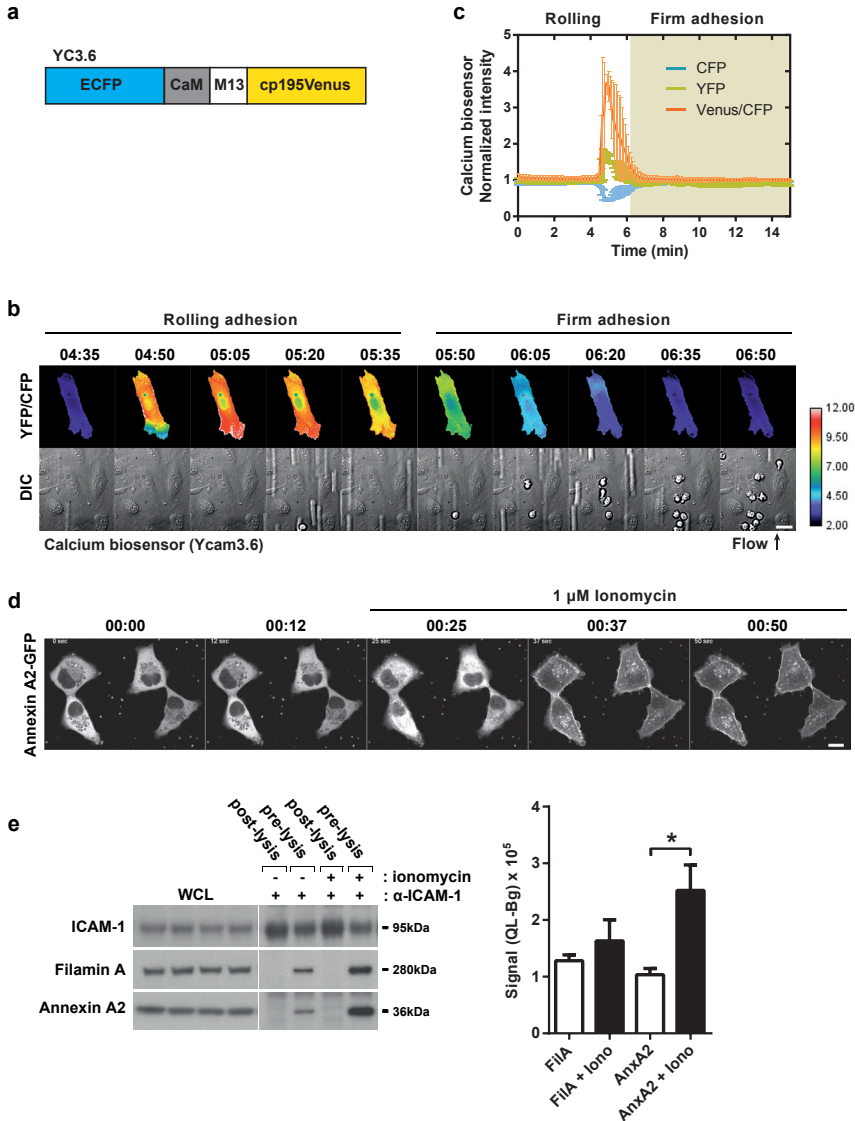
Figure 2. Rolling neutrophils transiently increase intracellular calcium levels in EC driving annexin A2 to associate with the plasma membrane and ICAM-1. (**a**) Schematic illustration of the Ycam3.6 calcium sensor design containing enhanced (E)CFP (blue), calmodulin E104Q (grey), the calmodulin-binding peptide M13p (white), and a circular permutated (cp)-Venus (yellow). (**b**) Time-lapse Venus/CFP ratio images of Ycam3.6 calcium biosensor simultaneously recorded with an epifluorescent microscope showing spatiotemporal calcium measurements during the onset of flow (0.9 dyne per cm^2) starting after 30 seconds, and upon neutrophil rolling, adhesion and transmigration (arrow). Calibration bar shows the increase in intracellular calcium concentrations (red) relative to basal calcium concentration (blue). Scale bar, 150µm. (**c**) Quantification of temporal intracellular calcium concentration in multiple EC during the onset of flow, and neutrophil rolling, adhesion and transmigration. Data

coated beads (Fig. 1b). Annexin A2 and Filamin A were not co-precipitated with anti-IgG isotype control antibody-coated beads (Fig. 1b). Thus, our findings show that annexin A2 binds to the intracellular tail of ICAM-1, but not to the intracellular tail of VCAM-1.

ROLLING NEUTROPHILS TRANSIENTLY INCREASE INTRACELLULAR CALCIUM LEVELS IN EC DRIVING ANNEXIN A2 TO ASSOCIATE WITH THE PLASMA MEMBRANE AND ICAM-1

Annexin A2 is a calcium effector protein comprising five calcium-binding domains that facilitate the binding of annexin A2 to the plasma membrane upon release of intracellular calcium (29). To investigate calcium signalling during leukocyte diapedesis under shear stress conditions, we used the fluorescence resonance energy transfer (FRET)-based genetically encoded calcium indicator Ycam3.6 (30) (Fig. 2a). The single chain Ycam3.6 biosensor consist of an enhanced (E)CFP, calmodulin E104Q, the calmodulin-binding peptide M13p, and a circular permutated (cp)-Venus. Binding of calcium makes calmodulin wrap around the M13 domain, increasing the FRET between the flanking FPs (30). EC transfected with Ycam3.6 biosensor were grown to confluence in FN-coated perfusion chambers, stimulated with TNF-α overnight and subsequently exposed to shear stress (0.8 Dyne/cm^2). Intracellular changes in calcium levels were measured by donor/acceptor ratio imaging and showed that the initial onset of flow rapidly triggered the transient influx of calcium, as was also shown by others (31-33) (Fig. S1). The levels of calcium influx normalized within 2 minutes. To exclude any flow-induced calcium signals, we perfused the neutrophils after at least 20 minutes of initial flow onset. The results showed that initial neutrophil contact during the rolling stage rapidly induced a transient increase in intracellular calcium concentration in EC, preceding the firm adhesion step (Fig. 2b and Supplementary Video 1). Interestingly, firm adhesion of neutrophils to the endothelium was observed directly after the temporary burst of released intracellular calcium (Fig. 2b and Supplementary Video 1). We measured

represents mean and s.e.m of three experiments including at least 12 cells per experiment. (**d**) Confocal imaging of cytosolic annexin A2-GFP translocation to the plasma membrane after ionomycin stimulation. Scale bar, 20µm. (**e**) Immunoblot analysis of protein extracts prepared from TNF-α-stimulated EC that were incubated with anti-ICAM-1-coated beads for 30 minutes pre lysis (meaning clustered ICAM-1) or post lysis (meaning non-clustered ICAM-1 conditions). EC were stimulated with ionomycin for 2 minutes to induce high intracellular calcium levels. Extracts were probed with antibodies directed against filamin A, ICAM-1 and annexin A2. Quantification of annexin A2 and filamin A binding, presented as 'quantum level' (sum of grayness of each pixel in blot) minus background (QL-Bg), normalized to that of ICAM-1. * $P < 0.05$ AnxA2 versus AnxA2 + ionomycin (ANOVA). Data represents mean and s.e.m of seven experiments (**b,c**) five experiments (**d**) three experiments (**e**).

a 5-fold increase in sensor ratio almost instantly when the neutrophil touched the endothelium, in line with previous findings by Ziegelstein and colleagues (34). Surprisingly however, only 20-30% of the sensor-expressing endothelial cells showed an increase in calcium signal upon rolling neutrophils. This may reflect the heterogenic expression of the adhesion molecules like selectin and ICAM-1 between mutual endothelial cells. Quantification of the biosensor activity showed the significance of the transient and rapid intracellular calcium changes preceding neutrophil adhesion (Fig. 2c). To test if the supernatant of the neutrophils may increase intracellular calcium levels, we treated endothelial cells with supernatant of PMA-stimulated neutrophils and did not observe any calcium influx (Fig. S2). This excludes that secreted molecules from the neutrophils induced the calcium influx in the endothelium.

In addition, increased levels of intracellular calcium drives the majority of annexin A2 to the plasma membrane as is indicated by the rapid translocation of cytosolic annexin A2-GFP to the plasma membrane after ionomycin treatment (Fig. 2d and Supplementary Video 2). Also endogenous stimuli like histamine induced annexin A2 translocation to the plasma membrane (Fig. S3). To study if the interaction between endogenous ICAM-1 and annexin A2 is regulated by high calcium, we immunoprecipitated ICAM-1 using magnetic beads coated with anti-ICAM-1 antibodies on intact ECs treated with ionomycin (pre-lysis). The co-precipitation of annexin A2 with anti-ICAM-1 antibody-coated beads was enhanced upon high intracellular calcium conditions (Fig 2e). Quantification showed that pre-treating EC with ionomycin significantly promoted the co-precipitation of annexin A2 with α-ICAM-1 antibody-coated beads, whereas filamin A levels were not significantly altered (Fig 2e). Note that addition of anti-ICAM-1 antibody-coated beads to an EC lysate (post-lysis) did not result in the co-precipitation of annexin A2 or filamin A, indicating that the interaction with endogenous annexin A2 required intact membranes to promote the interaction between annexin A2 and ICAM-1 upon ICAM-1 clustering. Together, these findings showed that rolling neutrophils transiently increase intracellular calcium levels in EC that may transiently drive annexin A2 to associate with the plasma membrane and ICAM-1.

ICAM-1 IS LOCALIZED IN F-ACTIN- AND ANNEXIN A2-RICH MICROVILLI

To study the spatial organization of ICAM-1 at the EC surface under non-ligand-bound conditions, we co-stained TNF-α-stimulated ECs for endogenous ICAM-1, F-actin and annexin A2. Overnight TNF-α-stimulated ECs showed heterogeneous distribution of ICAM-1 on the endothelial surface (Fig. 3a). Moreover, ICAM-1 is particularly enriched in F-actin-rich
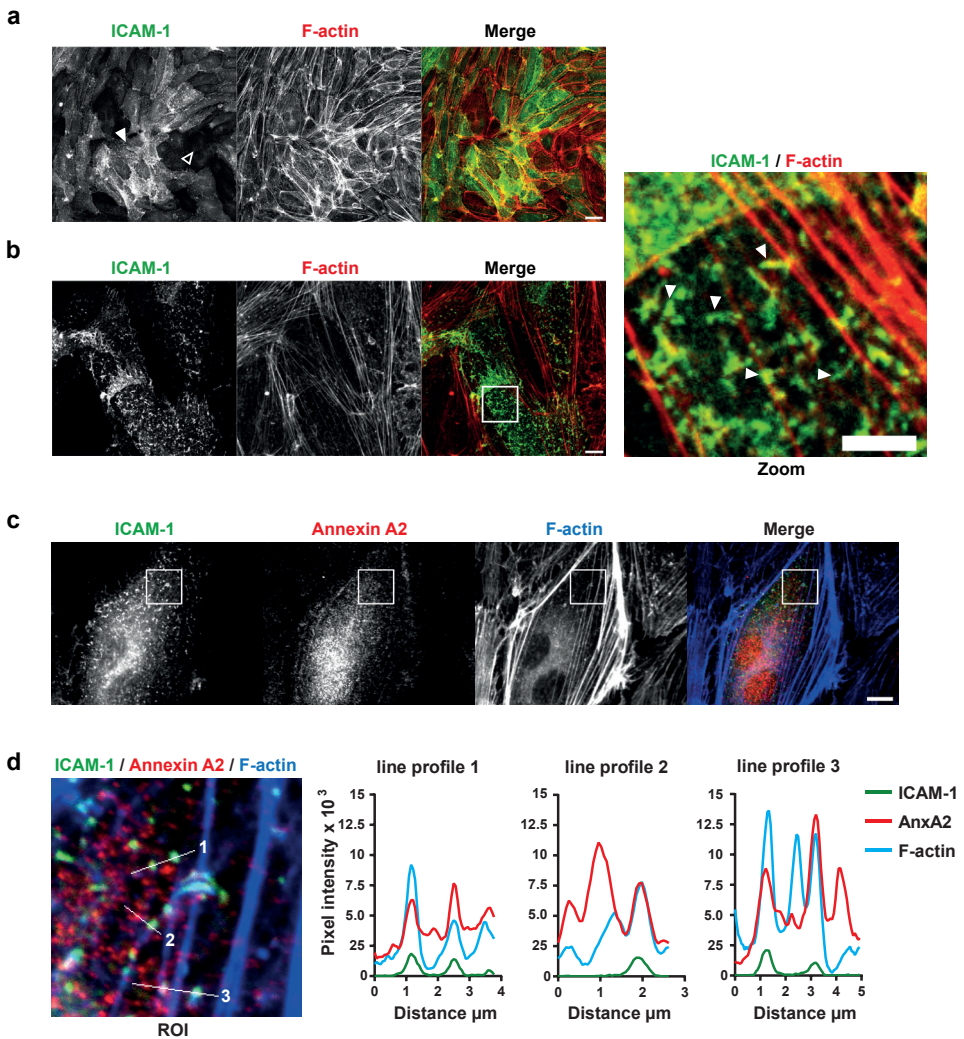
Figure 3. ICAM-1 at the EC surface is localized in microvilli rich in F-actin and annexin A2. (**a**) ECs show heterogeneous ICAM-1 surface expression after TNF-α stimulation. Immunofluorescence analyses of ICAM-1 and F-actin in TNF-α-stimulated ECs. Open and filled arrows indicate low and high endothelial surface expression of ICAM-1, respectively. (**b**) Immunofluorescence analyses of ICAM-1 and F-actin in TNF-α-stimulated ECs. Filled arrows indicate ICAM-1 localization at the plasma membrane in microvilli. (**c**) Immunofluorescence analyses of ICAM-1, F-actin and annexin A2 in TNF-α-stimulated ECs. Annexin A2 is localized in nanometer-scale clusters at the plasma membrane (**d**) Line profiles of ROI marked in Fig. 3 c. Line profile 1 indicates co-localization between ICAM-1, F-actin and annexin A2 in microvilli. Line profile 2 indicates annexin A2 membrane domains outside microvilli that does not co-localize with ICAM-1. Line profile 3 indicates membrane domains that are rich in ICAM-1, annexin A2 and F-actin and domains that only contain annexin A2 or F-actin.
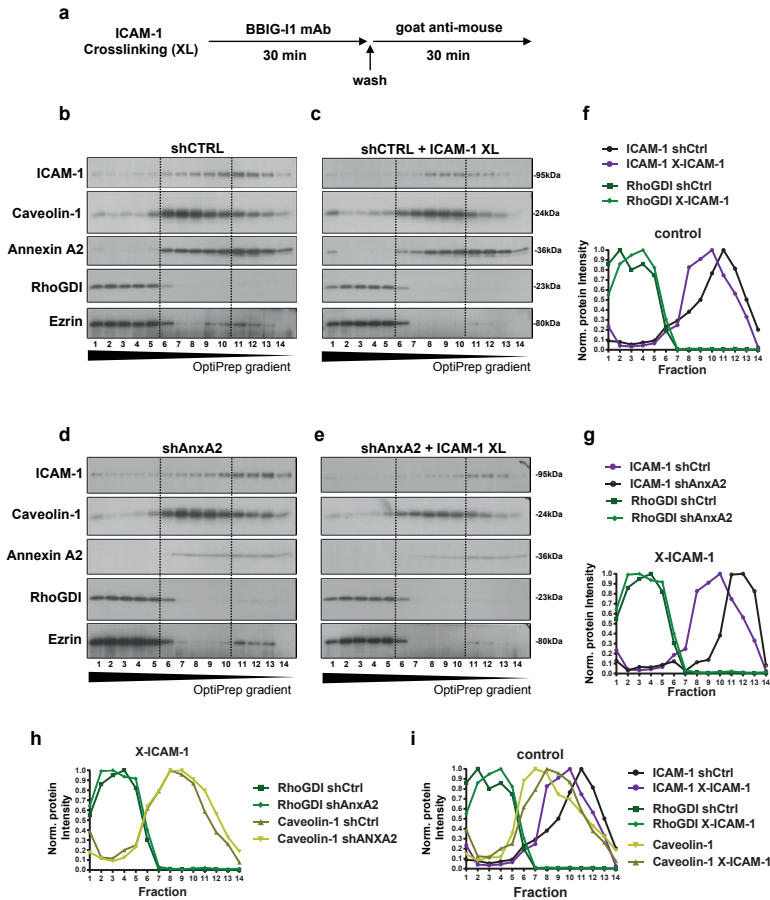
Figure 4. Annexin A2 regulates the spatial distribution of ICAM-1 at the EC surface and is required for ICAM-1 translocation to caveolin-1-rich membrane domains upon ICAM-1 clustering. (**a**) Schematic representation of ICAM-1 crosslinking prior membrane fractionation. ICAM-1 at the EC surface is clustered by incubation with the BBIG-I1 mAb for 30 minutes followed incubation with a secondary goat anti-mouse antibody for 30 minutes. (**b**) Immunoblot analysis of protein extracts that were separated on density by OptiPrep gradient centrifugation to visualize the spatial distribution of proteins at the plasma membrane in non-clustered and clustered ICAM-1 conditions. Extracts used for membrane fractionation were prepared 72 hours after transduction with control (**b**, **c**) or annexin A2 shRNA (**d**, **e**). Extracts were probed with antibodies directed against ICAM-1, caveolin-1, annexin A2, RhoGDI and Ezrin. Lane 1-5 indicate the cytosolic protein fraction. Lane 6-10 indicate high density membrane fractions rich in caveolin-1. Lane 11-14 indicate low density membrane fractions rich in Ezrin and Annexin A2. (**f**) Quantification of the spatial distribution of ICAM-1 at the plasma membrane in non-clustered and clustered ICAM-1 conditions. RhoGDI indicates the cytosolic fraction (**g**) Quantification of spatial distribution of ICAM-1 in control and annexin A2 depleted ECs after ICAM-1 clustering. (**h**) Quantification of the spatial distribution of caveolin-1 in control and annexin A2 depleted ECs after ICAM-1 clustering. (**i**) Quantification of the spatial distribution of ICAM-1 and caveolin-1 at the plasma membrane in non-clustered and clustered ICAM-1 conditions. RhoGDI indicates the cytosolic fraction.

extensions called microvilli that protrude out of the EC apical surface (Fig. 3b) (24,35). Immunofluorescent analysis of annexin A2 and ICAM-1 showed enrichment of both proteins in microvilli (Fig. 3c,d). In contrast to ICAM-1, annexin A2 is also enriched in membrane domains other than F-actin-rich microvilli (Fig. 3c,d). Thus, unengaged ICAM-1 is distributed at microvilli where it co-localized with F-actin and annexin A2.

ANNEXIN A2 REGULATES THE SPATIAL ORGANIZATION OF ICAM-1 AT THE PLASMA MEMBRANE

To examine the spatial organization of ICAM-1 at the plasma membrane during ICAM-1-mediated neutrophil TEM, we used a detergent-free membrane fractionation (36). Neutrophil-mediated ICAM-1 clustering was mimicked using antibody crosslinking, according to previous studies (37-39) (Fig. 4a). Without antibody-mediated clustering, ICAM-1 co-sedimented with ezrin and annexin A2 in fraction 10-12 outside of caveolin-1-rich membrane domains (fraction 6-10) (Fig. 4b). Antibody-mediated crosslinking of ICAM-1 drives ICAM-1 to the EC poles, regions that are rich in caveolin-1 (23). In line with these findings, we found that antibody-mediated clustering of ICAM-1 increased co-sedimentation of ICAM-1 with caveolin-1 to fractions 8-10, but also induced the dissociation of ezrin with the plasma membrane (Fig. 4c). Note that the membrane distribution of annexin A2 was not affected by ICAM-1 clustering (Fig. 4b,c). To investigate if annexin A2 regulated the spatial organization of ICAM-1 at the plasma membrane, we depleted annexin A2 using short hairpin RNA (shRNA). Annexin A2 depletion shifted non-clustered ICAM-1 to less dense fractions 11-13 (Fig. 4d). Strikingly, crosslinking ICAM-1 under these conditions prevented the co-sedimentation of ICAM-1 with caveolin-1, whereas annexin A2 depletion did not alter the distribution of caveolin-1 or ezrin dissociation from the plasma membrane upon ICAM-1 clustering (Fig. 4e). These findings showed that annexin A2 regulates the spatial ICAM-1 distribution at the EC surface and that annexin A2 is required for the translocation of ICAM-1 to caveolin-1-rich membrane domains upon ICAM-1 clustering.

ANNEXIN A2 NEGATIVELY REGULATES ICAM-1 MOBILITY AT THE EC SURFACE

To investigate whether annexin A2 affects ICAM-1 dynamics at the plasma membrane, we examined ICAM-1 mobility using FRAP. ECs were transiently transfected with ICAM-1-GFP, treated with TNF-α and subsequently a region of interest was bleached (Fig. 5a). The recovery of ICAM-1-GFP in the bleached region was measured using confocal laser scanning microscopy and showed that the mobile fraction of ICAM-1 was around 40% in control conditions (Fig. 5b). However, in annexin A2-

Figure 5. Annexin A2 regulates the lateral mobility of ICAM-1 at the EC surface. (**a**) Time-lapse confocal images showing FRAP of ICAM-1-GFP indicative for the lateral mobility of ICAM-1 at the plasma membrane and in microvilli. White box indicates the ICAM-1-GFP positive membrane part that has been bleached. Scale bar Scale bar, 10µm. (**b**) Quantification of ICAM-1-GFP recovery kinetics after photo bleaching showing the mobile fraction of ICAM-1-GFP at the EC surface in control (green line) and annexin A2 depleted (red line) ECs. Bar graph shows quantification of the mobile fraction of ICAM-1 after 150 seconds. (**c**) Endothelial annexin A2 depletion by shRNA. Immunoblot analysis of protein extracts prepared from HUVEC expressing ICAM-1-GFP. Extracts were prepared 72 hours after transduction with control or

deficient ECs, the mobile fraction of ICAM-1 was significantly increased to more than 55% (Fig. 5b). Subsequently, annexin A2, F-actin, endogenous ICAM-1 and ICAM-1-GFP, levels were analysed by Western blot. Importantly, Annexin A2-deficient ECs did not affect endogenous ICAM-1 as well as ICAM-1-GFP protein levels in TNF-α-treated ECs (Fig. 5c). Moreover, using anti-ICAM-1 antibody-coated beads, we found that ICAM-1-GFP was more rapidly and more frequently recruited to beads when annexin A2 was depleted than under control conditions (Fig. 5d,e and Supplementary Video 3). Quantification showed that the kinetics of ICAM-1-GFP recruitment to anti-ICAM-1 antibody-coated beads was significantly faster in annexin A2-deficient ECs than in control ECs (Fig. 5f). Also the number of ICAM-1-GFP-positive rings was increased in annexin A2-deficient ECs compared to the control (Fig. 5f). Thus, annexin A2 negatively regulates ICAM-1 mobility at the EC surface.

DOWN REGULATION OF ENDOTHELIAL ANNEXIN A2 INCREASES NEUTROPHIL ADHESION TO TNF-α STIMULATED ECs.

ICAM-1 at the EC surface has been described to support the rolling, arrest, crawling and transmigration of neutrophils (1-6). To investigate how altered ICAM-1 membrane distribution and dynamics in annexin A2-deficient ECs affect neutrophil TEM under physiological flow conditions, we simultaneously measured neutrophil TEM through control and annexin A2-deficient ECs in a parallel flow set-up (Fig. 6a). This set-up allowed us to use primary human neutrophils from the same donor. Neutrophils were simultaneously perfused over TNF-α-stimulated ECs under physiological shear stress conditions (0.8 Dyne/cm^2). Neutrophil rolling velocity, adhesion, crawling and transmigration was recorded by a wide-field microscope and subsequently quantified using ImageJ software. Annexin A2 depletion in ECs did not affect neutrophil rolling velocity (Fig. 6b). However, the adhesion of neutrophils to annexin A2-deficient ECs was significantly increased compared to control ECs (Fig 6c and Supplementary

annexin A2 shRNA. Extracts were probed with antibodies directed against ICAM-1, annexin A2 and actin. Quantification of actin, annexin A2 ICAM-1 and ICAM-1-GFP protein levels after 72 hours after transduction with control or annexin A2 shRNA, presented as 'quantum level' (sum of grayness of each pixel in blot) minus background (QL-Bg). (**d**) Confocal imaging of ICAM-1-GFP dynamics during incubation of anti-ICAM-1-coated beads at TNF-α-stimulated control and annexin A2 deficient primary ECs. (**e**) Kinetics of ICAM-1-GFP recruitment to anti-ICAM-1-coated beads in TNF-α-stimulated control and annexin A2 deficient primary ECs. (**f**) Quantification of ICAM-1-GFP-positive rings % after 30 minutes incubation with anti-ICAM-1-coated beads in TNF-α-stimulated control and annexin A2 deficient primary ECs. **** $P < 0.0001$ control versus AnxA2 (Student's t-test) (**b**). **** $P < 0.0001$ control versus AnxA2 (ANOVA). ** $P < 0.01$ control versus AnxA2 (Student's t-test) (**f**). Data represents mean and s.e.m of 20 experiments (**b**) 7 experiments (**e,f**).

Video 4). Quantification of the number of adherent neutrophils showed a 2-3 fold increase in neutrophil adhesion when annexin A2 was silenced using two distinct short hairpins targeting annexin A2 (Fig. 6d). Surprisingly, neutrophil crawling distance on the EC surface as well as their velocity was significantly reduced in annexin A2-deficient primary ECs (Fig. 7 a-c). Despite slower apical movement, neutrophils spend less time crawling over the EC cell surface before transmigration (Fig. 7d). In
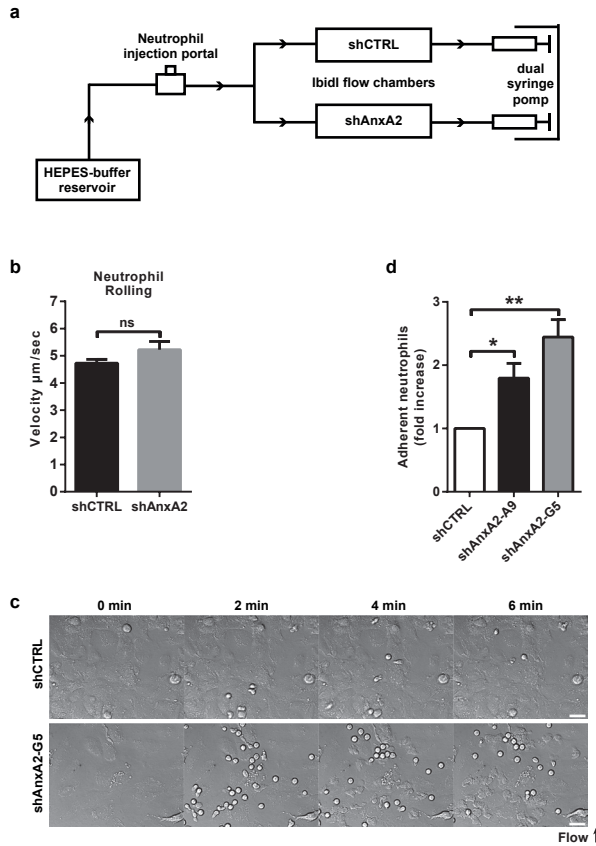
Figure 6. Annexin A2 depletion in EC enhanced the adhesive capacity of ICAM-1 to bind neutrophils β2-integrins (**a**) Schematic representation of the experimental set-up used to simultaneously measure two conditions with same donor neutrophils. (**b**) Quantification of neutrophil rolling velocities over TNF-α-stimulated control and annexin A2 deficient primary ECs. (**c**) Epi-fluorescent live-cell imaging of neutrophil TEM through TNF-α-stimulated control and annexin A2 deficient primary ECs under physiological flow conditions (0.9Dyne/cm^2). (**d**) Quantification of adherent neutrophils through TNF-α treated ECs under physiological flow conditions after 72 hours transduction with control shRNA (open bar), annexin A2 shRNA A9 (black bar) or annexin A2 shRNA G5 (grey bar). * $P < 0.05$ and ** $P < 0.01$ control versus AnxA2 (ANOVA) (**d**). Data are representative of five independent experiments with > 5 rolling events per group (**b**) five experiments with > 150 events per group (**d**) (error bars (**b,d**), s.e.m.).

line with this, we observed that most neutrophils crawled in a direct line to the EC junctions where they breeched the endothelial monolayer (data not shown). Consequently, the absolute number of neutrophils that finished the final step, i.e. crossing the endothelial barrier, was significantly increased when annexin A2 was depleted (Fig. 7e). When calculating the number of transmigrated neutrophils relative to the number of adhering neutrophils, there was no difference in percentage of neutrophils that
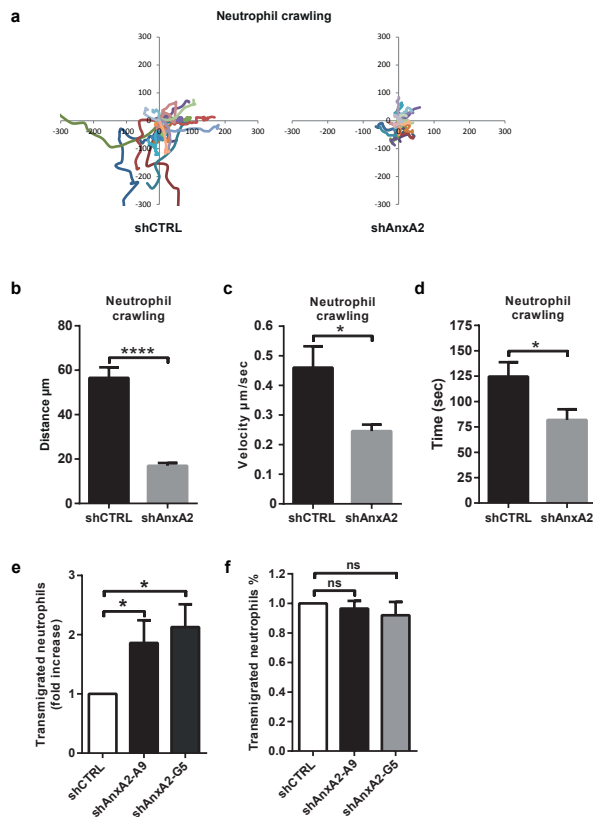
Figure 7. Neutrophil crawling distance and velocity was significantly reduced in annexin A2 deficient ECs, but neutrophil diapedesis was not affected. (**a**) Graphical representation of neutrophil crawling tracks over TNF-α-stimulated control and annexin A2 deficient primary ECs. (**b**) Quantification of neutrophil crawling distance, crawling velocity (**c**) and crawling time (**d**) over TNF-α-stimulated control and annexin A2 deficient primary ECs. (**e**) Quantification of transmigrated neutrophils through TNF-α treated ECs under physiological flow conditions after 72 hours transduction with control shRNA (open bar), annexin A2 shRNA A9 (black bar) or annexin A2 shRNA G5 (grey bar). (**f**) Quantification of percentage of adherent cells that completed transmigration after 20 minutes. **** $P < 0.0001$ control versus AnxA2 (Student's t-test) (**b**). * $P < 0.05$ control versus AnxA2 (Student's t-test) (**c,d**). * $P < 0.05$ control versus AnxA2 (ANOVA) (**e**). Data are representative of five independent experiments with > 5 crawling events per group (**a-d**) five experiments with > 150 events per group (**e,f**) (error bars (**a-f**), s.e.m.).

crossed the endothelium in the absence or presence of annexin A2 (Fig. 7f). Altogether, our results showed that annexin A2 regulates the adhesion, crawling and subsequent transmigration of neutrophils across the endothelium by controlling ICAM-1 membrane distribution and dynamics that in turn mediates the efficiency of neutrophil TEM.

Discussion

ICAM-1 at the EC surface functions as an adhesive ligand for neutrophil $\beta2$-integrins required for effective neutrophil TEM. However, little is known how cell-surface distribution of ICAM-1 is regulated and how this spatial organization controls the adhesive function of ICAM-1. It has been hypothesized that multiple ICAM-1 complexes with different protein content, spatial organization and subcellular localization regulate leukocyte behavior at different stages of leukocyte TEM (21,23,28). In agreement with this hypothesis, we found that altered ICAM-1 membrane distribution significantly alters neutrophil TEM efficiency. We found that clustered ICAM-1 translocates from ezrin-rich membrane domains to caveolin-1-rich membrane domains, which was impaired in annexin A2-depleted ECs. This altered ICAM-1 membrane distribution enhanced the lateral mobility and adhesive capacity of ICAM-1 to bind neutrophils. These findings suggest that the translocation of ICAM-1 into caveolae has a limiting effect on ICAM-1-mediated leukocyte adhesion. A previous study showed that ICAM-1 in caveolae is rapidly transcytosed and transported to the basolateral surface of ECs (23). This event together with the expression level of ICAM-1 on the cell surface has been suggested to regulate transcellular migration, but not paracellular migration of T cells and neutrophils (23,40,41).

Depletion of the intracellular domain of ICAM-1 impairs leukocyte transmigration, but not adhesion (8,9,42). Partly in line with these studies, we found that annexin A2-mediated alteration of ICAM-1 distribution affects neutrophil adhesion but not the percentage of transmigrating neutrophils. This suggests that the spatial organization of ICAM-1 at the endothelial surface is of primary importance for the adhesion, and less for the transmigration or diapedesis of leukocytes. Studies using LFA-1 ($\alpha_L\beta2$,CD11a/CD18) and MAC-1 ($\alpha_M\beta2$,CD11b/CD18) deficient mice show that neutrophil firm arrest depends mainly on LFA-1-ICAM-1 interactions, whereas neutrophil crawling requires MAC-1-ICAM-1 interactions (2,3). Interestingly, depletion of annexin A2 increased neutrophil adhesion efficiency, but reduced the time, velocity and distance of crawling neutrophils. Possibly, the increased ability of ICAM-1 to move through the

membrane may result in an increased efficiency to interact with neutrophil integrins. As a consequence, neutrophils adhere more rapidly to the endothelium. Why neutrophil crawling depends on the spatial distribution of ICAM-1 needs further investigation. Interestingly, overexpression of annexin A2 did not result in decreased leukocyte adhesion or TEM (data not shown). For annexin A2 to properly localize at the plasma membrane, it requires binding to the small molecule S100A10. However, if the expression of S100A2 is limiting, this may prevent the translocation of annexin A2 to the membrane and consequently its functionality in regulating ICAM-1.

Calcium signalling in EC has been implicated in all steps of leukocyte TEM (17,34,43-45). In fact, the major role for calcium signalling is believed to be involved in MLCK activation and subsequent actomyosin contraction to induce transient openings in the EC junctions allowing leukocyte transmigration (46-49). In contrast to multiple transient calcium spikes at each stage of diapedesis, we found that EC intracellular calcium was released upon initial neutrophil-EC contact prior neutrophil adhesion under flow conditions. As an alternative model for calcium being involved in junctional opening, we show that the calcium-effector annexin A2 is recruited to the plasma membrane upon release of intracellular calcium. Increased annexin A2 at the plasma membrane may modulate ICAM-1 function and thereby affect neutrophil TEM efficiency.

In conclusion, our work discovers that annexin A2 regulates ICAM-1 function through its spatial distribution on the endothelial surface, which limits neutrophil TEM efficiency. These findings may provide new targets for drug therapy to treat inflammatory-based diseases.

Footnotes

To whom correspondence should be addressed: Department of Molecular Cell Biology, Sanquin Research and Landsteiner Laboratory, Academic Medical Center, University of Amsterdam, Plesmanlaan 125, 1066 CX Amsterdam, the Netherlands. tel. +31-20-5121219; fax: +31-20-5123310; E-mail j.vanbuul@sanquin.nl

Abbreviations:

FRAP, Fluorescent Recovery After Photobleaching;

TEM, transendothelial migration;

ECs endothelial cells.

REFERENCE LIST

1. Bullard, D. C., L. Qin, I. Lorenzo, W. M. Quinlin, N. A. Doyle, R. Bosse, D. Vestweber, C. M. Doerschuk, and A. L. Beaudet. 1995. P-selectin/ICAM-1 double mutant mice: acute emigration of neutrophils into the peritoneum is completely absent but is normal into pulmonary alveoli. *J. Clin. Invest* 95: 1782-1788.
2. Gorina, R., R. Lyck, D. Vestweber, and B. Engelhardt. 2014. beta2 integrin-mediated crawling on endothelial ICAM-1 and ICAM-2 is a prerequisite for transcellular neutrophil diapedesis across the inflamed blood-brain barrier. *J. Immunol.* 192: 324-337.
3. Phillipson, M., B. Heit, P. Colarusso, L. Liu, C. M. Ballantyne, and P. Kubes. 2006. Intraluminal crawling of neutrophils to emigration sites: a molecularly distinct process from adhesion in the recruitment cascade. *J. Exp. Med.* 203: 2569-2575.
4. Sligh, J. E., C. M. Ballantyne, S. S. Rich, H. K. Hawkins, C. W. Smith, A. Bradley, and A. L. Beaudet. 1993. Inflammatory and immune responses are impaired in mice deficient in intercellular adhesion molecule 1. *Proceedings of the National Academy of Sciences* 90: 8529-8533.
5. Kadono, T., G. M. Venturi, D. A. Steeber, and T. F. Tedder. 2002. Leukocyte rolling velocities and migration are optimized by cooperative L-selectin and intercellular adhesion molecule-1 functions. *J. Immunol.* 169: 4542-4550.
6. Bourdillon, M. C., R. N. Poston, C. Covacho, E. Chignier, G. Bricca, and J. L. McGregor. 2000. ICAM-1 deficiency reduces atherosclerotic lesions in double-knockout mice (ApoE(-/-)/ICAM-1(-/-)) fed a fat or a chow diet. *Arterioscler. Thromb. Vasc. Biol.* 20: 2630-2635.
7. Etienne-Manneville, S., J. B. Manneville, P. Adamson, B. Wilbourn, J. Greenwood, and P. O. Couraud. 2000. ICAM-1-coupled cytoskeletal rearrangements and transendothelial lymphocyte migration involve intracellular calcium signaling in brain endothelial cell lines. *J. Immunol.* 165: 3375-3383.
8. Greenwood, J., C. L. Amos, C. E. Walters, P. O. Couraud, R. Lyck, B. Engelhardt, and P. Adamson. 2003. Intracellular domain of brain endothelial intercellular adhesion molecule-1 is essential for T lymphocyte-mediated signaling and migration. *J. Immunol.* 171: 2099-2108.
9. Lyck, R., Y. Reiss, N. Gerwin, J. Greenwood, P. Adamson, and B. Engelhardt. 2003. T-cell interaction with ICAM-1/ICAM-2 double-deficient brain endothelium in vitro: the cytoplasmic tail of endothelial ICAM-1 is necessary for transendothelial migration of T cells. *Blood* 102: 3675-3683.
10. Diamond, M. S., D. E. Staunton, S. D. Marlin, and T. A. Springer. 1991. Binding of the integrin Mac-1 (CD11b/CD18) to the third immunoglobulin-like domain of ICAM-1 (CD54) and its regulation by glycosylation. *Cell* 65: 961-971.
11. Otto, V. I., E. Damoc, L. N. Cueni, T. Schurpf, R. Frei, S. Ali, N. Callewaert, A. Moise, J. A. Leary, G. Folkers, and M. Przybylski. 2006. N-glycan structures and N-glycosylation sites of mouse soluble intercellular adhesion molecule-1 revealed by MALDI-TOF and FTICR mass spectrometry. *Glycobiology* 16: 1033-1044.

12. Carman, C. V., C. D. Jun, A. Salas, and T. A. Springer. 2003. Endothelial cells proactively form microvilli-like membrane projections upon intercellular adhesion molecule 1 engagement of leukocyte LFA-1. *J. Immunol.* 171: 6135-6144.

13. Shaw, S. K., S. Ma, M. B. Kim, R. M. Rao, C. U. Hartman, R. M. Froio, L. Yang, T. Jones, Y. Liu, A. Nusrat, C. A. Parkos, and F. W. Luscinskas. 2004. Coordinated Redistribution of Leukocyte LFA-1 and Endothelial Cell ICAM-1 Accompany Neutrophil Transmigration. *The Journal of Experimental Medicine* 200: 1571-1580.

14. Kanters, E., J. van Rijssel, P. J. Hensbergen, D. Hondius, F. P. Mul, A. M. Deelder, A. Sonnenberg, J. D. van Buul, and P. L. Hordijk. 2008. Filamin B mediates ICAM-1-driven leukocyte transendothelial migration. *J Biol. Chem* 283: 31830-31839.

15. van Buul, J. D., M. J. Allingham, T. Samson, J. Meller, E. Boulter, R. Garcia-Mata, and K. Burridge. 2007. RhoG regulates endothelial apical cup assembly downstream from ICAM1 engagement and is involved in leukocyte trans-endothelial migration. *J Cell Biol.* 178: 1279-1293.

16. Martinelli, R., M. Gegg, R. Longbottom, P. Adamson, P. Turowski, and J. Greenwood. 2009. ICAM-1-mediated endothelial nitric oxide synthase activation via calcium and AMP-activated protein kinase is required for transendothelial lymphocyte migration. *Mol. Biol. Cell* 20: 995-1005.

17. Pfau, S., D. Leitenberg, H. Rinder, B. R. Smith, R. Pardi, and J. R. Bender. 1995. Lymphocyte adhesion-dependent calcium signaling in human endothelial cells. *J. Cell Biol.* 128: 969-978.

18. van Rijssel J., J. Kroon, M. Hoogenboezem, F. P. van Alphen, R. J. de Jong, E. Kostadinova, D. Geerts, P. L. Hordijk, and J. D. van Buul. 2012. The Rho-GEF Trio controls leukocyte transendothelial migration by promoting docking structure formation. *Mol. Biol. Cell.*

19. Carpen, O., P. Pallai, D. E. Staunton, and T. A. Springer. 1992. Association of intercellular adhesion molecule-1 (ICAM-1) with actin-containing cytoskeleton and alpha-actinin. *J. Cell Biol.* 118: 1223-1234.

20. Heiska, L., K. Alfthan, M. Gronholm, P. Vilja, A. Vaheri, and O. Carpen. 1998. Association of ezrin with intercellular adhesion molecule-1 and -2 (ICAM-1 and ICAM-2). Regulation by phosphatidylinositol 4, 5-bisphosphate. *J Biol. Chem* 273: 21893-21900.

21. Schaefer, A., J. te Riet, K. Ritz, M. Hoogenboezem, E. C. Anthony, F. P. J. Mul, C. J. de Vries, M. J. Daemen, C. G. Figdor, J. D. Van Buul, and P. L. Hordijk. 2014. Actin-binding proteins differentially regulate endothelial cell stiffness, ICAM-1 function and neutrophil transmigration. *Journal of Cell Science.*

22. Yang, L., J. R. Kowalski, P. Yacono, M. Bajmoczi, S. K. Shaw, R. M. Froio, D. E. Golan, S. M. Thomas, and F. W. Luscinskas. 2006. Endothelial cell cortactin coordinates intercellular adhesion molecule-1 clustering and actin cytoskeleton remodeling during polymorphonuclear leukocyte adhesion and transmigration. *J Immunol.* 177: 6440-6449.

23. Millan, J., L. Hewlett, M. Glyn, D. Toomre, P. Clark, and A. J. Ridley. 2006. Lymphocyte transcellular migration occurs through recruitment of endothelial ICAM-1 to caveola- and F-actin-rich domains. *Nat. Cell Biol.* 8: 113-123.

24. Oh, H. M., S. Lee, B. R. Na, H. Wee, S. H. Kim, S. C. Choi, K. M. Lee, and C. D. Jun. 2007. RKIKK motif in the intracellular domain is critical for spatial and dynamic organization of ICAM-1: functional implication for the leukocyte adhesion and transmigration. *Mol. Biol. Cell* 18: 2322-2335.

25. Jun, C. D., C. V. Carman, S. D. Redick, M. Shimaoka, H. P. Erickson, and T. A. Springer. 2001. Ultrastructure and function of dimeric, soluble intercellular adhesion molecule-1 (ICAM-1). *J. Biol. Chem.* 276: 29019-29027.

26. Yang, Y., C. D. Jun, J. H. Liu, R. Zhang, A. Joachimiak, T. A. Springer, and J. H. Wang. 2004. Structural basis for dimerization of ICAM-1 on the cell surface. *Mol. Cell* 14: 269-276.

27. Barreiro, O., M. Yanez-Mo, M. Sala-Valdes, M. D. Gutierrez-Lopez, S. Ovalle, A. Higginbottom, P. N. Monk, C. Cabanas, and F. Sanchez-Madrid. 2005. Endothelial tetraspanin microdomains regulate leukocyte firm adhesion during extravasation. *Blood* 105: 2852-2861.

28. Barreiro, O., M. Zamai, M. Yanez-Mo, E. Tejera, P. Lopez-Romero, P. N. Monk, E. Gratton, V. R. Caiolfa, and F. Sanchez-Madrid. 2008. Endothelial adhesion receptors are recruited to adherent leukocytes by inclusion in preformed tetraspanin nanoplatforms. *J Cell Biol.* 183: 527-542.

29. Gokhale, N. A., A. Abraham, M. A. Digman, E. Gratton, and W. Cho. 2005. Phosphoinositide specificity of and mechanism of lipid domain formation by annexin A2-p11 heterotetramer. *J. Biol. Chem.* 280: 42831-42840.

3

30. Nagai, T., S. Yamada, T. Tominaga, M. Ichikawa, and A. Miyawaki. 2004. Expanded dynamic range of fluorescent indicators for Ca(2+) by circularly permuted yellow fluorescent proteins. *Proc. Natl. Acad. Sci. U. S. A* 101: 10554-10559.
31. Shen, J., F.W. Luscinskas, A. Connolly, C.F. Dewey Jr., and M.A. Gimbrone Jr. 1992. Fluid shear stress modulates cytosolic free calcium in vascular endothelial cells. *Am J Physiol.* 262, C384-390.
32. Geiger, R.V., and B.C. Berk, R.W. Alexander, R.M. Nerem. 1992, Flow-induced calcium transients in single endothelial cells: spatial and temporal analysis. *J Physiol.* 262, C1411-1417.
33. Dull, R.O., and P.F. Davies.1991. Flow modulation of agonist (ATP)-response (Ca2+) coupling in vascular endothelial cells. *Am J Physiol.* 261, H149-154 (1991).
34. Ziegelstein, R. C., S. Corda, R. Pili, A. Passaniti, D. Lefer, J. L. Zweier, A. Fraticelli, and M. C. Capogrossi. 1994. Initial contact and subsequent adhesion of human neutrophils or monocytes to human aortic endothelial cells releases an endothelial intracellular calcium store. *Circulation* 90: 1899-1907.
35. van Buul, J. D., J. van Rijssel, F. P. van Alphen, M. Hoogenboezem, S. Tol, K. A. Hoeben, M. J. van, E. P. Mul, and P. L. Hordijk. 2010. Inside-out regulation of ICAM-1 dynamics in TNF-alpha-activated endothelium. *PLoS. ONE.* 5: e11336.
36. Macdonald, J. L., and L. J. Pike. 2005. A simplified method for the preparation of detergent-free lipid rafts. *J. Lipid Res.* 46: 1061-1067.
37. Thompson, P. W., A. M. Randi, and A. J. Ridley. 2002. Intercellular adhesion molecule (ICAM)-1, but not ICAM-2, activates RhoA and stimulates c-fos and rhoA transcription in endothelial cells. *J. Immunol.* 169: 1007-1013.
38. Tilghman, R. W., and R. L. Hoover. 2002. E-selectin and ICAM-1 are incorporated into detergent-insoluble membrane domains following clustering in endothelial cells. *FEBS Lett.* 525: 83-87.
39. van Buul, J. D., C. Voermans, d. B. van, V, E. C. Anthony, F. P. Mul, S. van Wetering, C. E. van der Schoot, and P. L. Hordijk. 2002. Migration of human hematopoietic progenitor cells across bone marrow endothelium is regulated by vascular endothelial cadherin. *J. Immunol.* 168: 588-596.
40. Abadier, M., J. N. Haghayegh, A. L. Cardoso, R. Boscacci, D. Vestweber, S. Barnum, U. Deutsch, B. Engelhardt, and R. Lyck. 2015. Cell surface levels of endothelial ICAM-1 influence the transcellular or paracellular T-cell diapedesis across the blood-brain barrier. *Eur. J. Immunol.* 45: 1043-1058.
41. Yang, L., R. M. Froio, T. E. Sciuto, A. M. Dvorak, R. Alon, and F. W. Luscinskas. 2005. ICAM-1 regulates neutrophil adhesion and transcellular migration of TNF-alpha-activated vascular endothelium under flow. *Blood* 106: 584-592.
42. Sans, E., E. Delachanal, and A. Duperray. 2001. Analysis of the roles of ICAM-1 in neutrophil transmigration using a reconstituted mammalian cell expression model: implication of ICAM-1 cytoplasmic domain and Rho-dependent signaling pathway. *J. Immunol.* 166: 544-551.
43. Huang, A. J., J. E. Manning, T. M. Bandak, M. C. Ratau, K. R. Hanser, and S. C. Silverstein. 1993. Endothelial cell cytosolic free calcium regulates neutrophil migration across monolayers of endothelial cells. *J. Cell Biol.* 120: 1371-1380.
44. Kielbassa-Schnepp, K., A. Strey, A. Janning, L. Missiaen, B. Nilius, and V. Gerke. 2001. Endothelial intracellular Ca2+ release following monocyte adhesion is required for the transendothelial migration of monocytes. *Cell Calcium* 30: 29-40.
45. Su, W. H., H. I. Chen, J. P. Huang, and C. J. Jen. 2000. Endothelial [Ca(2+)](i) signaling during transmigration of polymorphonuclear leukocytes. *Blood* 96: 3816-3822.
46. Etienne, S., P. Adamson, J. Greenwood, A. D. Strosberg, S. Cazaubon, and P. O. Couraud. 1998. ICAM-1 signaling pathways associated with Rho activation in microvascular brain endothelial cells. *J. Immunol.* 161: 5755-5761.
47. Hixenbaugh, E. A., Z. M. Goeckeler, N. N. Papaiya, R. B. Wysolmerski, S. C. Silverstein, and A. J. Huang. 1997. Stimulated neutrophils induce myosin light chain phosphorylation and isometric tension in endothelial cells. *American Journal of Physiology - Heart and Circulatory Physiology* 273: H981-H988.
48. Saito, H., Y. Minamiya, S. Saito, and J. i. Ogawa. 2002. Endothelial Rho and Rho kinase regulate neutrophil migration via endothelial myosin light chain phosphorylation. *Journal of Leukocyte Biology* 72: 829-836.
49. Wojciak-Stothard, B., L. Williams, and A. J. Ridley. 1999. Monocyte adhesion and spreading on human endothelial cells is dependent on Rho-regulated receptor clustering. *J. Cell Biol.* 145: 1293-1307.

4

F-actin-rich contractile endothelial pores prevent vascular leakage during leukocyte diapedesis through local RhoA signaling

Niels Heemskerk[1], Lilian Schimmel[1], Chantal Oort[1], Jos van Rijssel[1], Taofei Yin[2], Bin Ma[3], Jakobus van Unen[4], Bettina Pitter[5], Stephan Huveneers[1], Joachim Goedhart[4], Yi Wu[2], Eloi Montanez[5], Abigail Woodfin[3], Jaap D. van Buul[1,*]

[1]Department of Molecular Cell Biology, Sanquin Research and Landsteiner Laboratory, Academic Medical Centre, University of Amsterdam, 1066CX, the Netherlands. [2]Center for Cell Analyses and Modelling, University of Connecticut Health Centre, Farmington, CT 06032. [3]Centre for Microvascular Research, William Harvey Research Institute, Barts and The London School of Medicine and Dentistry, Queen Mary, University of London, Charterhouse Square, London, EC1M 6BQ. [4]Swammerdam Institute for Life Sciences, University of Amsterdam, Amsterdam, the Netherlands. [5]Walter-Brendel-Center of Experimental Medicine Ludwig-Maximilians University Marchioninistr. 27 81377 Munich, Germany.

[*] Corresponding author:
Jaap D. van Buul; Sanquin Research and Landsteiner Laboratory; Academic Medical Centre; University of Amsterdam; Address: Plesmanlaan 125, 1066 CX, Amsterdam, the Netherlands. Phone: +31-20-5121219; Fax: +31-20-5123310; E-mail j.vanbuul@sanquin.nl

Abstract

During immune surveillance and inflammation, leukocytes exit the vasculature through transient openings in the endothelium without causing plasma leakage. However, the exact mechanisms behind this intriguing phenomenon are still unknown. Here, we report that maintenance of endothelial barrier integrity during leukocyte diapedesis requires local endothelial RhoA cycling. Endothelial RhoA depletion in vitro or Rho inhibition in vivo provokes neutrophil-induced vascular leakage that manifests during the physical movement of neutrophils through the endothelial layer. Local RhoA activation initiates the formation of contractile F-actin structures that surround emigrating neutrophils. These structures that surround neutrophil-induced endothelial pores prevent plasma leakage through actomyosin-based pore confinement. Mechanistically, we found that the initiation of RhoA activity involves ICAM-1 and the Rho GEFs Ect2 and LARG. Additionally, regulation of actomyosin-based endothelial pore confinement involves ROCK2b, but not ROCK1. Thus, endothelial cells assemble RhoA-controlled contractile F-actin structures around endothelial pores that prevent vascular leakage during leukocyte extravasation.

INTRODUCTION

The clinical signs of inflammation, redness, heat, swelling and pain are caused by the acute inflammatory response including increased vasodilatation, enhanced microvascular permeability and leukocyte recruitment. During inflammation the endothelial barrier becomes more permissive for large molecules, leading to local plasma proteins leakage and edema formation. Whether leukocyte transendothelial migration (TEM) directly causes increased microvascular permeability has been controversial for decades. Certain studies suggested leukocyte adhesion and transmigration to be the critical events leading to tissue damage and organ failure during inflammation and ischemia-reperfusion [1,2] since neutrophil depletion or CD11/CD18 blocking antibodies have been shown to attenuate vascular injury under these circumstances [2-5]. However, when microvascular permeability was measured simultaneously with leukocyte-endothelial interactions, local plasma leakage sites were often different from those of leukocyte adhesion or transmigration [6-11]. Recently, it has been shown that intravenous injection of TNF-α caused significant leukocyte adhesion and transmigration but did not affect basal microvessel permeability [12]. Moreover, several studies have shown that the timing of leukocyte adhesion and transmigration are not well linked with the evoked permeability change during acute inflammation [13-16]. Most of the abovementioned studies are descriptive, molecular evidence for the uncoupling between leukocyte TEM and vascular permeability has been recently shown by Wessel and colleagues. They mechanistically uncoupled leukocyte extravasation and vascular permeability by showing that opening of endothelial junctions in those distinct processes are controlled by different tyrosine residues of VE-cadherin *in vivo* [17]. However, how the endothelium maintains a tight barrier during leukocyte transendothelial migration is still unknown.

Here, we investigate the mechanism by which endothelial cells (ECs) prevent vascular leakage during leukocyte TEM. We examine the correlation between neutrophil extravasation and the evoked permeability changes during acute inflammation *in vitro* and *in vivo*. Spatiotemporal RhoA activation during leukocyte crossing is measured using a recently developed RhoA biosensor [19]. In addition, we use fluorescently-tagged Lifeact and Lifeact-EGFP transgenic knock-in mice to investigate endothelial filamentous (F)-actin dynamics in remodeling junctions during neutrophil diapedesis *in vitro* and *in vivo*, respectively. We show that endothelial pore restriction limits vascular leakage during leukocyte extravasation which is driven by a basolateral actomyosin-based structure that requires local endothelial RhoA activation.
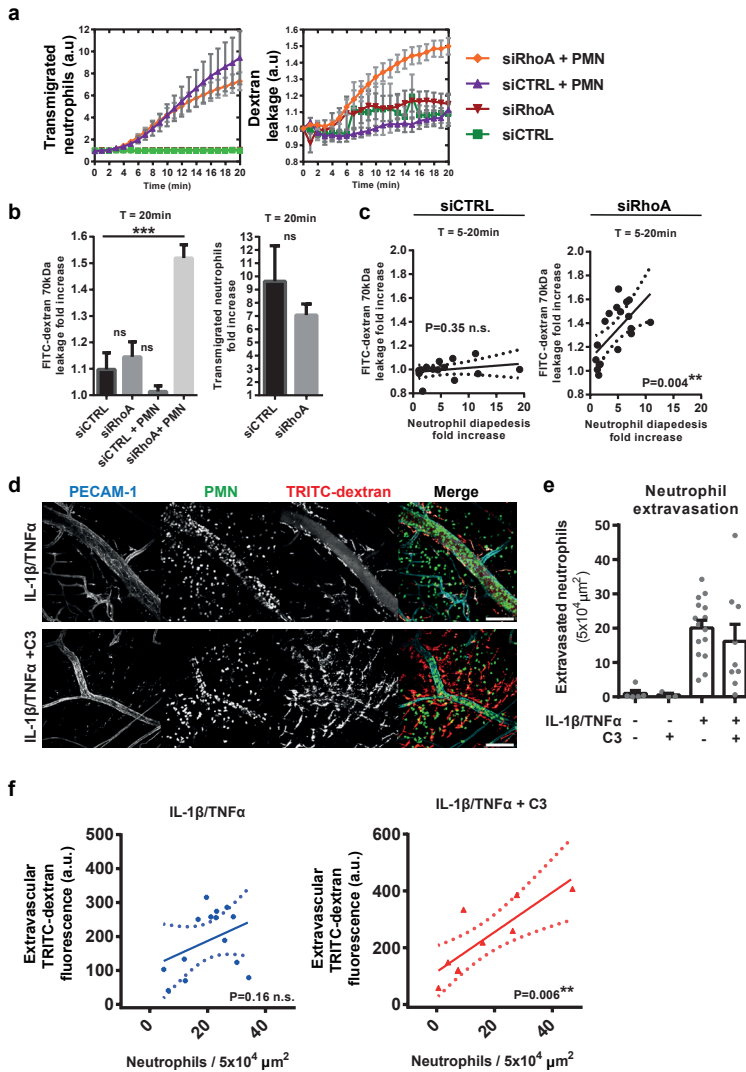
Figure 1 Impaired endothelial RhoA function results in increased vascular leakage during leukocyte diapedesis *in vivo*. (**a**) Extravasation kinetics of calcein-red labelled neutrophils and FITC-dextran through TNF-α treated ECs cultured on 3μm pore permeable filters. Neutrophils transmigrated towards a C5a chemotactic gradient in the lower compartment. Four conditions were tested; RhoA depletion (EC) + neutrophils (Orange line), control + neutrophils (purple line), RhoA depletion (EC) only (red line) and control only (green line). (**b**) Quantification of FITC-dextran and neutrophil extravasation after 20 minutes of neutrophil transmigration. (**c**) Correlation analysis of dextran and neutrophil extravasation kinetics through control and RhoA depleted ECs. (**d**) Confocal intravital microscopy of 20-80 μm diameter cremasteric venulesin LysM-GFP mice (green neutrophils) immunostained *in vivo* for EC junctions by intrascrotal injections of fluorescent-labeled PECAM-1 (blue) and stimulated for four hours with IL-1β and TNF-α only, or with Rho-inhibitor (C3). A second dose of Rho inhibitor was given intrascrotally and TRITC-dextran (40 kDa) was injected intravenously at T = 2 hours

RESULTS

RHOA CONTROLS VASCULAR LEAKAGE DURING LEUKOCYTE DIAPEDESIS

To investigate the molecular mechanism that controls endothelial barrier function during neutrophil TEM, we simultaneously measured neutrophil transmigration kinetics and FITC-dextran leakage across TNF-α -stimulated human umbilical vein endothelial cells (ECs) towards a C5a gradient, for 60 minutes. Neutrophil transmigration across control ECs was associated with minimal FITC-dextran leakage (Fig. 1a). Increasing neutrophil numbers in the upper compartment up to 10-fold did not induce FITC-dextran leakage, indicating that ECs maintained their barrier function, despite increased numbers of transmigrating neutrophils (Supplementary Fig. 1a). To investigate the functional role of RhoA in EC barrier maintenance during neutrophil TEM, we depleted RhoA using siRNA (Supplementary Fig. 1b). We found that endothelial RhoA depletion increased FITC-dextran leakage during neutrophil extravasation whereas minimal FITC-dextran leakage was measured during neutrophil crossing through control ECs (Fig. 1a,b). Correlation analysis showed that the increase in FITC-dextran leakage was highly correlated to neutrophil transmigration (Fig. 1c). Note that endothelial RhoA depletion did not alter FITC-dextran leakage under basal conditions which was comparable to control EC (Fig. 1a,b). Moreover, endothelial resistance measured under physiological flow conditions was significantly reduced during transmigration of neutrophils across Rho-inhibited endothelium (Supplementary Fig. 1c). We next investigated the role of RhoA in EC barrier maintenance during neutrophil TEM *in vivo*. Vessel permeability was monitored by TRITC-dextran leakage into the cremaster of C57BL/6 WT or LysM-GFP mice during IL-1β and TNF-α -stimulated neutrophil recruitment. Intrascrotal administration of anti-PECAM-1 labelling antibody resulted in a strong labelling of EC junctions in cremasteric venules (Fig. 1d). Administration of IL-1β and TNF-α

and allowed to circulate until T = 4 hours. Scale bar 100μm. (**e**) Neutrophil extravasation in animals left unstimulated (control), stimulated with C3 alone, IL-1β/TNF-α treated, IL-1β/TNF-α treated + C3 or IL-1β/TNF-α treated + neutrophil depletion. (**f**) Correlation analysis of dextran and neutrophil extravasation kinetics in animals stimulated with IL-1β/TNF-α alone or with IL-1β/TNF-α treated + C3. *** $P < 0.001$ control versus RhoA depleted HUVEC (ANOVA) or $P = 0.3504$ control versus RhoA depleted HUVEC (Student's t-test) (**b**). $r = 0.2547$ $P = 0.359$ (Pearson correlation) transmigrated neutrophils versus FITC-dextran leakage in control HUVECs or $r = 0.6345$ ** $P < 0.01$ (Pearson correlation) transmigrated neutrophils versus FITC-dextran leakage in RhoA depleted HUVECs (**c**). $P = 0.4230$ IL-1β/TNFα versus IL-1β/TNF-α + C3 (Student's t-test) (**e**). $r = 0.8258$ ** $P < 0.01$ (Pearson correlation) transmigrated neutrophils versus FITC-dextran leakage in IL-1β/TNF-α + Rho inhibitor treated mice (**f**). Data are from three experiments (**a-c**) or are representative of five to thirteen (**d-e**) or nine (**f**) independent experiments (**d-f**; one mouse per experiment; error bars (**a-c,e and f**), s.e.m.).

enhanced leakage of intravenous TRITC-dextran into the interstitium and neutrophil recruitment into the cremaster (Fig. 1d and Supplementary Fig. 1d). Rho inhibitor I (C3)-treated animals showed similar extravasated neutrophil levels, however TRITC-dextran leakage in those animals was highly increased compared to IL-1β and TNF-α administration alone (Fig 1d-e). Although no change in neutrophil extravasation was measured in the presence or absence of C3, we cannot exclude that the inhibitor affects other cells. Neutrophil extravasation and TRITC-dextran leakage in WT mice were not correlated in individual mice, although there was an overall association between extravasation and permeability, whereas the two processes in Rho-inhibited animals showed a highly significant correlation (Fig. 1f). Animals treated with C3 alone showed unaltered basal vascular permeability (Supplementary Fig. 1e). Thus, neutrophil extravasation and evoked changes in vascular permeability during inflammation are not correlated. However, when endothelial RhoA is inhibited, neutrophil diapedesis provokes vascular leakage, suggesting that endothelial RhoA is required to maintain a tight EC barrier during leukocyte diapedesis *in vivo*.

SPATIOTEMPORAL RHOA ACTIVATION DURING LEUKOCYTE DIAPEDESIS

To examine spatiotemporal RhoA activation in ECs during EC barrier maintenance associated with neutrophil TEM, we used a recently developed FRET-based RhoA biosensors called the Dimerization Optimized Reporter for Activation (DORA) RhoA sensors (Fig. 2a) [19]. DORA RhoA biosensors design were based on the published RhoA biosensor [20]. The ON-state Fluorescence Resonance Energy Transfer (FRET) efficiency of the GTPase was improved through modelling of the fluorescent protein dimers and the GTPase-effector domain complexes. Stable α-helical repeats from ribosomal protein L9, rather than an unstructured linker, were inserted between the fluorescent proteins to disrupt dimerization and diminish FRET efficiency in the inactive state (Fig. 2a). As a control, DORA RhoA mutant Protein kinase N (PKN) was developed to report misalignment of Cerulean3 (Cer3) and Venus image before and after image registration, motion artefacts or pH changes affecting the sensors fluorescent proteins. Glutamine substitution for a leucine at position 59 in the PKN domain prevents PKN binding to activated RhoA [21]. The characterizations of both DORA RhoA biosensors are described in online methods (Supplementary Fig. f,2 and 3a). From these validation experiments, we conclude that the DORA RhoA biosensor accurately reports RhoA dynamics in ECs downstream from endogenous stimuli such as thrombin (Fig. 2b and Supplementary Fig. 1f).

To study spatiotemporal RhoA activation in ECs during neutrophil TEM, we expressed the DORA RhoA biosensor in ECs and investigated

RhoA activation following neutrophil extravasation under physiological flow conditions. Important to note, Venus and Cer3 emission were simultaneously recorded utilizing a double camera system since sequential image acquisition resulted in motion artefacts induced by migrating leukocytes displacing fluorescent signals in ECs. We found unaltered RhoA biosensor activation during neutrophil rolling and crawling over the endothelium (Fig. 2c,g). Also RhoA activation during the initial opening of EC junctions was found to be unaltered (Fig. 2d). However, RhoA biosensor activity in the endothelium was locally increased at sites were neutrophils breeched the endothelium, between the first and second minute of neutrophil diapedesis (Fig. 2d-f, Supplementary Fig. 2d and Supplementary Movie 1). Based on the normalized ratiometric imaging and the relative displacement of the sensor, the data showed a 1.2-fold increase in FRET ratio upon diapedesis, comparable to what has been observed during RhoA activation after thrombin stimulation (Fig. 2h,i). The negative control DORA RhoA biosensor (mutant PKN) showed no change in FRET during leukocyte diapedesis (Supplementary Fig. 3b,c and Supplementary Movie 2). Importantly, expressing the DORA RhoA biosensors in ECs did not interfere with neutrophil TEM. Thus, endothelial RhoA is transiently and locally activated during the final stage of neutrophil diapedesis, but not during crawling or opening of endothelial junctions, indicating a role for local RhoA activity in EC barrier maintenance during the final stage of neutrophil extravasation.

F-actin-rich endothelial pores during diapedesis

To investigate endothelial F-actin dynamics during neutrophil diapedesis, we transfected ECs with GFP- and/or mCherry-tagged Lifeact [22]. It is important to note that phalloidin staining to visualize F-actin cannot be used to investigate endothelial actin structures that are in close proximity of transmigrating leukocytes, since F-actin in both leukocytes and ECs are visualized by phalloidin staining, making it impossible to discriminate between the two (Supplementary Fig. 3d). Transmigrating neutrophils initiated small endothelial pores in the endothelial lining. To study those endothelial pores at high resolution, transmigrating neutrophils were fixed with formaldehyde when partly breeched the endothelium. Confocal microscopy imaging and 3-D reconstruction showed that ECs assembled F-actin-rich structures around endothelial pores through which neutrophils transmigrated, both during transcellular and paracellular migration (Fig. 3a and Supplementary Movie 3-5). During paracellular migration, the junctional protein VE-cadherin was distributed to the endothelial pore margins (Fig. 3a). Interestingly, using ECs expressing either Lifeact-GFP or Lifeact-mCherry, we found that paracellular pores were formed by at

least two ECs. At the structures apical site, filopodia-like protrusions were found whereas at the basolateral site, a cortical actin-ring appeared during leukocyte crossing (Fig. 3b-d). In contrast to VE-cadherin distributed to the pores margins, the junctional protein PECAM-1 was localized around the basolateral F-actin-ring and distributed to apical protrusions surrounding migrating leukocytes during trans-and paracellular migration.
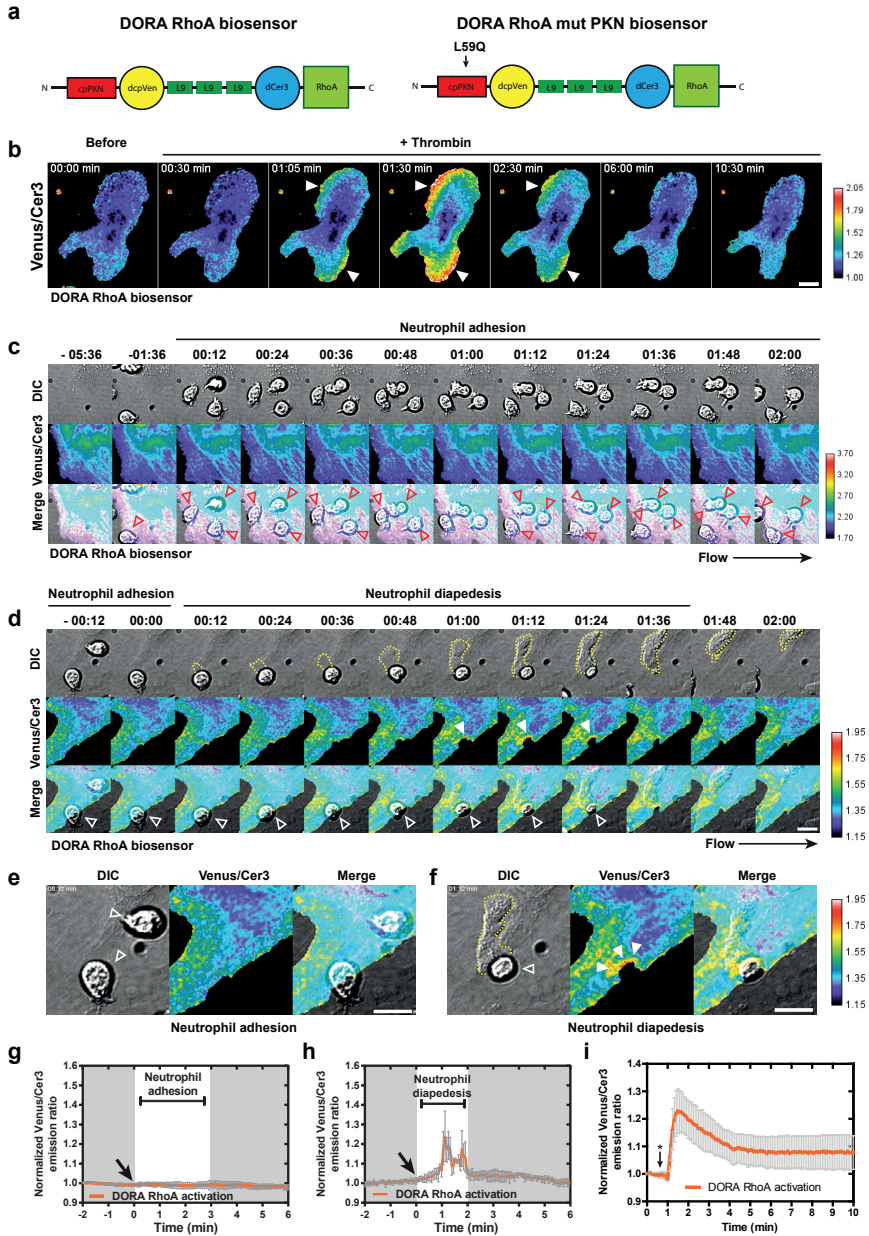
(Supplementary Fig. 3e,f). Moreover, we found that the adhesion molecule ICAM-1 was localized in the apical protrusions at endothelial pores (Supplementary Fig. 4a). We found that approximately 90% of all neutrophils and monocytes used the paracellular route, whereas approximately 10% migrated transcellular, in line with the migratory preference for neutrophils and monocytes found *in vivo* [23] (Fig. 3e). Note that all these diapedesis events by either neutrophils or monocytes were associated with basolateral F-actin-ring formation around endothelial pores (Fig. 3e). Within the paracellular route of migration, leukocyte transmigration through a bi-cellular or a multi-cellular junction was approximately 50 % (Supplementary Fig. 4b). In conclusion, ECs assemble F-actin-rich ring-like structures around endothelial pores through which neutrophils and monocytes transmigrate. This data indicates that maintenance of EC barrier function during leukocyte diapedesis involves actin cytoskeleton strengthening around endothelial pores. Basolateral F-actin ring formation may tighten the endothelial barrier during neutrophil crossing, making the leukocyte-induced endothelial pore impermeable for macromolecules.

Figure 2 Spatiotemporal RhoA activation during neutrophil TEM. Endothelial RhoA is locally and transiently activated during neutrophil extravasation (**a**) Schematic illustration of the DORA RhoA sensor design containing Rho effector PKN (red), circular permutated Venus (yellow), structured linker protein L9 (green), circular permutated Cer3 (blue) and RhoA GTPase (green),left panel. Right panel shows the DORA RhoA mutant PKN biosensor that was developed as a negative control biosensor, the glutamine was substituted for the leucine at position 59 in the PKN domain. This mutation prevents binding of PKN to activated RhoA. (**b**) Time-lapse Venus/Cer3 ratio images of DORA RhoA biosensor simultaneously recorded with an epifluorescent microscope showing spatiotemporal RhoA activation upon thrombin treatment (1U perml) in HUVECs. Filled arrows indicate RhoA activation. Scale bar, 10µm. Calibration bar shows RhoA activation (Red) relative to basal RhoA activity (Blue). (**c**) Epi-fluorescent live-cell imaging of HUVEC expressing the DORA RhoA biosensor during neutrophil adhesion under physiological flow conditions (0.8dyne per cm²). Red open arrows indicate adherent neutrophils. Scale bar 10µm. Calibration bar shows RhoA activation (red) relative to basal RhoA activity (blue). (**d**) Epi-fluorescent live-cell imaging of HUVECs expressing the DORA RhoA biosensor during neutrophil TEM. Time-lapse images of DIC (upper) Venus/Cer3 ratio images of DORA RhoA biosensor (middle) and Merge (bottom) during leukocyte diapedesis. Open arrows indicates adherent neutrophil at the apical side of the endothelium. Filled arrows indicate local RhoA activation during neutrophil diapedesis. Scale bar, 10µm. (**e**) Detailed zoom of RhoA activation during neutrophil adhesion (open arrows) prior diapedesis at time point t = -00:12 minutes. (**f**) Detailed zoom of local RhoA activation during neutrophil transmigration at time point t = 01:12 minutes. Filled arrows indicate local RhoA activation during neutrophil diapedesis. Scale bar, 10µm. (**g**) Quantification of temporal RhoA activation during multiple neutrophil adhesion events starting at time zero (arrow). (**h**) Quantification of temporal RhoA activation during multiple neutrophil transmigration events starting at time zero (arrow). (**i**) Quantification of DORA RhoA biosensor activation after thrombin treatment (1U permL) in HUVEC. Asterisk indicates thrombin addition. Data represents mean and s.e.m of seven experiments (**g**) five experiments (**h**). ten experiments (**i**).
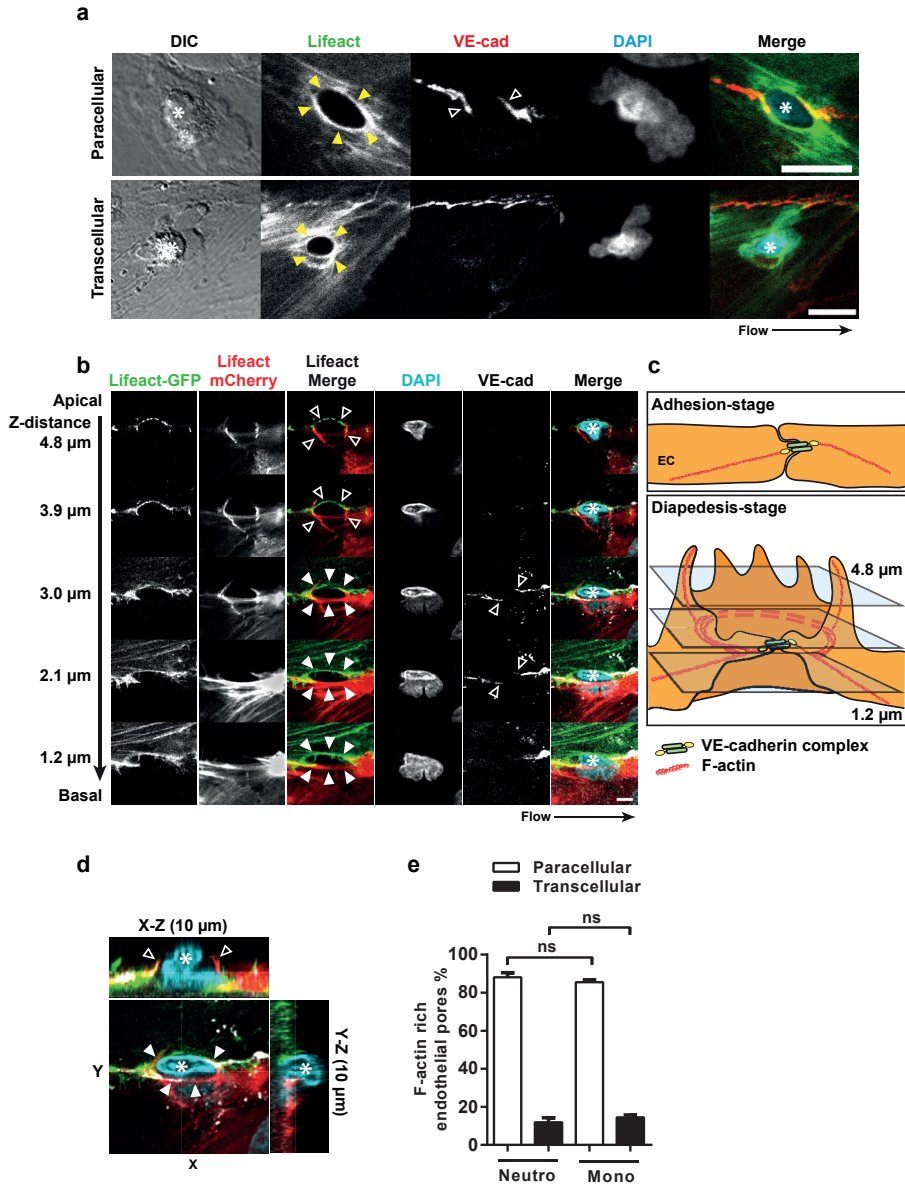
Figure 3 ECs assemble F-actin rich ring-like structures around transmigrating leukocytes. (**a**) Confocal imaging of para- and transcellular migrating leukocytes through Lifeact-GFP expressing HUVECs. Filled arrows indicate EC F-actin (Lifeact in green) assembly around extravasating leukocytes. Open arrows indicate VE-cadherin (directly labeled Alexa-647 antibody in red) distribution to the F-actin structure sites during paracellular diapedesis. Asterisks indicate extravasating leukocyte (DAPI in blue) in DIC. Flow speed 0.8 dyne per cm^2. Scale bar 5µm. (**b**) Confocal imaging showing a Z-stack of Lifeact-GFP and Lifeact-mCherry positive endothelial membrane structures from apical to basal plane. Open arrows indicate filopodia-like protrusions at the apical site of the structure.

F-ACTIN-RICH ENDOTHELIAL PORES ARE CONFINED IN SIZE

Electron microscopy studies showed that ECs maintain intimate contact with transmigrating neutrophils during the entire transmigration process [15,24]. To examine the dynamic contact between ECs and extravasating neutrophils, we examined F-actin-enriched endothelial pore shape and size in relation to neutrophil size. Real-time recordings of transmigrating neutrophils through ECs expressing GFP-tagged Lifeact showed increased F-actin assembly around endothelial pores (Supplementary Movie 6).

The kinetics of neutrophil diapedesis is on average two minutes and can be distinguished into early, mid and late diapedesis based on endothelial pore size and neutrophil morphology (Fig. 4a-c). Endothelial pore formation started when neutrophils partly breeched the endothelium, defined as early diapedesis. Following neutrophil diapedesis, most endothelial pores are maximal enlarged one minute after transmigration was initiated, defined as mid diapedesis (Fig. 4a-c). Subsequently, the endothelial pore is closed in conjunction with transmigrating neutrophils until completely under the endothelium, a stage defined as late diapedesis (Fig. 4a-c). Real-time imaging of neutrophil diapedesis under physiological flow conditions showed that neutrophil total surface area prior to TEM was roughly 100 µm^2, which was reduced to less than 20 µm^2 to fit the confined gap in the endothelium that had a maximal inner-surface area of 19 µm^2 (Fig. 4b,c). To investigate the morphology of *de novo* formed F-actin-positive rings and F-actin-positive apical protrusions that surround endothelial pores during neutrophil TEM, we trapped neutrophils at different stages of diapedesis. Interestingly, *de novo* formed F-actin-positive rings surrounding endothelial pores were found throughout all diapedesis steps, but not during neutrophil adhesion or crawling steps (Fig. 4d and Supplementary Fig. 4c). Quantification of endothelial pore size showed significant larger pores during mid diapedesis than during early and late diapedesis when pores open and close respectively (Fig. 4d). We next measured, the pore-size width, length and height of F-actin-

Filled arrows indicate the cortical actin-ring at the basolateral site that appeared during leukocyte crossing. Asterisk indicates extravasating leukocyte (DAPI in blue). Scale bar, 5µm. (**c**) Cartoon of endothelium during basal-stage and leukocytes diapedesis showing filopodia-like protrusions and the basolateral F-actin ring. (**d**) X-Z (10 µm) and Y-Z (10 µm) projections of confocal Z-stack shown in Fig. 1b. (**e**) Quantification of percentage F-actin rich endothelial pores associated with neutrophil and monocyte extravasation during para- and transcellular migration. Statistical significance was tested with ANOVA. Data are representative for three independent experiments (**a-e**) with 37-65 transmigration events per group (error bars (**e**), s.e.m).

rich endothelial pores surrounding transmigrating neutrophils and monocytes. On average, endothelial pores are 4 µm wide, 6 µm in length and mostly oval-shaped for all leukocytes migrating through the cell-cell junctions (Supplementary Fig. 4d and 4f). Additionally, we found that only during diapedesis approximately 40% of the endothelial pores contained F-actin-rich apical protrusions (Fig. 4d). No such structures were detected during the crawling step. These structures reached a maximal height of 6-7 µm (Supplementary Fig. 4e). Transcellular pores were found to be more round or circular shaped and had an average circularity of about 1.3 according to the circularity index (Supplementary Fig. 4f). Endothelial pore sizes showed remarkably little variation, despite leukocyte size, type or transmigration route (Fig. 4e). Thus, endothelial pores induced by extravasating neutrophils and monocytes are confined in size and close directly behind transmigrated cells. Active endothelial pore confinement and pore closure corroborated earlier findings that showed intimate contact between neutrophils and ECs during the entire TEM process and provides an explanation for limited transendothelial escape of macromolecules during neutrophil crossing.

Pore confinement and pore closure requires endothelial RhoA

Our data showed that increased endothelial RhoA activity during neutrophil TEM corresponded to endothelial pore restriction and closure during mid and late diapedesis. To investigate whether RhoA regulates endothelial pore confinement, we silenced endothelial RhoA using siRNA. RhoA was successfully depleted as shown by Western blot analysis (Supplementary Fig.5a). Confocal microscopy showed that RhoA depletion in ECs reduced Lifeact-GFP accumulation around endothelial pores, whereas Lifeact-GFP in the apical protrusions was still present (Fig. 5a). Basal F-actin rings in RhoA-depleted ECs were significantly reduced compared to control conditions (Fig. 5b). Endothelial RhoA depletion had no effect on the formation of F-actin-rich apical protrusions (Fig. 5b).

Quantification of endothelial pore size showed that in the absence of RhoA, endothelial pores were not only larger than endothelial pores formed in control ECs, but also did not close properly (Fig. 5c).Note that neutrophil adhesion and transmigration under physiological flow conditions were unaltered in RhoA-depleted ECs (Fig. 5d). To study if VE-cadherin signalling regulates endothelial pore size, we depleted VE-cadherin and analysed endothelial pore size. However, VE-cadherin depletion had no effect on endothelial pore size (Fig. 5e and Supplementary Fig. 5b-d). In conclusion, RhoA facilitates endothelial pore confinement and pore closure during leukocyte diapedesis.
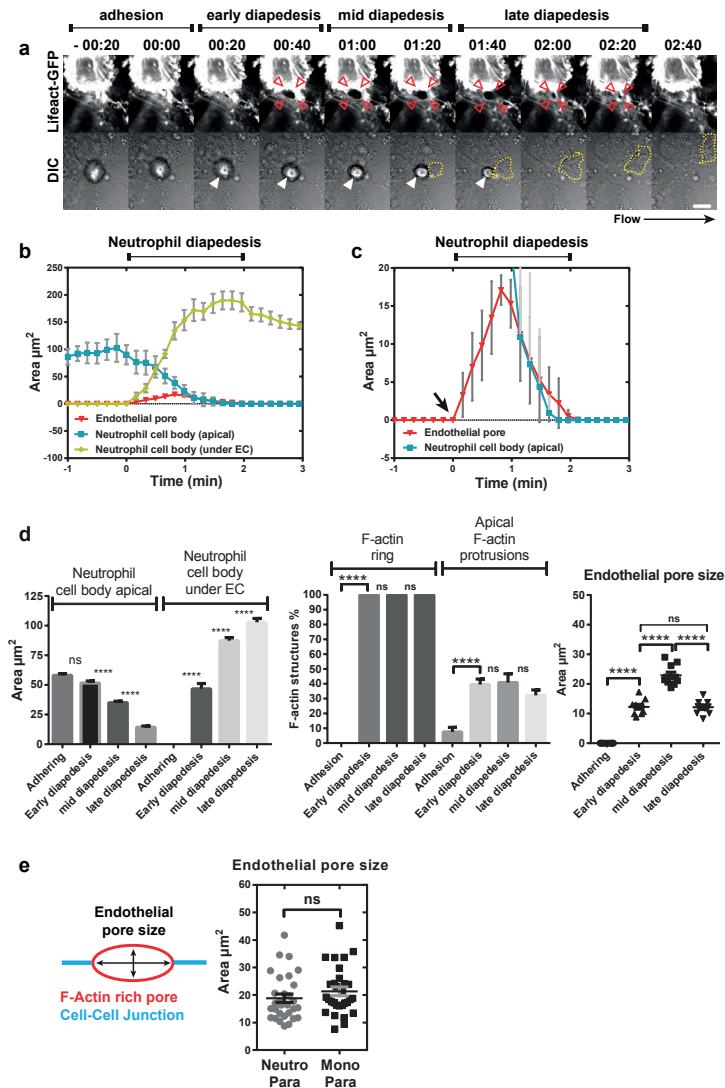
Figure 4 Endothelial pores formed during para- and transcellular leukocyte transmigration are confined in size. (**a**) Epi-fluorescent live-cell imaging of ECs expressing Lifeact-GFP. Red open arrows indicate F-actin-rich endothelial pore formation during leukocyte diapedesis under physiological flow conditions (0.8 dyne per cm^2). Filled arrows indicate extravasating leukocyte in DIC. Dashed lines indicates neutrophil localization under the endothelium. Scale bar, 10μm. (**b**, **c**) Quantification of size changes occurring in the neutrophil cell body and endothelial pore during neutrophil diapedesis. Endothelial pore size (red), neutrophil cell body apical (blue) and neutrophil cell body under EC (yellow), diapedesis starts at time zero. (**d**) Quantification of Neutrophil size, F-actin positive ring structures, F-actin positive apical protrusions and endothelial pore size. (**e**) Quantification of endothelial pore size for neutrophils and monocytes during paracellular migration. **** $P < 0.0001$ (ANOVA). Data are representative of four independent experiments (**d**, **e**) with 40 transmigration events per group. Data in (**b, c**) are representative of 10 transmigration events (error bars (**b-e**), s.e.m).

91
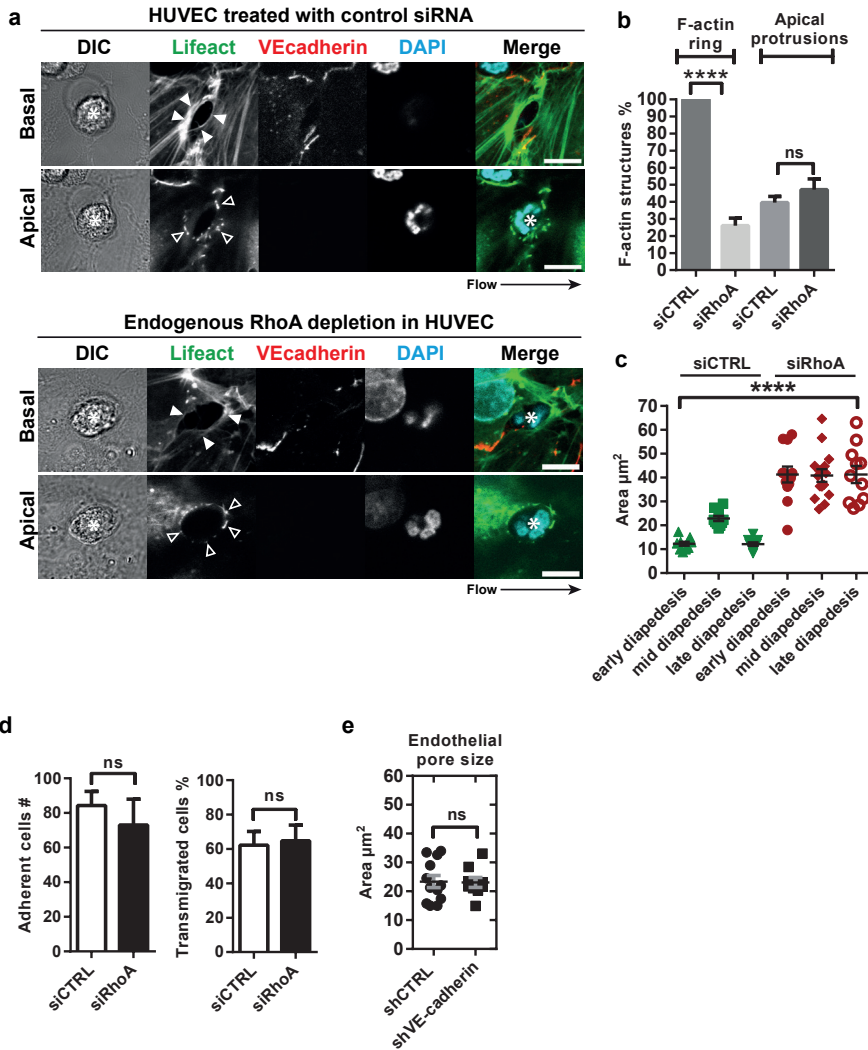
Figure 5 RhoA signalling is required for endothelial pore confinement. (**a**) Confocal imaging of paracellular migrating neutrophils through Lifeact-GFP expressing HUVECs after 72 hours transfection with control siRNA (upper panel) or RhoA siRNA (lower panel) under physiological flow conditions (0.8 dyne per cm^2). Open arrows and filled arrows indicate filopodia-like protrusions at the apical site and the cortical F-actin-ring at the basolateral site of the endothelial pore, respectively. Asterisk indicates extravasating neutrophil (DAPI in blue). VE-cadherin (Red). Scale bar, 5µm. (**b**) Quantification of F-actin-positive ring structures and F-actin-positive apical protrusions in control versus RhoA depleted ECs. (**c**) Quantification of endothelial pore size during early, mid and late diapedesis. (**d**) Quantification of neutrophil adhesion and diapedesis through TNF-α treated ECs under physiological flow conditions after 72 hours transfection with control siRNA (open bar) or RhoA siRNA (filled bar). (**e**) Quantification of endothelial pore size in control versus VE-cadherin depleted HUVECs. **** $P < 0.0001$ (ANOVA). Data are representative of four independent experiments (**a-e**) with > 12 transmigration events per group (error bars (**c**, **e**), s.e.m.).

Pore confinement is driven by actomyosin contractility

To investigate how RhoA regulates endothelial pore confinement during leukocyte diapedesis, we examined RhoA effector myosin II activation. To study myosin II activation we locally measured myosin light chain (MLC) phosphorylation on position Thr18 and Ser19. Immunofluorescent staining of pMLC showed an asymmetric phosphorylation pattern in F-actin-rich endothelial pores surrounding transmigrating neutrophils (Fig. 6a). MLC was particularly phosphorylated at cortical actin bundles as part of the F-actin ring (Fig. 6a and Supplementary Fig. 5e). Note that the uropod of the neutrophil is positive for MLC phosphorylation, most likely to retract its tail during transmigration [25]. In contrast to local MLC phosphorylation in control ECs, endothelial pores in RhoA-deficient ECs were enlarged and negative for local phospho-MLC (Supplementary Fig. 5e). In addition, we quantified Lifeact-GFP distribution around endothelial pores and found asymmetric F-actin distribution around endothelial pores, indicative of increased tension (Fig. 6b). To corroborate our findings *in vivo*, we studied F-actin localization during leukocyte diapedesis in retinal vasculature of Lifeact-EGFP-transgenic knock-in mice [26]. Lifeact-EGFP expression in the retinas of these mice is largely restricted to the endothelium and this allowed us to properly visualize F-actin in ECs *in situ* [26,27]. We found that endothelial pores induced by transmigrating neutrophils (isolectin B4-positive [28]) were surrounded by Lifeact-EGFP-positive rings in retinal ECs (Fig. 6c). Quantification of these rings showed that endothelial pore size *in vivo* was comparable to endothelial pores measured in the *in vitro* set-up (compare Fig. 6d and 4e). Lifeact was present in the basolateral ring and in apical protrusions that surrounded transmigrating neutrophils (Supplementary Fig. 5f). These data showed that apical membrane protrusions *in vivo* are rich for F-actin and surround adherent leukocytes. Next, we examined local MLC phosphorylation in WT mice during IL-1β and TNF-α-induced neutrophil recruitment in cremasteric venules. PECAM-1 was used as a marker to visualize endothelial pores *in vivo* [23] (Fig. 6e). In line with our *in vitro* findings, endothelial pores in mouse cremaster venules showed asymmetric MLC phosphorylation (Fig. 6f,g). In order to address the role of ROCK in endothelial pore confinement we depleted the ROCK isoforms ROCK1 and ROCK2b in endothelial cells and examined vascular permeability during neutrophil diapedesis. In line with RhoA inhibition, silencing ROCK 1 and ROCK2b did not prevent the adhesion or transmigration of neutrophils through the endothelial monolayer (Supplementary Fig. 6a,b). Basal endothelial barrier function in ROCK1 or ROCK2b deficient ECs was not affected. However, neutrophil diapedesis through ROCK2b, but not ROCK1 deficient ECs elicited increased endothelial permeability up to a twofold (Supplementary Fig. 6a,b). These
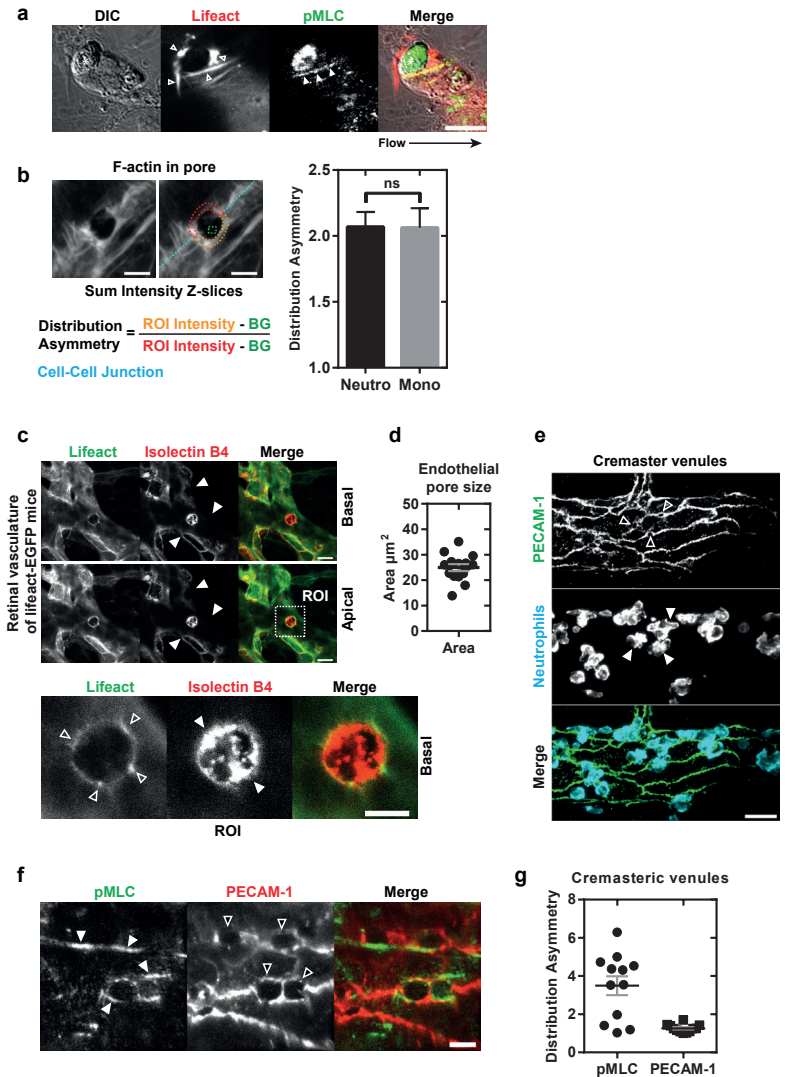
Figure 6 Endothelial pore confinement is driven by actomyosin contractility. (**a**) Immunofluorescence analyses of MLC phosphorylation during neutrophil transmigration. Open and filled arrows indicate Lifeact-mCherry (red) and MLC phosphorylation (green) localization respectively during neutrophil transmigration under physiological flow conditions (0.8 dyne per cm^2). Asterisk indicates extravasating leukocyte in DIC. Scale bar, 10 μm. (**b**) Quantification of F-actin distribution in endothelial pores surrounding transmigrating neutrophils and monocytes. Maximum intensity projection of F-actin in the endothelial pore was used to quantify F-actin distribution surrounding transmigrating leukocytes. Distribution asymmetry is defined by the ratio of region of interest ROI-1 and ROI-2 corrected for background. Scale bar, 5μm. (**c**) Confocal imaging of F-actin dynamics during leukocyte diapedesis in retina vasculature of Lifeact-EGFP C57BL6 mice. Filled arrows indicate the vasculature of mice retina, highly expressing Lifeact-GFP. Zoom of ROI, open arrows indicate the Lifeact-EGFP (green)-positive endothelial pore, filled arrows

findings may indicate that endothelial pore confinement is mediated through ROCK2b but not ROCK1.Altogether, local accumulation of F-actin and MLC phosphorylation is associated with neutrophil diapedesis *in vitro* and *in vivo,* suggesting that endothelial pore confinement is driven by local actomyosin contractility.

ENDOTHELIAL PORE CONFINEMENT REQUIRES ICAM-1, LARG AND ECT2

To investigate the signalling events upstream from RhoA, we focused on the involvement of guanine-nucleotide exchange factors (GEF) and performed a GEF screen that included: p115RhoGEF, Ect2 and LARG. Depletion of endothelial LARG together with Ect2 increased endothelial pore size, whereas depletion of LARG, p115 and Ect2 alone was not sufficient (Fig. 7a and Supplementary Fig. 6c). Quantification of endothelial pore size at different stages of diapedesis showed that endothelial pores in LARG- and Ect2-depleted endothelium were enlarged during early and mid-diapedesis but had no effect on endothelial pore closure (Fig. 7b). Under these conditions the number of F-actin-positive rings and F-actin-positive apical protrusions was unaltered (Fig. 7c). Enlarged endothelial pores in Ect2- and LARG-deficient ECs showed increased endothelial permeability during neutrophil diapedesis, whereas basal EC barrier function was not affected (Fig. 7d and Supplementary Fig. 6d-f). Neutrophil diapedesis through Ect2- and LARG-deficient ECs was slightly reduced (Fig. 7d and Supplementary Fig. 6d). To study LARG and Ect2 recruitment to the intracellular tail of PECAM-1 or ICAM-1 we performed clustering experiments induced by anti-ICAM-1 or anti-PECAM-1 coated beads. We found thatLARG and Ect2 are recruited to the intracellular tail of ICAM-1 (Supplementary Fig. 6g).Whereas PECAM-1recruited only LARG but not Ect2 to its intracellular tail upon clustering (Supplementary Fig. 6h). To investigate if ICAM-1 or PECAM-1 initiate and coordinate local RhoA activation and endothelial pore confinement during neutrophil diapedesis, we depleted ICAM-1 and PECAM-1 in ECs and

indicate transmigrating neutrophil. Scale bar, 5μm. (**d**) Quantification of endothelial pore size in retina vasculature. (**e**) Confocal imaging of PECAM-1 in cremasteric venules during TNF-α and IL-1β induced neutrophil recruitment. Open arrows indicate PECAM-1 positive endothelial pores that surround extravasating neutrophils (filled arrows). Scale bar, 20μm. (**f**) IF analyses of MLC phosphorylation during neutrophil transmigration into the cremaster of C57BL6 mice. Filled and open arrows indicate phospo-MLC and PECAM-1 localization to endothelial pores, respectively. Scale bar, 5μm. (**g**) Quantification of pMLC and PECAM-1 localization in endothelial pores. We quantified MLC phosphorylation defined as distribution asymmetry. The distribution asymmetry uses the intensity of one ROI vs another ROI as indicated in Figure 6b. Because MLC may occur at different heights within the pore we used max projection for this analysis. Data are representative of three independent experiments (**a-g**) with > 12 transmigration events per group (error bars (**b**, **d**, **g**), s.e.m.).
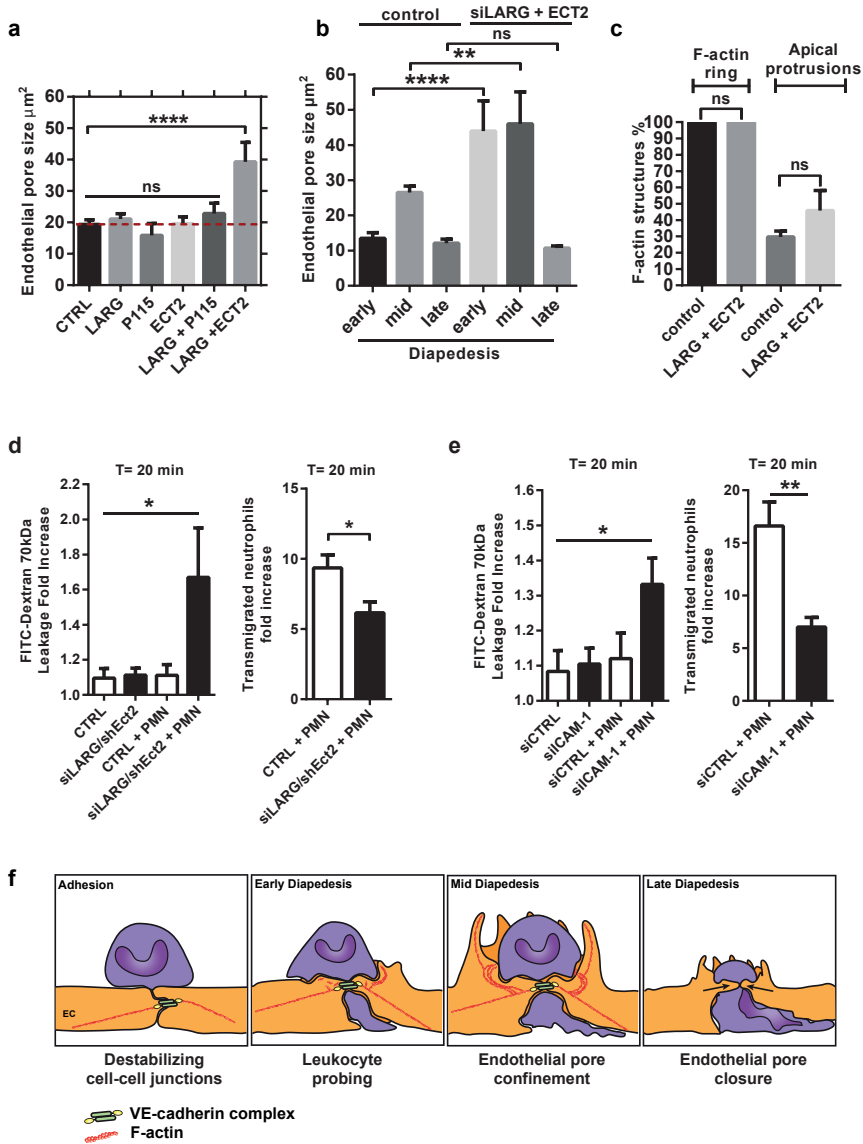
Figure 7 ICAM-1 regulates endothelial pore confinement through recruitment of the Rho GEFs LARG and Ect2. (**a**) Quantification of endothelial pore size in LARG, p115RhoGEF or Ect2 depleted ECs. (**b**) Quantification of endothelial pore size during early, mid and late diapedesis in control versus LARG + Ect2 depleted ECs. (**c**) Quantification of F-actin-positive ring structures and F-actin-positive apical protrusions in control versus LARG + Ect2 depleted ECs.(**d**) Quantification of FITC-dextran and neutrophil extravasation after 20 minutes of neutrophil transmigration through control and Ect2/LARG (**d**) or ICAM-1 deficient ECs (**e**). (**f**) Model of endothelial pore formation. Adherent leukocytes destabilizing cell-cell junctions subsequently insert small pseudopodia between transient openings in the endothelium (leukocyte probing) during early diapedesis. The next step (mid diapedesis) involves local

examined the extravasation of calcein-red-labeled-neutrophils and FITC-dextran across EC and measured endothelial pore size. We found that neutrophil transmigration through ICAM-1 deficient ECs compromised the endothelial barrier (Fig. 7e and Supplementary Fig. 7a-c), whereas PECAM-1 depletion did not alter endothelial pore size or vascular leakage (Supplementary Fig. 7d-e). ICAM-1 and PECAM-1 depletion alone had no effect on endothelial permeability (Fig. 7e and Supplementary Fig. 7d). In agreement with the existing literature endothelial ICAM-1 depletion significantly reduced the number of transmigrated neutrophils (Fig.7e). Neutrophil diapedesis through PECAM-1 deficient endothelial cells showed no reduction in transmigration numbers (Supplementary Fig. 7d). These data point out an important role for ICAM-1, Ect2 and LARG signalling in controlling RhoA-mediated endothelial pore confinement and EC barrier protection during neutrophil diapedesis.

DISCUSSION

Leukocytes that cross the endothelium induce large endothelial gaps without provoking leakage of plasma into the underlying tissue. However, the mechanisms behind this intriguing phenomenon are unclear. The present study shows how ECs limit vascular leakage during leukocyte TEM. We found that RhoA-mediated F-actin rings contribute to endothelial pore confinement that maintains endothelial barrier integrity during leukocyte diapedesis. Neutrophil diapedesis through ICAM-1, Ect2/LARG and RhoA-deficient ECs provokes vascular leakage that was highly correlated with neutrophil breeching events. Mechanistically, we found that the initiation of RhoA activity involves ICAM-1 and the Rho GEFs Ect2 and LARG. Additionally, we found that the regulation of actomyosin-based endothelial pore confinement involves ROCK2b, but not ROCK1. Our work identifies a novel mechanism that maintains endothelial barrier integrity during leukocyte extravasation which is driven by a basolateral actomyosin-based structure that requires spatiotemporal RhoA cycling (Fig. 7f).

and transient RhoA activation that mediates endothelial pore confinement through the formation of a *de novo* basolateral F-actin ring and actomyosin contractility. Finally, persistent actomyosin contractility closes the endothelial pore behind transmigrating leukocytes. ICAM-1 is involved in the regulation of endothelial pore confinement through recruitment of the Rho GEFs LARG and Ect2. Basolateral F-actin ring formation and actomyosin contractility tightens the endothelial barrier during leukocyte diapedesis, making the leukocyte-induced endothelial pore impermeable for macromolecules.**** $P < 0.0001$ (ANOVA) (**a-c**).** $P < 0.01$ (ANOVA) (**b**) * $P < 0.05$ (ANOVA) (**e,d**).* $P < 0.05$ control versus siLARG/shEct2 (**d**) ** $P < 0.01$ control versus siICAM-1 (**e**) (Student's t-test). Data are representative of three independent experiments (**a-e**) with > 12 transmigration events per group (**a-c**) (error bars (**a-e**), s.e.m).

Inflammation-driven leukocyte recruitment and vascular permeability are separable events [7,8,17]. In line with these observations, we discovered that during the TEM process endothelial RhoA plays a central role in EC barrier maintenance but is redundant for leukocyte transmigration. In agreement with previous reports, blocking RhoA activity or depleting RhoA in ECs did not perturb adhesion [29] or transmigration [30]. In contrast to the general concept that RhoA activation is required for leukocyte adhesion and opening of endothelial junctions [31-35], we found that endothelial RhoA was locally and transiently activated during the diapedesis step and not during neutrophil crawling, firm adhesion or opening of endothelial junctions prior to leukocyte extravasation. These processes require a separate, RhoA-independent mechanism that allows leukocyte-EC adhesion or opening of endothelial junctions. In agreement with our findings, for both transmigration routes, endothelial pore opening is in part mediated by mechanical forces that are generated by migrating leukocytes. Polarized actin polymerization in the leukocyte elicits pulling and pushing forces that support the movement of immune cells through the confined endothelial pore [36,37]. ICAM-1 is known to mediate leukocyte-EC interactions, and crosslinking ICAM-1 using ICAM-1-coated beads or ICAM-1 antibodies results in increased RhoA activation suggesting a role for ICAM-1-mediated RhoA activation in leukocyte adhesion [32,38-41]. However, based on the spatiotemporal activation of RhoA, we suggest that ICAM-1-mediated RhoA signaling specifically occurs during the diapedesis step, in agreement with our data that shows ICAM-1 enrichment only at diapedesis sites. PECAM-1 was also detected at sites of diapedesis, for either paracellular or transcellular migration. Recently, mechanical tension exerted on ICAM-1 and also PECAM-1 enhanced RhoA activation and MLC phosphorylation in ECs that was dependent on the recruitment of the RhoGEF LARG and ICAM-1 clustering [41,42]. Our work shows that ICAM-1 clustering indeed promotes the recruitment of LARG and we additionally found Ect2 to be recruited upon ICAM-1 clustering. Depletion of ICAM-1- and Ect2/LARG in ECs compromised the endothelial barrier during neutrophil diapedesis. Indicating that the ICAM-1-LARG/Ect2 signaling axis is likely to be activated upstream from RhoA activation, in order to regulate *de novo* F-actin rearrangements, endothelial confinement and barrier protection during neutrophil crossing. Together these data suggests that leukocytes exert mechanical forces on endothelial adhesion molecules that modulate endothelial F-actin cytoskeleton through mechanotransduction that may cause endothelial confinement.

The relationship between Ect2 and actomyosin contractility has been clearly established by several studies. For instance, Ect2 has been described to be involved in RhoA activation and contractile ring formation

during cytokinesis [43]. In addition, it has been shown that the molecular pathways that regulates local RhoA activation during cytokinesis are also used to control RhoA dynamics at the zonula adherens in interphase cells [44]. Although no proof for a role of Ect2 in endothelial junction regulation has been described we can speculate that Ect2 mediates similar functions in ECs, regulating actomyosin contractility around the pore. The latter is probable, since depletion of LARG and Ect2 simultaneously results in larger pores without affecting the number of F-actin rings. In agreement with this hypothesis overall endothelial pore size in RhoA-deficient endothelial cells was increased due to the lack of basal F-actin ring formation. In addition we observed that RhoA-deficient endothelial cells were unable to phosphorylate MLC near endothelial pores. Surprisingly, the length-to-width aspect ratio between paracellular and transcellular pores was found to be different, however this was not due a difference in nuclear size, shape or composition between neutrophils and monocytes. We speculate that in case of paracellular migration the amount of VE-cadherin disassembly at the pores margins may regulate pore size, which may affect the length/width ratio or circularity. In case of transcellular migration mechanical forces from the endothelium might counteract leukocyte induced forces from all directions forcing a circular passageway. A physical explanation for circular transcellular passages may also explained by cellular dewetting [45]. Despite different length-to-width ratio of the pores, the overall pore size is constant independent of leukocyte type, or transmigration route. This may indicate that the contractile forces generated during endothelial pore formation are high enough to counteract the mechanical forces generated by transmigrating leukocytes. Alternatively, the RhoA-induced basolateral F-actin ring itself may also add as a limiting factor for pore confinement on top of the actomyosin based contractility. Endothelial pore confinement is probably not restricted to neutrophil and monocyte diapedesis but may also occur during the diapedesis of other immune cells such as T-lymphocytes. Additional research is required to investigate this hypothesis. Surprisingly, we found that VE-cadherin depletion did not affect endothelial pore integrity, despite the prominent VE-cadherin localization at the pores margins. It is known that other junctional molecules such as N-cadherin may take over the function of VE-cadherin when VE-cadherin is depleted [46]. The fact that we see unaltered pore morphology in VE-cadherin deficient cells makes it conceivable that other molecules like N-cadherin take over the function of VE-cadherin controlling the integrity of the endothelial pore at its margins. It is evident that VE-cadherin plays a dominant role in endothelial barrier formation and regulation of leukocyte traffic through the endothelial barrier. For instance, locking VE-cadherin junctions reduces the number emigrating

leukocytes [47] and the phosphorylation of VE-cadherin at Y731 induced by adherent leukocytes prior diapedesis is a necessity for junctional destabilization and paracellular diapedesis [17]. We cannot exclude a supportive role for VE-cadherin in endothelial pore integrity, but we can exclude a direct role for VE-cadherin as a signaling molecule being involved in controlling and coordinating of endothelial pore confinement. Whether other junctional proteins such as JAM-A or CD99, that act distally from ICAM-1, and signal to RhoA to prevent leakage is currently unknown [23,48]. We found that many F-actin rings comprise apical membrane protrusions. These projections, also known as "*docking structures*" or "*transmigratory cups*", have been suggested to anchor endothelial adhesion receptors and therefore control leukocyte adhesion [30,39,49-52]. However, the biological function of these structures is still under debate. Interestingly, we found F-actin rings associated with leukocyte diapedesis that contained no apical protrusions suggesting that directional neutrophil diapedesis can occur through other mechanisms than "apical projection"-guidance for instance transendothelial migration-promoting endothelial chemokines that are locally released within the endothelial pore [53]. In agreement with studies showing that apical projection assembly requires RhoG and Rac1 but not RhoA activity [39,54], we still observed apical membrane protrusions around migrating leukocytes upon RhoA depletion, whereas the F-actin rings were significantly decreased. Suggesting that the basolateral F-actin ring and not the apical protrusions in the endothelial pore contribute to vascular leakage prevention during TEM. Interestingly, in drosophila, similar actomyosin networks have been found to rapidly close multicellular-wounds by actomyosin contraction [55]. Studies that investigated the mechanisms by which ECs repair gaps in the endothelial monolayer, show that mechanical induced micro-wounds in the endothelium are healed by ventral lamellipodia, a mechanism that may also be involved in the closure of leukocyte induced endothelial pores [56]. Our data shows that RhoA-mediated contractile force generation responsible for endothelial pore restriction precedes ventral lamellipodia formation. Moreover, RhoA-mediated pore constriction in ECs seems to be specific for the closure of leukocyte induced endothelial pores, whereas ventral lamellipodia are also observed in maintenance of basal junctional integrity [57]. Based on electron microscopy studies, it has been suggested that the intimate contact between neutrophils and ECs during the entire transendothelial migration process limits leakage of plasma proteins. Moreover, several studies showed that ECs reseal the endothelial barrier prior to or in conjunction with neutrophils penetrating the basal lamina [15,58]. In agreement with these ultra-structural studies we found that endothelial pores closed prior to or in conjunction with neutrophils that fully breeched the endothelial

lining. In the context of EC barrier maintenance it is well conceivable that endothelial pore confinement and closure directly prevents vascular leakage during leukocyte diapedesis whereas ventral lamellipodia restore junctional homeostasis after leukocyte crossing. Endothelial LSP1 has been implicated in a role for "dome" formation and controlling permeability during TEM [58] and has been found to be activated downstream from ICAM-1 clustering [59]. Together, this may open up the possibility that ICAM-1 clustering activates RhoA through LSP1. However, future experiments should show if this signaling axis indeed is operational during TEM.

In conclusion, we have discovered that local RhoA-mediated F-actin rings in the endothelial lining prevent vascular leakage during leukocyte diapedesis. Elucidating the molecular and cellular mechanisms of barrier maintenance during leukocyte diapedesis may have implications for the development of new therapies to restore normal homeostatic junctional remodeling to counteract vascular dysfunction during chronic inflammation.

4

METHODS

DNA AND RNA CONSTRUCTS

The Dimerization Optimized Reporter for Activation (DORA) RhoA and DORA RhoA mutant PKN biosensors were a very kind gift of Yi Wu (University of Connecticut Health centre, Farmington, USA). Briefly, circular permutated Protein kinase N (PKN) effector of RhoA coupled to dimeric circular permutated Venus is linked via a ribosomal protein-based linker (L9H) with dimeric Cerulean3 (Cer3) coupled to RhoA. The DORA RhoA sequence within a pTriEx-HisMyc backbone is cpPKN(S69-H97-GSG-S14-R68)-KpnI-GS-dcpVen-L9Hx3-BamHI-dCer3(G229)-NheI-RhoA-WT-HindIII. The DORA RhoA mutant PKN sequence within a pTriEx-HisMyc backbone is cpPKN (S69-H97-GSG-S14-R68, L59Q)-KpnI-GS-dcpVen-L9Hx3-BamHI-dCer3(G229)-NheI-RhoA-WT-HindIII. The Leucine (L) on position 59 in the PKN domain of the RhoA control biosensor is substituted for a glutamine (Q). The H1R, p63-RFP and mRFP-RhoGDI-α (pcDNA 3.1) were a kind gift of Joachim Goedhart (Swammerdam Institute for Life Sciences, University of Amsterdam, Amsterdam, the Netherlands). pLenti-Lifeact-mCherry, pLenti-Lifeact-GFP, were a kind gift of Stephan Huveneers (Sanquin, Amsterdam, the Netherlands). shRNA in pLKO.1 targeting VE-cadherin (12) B6 (TRCN 54090), GEF-H1 (TRCN 3174), GEF-H1 (TRCN 3175), p115RhoGEF (TRCN 33567), and Ect2 (TRCN 47686) were purchased from sigma Aldrich mission library. siRNA targeting RhoA (sc-29471) (working concentration 50 nM), ICAM-1 sc-29354 (50 nM), PECAM-1 sc-29445 (50 nM), LARG sc-41800 (50 nM), Rock-1 (sc-29473) (50 nM), Rock-2b (sc-29474) (50 nM),and scrambled non-silencing siRNA were purchased from (Santa Cruz Biotechnology, Santa Cruz, CA).

ANTIBODIES

Rabbit antibody against GEF-H1 (55B6) (Cat #4076) (1:1000 for WB), phospho Myosin light chain Thr18/Ser19 (Cat #3674) (1:100 for IF), p115RhoGEF (D25D2) (Cat #3669) (1:1000 for WB), RhoA (67B9) (Cat #2117X) (1:1000 for WB) and CD31 (PECAM-1) (89C2) (Cat #3528) (1:1000 for WB) were purchased from Cell signaling (BIOKE). Polyclonal rabbit antibody against Ect2 (Cat# 07-1364) (1:1000 for WB) was purchased from Millipore. Polyclonal goat antibody against LARG (Cat#AF4737) (1:1000 for WB) was purchased from R&D systems. Alexa Fluor 405 Phalloidin (1:100 for IF) was purchased from Promokine (Cat# PK-PF405-7-01). Polyclonal goat antibody against VE-cadherin (C-19) (Cat# SC-6458) (1:1000 for WB), Rock-2 (C-20) sc-1851 (1:1000 for WB), Rock-1 (H-85) sc-5560 (1:1000 for WB) were purchased from Santa Cruz (Bio-Connect). Polyclonal rabbit antibody against ICAM-1 (Cat #SC-7891) (1:1000 for WB) was purchased

from Santa Cruz Biotechnology. Monoclonal mouse antibody against Filamin A (Cat #MCA464S) (1:1000 for WB) was purchased from Serotec. Monoclonal mouse Alexa Fluor 647 VE-cadherin (55-7H1) (Cat# 560411) (1:100 for IF) and Alexa Fluor 488 PECAM-1 (Cat# 555445) (1:100 for IF) were purchased from Becton Dickinson. Monoclonal mouse antibody against Actin (AC-40) (Cat# A3853) (1:1000 for WB) was purchased from Sigma. The Alexa Fluor 405 goat anti-rabbit IgG (Cat# A31556) (1:100 for IF), Alexa Fluor 647 chicken anti-goat IgG (Cat# A21469) (1:100 for IF), Alexa Fluor 488 chicken anti-rabbit IgG (Cat# A21441) (1:100 for IF) and Texas red 568 Phalloidin (Cat #T7471) (1:100 for IF) were purchased from Invitrogen. Secondary HRP-conjugated goat anti-mouse, swine anti-rabbit antibodies (1:3000 for WB) were purchased from Dako (Heverlee, Belgium). Hoechst 33342 (H-1399) (1:50 for IF) was purchased from Molecular probes (Life Technologies). All antibodies were used according to manufacturer's protocol.

CELL CULTURES AND TREATMENTS

Pooled Human umbilical vein ECs (HUVECs) purchased from Lonza (P938, Cat # C2519A), were cultured on fibronectin-coated dishes in EGM-2 medium, supplemented with singlequots (Lonza, Verviers, Belgium) HUVECs were cultured until passage 9. HEK-293T were maintained in Dulbecco's Modified Eagle Medium (DMEM) (Invitrogen, Breda, The Netherlands) containing 10% (v/v) heat-inactivated fetal calf serum (Invitrogen, Breda, The Netherlands), 300 mg/ml L-glutamine, 100 U/ml penicillin and streptomycin and 1x sodium pyruvate (Invitrogen, Breda, The Netherlands). HeLa cells (American Tissue Culture Collection: Manassas, VA, USA) were cultured using Dulbecco's Modified Eagle Medium (DMEM) supplied with Glutamax, 10% FBS, Penicillin (100 U/ml) and Streptomycin (100µg/ml). Cells were cultured at 37°C and 5% CO_2. HUVECs were treated with 1U/ml thrombin (Sigma-Aldrich, St. Louis, USA) for periods as indicated, pre-treated with 10 ng/ml recombinant Tumor-Necrosis-Factor (TNF)-α (PeproTech, Rocky Hill, NJ) 24 hours before each leukocyte TEM experiment, For Rho inhibition cells were pre-incubated with cell-permeable Rho inhibitor I (C3) (Cytoskeleton, Cat# CT04) for 3 hours. Cells were transfected with the expression vectors according to the manufacturer's protocol with Trans IT-LT1 (Myrus, Madison, WI, USA). Lentiviral constructs were packaged into lentivirus in Human embryonic kidney (HEK)-293T cells by means of third generation lentiviral packaging plasmids (Dull et al., 1998; Hope et al 1990). Lentivirus containing supernatant was harvested on day 2 and 3 after transfection. Lentivirus was concentrated by Lenti-X concentrator (Clontech, Cat# 631232). Transduced target cells were used for assays after 72 hours. Cells were transfected with siRNA according to manufacturer's protocol using INTERFERin (Polyplus).

HeLa cell were transfected with Lipofectamine and imaged the next day. HeLa cells were treated with 100 µM histamine (Sigma-Aldrich, St. Louis, USA) and 10 µM Pyrilamine (mepyramine) (Sigma-Aldrich, St. Louis, USA) for periods as indicated.

NEUTROPHIL AND MONOCYTE ISOLATION

Polymorphonuclear (PMN) neutrophils and monocytes were isolated from whole blood derived from healthy donors and were conducted under the rules and legislation in place within the Netherlands. The rules and legislations are based on The Declaration of Helsinki (informed consent for participation of human subjects in medical and scientific research) and guidelines for Good Clinical Practice. Whole blood was diluted (1:1) with 5% (v/v) TNC in PBS. Diluted whole blood was pipetted carefully on 12.5 ml Percoll (room temperature) 1.076 g/ml. Tubes were centrifuged (Rotanta 96R) at 2000 rpm, slow start, low brake for 20 minutes. Ring fraction containing lymphocytes and monocytes was collected and further processed as indicated below*. After erythrocyte lysis in an ice-cold isotonic lysis buffer (155 mM NH_4CL, 10 mM $KHCO_3$, 0.1 mM EDTA, pH7.4 in Milli-Q(Millipore), neutrophils were centrifuged at 1500 rpm for five minutes at 4°C, incubated once with lysis buffer for 5 minutes on ice, centrifuged again at 1500 rpm for five minutes at 4°C, washed once with PBS, centrifuged again at 1500 rpm for five minutes at 4°C and resuspended in HEPES medium (20 mM HEPES, 132 mM NaCl, 6 mM KCL, 1 mM $CaCL_2$, 1 mM $MgSO_4$, 1.2 mM K_2HPO_4, 5 mM glucose (all from Sigma-Aldrich), and 0.4 % (w/v) human serum albumin (Sanquin Reagents), pH7.4) and kept at room temperature for not longer than four hours until use. *Ring fraction was washed three times with MACS buffer (0.5% (v/v) BSA in PBS, 2mM EDTA in PBS). Ring fraction was centrifuged at 1700 rpm for 7 minutes at 4°C and low break, and resuspended in 100 µl MACS buffer and incubated with 5 µl CD14 microbeads (Miltenyi biotec, # 130-050-201) for 30 minutes at 4°C and subsequently washed with 5 ml MACS buffer, centrifuged and resuspended in 1ml MACS buffer. LS columns (Miltenyi biotec, # 130-042-401) were placed in QuadroMACS separator (Miltenyi biotec, # 130-090-976) and cells were subsequently washed three times with 1 ml MACS buffer. Column was removed from the QuadroMACS separator and monocytes were collected in a collection tube. Neutrophil and monocyte counts were determined by cell counter (Casey).

FITC-DEXTRAN PERMEABILITY ASSAY

200,000 ECs were cultured in fibronectin (FN) treated 24 well cell culture inserts (Corning FluoroBlok, Falcon, 3.0 µm pore size # 351151)

and treated with TNF-α overnight. 30 µg FITC-dextran (70 kDa) (Sigma) in HEPES medium (20 mM HEPES, 132 mM NaCl, 6 mM KCL, 1 mM CaCL$_2$, 1 mM MgSO$_4$, 1.2 mM K$_2$HPO$_4$, 5 mM glucose (all from Sigma-Aldrich), and 0.4 % (w/v) human serum albumin (Sanquin Reagents), pH7.4) was added to the upper and 0.1 nM C5a (Sigma C-5788) in HEPES medium was added to the lower compartment. FITC-dextran and calcein red-orange (Molecular probes C34851) labeled neutrophil (200,000 cells) extravasation was monitored simultaneously for a period of 60 minutes with an interval of 1 minute by an Infinite F200 pro plate reader (TECAN) at 37 ˚C. EX BP 485/9 and EM BP 535/20 was used to measure FITC-dextran kinetics. EX BP 535/9 and EM BP 595/20 was used to measure neutrophil (calcein red-orange) transmigration kinetics.

NEUTROPHIL AND MONOCYTE TEM UNDER PHYSIOLOGICAL FLOW

HUVECs were cultured to 70% confluence in FN-coated 6 well plate, and transfected with different expression vectors (e.g. DORA RhoA biosensor) according to the manufacturer's protocol with Trans IT-LT1 (Myrus, Madison, WI, USA) for 24 hours or transduced with expression vectors in lentivirus (e.g. pLenti-Lifeact-mCherry) for 72 hours. HUVECs were cultured in a FN-coated ibidi µ-slide VI$^{0.4}$ (ibidi, Munich, Germany) the day before the experiment was executed and stimulated overnight with TNF-α (10 ng/ml). Freshly isolated neutrophils and monocytes were resuspended at 1x10^6 cells/ml in HEPES medium and were incubated for 30 minutes at 37ºC. Cultured HUVECs in ibidi flow chambers were connected to a perfusion system and exposed to 0.5 ml/minute HEPES shear flow for 10 minutes (0.8 dyne/cm^2). Actual levels of injected neutrophils ranged between 0.5-2*10^6 dependent on the donor and activity of the neutrophils. Actual levels of monocytes ranged between 1.5-2.2*10^6. Neutrophils or monocytes were subsequently injected into the perfusion system and real-time leukocyte-endothelial interactions were recorded for 20 minutes by a Zeiss Observer Z1 microscope using a 40x NA 1.3 oil immersion objective or samples were fixed for immunofluorescent staining and subsequent analysis. All live imaging was performed at 37˚C in the presence of 5% CO$_2$. Transmigrated neutrophils were distinguished from those adhering to the apical surface of the endothelium by their transition from bright to phase-dark morphology. Percentage adherent or transmigrated neutrophils were manually quantified using the ImageJ plug-in Cell Counter (type 1, adherent cells, type 2, transmigrated cells).

CONFOCAL LASER SCANNING MICROSCOPY

Cells were cultured in FN-coated ibidi µ-slide VI$^{0.4}$ (ibidi, Germany) and transfected or stimulated as indicated. After treatment, cells were washed

with cold PBS, containing 1 mM $CaCl_2$ and 0.5 mM $MgCl_2$, and fixed in 4% (v/v) formaldehyde for 10 minutes. After fixation, cells were permeabilized in PBS supplemented with 0.5% (v/v) Triton X-100 for 10 minutes followed by a blocking step in PBS supplemented with 2.5% (w/v) BSA. Cells were incubated with primary and secondary antibodies and after each step washed with PBS. Z-stack image acquisition was performed on a confocal laser scanning microscope (LSM510/Meta; Carl Zeiss Micro-Imaging) using a voxel size of 0.06x0.06x0.48 µm and a 63x NA 1.4 oil immersion objective. Following acquisition, the sequences of Z-stack images were analyzed off-line using Imaris which renders the optical sections into 3D models enabling analysis of leukocyte-endothelial interaction dynamics.

QUANTIFICATION ENDOTHELIAL PORE STRUCTURES

Real-time endothelial pore dynamics in HUVECs expressing Lifeact-GFP was analyzed by ImageJ. Three parameters were scored; the area of the neutrophil cell body (luminal site), the area of the pore, and the area of the neutrophil cell body under the endothelium (abluminal site). The area (μm^2) of each parameter was measured manually by drawing a ROI resembling the parameter (e.g pore size) and measured in ImageJ using analyze measure. Endothelial pore sizes of fixed HUVECs were measured by drawing a ROI resembling various parameters (width, length, height, circularity, and pore size). Length of the endothelial pore was defined as the total distance of the pore parallel to the junction and width was defined as the total distance perpendicular to the junction. Circularity of the pore is defined by the length over width ratio. Pore size was defined as the total surface area of endothelial pore. Total F-actin in the pore (sum intensity Z-slices) was divided in two equal ROI. Distribution asymmetry was defined by ROI (1)-BG over ROI (2)-BG ratio. Leukocytes migrating through the EC body not interrupting junctional VE-cadherin were scored as transcellular migration, whereas leukocyte migrating between ECs interrupting junctional VE-cadherin were scored as paracellular migration.

CHARACTERIZATION OF DORA RHOA BIOSENSOR

The design of the DORA RhoA sensor is based on the published RhoA biosensor [20]. Importantly, the GTPase is placed at the C-terminus of the construct enabling the DORA RhoA biosensor to localize at the plasma membrane similar to endogenous RhoA (Fig. 2a). FRET efficiency of the ON-state of the GTPase is improved through modelling of the fluorescent protein dimers and the GTPase-effector domain complexes. Repeats of stable α-helix from ribosomal protein L9, rather than an unstructured linker, is inserted between the fluorescent proteins to disrupt dimerization and diminish FRET efficiency in the inactive state

(Fig. 2a). In ECs, the DORA RhoA sensor accurately reported thrombin induced RhoA activation, showing a fast and transient RhoA activation (Fig. 2b and Supplementary Fig. 1f and Supplementary Movie 7). Quantification of 10 independent experiments showed reproducible RhoA activation patterns upon thrombin treatment (Supplementary Fig. 1f). As a control, DORA RhoA mutant PKN was generated to report misalignment of Cer3 and Venus image before and after image registration, motion artefacts or pH changes affecting the sensors fluorescent proteins. The substitution of glutamine for the leucine at position 59 in PKN prevents the binding of PKN to activated RhoA, in the DORA RhoA mutant PKN [21]. The DORA RhoA mutant PKN showed no change in Venus/Cer3 ratio after thrombin stimulation (Supplementary Fig. 2a and Supplementary Movie 8). Quantification of 10 independent experiments showed no change in Venus/Cer3 ratio after thrombin addition in ECs that expressed the DORA RhoA mutant PKN biosensor (Supplementary Fig. 2a). In addition, Hela cells that over-expressed the histamine receptor, histamine stimulation induced a fast and sustained RhoA activation (Supplementary Fig. 2b and Supplementary Movie 9). Subsequent addition of Pyrilamine reduced RhoA activity to baseline levels, showing that the sensor dynamically reports RhoA activation and inactivation [60]. The DORA RhoA mutant PKN showed no change in Venus/Cer3 ratio after histamine stimulation (Supplementary Fig. 2c and Supplementary Movie 10). To show that the sensor is cycling between an active and inactive, Rho-GDI-bound form, we co-expressed Rho-GDI and found a reduced FRET ratio, illustrative for binding to Rho-GDI (Supplementary Fig. 3a). In conclusion, the DORA RhoA biosensor accurately reports RhoA dynamics in ECs. Important to note, Venus and Cer3 emission were simultaneously recorded utilizing a double camera system since sequential image acquisition results in motion artefacts induced by migrating leukocytes displacing fluorescent signals in the ECs.

CHARACTERIZATION OF DORA FRET RHoA-SENSOR

The intrinsic single-chain nature of the DORA RhoA biosensor rules out the possibility of unequal Cer3 and Venus localization within the EC. Therefore, DORA RhoA sensor translocation always results in a paired translocation of Cer3 and Venus emission. In case the biosensor does translocate (e.g in response to EC shape alterations induced by migrating neutrophils lowering the local Venus and Cer3 emission dramatically) sequential imaging may result in erroneous measurements. The delay in the acquired Cer3 and Venus emission image of around 400-800 milliseconds may therefore contain an intrinsic local CFP-YFP pixel shift that cannot be solved by registration software. Therefore, quality of the obtained Venus/Cer3 Ratio acquired by sequential image acquisition is dependent

on the transmigration speed of the neutrophil. To control for erroneous measurements during sequential image acquisition one could change the acquisition order of sequential image acquisition from Cer3-Venus to Venus-Cer3, the DORA RhoA activity status will change from high to a low activity pattern. If the activity pattern alters, it indicates that an intrinsic local CFP-YFP pixel shift is present in the sequentially acquired Cer3 and Venus dataset. To circumvent motion artefacts a dual camera setup was used to acquire Cer3 and Venus emission images simultaneously. In our setup photo bleaching-rates of Cer3 and Venus are more or less equivalent. Photo bleaching (average ± s.d.) was determined by the reduction in fluorescence (1-F/F0) in living cells after 30 minutes illumination with HXP V at 20%, 800ms illumination with an interval of 5 seconds. dCer3 photo bleaching was 16.3% ±7.6%) and dcpVenus bleaching was 13.3% ±7.9%). All ratio-metric images and normalized intensity graphs were not corrected for photo bleaching, since photobleaching kinetics may change when FRET changes. Cer3 bleed through into the Venus channel is 57 %. All normalized intensity graphs were corrected for bleed through using the equation (YFP-BG)-(0.57*(CFP-BG).

DORA FRET RhoA-sensor analysis

We use a Zeiss Observer Z1 microscope with 40x NA 1.3 oil immersion objective, a HXP 120 V excitation light source, a Chroma 510 DCSP dichroic splitter, and two Hamamatsu ORCA-R2 digital CCD cameras (2x2 binning) for simultaneous monitoring of Cer3 and Venus emissions. Image acquisition was performed using Zeiss Zen 2011 microscope software. The lowest achievable HXP excitation power, through a FRET filter cube (Exciter ET 436/20x, and 455 DCLP dichroic mirror (Chroma), the emission filter is removed) was used to excite the Cer3 donor. The emission is directed to the left side port by a 100% mirror, to an attached dual camera adaptor (Zeiss) controlling a 510 DCSP dichroic mirror. Emission wavelengths between 455-510 nm are directed to an emission filter (ET 480/40, Chroma) and then captured by the 'straight' Hamamatsu ORCA-R2 camera resulting in Cer3 image acquisition. The Emission wavelength 510 nm and higher are directed to a six positions LEP filter wheel (Ludl Electronic Products) placed in front of the second 'rear' Hamamatsu ORCA-R2 camera. Position 1 in the emission filter wheel is equipped with an ET 540/40m used for venus image acquisition. Position 2 is left empty to allow mCherry image acquisition (EX BP 572/25, BS FT 590, EM BP 629/62, Zeiss). The LEP filter wheel is controlled by the MAC 6000 controller system (Ludl Electronic Products). Exposure time of DIC image was set to 76 ms and exposure time of simultaneous CFP and YFP acquisition was set to +/-800 ms, images were subsequently recorded

every 5 seconds for periods as indicated. Offline ratio analysis between Cer3 and Venus images was done utilizing the MBF ImageJ collection (Tony Collins). Individual images in the raw Cer3 and Venus image stacks were background (BG) corrected using the plug-in 'ROI, BG subtraction from ROI'. An region of interest (ROI) in the image were no cells were present was selected as the background. Next, the Cer3 and Venus stacks were aligned using the registration plug-in 'Registration, MultiStackReg'. A smooth filter was applied to both image stacks to improve image quality by reducing the noise. The smooth filter (mean filter) was applied over the entire image and replaces each pixel with the average of its 3×3 neighborhood. Next, both image stacks were converted to a 32-bit image format, required for subsequent masking. A user defined threshold was applied exclusively to the Venus image stack, converting the background pixels to 'not a number' (NaN). It allows elimination of artifacts in ratio image stemming from the background noise. Finally the Venus/Cer3 ratio was calculated using the plug-in 'Ratio Plus', and a custom lookup table was applied to generate a color-coded image illustrating the high 'red' and low 'blue' activities. Note that some of the plug-ins, namely MultiStackReg, and Ratio Plus are not included in the basic MBF ImageJ collection and should be downloaded from the plug-in page in the ImageJ website (http://rsb.info.nih.gov/ij/plugins/index.html). Normalized intensity graphs; the intensity of an manually selected ROI of interest and the BG of the raw Cer3 and Venus image stacks were measured using the plug-in ROI, Multi Measure in ImageJ. The raw Cer3 and Venus intensities were BG subtracted using equation Cer3 = (Cer3 raw - BG), subsequently Venus only was corrected for bleed through using the equation VenusC = (Venus)-(0.5748*(Cer3). Normalization of the individual intensity traces was done by dividing the data by the average over acquisition 3 to 13. The Venus/Cer3 ratio was calculated from the normalized data using Excel.

CONFOCAL INTRAVITAL MICROSCOPY OF MOUSE CREMASTER MUSCLES

To investigate local myosin light chain phosphorylation during leukocyte diapedesis, whole-mounted cremaster muscles of mice expressing endogenously labeled GFP-leukocytes (*Lys-EGFP-ki, CX3CR1-EGFP-ki*, Tie-2Cre) or C57BL6 mice were fixed, immunostained and analyzed by confocal microscopy. Inflammation in mouse cremaster muscles was induced by intrascrotal injection (i.s.) of IL-1β/TNF-α (50 ng IL-1β, 300 ng TNF-α in 400μl saline) or saline (400 μl) for 2 hours. EC junctions were labeled through co-administration of Alexa Fluor-555 or 647-labeled anti-PECAM-1 mAb (clone 390; 3μg i.s.). Anti-PECAM mAb clone 390 was conjugated to Alexa Fluor-555 using a commercially available kit (Invitrogen, Paisley, UK). The cremasters were surgically

exteriorized and TEM was analyzed by intravital microscopy. Straight post-capillary venules of 20-40 μm in diameter were selected for analysis of leukocyte-vessel wall interactions. Z-stacks of images were captured by confocal microscopy as described by Abigail Woodfin [23]. The tissues were fixed with 4% paraformaldehyde for 30 minutes at a time point with several paracellular pores visible in the PECAM-1 labelling. Subsequently, tissues were permeabilised with 0.5% Triton and blocked with 10% BSA and 10 μg/μl FC block for 2 hours. Tissues were incubated with anti-phospho Myosin light chain Thr18/Ser19 (Cat #3674) purchased from Cell signaling (BIOKE) antibody for 2 days and a further 2 days with the secondary antibody or IgG isotype control (1:100). Transmigration induced permeability was examined by looking at fluorescent TRITC-dextran leakage into the cremaster of C57BL/6 WT or LysM-GFP mice during IL-1β and TNF-α stimulated neutrophil recruitment. Four different groups were defined; unstimulated, Rho inhibitor I (C3) alone, IL-1β/TNF-α treated, IL-1β/TNF-α treated + C3. IL-1β (50 ng), TNF-α (300 ng), Rho-inhibitor (1 μg) and anti-PECAM-1 labelling antibody (4 μg) were given intrascrotally at T = 0 hours. A second dose of C3 (1 μg) was given intrascrotally and TRITC-dextran (40 kDa, 200 μl/40 μM) was injected intravenously at T = 2 hours and allowed to circulate until T = 4 hours. At T = 4 hours animals were sacrificed and tissues were subjected to vascular wash-out by perfusion of 10 ml PBS via the left ventricle. Tissues were examined by confocal microscopy (Leica SP5, 20X objective) and the level of TRITC-dextran fluorescence by region of interest in the surrounding tissue was quantified using the LAS-AF Lite software. Neutrophil extravasation per 5×10^4 μm^2 tissue area was quantified by endogenous GFP fluorescence in the neutrophils of LysM-GFP mice, or by fixation and labelling of neutrophils with anti-MRP14-alexa647 in WT mice after analysis of TRITC-dextran leakage in unfixed tissues.

F-ACTIN VISUALIZATION IN RETINAL VASCULATURE OF LIFEACT-GFP MICE

Lifeact-EGFP transgenic mice have been previously described [26]. All experiments with mice were performed in accordance to German guidelines and regulations. Mice were analysed at p7 and gender was randomly picked. The protocol was approved by the Committee on the Ethics of Animal Experiments of the Ludwig-Maximilians University Munich.

WHOLE RETINA IMMUNOHISTOCHEMISTRY

Dissection and labelling of retinas was performed as previously described [27]. Briefly, retinas were fixed for 2 hours on ice in 4% paraformaldehyde (PFA), incubated in 1% BSA and 0.3% Triton X-100, washed two times in

Pblec (1% Triton X-100, 1 mM CaCl2, 1 mM MgCl2, and 1 mM MnCl2 PBS [pH 6.8]), and incubated overnight with isolectin-B4 (1:50) and antibodies diluted in Pblec. Images were acquired and processed using a Leica TCS SP5 II microscope, LAS Montage Imaging software (Leica) and the IMARIS Digital Imaging software (Biplane). Biotinylated *Griffonia simplicifolia* lectin I (IB4), (B-1205) was purchased from Vector Laboratories.

Western blotting

Cells were washed twice with PBS, and lysed with 95°C SDS-sample buffer containing 4% β-mercapto-ethanol. Samples were boiled at 95°C for 4 minutes to denature proteins. Proteins were separated on 4–12% NuPAGE Novex Bis-Tris gels (Invitrogen), transferred to Immobilon-PVDF transfer membranes (Millipore Corp., Billerica, MA) and subsequently blocked with 2.5% (w/v) bovine serum albumin (BSA) in Tris-buffered saline with Tween 20 (TBST) for 60 minutes. The immunoblots were analyzed using primary antibodies incubated overnight at 4°C and secondary antibodies linked to horseradish peroxidase (HRP) (GE Healthcare, UK), after each step immunoblots were washed 6x with TBST. Signals were visualized by enhanced chemiluminescence and light sensitive films (GE Healthcare, UK).

Pull-out assay and immunoprecipitation

1.2 mg/ml dynabeads goat-x-ms IgG (Dynal, Invitrogen) per condition were washed ones with 1 ml buffer 1 containing PBS + 2 mM EDTA and 0.1% BSA (Millipore) using a magnetic holder. Dynabeads were coated with 1.6 µg α-ICAM-1 CD54 (BBIG-I1/IIC81, R&D systems (Cat #BBA9) antibodies per condition and incubated head-over-head at 4°C for 45 min. The beads were washed twice using buffer 1 and resuspended in PBS containing 0.5 $MgCl_2$ and 1 mM $CaCl_2$. Overnight TNF-α treated (10 ng per ml) HUVEC (2-5 million cells) were pre-treated with 1 µM Ionomycin (Invitrogen, I-24222) for 10 min. 1.2 mg per ml dynabeads per condition were used to cluster ICAM-1 for 10-30 minutes. Cells were washed once on ice using PBS containing 0.5 $MgCl_2$ and 1 mM $CaCl_2$. Next, cells were lysed in 1 ml cold pH7.4 RIPA buffer containing 50 mM Tris, 100 mM NaCl, 10 mM $MgCl_2$, 1% NP40, 10% glycerol, 0.1% SDS, 1% DOC (Sigma-Aldrich), DNAse inhibitor and protease phosphatase inhibitor cocktail for 5 min. Cells were scraped together and lysates were transferred to a new tube. Then, ICAM-1 coated dynabeads were added to non-clustered-control cells. 50 µl whole cell lysate was taken from all conditions. Beads and cell-lysates were subsequently incubated head-over-head for 1-2h at 4° C. Next cells were washed twice with Ripa buffer and three times with NP-40 lysis buffer. Beads were resuspended in 30 µl 2x SDS-sample buffer and assessed by Western blotting.

Electric cell-substrate impedance sensing under flow

Endothelial monolayer integrity during leukocyte diapedesis was determined by measuring the electrical resistance using Electric Cell-substrate Impedance Sensing (ECIS). Flow chamber electrode arrays (8F10E; Applied Biophysics, Troy, NY) were pretreated with 10 mM L-cysteine (Sigma-Aldrich) for 15 minutes at 37°C, subsequently washed twice with 0.9% NaCl and coated with FN (Sanquin) in 0.9% NaCl for 1 hour at 37°C. Cells were seeded at 300,000 cells per slide (2.5 cm^2) and grown to confluence. Continuous resistance measurements were performed at 37°C at 5% CO_2 with the ECIS Zθ (Theta) system controller (Applied Biophysics). After forming a stable monolayer, HUVECs were subjected to flow (0.8 dynes/cm^2) for periods as indicated.

Statistics

Endothelial pore analyses between leukocyte subtypes was tested using a one-way ANOVA assuming no matching or pairing, comparing the mean of each column with the mean of every other column, that were corrected for multiple comparisons by Tukey multiple comparisons test, with a single pooled variance. Statistical comparison between experimental groups was performed by the student T-test. A two-tailed p-value of < 0.05 was considered significant. Correlation analysis of dextran and neutrophil extravasation kinetics was performed by Pearson's correlation. Unless otherwise stated, a representative experiment out of at least three independent experiments is shown.

Author contributions

NH, LS, CO, JvR, TY, BM, JvU, BP, SH, JG, YW, EM, AW, JDvB performed the experiments; NH, SH, JG, YW, EM, AW and JDvB analyzed and interpreted the data; NH and JDvB did study conception and design; NH and JDvB wrote the manuscript.

Competing Financial Interest

The authors declare that they have no competing financial interest

References

1. Oliver, M. G., Specian, R. D., Perry, M. A. & Granger, D. N. Morphologic assessment of leukocyte-endothelial cell interactions in mesenteric venules subjected to ischemia and reperfusion. *Inflammation* **15,** 331–346 (1991).
2. Hernandez, L. a *et al.* Role of neutrophils in ischemia-reperfusion-induced microvascular injury. *Am. J. Physiol.* **253,** H699–H703 (1987).
3. Kubes, P., Suzuki, M. & Granger, D. N. Modulation of PAF-induced leukocyte adherence and increased microvascular permeability. *Am. J. Physiol.* **259,** G859–G864 (1990).
4. Sumagin, R., Lomakina, E. & Sarelius, I. H. Leukocyte-endothelial cell interactions are linked to vascular permeability via ICAM-1-mediated signaling. *Am. J. Physiol. Heart Circ. Physiol.* **295,** H969–H977 (2008).
5. Carden, D. L., Smith, J. K. & Korthuis, R. J. Neutrophil-mediated microvascular dysfunction in postischemic canine skeletal muscle. Role of granulocyte adherence. *Circ. Res.* **66,** 1436–1444 (1990).
6. McDonald, D. M., Thurston, G. & Baluk, P. Endothelial gaps as sites for plasma leakage in inflammation. *Microcirculation* **6,** 7–22 (1999).
7. Baluk, P., Bolton, P., Hirata, A., Thurston, G. & McDonald, D. M. Endothelial gaps and adherent leukocytes in allergen-induced early- and late-phase plasma leakage in rat airways. *Am. J. Pathol.* **152,** 1463–76 (1998).
8. McDonald, D. M. Endothelial gaps and permeability of venules in rat tracheas exposed to inflammatory stimuli. *Am. J. Physiol.* **266,** L61–L83 (1994).
9. Baluk, P., Bertrand, C., Geppetti, P., McDonald, D. M. & Nadel, J. A. NK1 receptors mediate leukocyte adhesion in neurogenic inflammation in the rat trachea. *Am. J. Physiol.* **268,** L263–L269 (1995).
10. Gawlowski, D. M., Benoit, J. N. & Granger, H. J. Microvascular pressure and albumin extravasation after leukocyte activation in hamster cheek pouch. *Am. J. Physiol.* **264,** H541–6 (1993).
11. Rosengren, S., Ley, K. & Arfors, K. E. Dextran sulfate prevents LTB4-induced permeability increase, but not neutrophil emigration, in the hamster cheek pouch. *Microvasc. Res.* **38,** 243–254 (1989).
12. Zeng, M., Zhang, H., Lowell, C. & He, P. Tumor necrosis factor-alpha-induced leukocyte adhesion and microvessel permeability. *Am. J. Physiol. Heart Circ. Physiol.* **283,** H2420–30 (2002).
13. Valeski, J. E. & Baldwin, a L. Effect of early transient adherent leukocytes on venular permeability and endothelial actin cytoskeleton. *Am. J. Physiol.* **277,** H569–H575 (1999).
14. Kim, M.-H., Curry, F.-R. E. & Simon, S. I. Dynamics of neutrophil extravasation and vascular permeability are uncoupled during aseptic cutaneous wounding. *Am. J. Physiol. Cell Physiol.* **296,** C848–56 (2009).
15. Lewis, R. E. & Granger, H. J. Diapedesis and the permeability of venous microvessels to protein macromolecules: the impact of leukotriene B4 (LTB4). *Microvasc. Res.* **35,** 27–47 (1988).
16. Lewis, R. E., Miller, R. A. & Granger, H. J. Acute microvascular effects of the chemotactic peptide N-formyl-methionyl-leucyl-phenylalanine: Comparisons with leukotriene B4. *Microvasc. Res.* **37,** 53–69 (1989).
17. Wessel, F. *et al.* Leukocyte extravasation and vascular permeability are each controlled in vivo by different tyrosine residues of VE-cadherin. *Nat. Immunol.* **15,** 223–30 (2014).
18. Vestweber, D., Wessel, F. & Nottebaum, A. F. Similarities and differences in the regulation of leukocyte extravasation and vascular permeability. *Seminars in Immunopathology* **36,** 177–192 (2014).
19. Lin, B., Yin, T., Wu, Y. I., Inoue, T. & Levchenko, A. Interplay between chemotaxis and contact inhibition of locomotion determines exploratory cell migration. *Nat. Commun.* **6,** 6619 (2015).
20. Pertz, O., Hodgson, L., Klemke, R. L. & Hahn, K. M. Spatiotemporal dynamics of RhoA activity in migrating cells. *Nature* **440,** 1069–72 (2006).
21. Maesaki, R. *et al.* The structural basis of Rho effector recognition revealed by the crystal structure of human RhoA complexed with the effector domain of PKN/PRK1. *Mol. Cell* **4,** 793–803 (1999).
22. Riedl, J. *et al.* Lifeact: a versatile marker to visualize F-actin. *Nat. Methods* **5,** 605–7 (2008).
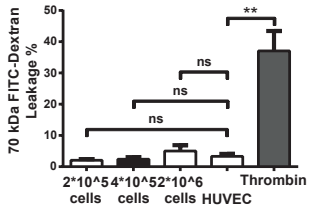23. Woodfin, A. *et al.* The junctional adhesion molecule JAM-C regulates polarized

transendothelial migration of neutrophils in vivo. *Nat. Immunol.* **12,** 761–9 (2011).

24. Thureson-Klein, A., Hedqvist, P. & Lindbom, L. Leukocyte diapedesis and plasma extravasation after leukotriene B4: lack of structural injury to the endothelium. *Tissue Cell* **18,** 1–12 (1986).
25. Worthylake, R. A., Lemoine, S., Watson, J. M. & Burridge, K. RhoA is required for monocyte tail retraction during transendothelial migration. *J. Cell Biol.* **154,** 147–60 (2001).
26. Riedl, J. *et al.* Lifeact mice for studying F-actin dynamics. *Nat. Methods* **7,** 168–9 (2010).
27. Fraccaroli, A. *et al.* Visualization of endothelial actin cytoskeleton in the mouse retina. *PLoS One* **7,** e47488 (2012).
28. Matsumoto, H. *et al.* Antibodies to CD11b, CD68, and lectin label neutrophils rather than microglia in traumatic and ischemic brain lesions. *J. Neurosci. Res.* **85,** 994–1009 (2007).
29. Strey, A., Janning, A., Barth, H. & Gerke, V. Endothelial Rho signaling is required for monocyte transendothelial migration. *FEBS Lett.* **517,** 261–6 (2002).
30. Carman, C. V. & Springer, T. A. A transmigratory cup in leukocyte diapedesis both through individual vascular endothelial cells and between them. *J. Cell Biol.* **167,** 377–388 (2004).
31. Hixenbaugh, E. A. *et al.* Stimulated neutrophils induce myosin light chain phosphorylation and isometric tension in endothelial cells. *Am J Physiol Hear. Circ Physiol* **273,** H981–988 (1997).
32. Etienne, S. *et al.* ICAM-1 signaling pathways associated with Rho activation in microvascular brain endothelial cells. *J. Immunol.* **161,** 5755–61 (1998).
33. Wójciak-Stothard, B., Williams, L. & Ridley, A. J. Monocyte adhesion and spreading on human endothelial cells is dependent on Rho-regulated receptor clustering. *J. Cell Biol.* **145,** 1293–307 (1999).
34. Saito, H., Minamiya, Y., Saito, S. & Ogawa, J. Endothelial Rho and Rho kinase regulate neutrophil migration via endothelial myosin light chain phosphorylation. *J. Leukoc. Biol.* **72,** 829–36 (2002).
35. Heemskerk, N., Van Rijssel, J. & Van Buul, J. D. Rho-GTPase signaling in leukocyte extravasation: An endothelial point of view. *Cell Adhesion and Migration* **8,** 67–75 (2014).
36. Rabodzey, A., Alcaide, P., Luscinskas, F. W. & Ladoux, B. Mechanical forces induced by the transendothelial migration of human neutrophils. *Biophys. J.* **95,** 1428–1438 (2008).
37. Toyjanova, J., Flores-Cortez, E., Reichner, J. S. & Franck, C. Matrix Confinement Plays a Pivotal Role in Regulating Neutrophil-generated Tractions, Speed and Integrin Utilization. *J. Biol. Chem.* **290,** jbc.M114.619643 (2014).
38. Thompson, P. W., Randi, A. M. & Ridley, A. J. Intercellular adhesion molecule (ICAM)-1, but not ICAM-2, activates RhoA and stimulates c-fos and rhoA transcription in endothelial cells. *J. Immunol.* **169,** 1007–1013 (2002).
39. Van Buul, J. D. *et al.* RhoG regulates endothelial apical cup assembly downstream from ICAM1 engagement and is involved in leukocyte trans-endothelial migration. *J. Cell Biol.* **178,** 1279–1293 (2007).
40. Adamson, P., Etienne, S., Couraud, P. O., Calder, V. & Greenwood, J. Lymphocyte migration through brain endothelial cell monolayers involves signaling through endothelial ICAM-1 via a rho-dependent pathway. *J. Immunol.* **162,** 2964–73 (1999).
41. Lessey-Morillon, E. C. *et al.* The RhoA guanine nucleotide exchange factor, LARG, mediates ICAM-1-dependent mechanotransduction in endothelial cells to stimulate transendothelial migration. *J. Immunol.* **192,** 3390–8 (2014).
42. Collins, C. *et al.* Localized tensional forces on PECAM-1 elicit a global mechanotransduction response via the integrin-RhoA pathway. *Curr. Biol.* **22,** 2087–94 (2012).
43. Su, K.-C., Takaki, T. & Petronczki, M. Targeting of the RhoGEF Ect2 to the equatorial membrane controls cleavage furrow formation during cytokinesis. *Dev. Cell* **21,** 1104–15 (2011).
44. Ratheesh, A. *et al.* Centralspindlin and α-catenin regulate Rho signalling at the epithelial zonula adherens. *Nat. Cell Biol.* **14,** 818–828 (2012).
45. Lemichez, E., Gonzalez-Rodriguez, D., Bassereau, P. & Brochard-Wyart, F. Transcellular tunnel dynamics: Control of cellular dewetting by actomyosin contractility and I-BAR proteins. *Biol. Cell* **105,** 109–117 (2013).
46. Luo, Y. & Radice, G. L. N-cadherin acts upstream of VE-cadherin in controlling vascular morphogenesis. *J. Cell Biol.* **169,** 29–34 (2005).
47. Schulte, D. *et al.* Stabilizing the VE-cadherin–catenin complex blocks leukocyte extravasation and vascular permeability. *EMBO J.* **30,** 4157–4170 (2011).
48. Schenkel, A. R., Mamdouh, Z. & Muller, W. a. Locomotion of monocytes on endothelium

is a critical step during extravasation. *Nat. Immunol.* **5,** 393–400 (2004).

49. Barreiro, O. *et al.* Dynamic interaction of VCAM-1 and ICAM-1 with moesin and ezrin in a novel endothelial docking structure for adherent leukocytes. *J. Cell Biol.* **157,** 1233–1245 (2002).
50. Vestweber, D., Zeuschner, D., Rottner, K. & Schnoor, M. and ICAM-1 clustering in endothelium Implications for the formation of docking structures. 1–5 (2013).
51. Sandig, M., Negrou, E. & Rogers, K. A. Changes in the distribution of LFA-1, catenins, and F-actin during transendothelial migration of monocytes in culture. *J. Cell Sci.* **110 (Pt 2,** 2807–2818 (1997).
52. Millán, J. *et al.* Lymphocyte transcellular migration occurs through recruitment of endothelial ICAM-1 to caveola- and F-actin-rich domains. *Nat. Cell Biol.* **8,** 113–123 (2006).
53. Shulman, Z. *et al.* Transendothelial migration of lymphocytes mediated by intraendothelial vesicle stores rather than by extracellular chemokine depots. *Nat. Immunol.* **13,** 67–76 (2011).
54. Van Rijssel, J. *et al.* The Rho-guanine nucleotide exchange factor Trio controls leukocyte transendothelial migration by promoting docking structure formation. *Mol. Biol. Cell* **23,** 2831–2844 (2012).
55. Fernandez-Gonzalez, R. & Zallen, J. A. Wounded cells drive rapid epidermal repair in the early Drosophila embryo. *Mol. Biol. Cell* **24,** 3227–37 (2013).
56. Martinelli, R. *et al.* Release of cellular tension signals self-restorative ventral lamellipodia to heal barrier micro-wounds. *J. Cell Biol.* **201,** 449–65 (2013).
57. Abu Taha, A., Taha, M., Seebach, J. & Schnittler, H.-J. ARP2/3-mediated junction-associated lamellipodia control VE-cadherin-based cell junction dynamics and maintain monolayer integrity. *Mol. Biol. Cell* **25,** 245–56 (2014).
58. Kaur, J. *et al.* Endothelial LSP1 is involved in endothelial dome formation , minimizing vascular permeability changes during neutrophil transmigration in vivo. **117,** 942–953 (2014).
59. Hossain, M., Qadri, S. M., Su, Y. & Liu, L. ICAM-1-mediated leukocyte adhesion is critical for the activation of endothelial LSP1. *Am. J. Physiol. Cell Physiol.* **304,** C895–904 (2013).
60. Van Unen, J., Reinhard, N.R., Yin, T., Wu, Y.I., Postma, M., Gadella Jr., T.W., Goedhart, J. Plasma membrane restricted RhoGEF activity is sufficient for RhoA-mediated actin polymerization. *Sci. Rep.* (2015).
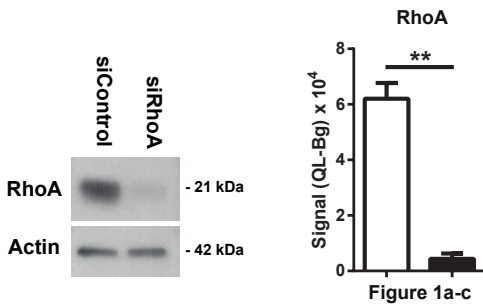
4

Supplementary Figure 1 Neutrophil transmigration through ECs is associated with minimal FITC-dextran leakage. (**a**) Quantification of FITC-dextran (70 kDa) leakage during neutrophil diapedesis through TNF-α treated HUVECs cultured on 3μm pore permeable filters. Neutrophils transmigrated towards a C5a chemotactic gradient in the lower compartment. (**b**) Endothelial RhoA depletion by siRNA. Immunoblot analysis of protein extracts prepared from HUVEC treated with TNF-α overnight. Extracts were prepared 72 hours after transfection with control and RhoA siRNA duplexes. Extracts were probed with antibodies directed against RhoA and actin. Quantification of RhoA depletion, presented as 'quantum level' (sum of grayness of each pixel in blot) minus background (QL-Bg), normalized to that of actin. (**c**) Normalized resistance of endothelial monolayer during leukocyte diapedesis through HUVECs treated with or without C3 inhibitor measured with ECIS in real-time under flow conditions. Green and red line indicates untreated and C3-pretreated ECs, respectively. Lines represent average of eight wells. Numbers: 1: Onset of flow (0.8 dyne per cm^2); 2: addition of neutrophils (approximately 1*10^6 per mL); 3: addition of thrombin (1U per mL). (**d**) Confocal intravital microscopy of 20 μm diameter cremasteric venules in LysM-GFP mice (green neutrophils) immunostained *in vivo* for EC junctions by intrascrotal injections of fluorescent-labeled PECAM-1 (blue) and stimulated for four hours with IL-1β and TNF-α only, or with Rho-inhibitor (C3). A second dose of Rho inhibitor was given intrascrotally and TRITC-dextran (40 kDa) was injected intravenously at T = 2 hours and allowed to circulate until T = 4 hours. Scale bar 100μm. (**e**) Quantification of TRITC-dextran extravasation in animals left unstimulated (control), stimulated with C3 alone or IL-1β/TNF-α. (**f**) Characterization of DORA RhoA biosensor and DORA RhoA mutant PKN biosensor. Time-lapse Venus/Cer3 ratio images of DORA RhoA biosensor after thrombin treatment in HUVECs. Filled arrows indicate RhoA activation. Scale bar, 10μm. Calibration bar shows RhoA activation (Red) relative to basal RhoA activity (Blue). Graph on the right shows quantification of DORA RhoA biosensor ** $P < 0.01$ (ANOVA) (**a**) ** $P < 0.01$ control versus RhoA depletion (Student's t-test) (**b**). * $P < 0.05$ Saline versus IL-1β/TNF-α (Student's t-test) (**e**). Data are representative of three independent experiments (**a-c**) 10 experiments (**f**) (error bars (**a-e**), s.e.m).

Supplemental Figure 1.

a

b

RhoA

- 21 kDa

- 42 kDa

c

1. Flow
2. Neutrophils
3. Thrombin

— Control
— C3

4

Figure 1a-c

d

IL-1β/TNFα   IL-1β/TNFα +C3

Venule diameter of 20 μm

e

| IL-1β/TNFα | - | - | + |
| C3 | - | + | - |

f

Before   + Thrombin

Venus/Cer3

DORA RhoA biosensor

— Cer3
— Venus
— DORA RhoA activation
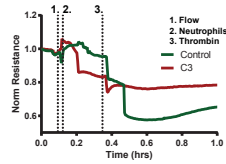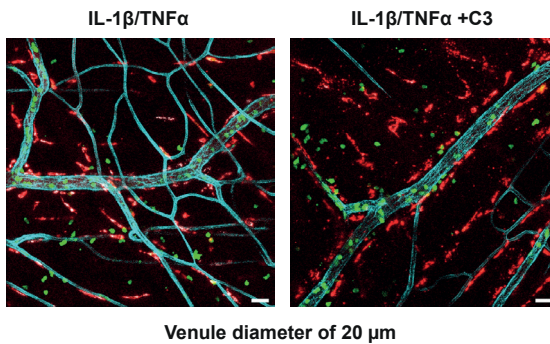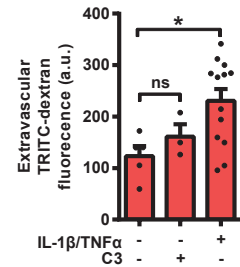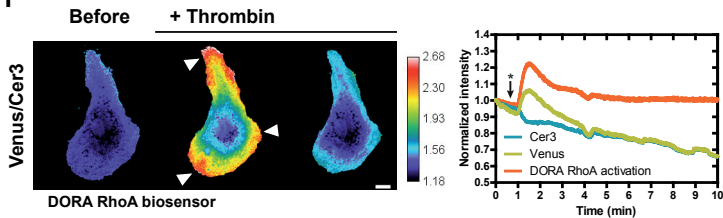
Supplementary Figure 2 Characterization of DORA RhoA biosensor and DORA RhoA mutant PKN biosensor. (**a**) Time-lapse Venus/Cer3 ratio images of DORA RhoA mutant PKN biosensor after thrombin treatment in HUVECs. Scale bar, 10μm. Calibration bar shows RhoA activation (Red) relative to basal RhoA activity (Blue). Graph on the right shows quantification of DORA RhoA mutant PKN biosensor after thrombin treatment (asterisk) in HUVECs. (**b**) Time-lapse Venus/Cer3 ratio images of DORA RhoA biosensor or DORA RhoA mutant PKN biosensor (**c**) after histamine and subsequent antagonist pyrilamine stimulation in Hela cells expressing the histamine receptor. Filled arrows indicate RhoA activation. Graph on the right shows quantification of DORA RhoA activation. Asterisk indicate addition of histamine; second asterisk shows addition of pyrilamine. (**d**) Epi-fluorescent live-cell imaging of HUVECs expressing the DORA RhoA biosensor during neutrophil adhesion under physiological flow conditions (0.8dyne per cm^2). Open arrows indicate adherent neutrophil at the apical side of the endothelium. Filled arrows indicate local RhoA activation during neutrophil diapedesis. Scale bar 10μm. Calibration bar shows RhoA activation (red) relative to basal RhoA activity (blue). Data are representative of 10 experiments (**a-c**).

Supplemental Figure 2.
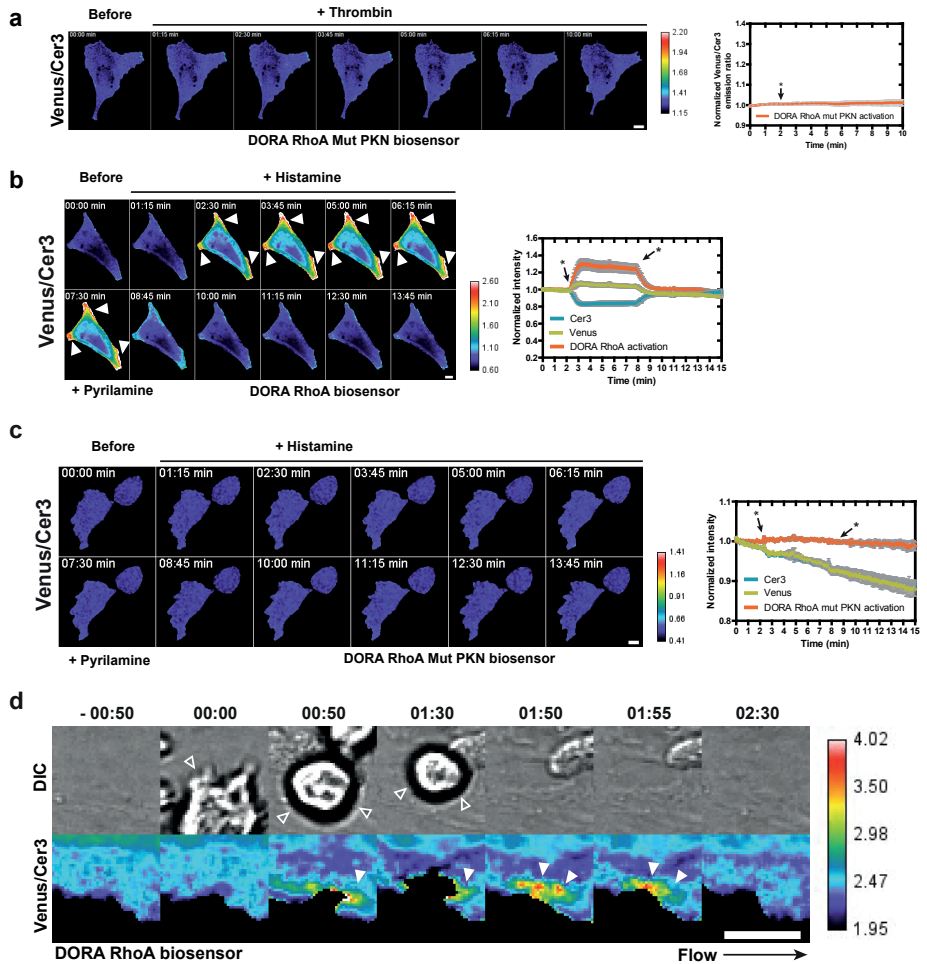
Supplementary Figure 3 F-actin rich endothelial pores. (**a**) Quantification of basal DORA RhoA biosensor ratios in Hela cells with and without RhoGDI overexpression. Box plot shows median with 95% confidence interval (notches) and the limits of the box indicate the 25th and 75th percentiles; whiskers extend 1.5 times the interquartile range from the 25th and 75th percentiles. The Venus/Cer3 ratios of individual cells are plotted as open circles. The lower FRET ratio in presence of RhoGDI reflectes reduced GTP-loading, which is in agreement with regulation by RhoGDIs. (**b**) Time-lapse Venus/Cer3 ratio images of DORA RhoA mutant PKN biosensor during neutrophil transmigration. (**c**) Quantification of DORA RhoA mutant PKN biosensor activation during neutrophil TEM. First asterisk indicates leukocyte adhesion; second asterisk shows leukocyte diapedesis. (**d**) Confocal imaging of extravasating neutrophils through Lifeact-GFP expressing HUVECs under physiological flow conditions, cells were fixed and stained for phalloidin. Open and filled arrows indicate F-actin visualized using phalloidin or Lifeact-GFP, respectively. Scale bar, 20µm. PECAM-1 localization in para-and transcellular endothelial pores. (**e**) Paracellular migration of monocytes. Open and filled arrows indicate PECAM-1 localization to the endothelial pore at the basolateral or apical site, respectively. Lifeact (red), VE-cadherin (green) and neutrophil nuclei (blue). Asterisk indicates transmigrating neutrophil in DIC. Merge shows all colours. Scale bar, 5µm. (**f**) Transcellular migration of monocytes. Open and filled arrows indicate PECAM-1 localization to the endothelial pore at the basolateral or apical site, respectively. Lifeact (red), VE-cadherin (green) and neutrophil nuclei (blue). Asterisk indicates transmigrating neutrophil in DIC. Merge shows all colours. Scale bar, 5µm. Data are representative of ten independent experiments (**a**) seven experiments (**c**) > 20 transmigration events (**e**, **f**) (error bars (**a,c**), s.e.m).

Supplemental Figure 3.

a

b

c

d

e

f
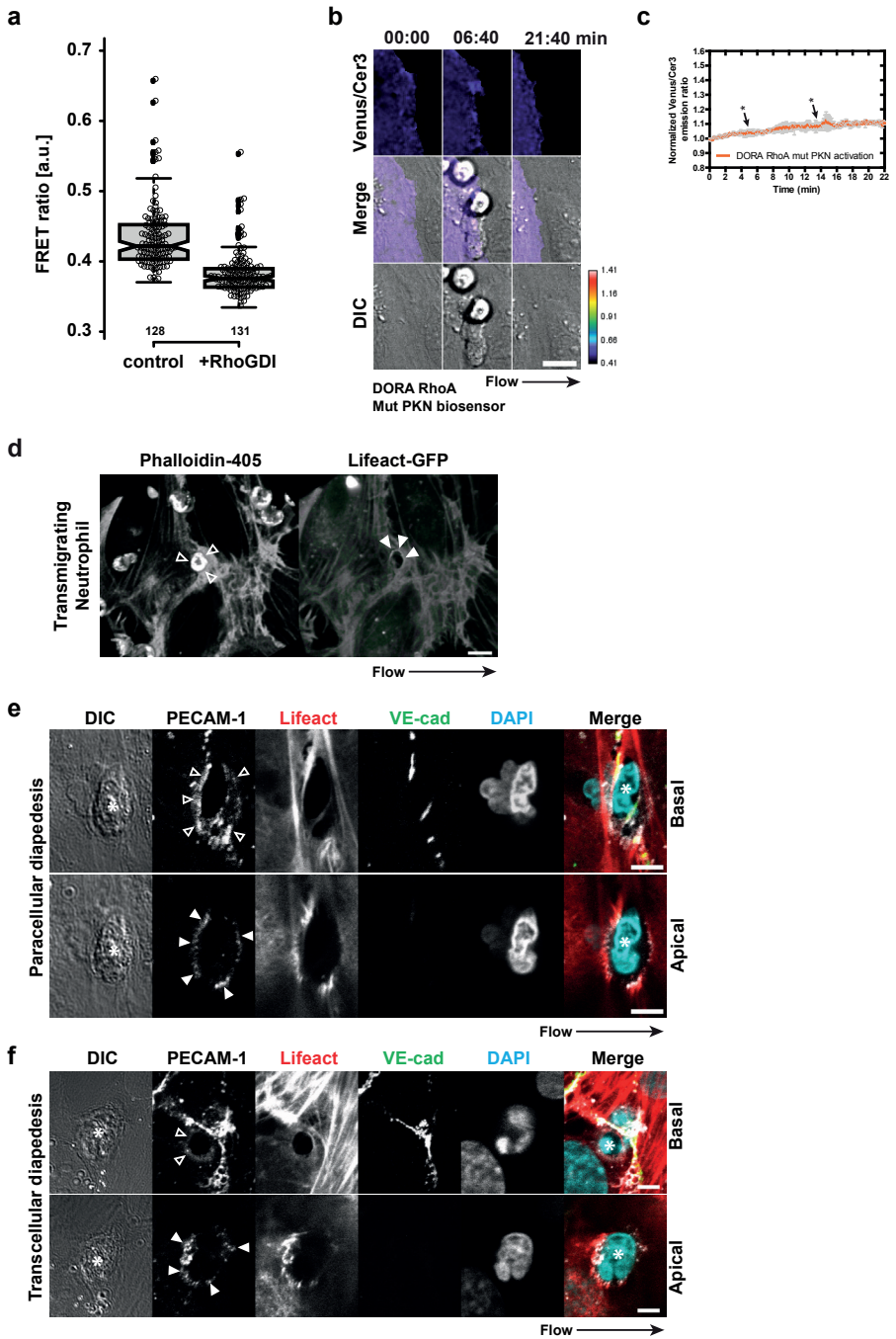
Supplementary Figure 4 Endothelial pore morphology at distinct stages of neutrophil diapedesis. (**a**) Confocal imaging of paracellular migrating neutrophils through ICAM-1-GFP and Lifeact-mCherry expressing HUVEC under physiological flow conditions. Open and filled arrows indicate ICAM-1-GFP and Lifeact-mCherry localization to endothelial pore, respectively. Asterisk indicates extravasating neutrophil (DAPI in blue). VE-cadherin (white). Scale bar, 5µm. (**b**) Quantification of paracellular migration route through bi-cellular (i.e. junctions of two adjacent ECs) or multi-cellular (i.e. junctions formed by three or more ECs). (**c**) Confocal imaging of Lifeact-GFP-positive endothelial pores at distinct stages of neutrophil diapedesis, defined as adhesion, early, mid, and late diapedesis. Open arrows indicate filopodia-like protrusions at the apical site of the structure. Filled arrows indicate the cortical actin-ring at the basolateral site that appeared during leukocyte crossing. Asterisk indicates extravasating leukocyte (DAPI in blue). Scale bar, 10µm. (**d**) Quantification of pore length and pore width defined as the distance parallel and perpendicular to the cell-cell junction, respectively. (**e**) Quantification of F-actin rich apical protrusions height for neutrophils and monocytes. (**f**) Quantification of endothelial circularity for para- and transcellular migrating neutrophils and monocytes according to the circularity index, Circle = 1 and oval = 2. Diagram on the left indicates the orientation of the pore for the paracellular route. Statistical significance was tested using a student's t-test. Data are representative of four independent experiments (**a**-**f**) with 40 transmigration events per group (error bars (**d**-**f**), s.e.m).

Supplemental Figure 4.

a

b

c

d Pore length / Pore width — F-Actin rich pore / Cell-Cell Junction

e

f Circularity index
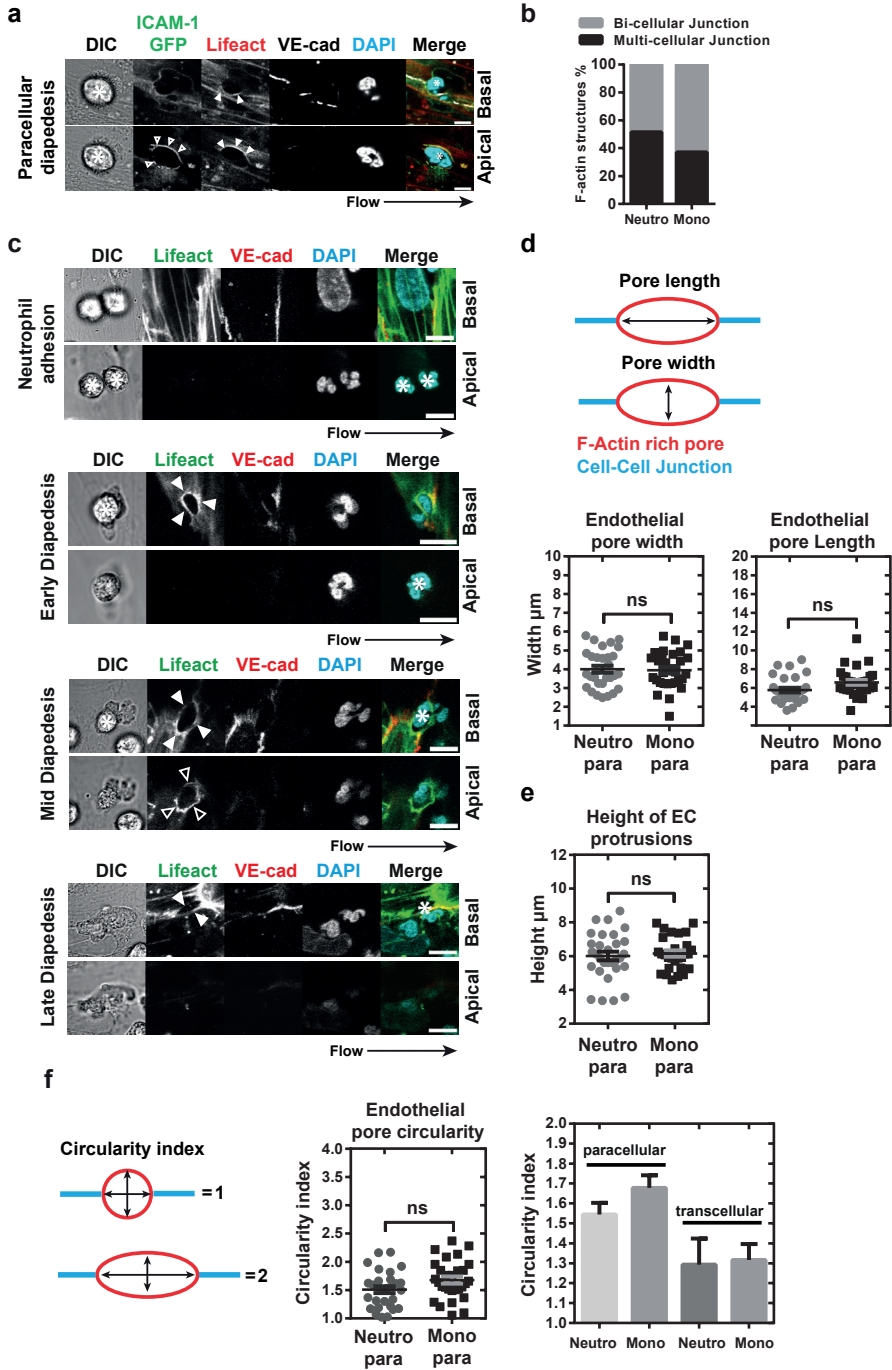
Supplementary Figure 5 RhoA signalling is required for local MLC phosphorylation and endothelial pore confinement during neutrophil transmigration. Endothelial RhoA and VE-cadherin depletion by siRNA. (**a**) Immunoblot analysis of protein extracts prepared from HUVEC treated with TNF-α overnight. Extracts were prepared 72 hours after transfection with control and RhoA siRNA duplexes. Extracts were probed with antibodies directed against RhoA and actin. Quantification of RhoA depletion, presented as 'quantum level' (sum of grayness of each pixel in blot) minus background (QL-Bg), normalized to that of actin. (**b**) Confocal imaging of paracellular migrating neutrophils through Lifeact-GFP expressing HUVEC after 72 hours transduction with control shRNA (left panel) or VE-cadherin shRNA (right panel) under physiological flow conditions. Open and filled arrows indicate PECAM-1 (white) and VE-cadherin (green) localization to the endothelial pore, respectively. Open and filled arrows indicate Lifeact-GFP localization to endothelial pore after 72 hours transduction with control shRNA (left panel) or VE-cadherin shRNA, respectively. Asterisks indicate extravasating neutrophils in DIC. VE-cadherin (green) and DAPI (blue). Merge shows all colours. Scale bar, 5µm. (**c**) Quantification of endothelial pore length, width, height, circularity of the endothelial pore in HUVECs after 72 hours transfection with control shRNA or VE-cadherin shRNA under physiological flow conditions. (**d**) Immunoblot analysis of protein extracts prepared from HUVECs treated with TNF-α overnight. Extracts were prepared 72 hours after transduction with control and VE-cadherin shRNA duplexes. Extracts were probed with antibodies directed against VE-cadherin and actin. (**e**) RhoA signalling is required for local MLC phosphorylation and endothelial pore confinement during neutrophil transmigration. Confocal imaging of paracellular migrating neutrophils through Lifeact-mCherry (red) expressing HUVECs after 72 hours transfection with control siRNA (upper panel) or RhoA siRNA (lower panel) under physiological flow conditions (0.8 dyne/cm^2). Open arrows in the apical and basal plane indicate filopodia-like protrusions at the apical site and the cortical F-actin-ring at the basolateral site of the endothelial pore, respectively. Filled arrows indicate MLC phosphorylation (green) localization during neutrophil transmigration under physiological flow conditions (0.8 dyne per cm^2). Asterisk indicates extravasating leukocyte in DIC. Scale bar, 10 µm. (**f**) Confocal imaging of F-actin dynamics during leukocyte diapedesis in retina vasculature of Lifeact-EGFP mice. Upper panel shows x-y and z-x projection of Lifeact-EGFP surrounding isolectin B4 (IB4) positive neutrophil. Open and filled arrows indicate Lifeact-EGFP localization to the endothelial pore at the basolateral or apical site, respectively. Asterisk indicates transmigrating neutrophil. Scale bar, 2µm. ** $P < 0.01$ and * $P < 0.05$ siCTRL vs siRhoA (Student's t-test) (**a**).Data are representative of four independent experiments (**a-d**) with >12 transmigration events per group (**c**) (error bars (**a**), s.e.m, (**c**), SD).
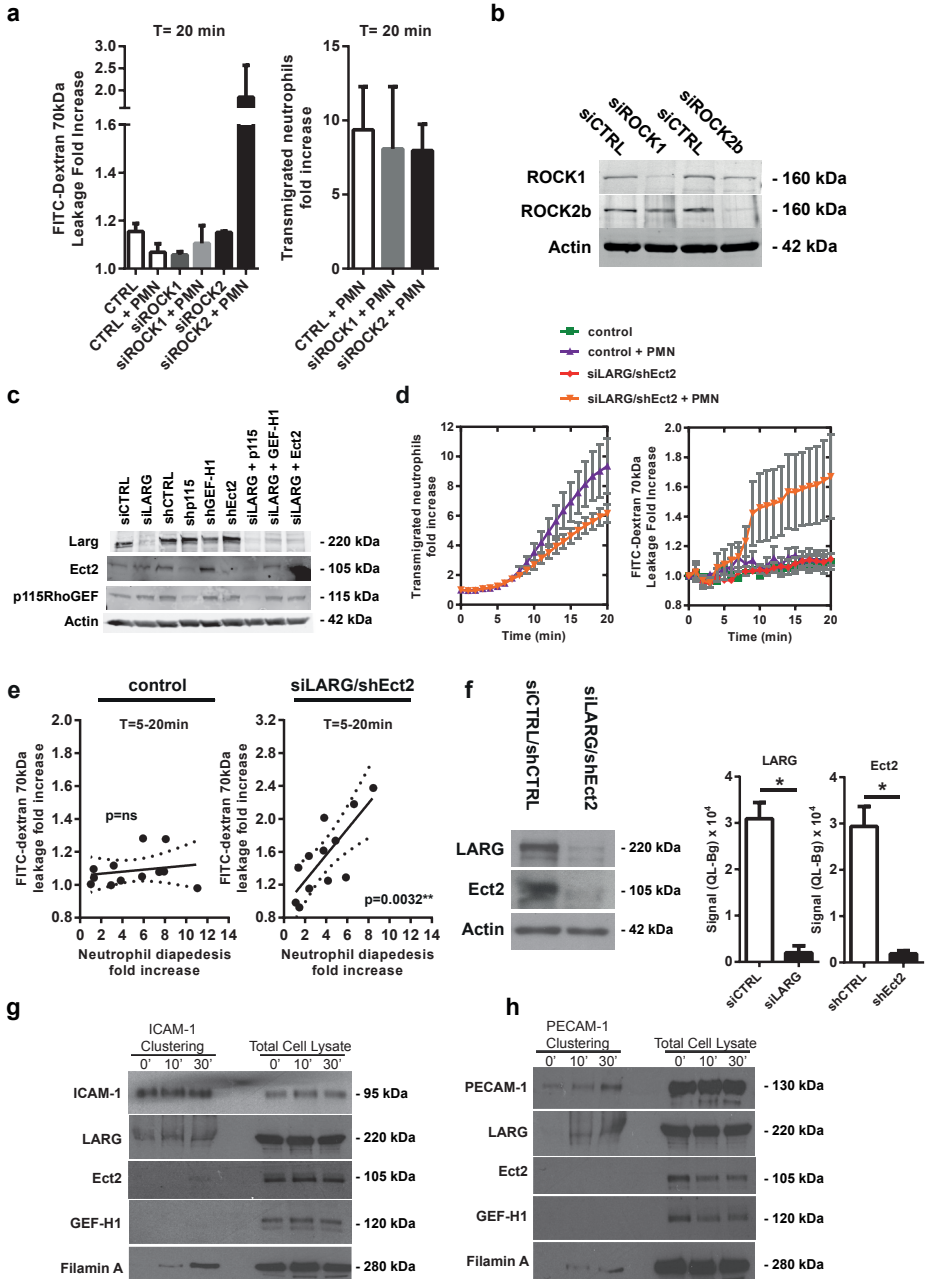
Supplementary Figure 5

a

b

c

d

e

f

4
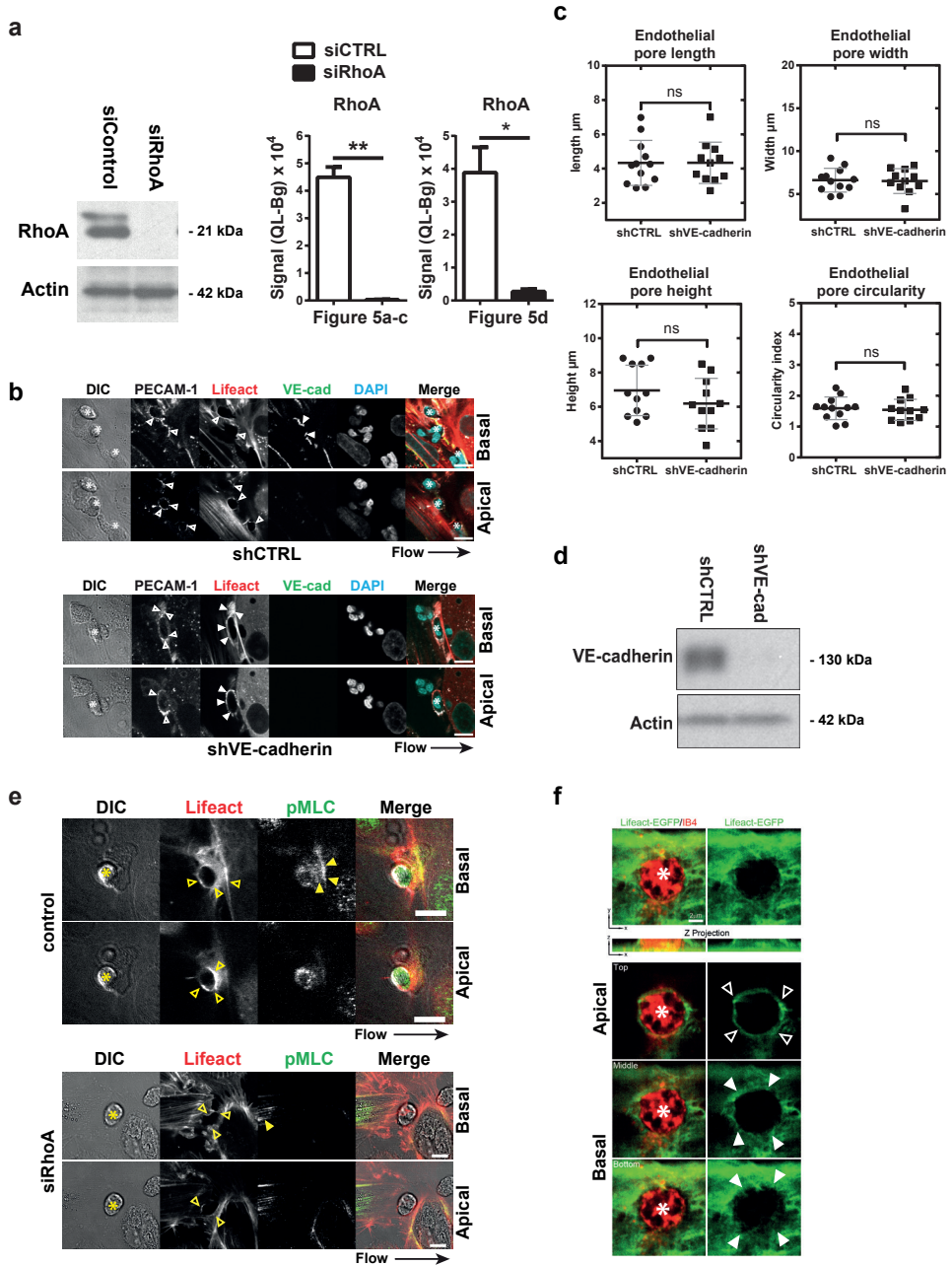
Supplementary Figure 6 LARG and Ect2 are recruited to intercellular tail of ICAM-1 upon clustering (**a**) Quantification of FITC-dextran and neutrophil extravasation after 20 minutes of neutrophil transmigration through control and ROCK1 or ROCK2b deficient ECs (**b**) Immunoblot analysis of protein extracts prepared from ECs treated with TNF-α overnight. Extracts were prepared 72 hours after transfection with control, ROCK1 or ROCK2b siRNA duplexes. Extracts were probed with antibodies directed against ROCK1, ROCK2b and actin. (**c**) Immunoblot analysis of protein extracts prepared from ECs treated with TNF-α overnight. Extracts were prepared 72 hours after transduction with control, Ect2, p115RhoGEF shRNA or transfection with LARG siRNA duplexes. Extracts were probed with antibodies directed against LARG, Ect2, p115RhoGEF and actin. (**d**) Extravasation kinetics of calcein-red labelled neutrophils and FITC-dextran through TNF-α treated ECs cultured on 3μm pore permeable filters. Neutrophils transmigrated towards a C5a chemotactic gradient in the lower compartment. Four conditions were tested; LARG/Ect2 deficient ECs + neutrophils (Orange line), control + neutrophils (purple line), LARG/Ect2 deficient ECs only (red line) and control only (green line). (**e**) Correlation analysis of dextran and neutrophil extravasation kinetics through control and LARG/Ect2 deficient ECs. (**f**) Endothelial LARG/Ect2 depletion by RNAi. Immunoblot analysis of protein extracts prepared from HUVEC treated with TNF-α overnight. Extracts were prepared 72 hours after transfection with control and Ect2 shRNA or transfection with control and LARG siRNA duplexes. Extracts were probed with antibodies directed against LARG, Ect2 and actin. Quantification of LARG/Ect2 depletion, presented as 'quantum level' (sum of grayness of each pixel in blot) minus background (QL-Bg), normalized to that of actin. (**g**) ICAM-1 clustering using beads coated with anti-ICAM-1 antibodies pre-and post-membrane lysis. Extracts were probed with antibodies directed against ICAM-1, LARG, Ect2, GEF-H1 and Filamin A. (**h**) PECAM-1 clustering using beads coated with anti-PECAM-1 antibodies pre-and post-membrane lysis. Extracts were probed with antibodies directed against PECAM-1, LARG, Ect2, GEF-H1 and Filamin A. $r = 0.1994$ $P = 0.5345$ (Pearson correlation) transmigrated neutrophils versus FITC-dextran leakage in control HUVECs or $r = 0.7734$ ** $P < 0.01$ (Pearson correlation) transmigrated neutrophils versus FITC-dextran leakage in LARG/Ect2 depleted ECs (**b**). * $P < 0.05$ siCTRL vs siLARG (Student's t-test) * $P < 0.05$ shCTRL vs shEct2 (Student's t-test) (**f**). Data are representative for three independent experiments (**d-h**) (error bars (**d-f**), s.e.m).

Supplemental Figure 6.

Supplementary Figure 7 ICAM-1, but not PECAM-1 depletion elicits vascular permeability during neutrophil diapedesis. (**a**) Extravasation kinetics of calcein-red labelled neutrophils and FITC-dextran through TNF-α treated ECs cultured on 3µm pore permeable filters. Neutrophils transmigrated towards a C5a chemotactic gradient in the lower compartment. Four conditions were tested; ICAM-1 depletion (EC) + neutrophils (Orange line), control + neutrophils (purple line), ICAM-1 depletion (EC) only (red line) and control only (green line). (**b**) Correlation analysis of dextran and neutrophil extravasation kinetics through control and ICAM-1 depleted ECs. (**c**) Endothelial ICAM-1 depletion by siRNA. Immunoblot analysis of protein extracts prepared from HUVEC treated with TNF-α overnight. Extracts were prepared 72 hours after transfection with control or ICAM-1 siRNA duplexes. Extracts were probed with antibodies directed against ICAM-1 and actin. Quantification of ICAM-1 depletion, presented as 'quantum level' (sum of grayness of each pixel in blot) minus background (QL-Bg), normalized to that of actin. (**d**) Quantification of FITC-dextran and neutrophil extravasation after 20 minutes of neutrophil transmigration through control and PECAM-1 deficient ECs. (**e**) Immunoblot analysis of protein extracts prepared from HUVECs treated with TNF-α overnight. Extracts were prepared 72 hours after transduction with control and PECAM-1 siRNA duplexes. Extracts were probed with antibodies directed against PECAM-1 and actin and quantification of endothelial pore size in control and PECAM-1 deficient ECs. $r = 0.5688$ $P = 0.053$ (Pearson correlation) transmigrated neutrophils versus FITC-dextran leakage in control HUVECs or $r = 0.6078$ * $P < 0.05$ (Pearson correlation) transmigrated neutrophils versus FITC-dextran leakage in ICAM-1 depleted ECs (**b**). ** $P < 0.01$ siCTRL vs siICAM-1 (Student's t-test) (**c**). Data are from three experiments (**a-d**) or are representative of > 20 transmigration events error bars (**a-e**) are s.e.m.

Supplemental Figure 7.

a

b

siCTRL

T=5-20min

p=ns

FITC-dextran 70kDa leakage fold increase

Neutrophil diapedesis fold increase

silCAM-1

T=5-20min

p=0.036*

FITC-dextran 70kDa leakage fold increase

Neutrophil diapedesis fold increase

c

ICAM-1

ICAM-1 - 95 kDa

Actin - 42 kDa

Signal (QL-Bg) x 10^4

**

siCTRL silCAM-1

d

T= 20 min

ns

FITC-Dextran 70kDa Leakage Fold Increase

CTRL
CTRL + PMN
siPECAM-1
siPECAM-1 + PMN

T= 20 min

ns

Transmigrated neutrophils fold increase

CTRL + PMN
siPECAM-1 + PMN

e

PECAM-1 - 130 kDa

Actin - 42 kDa

Endothelial pore size

ns

Area µm^2

siCTRL siPECAM1

4

5

A local VE-cadherin/Trio-based signaling complex stabilizes endothelial junctions through Rac1

Ilse Timmerman[1], Niels Heemskerk[1], Jeffrey Kroon[1], Antje Schaefer[1], Jos van Rijssel[1], Mark Hoogenboezem[1], Jakobus van Unen[2], Joachim Goedhart[2], Theodorus W.J. Gadella Jr.[2], Taofei Yin[3], Yi Wu[3], Stephan Huveneers[1] and Jaap D. van Buul[1,*]

[1] Department of Molecular Cell Biology, Sanquin Research and Landsteiner Laboratory, Academic Medical Center, University of Amsterdam, 1066 CX, the Netherlands. [2] Swammerdam Institute for Life Sciences, Section of Molecular Cytology, van Leeuwenhoek Centre for Advanced Microscopy, University of Amsterdam, 1098 XH Amsterdam, the Netherlands. [3] Center for Cell Analysis and Modelling, University of Connecticut Health Center, Farmington, CT 06032, USA.

[*] Corresponding author:
Jaap D. van Buul; Sanquin Research and Landsteiner Laboratory; Academic Medical Center; University of Amsterdam; Address: Plesmanlaan 125, 1066 CX, Amsterdam, the Netherlands. Phone: +31-20-51233219; Fax: +31-20-5123310; E-mail: j.vanbuul@sanquin.nl

Abstract

Endothelial cell-cell junctions maintain a restrictive barrier that is tightly regulated to allow dynamic responses to permeability-inducing angiogenic factors as well as inflammatory agents and adherent leukocytes. The ability of these stimuli to transiently remodel adherens junctions (AJs) depends on Rho-GTPase-controlled cytoskeletal rearrangements. How activity of Rho-GTPases is spatio-temporally controlled at endothelial AJs by guanine-nucleotide exchange factors (GEFs) is incompletely understood. Here, we identify a crucial role for the Rho-GEF Trio in stabilizing VE-cadherin-based junctions. Trio interacts with VE-cadherin and locally activates Rac1 at AJs during nascent contact formation, assessed using a novel FRET-based Rac1 biosensor and biochemical assays. The Rac-GEF domain of Trio is responsible for remodeling of junctional actin from radial to cortical actin bundles, a critical step for junction stabilization. This promotes the formation of linear AJs and increases endothelial monolayer resistance. Collectively, our data show the importance of spatio-temporal regulation of the actin cytoskeleton through Trio and Rac1 at VE-cadherin-based cell-cell junctions to maintain the endothelial barrier.

INTRODUCTION

The endothelium lining the vessel wall forms a major barrier between the circulation and the surrounding tissues, preventing plasma leakage. Endothelial adherens junctions, comprising the vascular endothelial (VE)-cadherin-catenin complex, function to maintain the monolayer integrity. VE-cadherin-based cell-cell junctions are dynamic and remodeled during processes such as leukocyte extravasation or angiogenesis, and also during homeostasis (Dejana, 2004; Vestweber et al., 2009). Therefore, cell-cell junctions are tightly regulated. VE-cadherin's extracellular domain mediates homophilic calcium-dependent adhesion, whereas β-catenin indirectly links the intracellular domain of VE-cadherin to the actin cytoskeleton via α-catenin (Lampugnani et al., 1992; Navarro et al., 1995). Additional F-actin binding and regulating proteins are recruited to modify the strength of VE-cadherin-based adhesions (Bershadsky, 2004; Huveneers and de Rooij, 2013).

Changes in the actin cytoskeleton have a major impact on the morphology and stability of VE-cadherin-based cell-cell junctions (Hultin et al., 2014; Noda et al., 2010; Phng et al., 2015; Sauter et al., 2014; Schulte et al., 2011), in part by altering the magnitude and direction of forces exerted on cell-cell junctions (Oldenburg and Rooij, 2014). Distinct types of cell-cell junctions exist depending on the organization of the junction-associated actin cytoskeleton. Destabilization of cell-cell junctions in response to permeability-inducing factors, such as thrombin and Vascular Endothelial Growth Factor (VEGF), is associated with the presence of radial contractile actin bundles that terminate at cell-cell junctions. These remodeling junctions have a discontinuous morphology and a different molecular build-up. In this study, we will refer to these junctions as Focal Adherens Junctions (FAJs) to make a distinction from other junction conformations (Huveneers et al., 2012). On the other hand, cell-cell adhesion stabilization is supported by cortical actin bundles that run parallel to the cell-cell junction (Noda et al., 2010). The presence of thick cortical actin bundles near junctions correlates with the appearance of stable, continuous junctions (Oldenburg and Rooij, 2014). Interestingly, homophilic ligation of cadherins has been reported to directly recruit and activate actin regulators that reorganize the cytoskeleton, indicative for bidirectional interplay (Huveneers and de Rooij, 2013; Kovacs et al., 2002; Lambert et al., 2002).

Members of the Rho family of GTPases are of key importance in the control of actomyosin organization. In epithelial cells, the small GTPase Rac1 initiates cell-cell adhesion by promoting Arp2/3-based membrane protrusions and eventually stabilizes these contacts by promoting the

formation of cortical actin bundles adjacent to the junction (Yamada and Nelson, 2007; Yamazaki et al., 2007; Zhang et al., 2005). However, junction formation in endothelium and epithelium does not follow the exact same mechanism. Hoelzle and Svitkina for example showed that endothelial cells use lamellipodia as the initial contact and then transform these into filopodia-like bridges that develop into nascent VE-cadherin-based junctions (Hoelzle and Svitkina, 2012). Moreover, Rac1 is reported to be required for barrier maintenance, but also needed for VE-cadherin endocytosis and reactive oxygen species (ROS)-mediated loss of VE-cadherin-mediated cell-cell contacts (Gavard & Gutkind, 2006; Spindler, Schlegel, & Waschke, 2010; van Wetering et al., 2002). Thus, Rac1 controls signaling mechanisms that have opposing effects on endothelial cell-cell junctions, suggesting a need for fine-balanced spatial and temporal regulation of its activity.

A possible mechanism for the spatio-temporal activation of Rac1 at cell-cell junctions is through localized activation of guanine-nucleotide exchange factors (GEFs); factors that activate small GTPases by promoting the exchange of bound GDP for GTP (Rossman et al., 2005). It is still unclear which of the many identified Rac-GEFs function in endothelial cells control VE-cadherin-based cell-cell junctions. Previous work of our group implicated the Rac1-GEF Trio in primary human endothelium as an important regulator of transendothelial migration of leukocytes (van Rijssel et al., 2012b). Because we observed that Trio localizes at endothelial cell-cell junctions, we further studied whether Trio has a role in the regulation of endothelial junctions. Here, we show that Trio binds to VE-cadherin during junction (re-) formation, locally activates Rac1 and thereby promotes the transition from nascent-to-stable VE-cadherin-based adhesion.

RESULTS

TRIO CONTROLS ENDOTHELIAL CELL-CELL JUNCTION ORGANIZATION AND BARRIER FUNCTION.

Our previous work identified a role for the endothelial GEF Trio in inflammation and leukocyte diapedesis. Also we observed that Trio-deficient endothelial cells (ECs) form less linearly organized cell-cell junctions (van Rijssel et al., 2012b; Van Rijssel et al., 2013). To investigate the role of Trio in endothelial junction regulation, we silenced Trio expression in ECs with short hairpin RNAs (shRNAs). Trio-deficient cells showed a larger phenotype compared to control cells. Using real-time imaging of VE-cadherin-GFP, we found that cell-cell junctions of

Trio-deficient ECs (marked by TagRFP) remained unstable compared to shCTRL-treated cells (Fig. 1A and Movie S1). Detailed analysis showed that both control and Trio-deficient ECs displayed linear and irregular cell-cell junctions (Fig. 1B). These irregular junctions were previously described and named focal adherens junctions (FAJ), which are sites of junction remodelling (Huveneers et al., 2012) (Fig. 1B). We quantified the amount of FAJ in monolayers by using VE-cadherin as a marker for cell-cell junctions and compared the length of the FAJ to the total junction length, according to the quantification approach described by Wilson and colleagues (Wilson et al., 2013) (Fig. S1B). This revealed that ECs lacking Trio showed increased FAJs (Fig. 1B, S1B). Moreover, studying the amount of FAJ area in time revealed that a major portion of the junctions between Trio-deficient cells remain organized as FAJs (Fig. S1B). We wish to note that some of the FAJ in control cells showed a thicker phenotype, whereas FAJ from Trio-deficient cells showed a more focal phenotype. Both phenotypes were quantified as FAJ (Fig. S1B). This indicates that cell-cell junctions in Trio-deficient cells remained unstable and continuously dis- and re-assemble.

To test if Trio deficiency has functional consequences for monolayer barrier function, we measured the electrical resistance of endothelial monolayers using electrical cell-substrate impedance sensing (ECIS). We found that silencing Trio, using two independent shRNA constructs, strongly reduced EC monolayer resistance compared to control cells, indicating that a lack of Trio reduces junction integrity (Fig. 1C). Also permeability was increased in Trio-deficient ECs, as was assessed by determining leakage of fluorescently-labeled dextran across Transwell filters (Fig. S1C). Thus, these data showed that Trio is required for barrier function by regulating endothelial cell-cell junction organization.

Trio is a Rho-GEF comprising three catalytic domains: two GEF domains, to activate small GTPases and a serine/threonine kinase domain (Fig. 1D). The N-terminal GEF domain (GEF1) activates Rac1 and RhoG whereas the C-terminal GEF domain (GEF2) activates RhoA (Blangy et al., 2000; Debant et al., 1996; van Rijssel et al., 2012a). Using the GEF1 inhibitor ITX3, we showed that the activity of GEF1 is required to maintain endothelial resistance (Fig. S1D). To further test if Trio activity is involved in the regulation of the barrier function of the endothelium, we rescued the impaired resistance of shTrio-expressing ECs by expressing the N-terminus of Trio (TrioN), which includes GEF1 and which expression is not targeted by the shRNA (van Rijssel et al., 2012a). The endothelial barrier defect of Trio-deficient cells was readily rescued by expression of TrioN (Fig. 1E, S1E). Moreover, TrioN overexpression in wild type HUVECs enhanced endothelial monolayer resistance, whereas overexpression

5
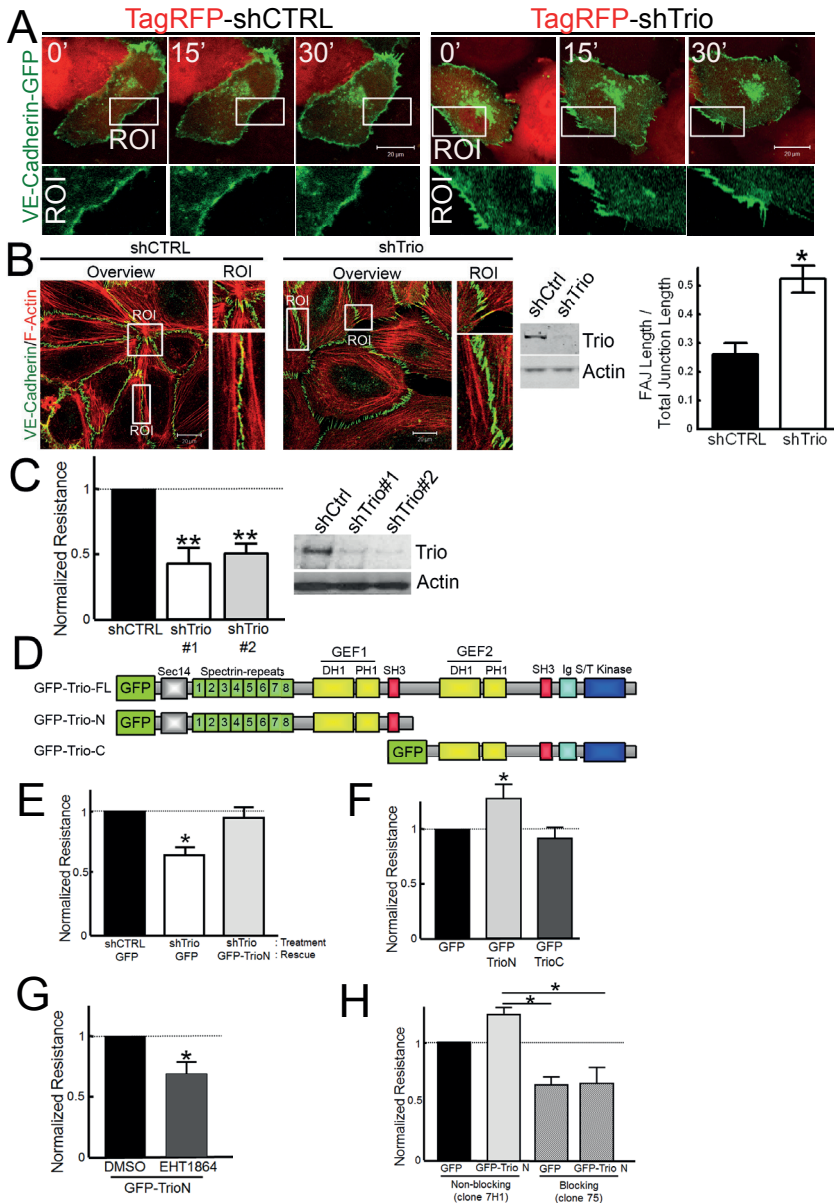
Figure 1. *Trio promotes endothelial barrier function.* (**A**) ECs are transfected with TagRFP-shCTRL or TagRFP-shTrio (red) and VE-cadherin-GFP (green). Dynamics of cell-cell junctions were followed over time as indicated. Regions of interest (ROI) show VE-cadherin-GFP distribution in time. Bar: 20 μm. (**B**) HUVECs were transduced with shCTRL or shTrio and stained as indicated. Western blot shows Trio knock down. FAJ length versus total junction length was quantified. (**C**) ECs were transduced with control or two different Trio shRNAs and electrical resistance was monitored by ECIS. Bar graph represents electrical resistance one day after seeding. Western blot shows Trio knock down. (**D**) Overview of GFP-Trio

of the C-terminus of Trio (TrioC), including GEF2, did not (Fig. 1F, S1E). Inhibiting Rac1 by EHT-1864 (Onesto et al., 2008) in cells expressing TrioN additionally showed that TrioN promoted the endothelial electrical resistance through the activation of Rac1 (Fig. 1G). In order to investigate if TrioN-mediated increase in resistance involves VE-cadherin, we used a VE-cadherin blocking antibody. This antibody efficiently reduces VE-cadherin-mediated barrier function (Corada et al., 2001; van Buul et al., 2005). When ECs were pretreated with this antibody, overexpression of TrioN in Trio-deficient cells failed to rescue the drop in electrical resistance, indicating the involvement of VE-cadherin in Trio-mediated barrier enhancement (Fig. 1H). Together, these data indicate that Trio is required to maintain the endothelial barrier function in a Rac1-dependent manner.

Since junctions of Trio-deficient ECs rapidly dis- and re-assemble, we next focused on the role of Trio during junction remodeling and used the permeability mediator thrombin to induce actomyosin-dependent junction disruption (Huveneers et al., 2012; van Hinsbergh, 2002). Thrombin rapidly destabilized cell-cell junctions (within 5 minutes) followed by recovery of cell-cell junctions after 30 minutes, resulting in full restoration of EC monolayer integrity after approximately 2-3 hours (Movie S2). Interestingly, overexpression of TrioN promoted the formation of linear junctions in ECs and prevented the loss of cell-cell contact induced by thrombin (Fig. 2A, Movie S3), indicating that Trio promotes the stabilization of cell-cell junctions. Conversely, ECIS experiments showed that depletion of Trio delayed recovery of barrier function after thrombin treatment (Fig. 2B). Quantification of the recovery after 3h of thrombin treatment showed that the control cells reached maximal recovery, whereas in Trio-deficient cells, the recovery was significantly delayed to 59%. To investigate if during recovery, Trio directly controls VE-cadherin-based junction assembly, we performed real-time imaging of VE-cadherin-GFP in Trio-depleted and control ECs. In control conditions, thrombin rapidly remodeled and disrupted VE-cadherin-positive cell-cell junctions, followed by re-assembly of cell-cell contacts and formation of linear junctions (Fig. 2C, Movie S4). In Trio-deficient cells, cell-cell junctions were

constructs: GFP-Trio full length (FL), the N-terminus of Trio containing GEF1 (GFP-TrioN) and the C-terminus containing GEF2 (GFP-TrioC). (**E**) ECs were transduced with Trio or control shRNA, followed after 2 days by infection with adenovirus expressing GFP or GFP-TrioN. Bar graph represents electrical resistance. (**F**) ECs were transduced with adenovirus encoding GFP-TrioN or GFP-TrioC. (**G**) ECs were transduced with adenovirus encoding GFP-TrioN. Rac1 activity was inhibited by 50mM EHT-1864. (**H**) ECs expressing GFP or GFP-TrioN were grown to confluence on electrode-arrays. One day after cell seeding a non-blocking (clone 7H1) or blocking (clone 75) VE-cadherin antibody was added (6.25 ug/mL). All experiments have been performed at least three times. Data are mean±SEM. *p<0.05; **p<0.01.
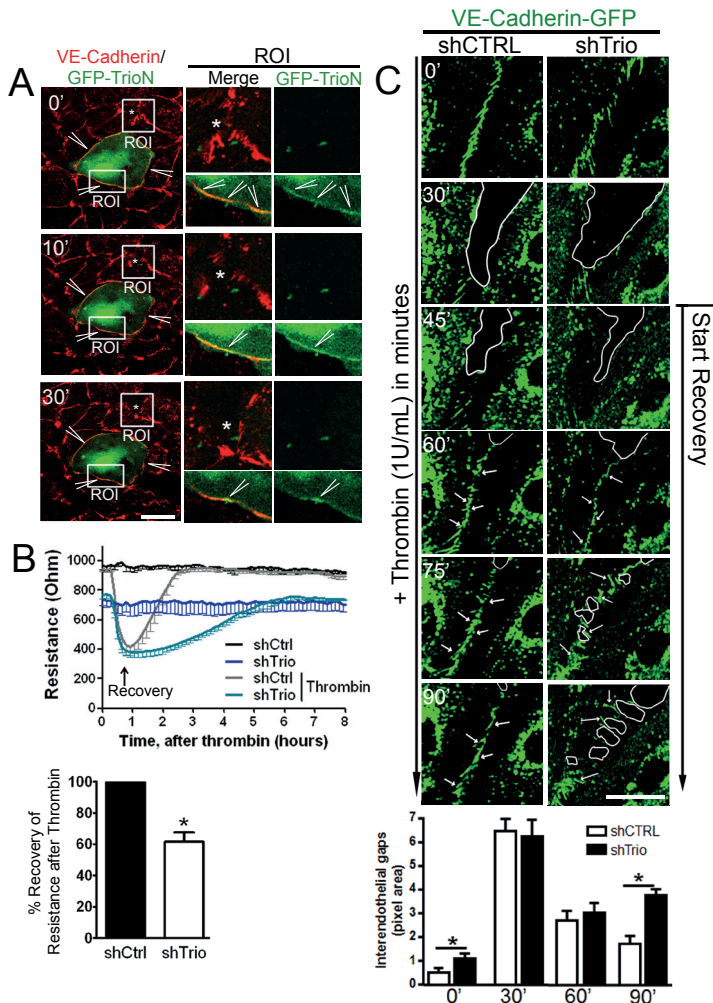
Figure 2. *Trio is required for efficient cell-cell junction recovery.* (**A**) Still images and ROIs from time-lapse recordings (Movie S3) showing linear stable cell-cell junctions (arrowheads) in GFP-TrioN-expressing cells, 10-30 min. after thrombin stimulation, whereas a major part of cell-cell junctions of non-transfected cells are disrupted (asterisks). VE-cadherin is visualized using VE-cadherin-ALEXA-647 antibody. Bar: 20 µm. (**B**) ECs were transfected with control (dark line) or Trio (blue line) shRNA and grown to confluence on FN-coated electrode-arrays. At time-point 0, cells were incubated with (dashed line) or without (solid line) thrombin. Resistance was monitored in time by ECIS. Arrow indicates starting point of recovery phase. Bar graph represents percentage recovery of the endothelial monolayer resistance after thrombin at time-points when control monolayers were completely restored. (**C**) Still images of time-lapse recording of thrombin-stimulated control or Trio-depleted ECs expressing VE-cadherin-GFP. See also corresponding Movie S4 as representative of multiple experiments. Arrows indicate formation of cell-cell junctions during recovery phase, indicated by arrow on the right and white lines indicate gaps appearing in Trio-deficient cells. Bar: 10 µm. Analysis of interendothelial gaps based on DIC imaging showed increased gaps in Trio-deficient cells after thrombin. All experiments have been repeated three times. Data are mean±SEM. *p<0.05.

remodeled likewise, followed by re-assembly of the junctions. However, newly formed VE-cadherin-based junctions remained instable and rapidly dis-assembled again (Fig. 2C, Movie S4). Quantification of interendothelial gaps based on DIC after 90 minutes of thrombin showed significantly larger gaps in Trio-deficient cells compared to control cells (Figure 2C, S1F). Thus, Trio is required for stabilization of VE-cadherin-based cell-cell junctions.

Trio localizes at endothelial cell-cell junctions.

To further assess the role of Trio in the regulation of endothelial cell-cell junctions, we focused on the subcellular distribution of Trio. Due to the lack of proper antibodies to detect endogenous Trio in immunofluorescence, we transfected GFP-Trio full length (FL) in primary ECs and observed that Trio localized at cell-cell junctions (Fig. 3A). By expressing different Trio truncation mutants, we found that TrioN, but not TrioC localized at cell-cell junctions (Fig. 3A). This indicates that the N-terminus of Trio, encoding the Sec14 domain, spectrin-repeats and the Rac1/RhoG GEF1 domain, is required for targeting of Trio to cell-cell junctions. We next examined the localization of Rac1 and RhoG and expressed the constitutively active forms of these GTPases in ECs. We found that active Rac1, but not RhoG, co-localized with VE-cadherin, indicating that Rac1 is involved in regulating endothelial cell-cell contacts downstream of Trio (Fig. S1G).

To test if VE-cadherin is necessary for Trio localization at cell-cell junctions, we used Chinese Hamster Ovary (CHO) cells that lack endogenous cadherin expression. We found that myc-tagged Trio-FL only localized at cell-cell contacts when VE-cadherin was co-expressed (Fig. 3B). Additionally, silencing VE-cadherin in ECs prevented Trio localization at cell-cell junctions (Fig. 3C, S1H). Interestingly, silencing VE-cadherin did not prevent β-catenin from localizing at cell-cell junctions. Previous work from the group of Dejana showed that under these conditions, N-cadherin localizes at cell-cell junctions (Navarro et al., 1998). Thus, these experiments show that Trio localization at cell-cell contacts depends on the specific presence of VE-cadherin.

Trio interacts with VE-cadherin.

We next investigated whether Trio interacts with the VE-cadherin-catenin complex. Therefore, immunoprecipitation of endogenous Trio from EC lysates was analyzed by Western blotting. These experiments revealed that Trio associates with the VE-cadherin complex, but not with N-cadherin, PECAM-1, VEGFR-2 or the tight junction protein ZO-1 (Fig. 4A). Of interest, inhibition of Trio-GEF1 activity using ITX3 did not dissociate
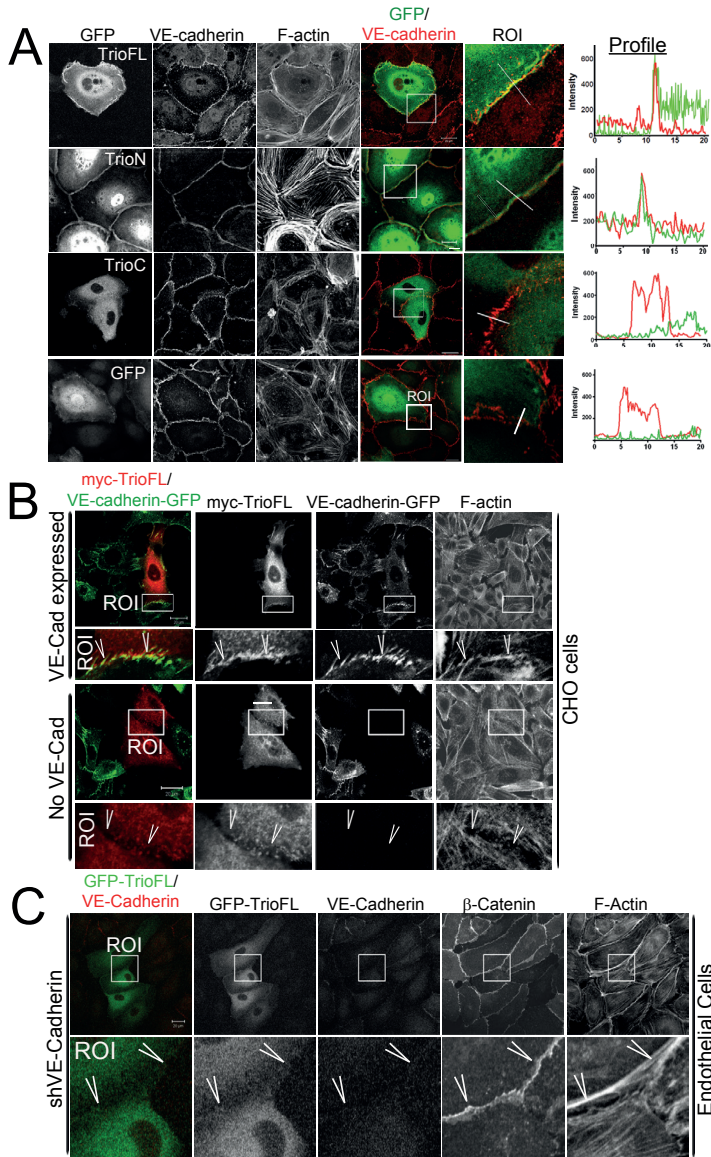
Figure 3. *Trio localizes at endothelial cell-cell contacts.* **(A)** ECs were transfected with GFP-TrioFL, GFP-TrioN or GFP-TrioC and stained as indicated. ROIs show co-localization between Trio and VE-cadherin. Profile shows fluorescence intensity of VE-cadherin (red) and GFP proteins (green) according to the line present in ROI. Bar: 20 µm. **(B)** CHO cells were transfected with myc-TrioFL and transduced with adenovirus containing VE-cadherin-GFP. Cells were stained as indicated. ROIs show that myc-TrioFL localization at cell-cell contacts depends on VE-cadherin expression. Arrow heads indicate cell-cell contact areas. Bar: 20 µm. **(C)** ECs were silenced for VE-cadherin and transfected with GFP-TrioFL and stained as indicated. ROIs show no localization of Trio at VE-cadherin-deficient cell-cell contact, but do show β-catenin. Arrowheads indicate cell-cell contact area. Bar: 20 µm.

VE-cadherin from Trio (Fig. S1I), demonstrating that the interaction did not depend on the activity of GEF1. To determine which component of the VE-cadherin complex is required for the interaction with Trio, we used several VE-cadherin truncation mutants and alpha-catenin fusion proteins to examine binding capacity to Trio in cells (Noda et al., 2010) (Fig. 4B). All VE-cadherin-GFP mutants as well as wild type VE-cadherin-GFP localize to cell-cell contacts (Noda et al., 2010). Western blot analysis of immunoprecipitations of these VE-cadherin mutants revealed that Trio showed the strongest binding to the full length VE-cadherin construct (Fig. 4C). The interaction of Trio with the VE-cadherin complex was reduced in the absence of the β-catenin binding domain (VEΔβ-GFP), as well as when the complete cytoplasmic domain of VE-cadherin was replaced by full length α-catenin (VEΔC-α-GFP) or α-catenin lacking the N-terminal β-catenin binding domain (VEΔC-αΔN-GFP) (Fig. 4C). Because β-catenin did co-precipitate with VEΔC-α-GFP, and not with VEΔβ-GFP, together with the localization studies presented in figure 3C, these results indicate that Trio interacts with VE-cadherin through a region in the intermediate domain proximal to the β-catenin binding domain.

To study if Trio directly interacts with VE-cadherin, we designed two peptides that encode for the intermediate domain of human VE-cadherin (Fig. 4D). Precipitation experiments from cell lysates showed that Trio has higher affinity to the region of VE-cadherin that partially overlapped with the β-catenin binding site (aa 726-765; Fig. 4E) as compared to the region that includes aa 697-735. Since TrioN, but not the GEF1 domain only co-localized with VE-cadherin (Fig. 3A, S1J) and immunoprecipitation studies between VE-cadherin and different Trio mutants showed strong binding of TrioN with endogenous VE-cadherin (Fig. 4F), we focused on the N-terminal spectrin-repeats, known as protein-protein binding regions, as potential binding sites of Trio for VE-cadherin (Djinovic-Carugo et al., 2002). Using GST-fusion constructs of Trio spectrin-repeats 1-4 and 5-8, we found that the VE-cadherin peptide directly associated with the spectrin-repeats 5-8, whereas a scrambled peptide did not (Fig. S2A, S2B). Further analysis showed that VE-cadherin directly associated to the spectrin-repeats 5-6 through its intracellular region 726-765 (Fig. 4G, S2B). These data show that Trio may directly interact with the intracellular tail of VE-cadherin.

Trio dynamically interacts with VE-cadherin.

We next questioned if the Trio-VE-cadherin interaction is regulated during assembly, stabilization and remodeling of junctions. Since most junctions are stabilized in confluent monolayers, we first tested whether the interaction of Trio with the VE-cadherin-catenin complex is confluency-dependent. Trio immunoprecipitations were performed using
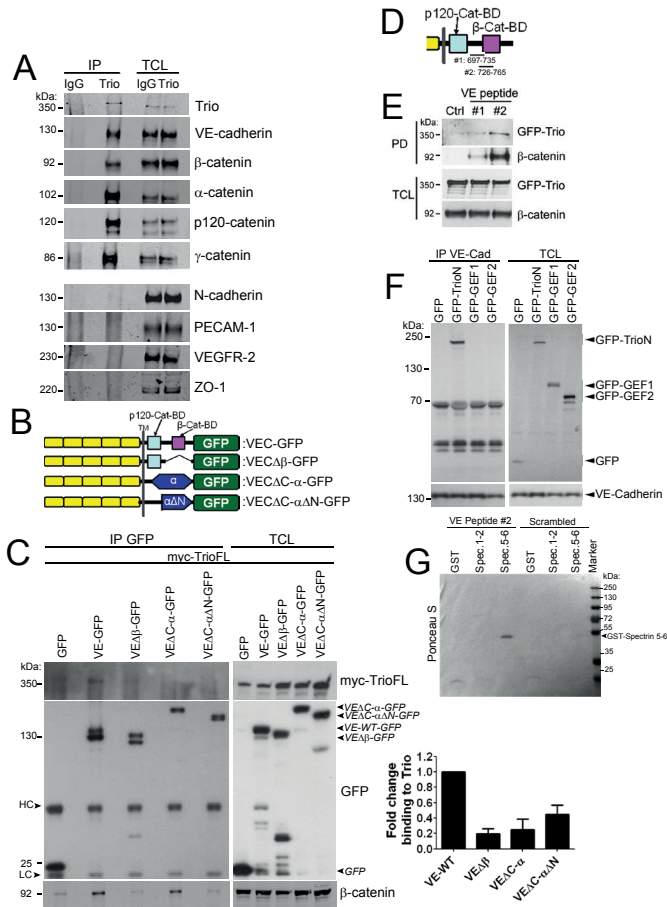
Figure 4. *Interaction of Trio with VE-cadherin.* **(A)** Trio IP from EC lysates and analyzed with Western blot. VE-cadherin and the catenins were precipitated whereas N-cadherin, PECAM-1, VEGFR2 and ZO-1 were not. **(B)** Overview VE-cadherin constructs. VEΔβ-GFP: deletion of α-catenin binding domain, VEΔC-α-GFP: cytoplasmic domain is replaced with α-catenin, VEΔC-αΔN-GFP: cytoplasmic domain is replaced with α-catenin lacking the N-terminal α-catenin binding domain. **(C)** Cos7 cells were transfected with myc-tagged TrioFL and wild type (WT) VE-cadherin-GFP or a VE-cadherin mutant as indicated. VE-cadherin-GFP was IP-ed using an anti-GFP antibody and binding of myc-TrioFL was determined by Western blotting. Panel at the right shows quantification of three independent experiments. Data are mean±SEM. **(D)** Illustration of the designed VE-cadherin peptides #1 and #2. **(E)** HEK293 cells were transfected with GFP-TrioFL and lysed. Specific biotin-tagged peptides, encoding regions of the VE-cadherin cytoplasmic tail as indicated, were used to pull down (PD) GFP-Trio. VE #2 efficiently precipitated TrioFL as well as α-catenin. **(F)** HUVECs were transfected with GFP-Trio mutants as indicated and VE-cadherin was immunoprecipitated (IP). Western blot shows interaction of VE-cadherin with TrioN but not with GEF1, GEF2 or GFP. Panels on the right show protein expression in total cell lysates (TCL). **(G)** VE-cadherin peptide #2 was co-incubated with GST-spectrin-repeats as indicated. Western blot analysis shows that Trio spectrin-repeats 5-6 interacted with VE #2 and not with the scrambled peptide. Experiments are carried out three times independently.

cell lysates of endothelial monolayers lysed 1 day after plating (recently confluent), and monolayers lysed 6 days after plating (long confluent) (Fig. 5A). Immunoprecipitates of Trio contained considerably more VE-cadherin and β-catenin when obtained from cells lysed 1 day after plating as compared to lysates from cells lysed 6 days after plating. Note that we corrected for total protein concentration, i.e. similar amounts of total Trio and VE-cadherin protein were present in the cell lysates used for immunoprecipation. Thus, the binding of Trio to the VE-cadherin complex depends on monolayer confluency, being reduced when junction stability is increased.

To study if the Trio-VE-cadherin interaction is regulated during nascent cell-cell junction assembly, the interaction was analyzed in cells during a calcium-switch assay. Confluent endothelial monolayers were treated with the calcium chelator EGTA, disrupting adherens junctions, followed by a washout and re-addition of calcium to restore cell-cell contact. Immunoprecipitation studies showed that the interaction of Trio with VE-cadherin significantly increased after already 15 minutes of calcium re-addition. After 5 hours of re-addition of calcium, Trio-VE-cadherin interactions were back to basal level (Fig. 5B). The phenotypic re-assembly of cell-cell junctions after EGTA treatment is visible after 60 minutes of re-addition of calcium. However, in Trio-deficient cells, junction recovery was still largely impaired at these time points (Fig. S2C).

Additionally, we used thrombin to induced junction remodeling and study the regulation of the Trio-VE-cadherin interaction. Trio immunoprecipitations showed that 30 minutes after thrombin stimulation, when thrombin-induced cell-cell junction disruption and resistance drop were maximal (Fig. 2B), Trio binding to VE-cadherin was reduced compared to untreated cells. However, Trio-VE-cadherin interaction significantly increased during the recovery phase, i.e. when cell-cell junctions are re-assembled and the resistance is restored (Fig. 5C, 2B). The Trio-VE-cadherin interaction was also reduced after stimulation with the permeability factor VEGF (Fig. S2D). Together, these experiments show that Trio dynamically associates with the VE-cadherin complex primarily at nascent cell-cell contacts.

TRIO CONTROLS JUNCTION-ASSOCIATED ACTIN ORGANIZATION.

To examine the mechanism how Trio controls endothelial cell-cell junction integrity, we next studied the effect of Trio silencing on the organization of the VE-cadherin complex and the actin cytoskeleton in more detail. Loss of cell-cell junction integrity in Trio-deficient ECs did not result from changes in the expression levels of VE-cadherin, α/β/γ/p120-catenin or other junction adhesion molecules (Fig. S2E). Also, by

immunoprecipitating VE-cadherin from lysates, no changes were found in the composition of the VE-cadherin-catenin complex in Trio-deficient cells compared to controls (Fig. S2F). Interestingly, overexpression of TrioN induced strong cortical actin bundles at VE-cadherin-based junction regions (Fig. 3A, S3A). Since the function of VE-cadherin is known to be strongly influenced by re-arrangements of the actin cytoskeleton (Oldenburg and De Rooij, 2014), we next examined whether Trio controls junctional actin organization through the small GTPase Rac1.

VE-cadherin ligation activates Rac1 through Trio.

In epithelial cells, replacement of radial actin bundles by a peri-junctional actin belt has been proposed to be controlled by cadherins whose homophilic ligation can directly recruit and activate actin regulators (Cavey, 2009). Therefore, we studied whether VE-cadherin homophilic ligation induces Trio-dependent Rac1 activation. To biochemically analyze a defined number of nascent VE-cadherin-mediated adhesive contacts, endothelial cells were incubated with magnetic beads coated with the ecto-domain of VE-cadherin. VE-cadherin-coated beads specifically ligate endogenous VE-cadherin complexes (Fig. S3B). Interestingly, Rac1 activation was increased 15-30 minutes following VE-cadherin ligation, after which activation levels declined (Fig. 6A). In contrast, VE-cadherin ligation reduced the activation of both RhoG and RhoA (Fig. S3C, S3D). We next studied if Trio underlies VE-cadherin ligation-induced Rac1 activation. Although basal levels of Rac1 activity were increased in Trio-depleted cells compared to controls, Trio silencing blocked the increase in Rac1 activity observed after VE-cadherin ligation (Fig. 6B). We confirmed this with a different shRNA targeting Trio expression (Fig. S3E). Additionally, we observed that inhibition of GEF1 by ITX3 blocked VE-cadherin ligation-dependent Rac1 activation (Fig. 6C).

To show functional involvement of the GEF1 domain in junction regulation, we expressed TrioN in Trio-deficient endothelial cells and studied the amount of FAJ (Fig. 6D). To check whether the activity of the GEF1 domain is required, we induced two point mutants (N1406A/D1407A) in GEF1, resulting in a catalytic dead protein unable to activate Rac1 (Fig. S3F). Expression of the catalytic dead mutant did not reduce FAJ length in Trio-deficient cells (Fig. 6D). Additional experiments showed that TrioN-induced linearization of cell-cell junctions is independent of RhoG (Fig. S3G). Collectively, these data indicate that Trio is involved in Rac1 activation upon VE-cadherin ligation and mediates linearization of cell-cell junctions.

We next studied the spatial and temporal activation of Rac1 during endothelial cell-cell junction formation, using a novel Rac1 sensor called

the Dimerization-Optimized Reporter for Activation (DORA)-based Rac1-sensor (Fig. S4A). We first characterized the sensor for local Rac1 activation in random migrating endothelial cells (Fig. S4B, Movie S5), as well as EGF-treated HeLa cells (Fig. S4C, S4D). Additionally, we measured spatial and temporal Rac1 inactivation and activation upon thrombin treatment in endothelial cells (Fig. S4E, Movie S5). Moreover, we have performed FLIM measurements in cells expressing the Rac-wt or the constitutively active (Q61L) mutant sensor, showing reduced lifetime of the Q61L compared to

5
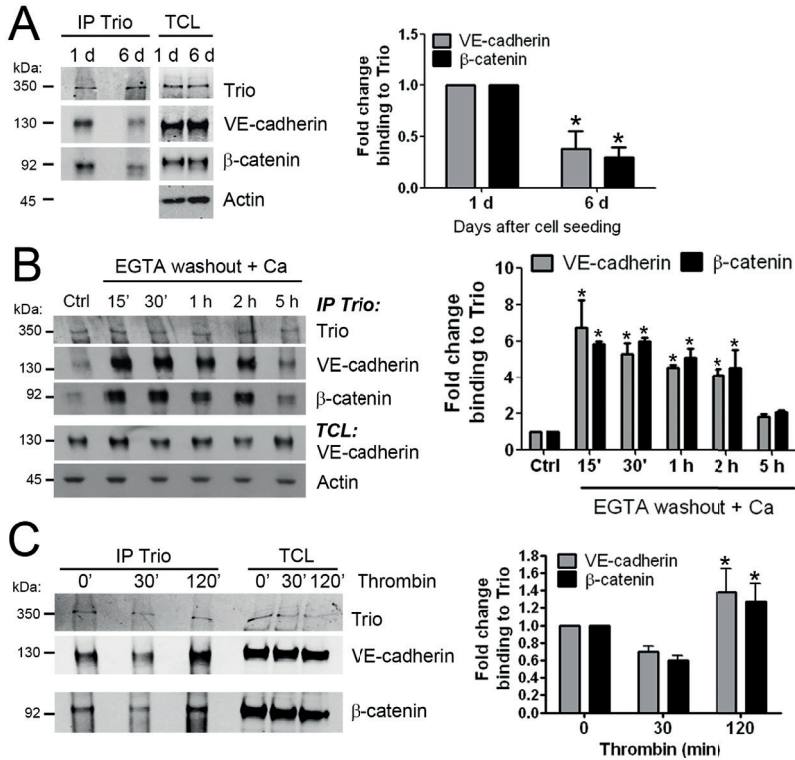
Figure 5. *Dynamic Trio-VE-cadherin interaction* **(A)** ECs of different confluency (days after seeding are indicated above) were lysed and subjected to Trio IP. Association of VE-cadherin and β-catenin to Trio was determined by Western blotting. Quantification is shown in right panel. **(B)** Long confluent ECs were subjected to calcium switch: EGTA treatment to chelate extracellular calcium leading to cell-cell junction disruption, followed by EGTA washout and calcium re-addition resulting in junction re-assembly. ECs were lysed at the indicated times after calcium re-addition and Trio IP was performed. Quantification is shown in right panel. **(C)** ECs were grown to confluence, stimulated with thrombin for 30 or 120 min., reflecting time-points of cell-cell junction disassembly and re-assembly, respectively. Cells were lysed and subjected to Trio IP. Association of VE-cadherin and β-catenin to Trio was determined by Western blotting. Quantification is shown in right panel. All experiments are performed at least three times. Data are mean±SEM. *p<0.05.

wild type version (2.4 vs. 2.9 ns, respectively) (Fig. S4F). Importantly, the dominant negative Rac1 sensor did not show any activity upon random migration of ECs (Fig. S4G). For more detailed text, see supplemental information section. These experiments showed an active and useful DORA Rac1 sensor with high FRET efficiency to measure spatio-temporal
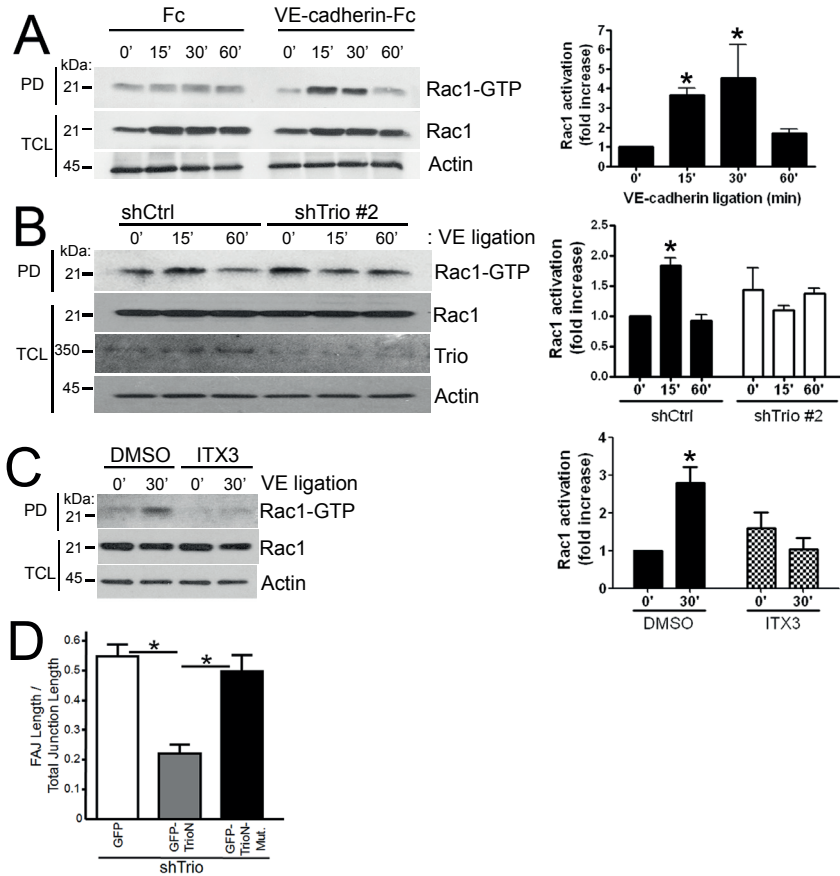
Figure 6. *VE-cadherin-induced Rac1 activation depends on Trio.* (**A-D**) VE-cadherin-ectodomain-Fc- or Fc-coated magnetic beads were added to an endothelial monolayer to induce VE-cadherin ligation. (**A**) Rac1 activation increases 15-30 min. after adding VE-cadherin-coated beads, as analyzed using a CRIB-peptide pull-down (PD) assay. Right panel shows quantification. (**B**) ECs were transduced with control or Trio shRNA. VE-cadherin ligation did not increase Rac1 activation in Trio-deficient cells. Right panel shows quantification. (**C**) VE-cadherin ligation was induced in ECs treated with DMSO or the Trio-GEF1 inhibitor ITX3. Treatment with ITX3 blocks VE-cadherin ligation-induced Rac1 activation. Right panel shows quantification. (**D**) Trio-deficient ECs (shTrio) were transfected with GFP, GFP-TrioN-wt or GFP-TrioN-1406A/D1407A and FAJ were quantified as described previously. Per condition, 25 cells are analyzed. All experiments are carried out at least three times independently. Data are mean±SEM. *p<0.05.

activation of Rac1 upon cell-cell junction assembly.

Endothelial cells were transfected with the DORA Rac1 sensor and α-catenin-mCherry to visualize the VE-cadherin complex. We monitored FRET during the assembly and disassembly cycle of forming junctions. At the initial stage of junction assembly, marked by α-catenin-mCherry, no FRET signal was detected (Fig. 7A, Movie S6). However, after approximately 15 minutes, increased FRET at α-catenin-selected regions of interest (ROI) was detected, showing local Rac1 activity at cell-cell junction regions (Fig. 7A, 7C, Movie S6). These data indicate that formation of nascent cell-cell junctions triggered local activation of Rac1. To investigate if Trio is involved in local activation of Rac1 at nascent cell-cell junctions, we analyzed ECs expressing TagRFP-Trio shRNAs and the DORA-Rac1 biosensor. To properly discriminate cell-cell junctions we additionally live-labeled with a VE-cadherin-ALEXA-647 antibody (Fig. 7B). We previously showed that this antibody did not interfere with the dynamics of VE-cadherin or the barrier function (Kroon et al., 2014). Using this set-up, we observed that junctions in Trio-deficient ECs rapidly dis- and re-assemble, as shown before. Interestingly, no increase in local Rac1 activity was measured at VE-cadherin-based junctions in Trio-deficient cells (Fig. 7D, Movie S7). Quantification of the emission ratio of the FRET showed a lack of Rac1 activity at selected cell-cell contact regions (ROI), marked by VE-cadherin, in Trio-deficient cells (Fig. 7C). Interestingly, we observed local Rac1 activity at the edge of non-junctional membrane protrusions in Trio-deficient cells, indicating that Rac1-mediated induction of protrusions per se is not regulated through Trio (Fig. S4G, Movie S8). However and in line with the previous experiment, at sites of junction assembly, marked by VE-cadherin, no increase in FRET is detected (Fig. S4G, Movie S8). Together, these data show that Trio controls spatial and temporal activation of Rac1 at sites of newly formed VE-cadherin-based junctions.

Discussion

Here we show that Trio regulates stabilization of nascent, VE-cadherin-based cell-cell adherens junctions (AJ) to maintain endothelial barrier properties. Mechanistically, we show that VE-cadherin ligation recruits and directly binds Trio, triggering spatio-temporal activation of the small GTPase Rac1, followed by stabilization of endothelial AJs.

The process of AJ formation can be subdivided in distinct stages: first, membrane protrusions generate initial contacts; second, cadherin molecules engage in homophilic interactions and form clusters; and third, homophilic ligation of cadherins triggers actin cytoskeleton
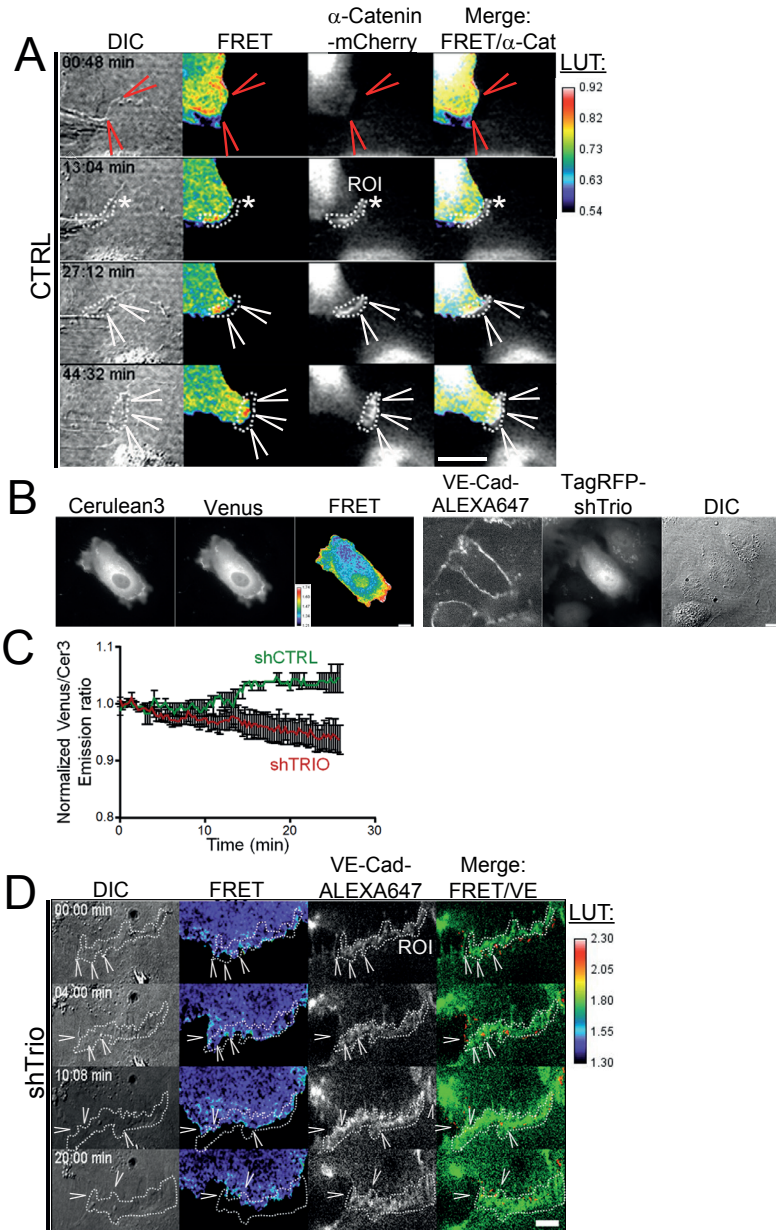
Figure 7. *Spatio-temporal Rac1 activity.* **(A)** ECs were transfected with the DORA Rac1 biosensor and α-catenin-mCherry to mark cell-cell junctions. Panels show DIC, ratiometric images with warm colors as increased FRET (Venus/Cer3) signals (see LUT on the right), α-catenin-mCherry and the merge with FRET in red and α-catenin-mCherry in white. Arrowheads show co-localization of local active Rac1 with α-catenin. Asterisk shows formation of nascent cell-cell junctions. Bar: 10 µm. **(B)** Trio-deficient ECs are marked by RFP tag; junction region is marked by VE-cadherin-ALEXA-647, since red channel is used by the RFP tag. All fluorescent signals

rearrangements, driving expansion and stabilization of the cadherin adhesive interface (Cavey, 2009). Rac1 activity has been shown to be involved in multiple of these stages of AJ formation, but also in AJ dissociation (reviewed in Spindler *et al.* (Spindler et al., 2010)). These apparently contradictory data underscore the importance of addressing spatial and temporal differences in Rac1 activity and understanding involvement of specific GEF-GTPase-effector complexes. We propose that Trio activity is in particular crucial during the above described third stage of the AJ formation process. This is based on our observation that local Rac1 activity at AJs was rapidly increased in a Trio-dependent manner during nascent contact formation, as was assessed using a novel FRET-based Rac1 biosensor. Moreover, homophilic ligation of VE-cadherin, triggered by VE-cadherin-coated beads, stimulated a rapid and transient Trio-dependent Rac1 activation. In line with this, AJs in Trio-deficient cells remained unstable and underwent continuous dis- and re-assembly. Importantly, Trio-deficiency did not prevent Rac1-induced membrane protrusive activity and formation of initial cell-cell contact. Thus, prior to stabilization of the nascent cell-cell contact induced by local signaling through the VE-cadherin-Trio-Rac1 axis, other Rac-GEFs likely contribute to promote initial cell-cell contact formation. For example Tiam-1, which is well recognized for its role in promoting epithelial cell-cell adhesion (Hordijk et al., 1997), has also been suggested for a role in controlling endothelial cell-cell junctions; re-introduction of VE-cadherin in VE-cadherin-null cells induced Rac1 activation and recruited Tiam-1 to cell-cell junctions (Birukova et al., 2012; Lampugnani et al., 2002). Conversely, Tiam-1 is reported to be required for platelet-activating factor-increased permeability (Knezevic et al., 2009). Clearly further study is needed to unravel how Trio may act in concert with other Rac-GEFs, such as Tiam-1, Vav2 (Gavard and Gutkind, 2006) and P-Rex1 (Naikawadi et al., 2012), to control endothelial AJs under resting or inflammatory conditions.

To our knowledge, Trio is the first example of a GEF binding to the cytoplasmic domain of VE-cadherin. Other GEFs like Tiam1, Syx and TEM4 have been shown to localize at endothelial cell-cell junctions or to co-IP with one of the VE-cadherin complex members but no *in vitro* interaction

5

were recorded in real-time. Bar: 10 μm. **(C)** Quantification of ratiometric changes at regions of nascent cell-cell junctions, marked by α-catenin or VE-cadherin (dotted line in panels A and D), show increased FRET signal after approx. 15 min. in shCTRL but not in Trio-deficient ECs. Graph shows representative presentation of three independent experiments. Data are mean±SEM. (**D**) Trio-deficient ECs (marked by TagRFP-shTrio) show no increase in FRET signal at sites of newly formed cell-cell junctions, marked by VE-cadherin-ALEXA-647 (arrowheads). Note that the basal FRET signals (LUT) are higher in Trio-deficient cells than in control cells (see LUT in A), in line with the biochemical data. Bar: 5 μm.

studies using peptides or GST–tagged proteins have been performed so far (Di Lorenzo et al., 2013; Lampugnani et al., 2002; Ngok et al., 2012; Ngok et al., 2013). We found that Trio especially interacted with the pool of VE-cadherin at (re-) assembling junctions, enabling temporally coordinated Rac1 activation. Although we could show that Trio binds to a region in VE-cadherin proximal to the β-catenin binding domain, our experiments indicate that Trio does not seem to compete with β-catenin for binding to VE-cadherin but may in fact form a ternary complex. Previously, Trio was reported to biochemically co-precipitate with M-cadherin, cadherin-11 and E-cadherin (Backer, 2007; Charrasse, 2007; Kashef, 2009; Li, 2011; Yano, 2011). In the latter study, activity of Trio at E-cadherin-based epithelial cell-cell junctions was described to down-regulate E-cadherin expression levels by activating a transcriptional E-cadherin repressor (Yano, 2011). In contrast, our data show that VE-cadherin and N-cadherin total protein levels are unaltered in Trio-deficient endothelial cells. Thus, Trio has distinct regulatory roles at AJs depending on the cadherin and cell type involved. Elucidating the mechanism how Trio is activated and recruited to the VE-cadherin complex will be exciting goals for future research.

Our finding that Trio silencing impairs endothelial barrier recovery in response to thrombin treatment supports our hypothesis that Trio activity is not only crucial for *de novo* assembly of AJs, but also for re-assembly of AJs following inflammatory remodeling of the vascular endothelium. In addition, even apparently stable endothelial monolayers display ongoing remodeling of cell-cell junctions and Rac1 activation in confluent endothelial monolayers has been suggested to reflect such local remodeling (Braga, 2005). Our finding that Trio-induced Rac1 activity contributes to maintain the endothelial barrier may therefore reflect on a smaller scale the requirement of Trio for re-assembly of cell-cell contacts. During endothelial AJ remodeling, the morphology of cell-cell junctions switches between linear AJs, paralleled by cortical actin bundles and focal AJs, connected to radial actin bundles (Huveneers, 2012). We found that Trio contributes to transition of radial to cortical actin bundles, promoting the formation of stable linear AJs. This transition in junctional actin organization has been suggested to take place very shortly after the initial clustering of cadherins (Cavey, 2009). This is in full accordance with our observations when measuring active Rac1 in real-time. We observed that Rac1 is activated several minutes after initial cell-cell junctions are formed. And although Rac1 is well-known to localize at de novo adhesion sites and promote lamellipodia formation through actin remodeling (Yamada and Nelson, 2007; Yamazaki et al., 2007; Zhang et al., 2005), further study is required to elucidate the detailed mechanism how Trio-induced Rac1 activity triggers actin cytoskeletal re-arrangements upon VE-cadherin

ligation. An interesting side observation was that Trio-deficient cells show a higher basal Rac1 activity and increased cell migration. One explanation for increased Rac1 activation may be that the instable cell-cell junctions in Trio-deficient cells trigger the release of a different Rac1 pool that becomes activated. This may also explain the increased spread surface area that was observed for Trio-deficient cells. In other cell types, cadherin ligation has been shown to recruit and activate actin-regulators, including Arp2/3 (Kovacs, 2002; Verma, 2004), Cortactin (Helwani, 2004), N-WASP (Ivanov, 2005) and Formin1 (Kobielak, 2004) (for review, see (Bershadsky, 2004; Yap, 2003)). Some of these factors that promote branched actin polymerization were found to be relatively depleted from older, more stable regions of epithelial cell-cell contacts (Helwani, 2004; Yamada and Nelson, 2007). Although there are notable differences between epithelial and endothelial cell-cell contacts with respect to the organization of the junction-associated actin cytoskeleton, similar actin regulators may be involved in VE-cadherin-based AJ strengthening.

In conclusion, Trio regulates spatial and temporal activation of Rac1 to drive VE-cadherin-based AJ re-assembly, not only after EC barrier disruption induced by inflammatory agents such as thrombin, but also for *de novo* assembly of AJs. Eventually, enhancing the VE-cadherin-Trio interaction may be considered as a potential novel therapeutic approach that may serve to counteract vascular leakage and/or inflammation.

Experimental Procedures

Antibodies

Monoclonal antibodies (mAb) to b-catenin, p120-catenin, g-catenin, Cdc42 (clone 44), Rac1, VE-cadherin (clone 75; used at 6.25 µg/ml) and an Alexa-647-conjugated VE-cadherin antibody (clone 7H1) were from BD Transduction Laboratories (Amsterdam, The Netherlands). mAbs to VE-cadherin (clone F8), RhoA and polyclonal Abs (pAb) to b-catenin, a-catenin and Trio (clone D-20) were purchased from Santa Cruz Biotechnology (Heidelberg, Germany). mAb to Trio was from Abnova (Heidelberg, Germany). VE-cadherin mAb clone 7H1 was from Pharmingen (San Diego, USA), VE-cadherin clone BV6 and RhoG mAbs were from Millipore (Amsterdam, The Netherlands). pAb to VE-cadherin was from Cayman (Michigan, USA). mAbs to a-tubulin (DM1A), actin (clone AC-40), HA was purchased from Sigma (Zwijndrecht, The Netherlands). pAb to VEGFR2 and pAb to mouse PECAM-1 were from R&D (Abingdon, UK). PECAM-1 Ab (CD31 clone 12F11) was from Sanquin (Amsterdam, The Netherlands). mAb for GFP (JL-8), secondary goat-anti-rabbit IR 680, goat-

anti-mouse IR 800 and donkey anti-goat IR 800 Abs were purchased from Licor Westburg (Leusden, The Netherlands). Abs to N-cadherin, myc, ZO-1 (A12), secondary Alexa-labelled Abs and Alexa-633-conjugated phalloidin and phallodin-texas red were from Invitrogen (Breda, The Netherlands). Secondary HRP-conjugated goat-anti-mouse, swine-anti-rabbit and rabbit-anti-goat Abs were purchased from Dako (Heverlee, Belgium).

Cell cultures, Treatments and Transfections

Human umbilical vein endothelial cells (HUVECs) were purchased from Lonza and cultured on FN-coated dishes in EGM-2 medium, supplemented with singlequots (Lonza, Verviers, Belgium). HUVECs were cultured until passage 7. HEK-293T, Cos7 and CHO (Chinese Hamster Ovary) cells were maintained in IMDM (Iscove's Modified Dulbecco's Medium) (BioWhittaker, Verviers, Belgium) containing 10% (v/v) heat-inactivated fetal calf serum (Invitrogen, Breda, The Netherlands), 300 mg/ml L-glutamine, 100 U/ml pen/strep. Cells were cultured at 37°C and 5% CO_2. Cells were pretreated for 20h at 37°C with 100 mM ITX3, purchased from ChemBridge (San Diego, USA) (Bouquier et al., 2009). Cells were pretreated for 1 hour with 12,5 mM EHT 1864 (Sigma) (Onesto et al., 2008). Cells were transfected according to the manufacturer's protocol with Trans IT-LT1 reagent (Myrus, Madison, WI, USA) or electroporation (1 pulse, 1350V, 30 msec) (Invitrogen). GFP-tagged VE-cadherin constructs (VEDbDIMD-GFP, VEDC-a-GFP and VEDC-aDN-GFP) were a kind gift of Dr. N. Mochizuki (National Cardiovascular Center Research Institute, Osaka, Japan) (Noda, 2010). Adenovirus Trio and VE-cadherin-GFP constructs were generated as described (Allingham et al., 2007; van Rijssel J. et al., 2012b). One day after adenoviral infection, medium was replaced; 2-3 days after infection, cells were used for assays. a-catenin-mCherry and shRNA constructs (Sigma Mission library) targeting Trio (shTrio#1, TRC_10561; shTrio#2, TRC_873;), VE-cadherin (TRC_54090) or a non-targeting shCtrl (shC002) were packaged into lentivirus in HEK293T cells by means of third generation lentiviral packaging plasmids (Dull et al., 1998;Hope et al., 1990). Lentivirus-containing supernatant was harvested on day 2 and 3 after transfection. Lentivirus was concentrated by centrifugation at 20,000 x g for 2 hours. Target cells were infected and 3 days after the addition of virus, cells were used for assays.

Confocal laser scanning Microscopy

Cells were cultured on FN-coated glass coverslips and transfected/stimulated as indicated. After treatment, cells were washed with ice-cold PBS, containing 1mM $CaCl_2$ and 0.5mM $MgCl_2$, and fixed in 4% (v/v) formaldehyde for 10 min. After fixation, cells were permeabilized in PBS

with 0.2% (v/v) Triton X-100 for 10 min followed by a blocking step in PBS with 2% (w/v) BSA and incubated with primary and secondary antibodies and after each step washed with PBS. Fluorescent imaging was performed with a confocal laser-scanning microscope (LSM510/Meta; Carl Zeiss MicroImaging) using a 63x NA 1.40 or a 40x NA 1.30 oil lens. Pixel area was determined as described (Timmerman et al., 2012).

DORA Rac1-sensor constructs

Development of the Dimerization-Optimized Reporter for Activation (DORA) single-chain Rac1 biosensor: dimeric Cerulean3 coupled to the Rac1 effector p21-activated protein kinase (PAK) is linked via ribosomal protein-based linker (L9H) with circular-permutated Venus coupled to Rac1. The DORA Rac1 sequence within a pTriEx-HisMyc backbone is dCer3(G229)-KpnI-GS-PAK(I75-K118)-L9H-L9H-BamHI-GS-dcpVen-NheI-Rac-WT-HindIII. The DORA Rac1 mutant PAK biosensor sequence within a pTriEx-HisMyc backbone is dCer3(G229)-KpnI-GS-PAK(I75-K118, H83,86D)-L9H-L9H-BamHI-GS-dcpVen-NheI-Rac-WT-HindIII. The Histidine (H) on position 83 and 86 in the PAK domain of the Rac1 control biosensor is substituted for an Aspartic acid (D) and used as a negative control.

FRET measurements

Rac1 activity was measured in living cells by monitoring YFP FRET over donor CFP intensities. A Zeiss Observer Z1 microscope with 40x NA 1.3 oil immersion objective, a HXP 120 V excitation light source, a Chroma 510 DCSP dichroic splitter, and two Hamamatsu ORCA-R2 digital CCD cameras for simultaneous monitoring of Cer3 and Venus emissions were used. Image acquisition was performed using Zeiss-Zen 2011 microscope software. Offline ratio analysis between Cer3 and Venus images were processed using MBF ImageJ collection. Raw Cer3 and Venus images were background (BG) corrected using the plug-in 'ROI, BG subtraction from ROI'. Cer3 and Venus stacks were aligned using the registration plug-in 'Registration, MultiStackReg'. A smooth filter was applied to both image stacks to improve image quality by reducing noise. Image stacks were converted to a 32-bit image format and a threshold was applied exclusively to the Venus image stack, converting the background pixels to 'not a number' (NaN), allowing elimination of artifacts in ratio image stemming from the background noise. Finally, the Venus/Cer3 ratio was calculated using the plug-in 'Ratio Plus', and a custom look-up table was applied to generate a heatmap. MultiStackReg, and Ratio Plus are available through the ImageJ website (http://rsb.info.nih.gov/ij/plugins/index.html).

To label cell-cell junctions, we have used alpha-catenin-mCherry in the control cells. In Tag-RFP Trio-deficient cells, the red channel was in use.

Therefore, a directly fluorescently-labelled antibody to VE-Cadherin (VE-Cadherin-ALEXA-647, Millipore). Fluorescent-lifetime imaging microscopy (FLIM) was done using a dedicated Zeiss Axiovert wide field microscope equipped with instruments for frequency-domain FLIM imaging and a 63X (Plan Apochromat NA 1.4 oil) objective.

IMMUNOPRECIPITATION AND WESTERN BLOT ANALYSIS

Cells were washed twice with ice-cold PBS, containing 1 mM $CaCl_2$ and 0.5 mM $MgCl_2$, and lysed in cold NP-40 lysis buffer (25 mM Tris, 100 mM NaCL, 10 mM $MgCl_2$, 10% (v/v) glycerol and 1% (v/v) Nonidet P-40, pH 7.4), supplemented with a phosphatase inhibitor cocktail (Sigma) and fresh protease-inhibitor-mixture tablets (Roche Applied Science). After 10 min., cell lysates were collected and centrifuged at 10.000 rpm for 10 min. at 4°C. The supernatant was incubated with 0.5 µg mAb to VE-cadherin (BV6, Millipore) or 2 µg goat pAb to Trio (D-20, Santa Cruz) and 50 µl of protein G-Sepharose at 4°C under continuous mixing. In other experiments, biotinylated-peptides (1 µg/mL) together with streptavidin-agarose were used. Subsequently, beads were centrifuged at 5000 rpm for 20 sec. at 4°C, washed 5 times with NP-40 lysis buffer and boiled in SDS-sample buffer containing 4% β-mercapto-ethanol. Samples were analyzed by SDS-PAGE. Proteins were transferred to a 0.2 µm nitrocellulose membrane (Whatman, Dassel, Germany), subsequently blocked with 5% (w/v) milk powder in Tris-buffered saline with Tween20 (TBST). The nitrocellulose membrane was incubated with specific primary antibodies overnight at 4°C, followed by incubation with secondary HRP-labelled antibodies for 1h at RT. Between the incubation steps, blots were washed with TBST. Staining was visualized with an enhanced chemiluminescence (ECL) detection system (ThermoScientific, Amsterdam, The Netherlands). Alternatively, blots were incubated with IR 680 or IR 800 dye-conjugated secondary antibodies. Infrared signal was detected and analyzed with the Odyssey infrared detection system (Li-cor Westburg).

GTPASE ACTIVITY ASSAYS

Cells were lysed in 50 mM Tris, pH 7.4, 0.5 mM $MgCl_2$, 500 mM NaCl, 1% (v/v) Triton X-100, 0.5% (w/v) deoxycholic acid (DOC), and 0.1% (w/v) SDS supplemented with protease inhibitors. Subsequently, lysates were cleared at 10.000 rpm for 10 min. GTP-bound Rac1 and Cdc42 was isolated by rotating supernatants for 30 min with 30µg of a biotinylated PAK1-CRIB peptide, coupled to streptavidin agarose (Price et al., 2003). GTP-bound RhoG was isolated by rotating supernatants for 30 min with 60µg of GST-ELMO, precoupled to glutathione sepharose beads (GE Healthcare, Zeist, The Netherlands) (van Buul et al., 2007; Wittchen and

Burridge, 2008). Beads were washed five times in 50 mM Tris, pH 7.4, 0.5 mM MgCl2, 150 mM NaCl, 1% (v/v) Triton X-100 and boiled in SDS-sample buffer containing 4% β-mercapto-ethanol. Samples were analyzed by SDS-PAGE as described above. RhoA activation was measured using a G-LISA kit, according to the manufacturer's protocol (Cytoskeleton, Denver, USA).

VE-cadherin Ectodomain-Fc-coated Beads

Freestyle HEK cells were transfected with pcDNA-VE-Cad-Ect-Fc-His and pcDNA-Fc-His using 293Fectin. After 4 days, VE-cadherin-Fc (VE-Fc) protein secreted into the medium was collected and centrifuged to remove cell debris. His-tagged proteins were purified using a Chelating Sepharose column (GE Healthcare) charged with nickel. VE-Fc or Fc protein was eluted with 250 mM imidazole after which the buffer was exchanged into PBS containing 1 mM $CaCl_2$ by dialysis. Dynabeads (Invitrogen) were incubated with 2 µg of VE-Fc or Fc diluted in PBS containing 2mM EDTA and 0,1% (w/v) BSA for 45 min. under constant head-over-head rotation at 4°C. Dynabeads were washed and added to the cells for the indicated time to allow homophilic VE-cadherin engagement. Cells were washed twice with ice-cold PBS, containing 1 mM $CaCl_2$ and 0.5 mM $MgCl_2$, and lysed in cold NP-40 lysis buffer. Subsequently a CRIB peptide-based pull-down was done (see section GTPase Activity Assays) or VE-Fc-and Fc-coated Dynabeads were isolated using a magnetic holder and the interacting proteins were studied. Dynabeads were washed twice with RIPA-buffer, three times with NP40-lysis buffer and resuspended in SDS-PAGE sample buffer.

Electric Cell-substrate Impedance Sensing (ECIS)

Monolayer integrity was determined by measuring the electrical resistance using ECIS. Electrode-arrays (8W10E; IBIDI, Planegg, Germany) were treated with 10 mM L-cysteine (Sigma) for 15 minutes at 37˚C and subsequently coated with 10 µg/ml fibronectin (Sigma) in 0.9% NaCl for 1 hour at 37˚C. Cells were seeded at 100.000 cells per well (0.8 cm²) and grown to confluency. Electrical resistance was continuously measured at 37˚C at 5% CO_2 using ECIS model 9600 (Applied BioPhysics, New York, USA). Permeability was measured using Transwell filters with FN-coated 0.1 µm pore size filters. Fluorescently labelled 3 or 10kDa Dextran were added to the upper compartment and 5 hours later the fluorescence in the lower compartment was measured using a fluorimeter.

VE-Cadherin peptides

Peptides were synthesized corresponding to the intracellular sequence for VE-cadherin as indicated. Scrambled peptides were synthesized as

negative controls with the lowest Needleman-wunsch alignment score and highest Levenshtien distance to original sequence. VE-cadherin peptide #1 sequence: GAHGGPGEMAAMIEVKKDEADHDGDGPPYDTLH IYGYEG. VE-cadherin peptide #2 sequence: TLHIYGYEGSESIA ESLSSLGTDSSDSDVDYDFLNDWGP. Scrambled peptide sequence: SLEDISLEAYSGHYSEGTSGDDVSPDFSNDLSLGDTWDY. Protein-transduction domain (PTD) sequence: YARAAARQARA. Glycine was used as a linker. All peptides were biotinylated at the N-terminus. Pull down assays were performed using steptavadin-coated magnetic beads.

GST PULL DOWN ASSAY

The different constructs of GST-Trio spectrin repeats (spectrin 1-2, spectrin 1-4, spectrin 5-6, spectrin 5-8) as well as GST in pGEX6P1 vectors were expressed in *Escherichia coli* BL21 overnight at 18ºC and purified according to the manufacturers' recommendations (Amersham Biosciences) using 50 mM Tris/HCl, pH 7.4, 500 mM NaCl, 10% glycerol, 5 mM β-Mercaptoethanol, supplemented with protease inhibitor mixture tablets (Roche), as lysis buffer. GST-Trio spectrin-repeats or GST were eluted with 20 mM glutathione, 50 mM Tris/HCl, pH 7.4, 150 mM NaCl, 5% glycerol, 5 mM β-Mercaptoethanol, from glutathione-Sepharose-4B beads and dialyzed twice using the same buffer but without glutathione. Proteins were aliquoted and stored at -80ºC upon flash freezing in liquid N_2. To test for direct binding, the biotinylated peptides encoding intracellular domains of VE-cadherin as described and scrambled peptide (CTRL) were coupled to streptavidin agarose beads and incubated with purified GST-Trio spectrin repeats (molar ratio 1:2, spectrin 1-2, spectrin 1-4, spectrin 5-6 or spectrin 5-8) in 50 mM Tris/HCl, pH 7.4, 150 mM NaCl, 10 mM $MgCl_2$, 5 % glycerol, 5 mM β-Mercaptoethanol for 1 h at 4˚C under continuous mixing. Beads were washed five times and resuspended in SDS-sample-buffer. GST was used as control. Rate of activity was normalized by comparing the in/decrease of GTPase activity to the expression levels of the GTPase in the total cell lysates.

STATISTICAL ANALYSIS

Statistical comparisons between experimental groups were performed by the student T-test. A two-tailed p-value of ≤ 0.05 was considered significant.

AUTHOR CONTRIBUTION

IT and JDvB designed the study, performed and analyzed the experiments and wrote the paper. NH, JK, AS, JvR and MH performed the experiments. JvU and JG performed and analyzed the characterization

of the sensor experiments. TWJG supervised and analyzed the sensor characterization experiments. TY and YW generated and characterized the sensor. SH designed and analyzed the experiments, wrote the paper.

5

Conflict of Interest

The authors declare no conflict of interest.

Non-standard Abbreviations:

AJ	Adherens Junction
ECIS	Electric Cell-substrate Impedance Sensing
FAJ	Focal Adherens Junction
GEF	Guanine-nucleotide Exchange Factor
HUVEC	Human Umbilical Vein Endothelial Cell
TER	Transendothelial Electrical Resistance
VE-cadherin	Vascular Endothelial-Cadherin

REFERENCE LIST

Allingham, M. J., van Buul, J. D. and Burridge, K. (2007). ICAM-1-mediated, Src- and Pyk2-dependent vascular endothelial cadherin tyrosine phosphorylation is required for leukocyte transendothelial migration. *J Immunol*. 179, 4053-4064.

Backer, S. (2007). Trio controls the mature organization of neuronal clusters in the hindbrain.

Bershadsky, A. (2004). Magic touch: how does cell-cell adhesion trigger actin assembly?

Birukova, A. A., Tian, Y., Dubrovskyi, O., Zebda, N., Sarich, N., Tian, X., Wang, Y. and Birukov, K. G. (2012). VE-cadherin trans-interactions modulate Rac activation and enhancement of lung endothelial barrier by iloprost. *J. Cell Physiol* 227, 3405-3416.

Blangy, A., Vignal, E., Schmidt, S., Debant, A., Gauthier-Rouviere, C. and Fort, P. (2000). TrioGEF1 controls Rac- and Cdc42-dependent cell structures through the direct activation of rhoG. *J. Cell Sci*. 113 (Pt 4), 729-739.

Bouquier, N., Vignal, E., Charrasse, S., Weill, M., Schmidt, S., Leonetti, J. P., Blangy, A. and Fort, P. (2009). A cell active chemical GEF inhibitor selectively targets the Trio/RhoG/Rac1 signaling pathway. *Chem. Biol*. 16, 657-666.

Braga, V. M. (2005). The challenges of abundance: epithelial junctions and small GTPase signalling.

Cavey, M. (2009). Molecular bases of cell-cell junctions stability and dynamics.

Charrasse, S. (2007). M-cadherin activates Rac1 GTPase through the Rho-GEF trio during myoblast fusion.

Corada, M., Liao, F., Lindgren, M., Lampugnani, M. G., Breviario, F., Frank, R., Muller, W. A., Hicklin, D. J., Bohlen, P. and Dejana, E. (2001). Monoclonal antibodies directed to different regions of vascular endothelial cadherin extracellular domain affect adhesion and clustering of the protein and modulate endothelial permeability. *Blood* 97, 1679-1684.

Debant, A., Serra-Pages, C., Seipel, K., O'Brien, S., Tang, M., Park, S. H. and Streuli, M. (1996). The multidomain protein Trio binds the LAR transmembrane tyrosine phosphatase, contains a protein kinase domain, and has separate rac-specific and rho-specific guanine nucleotide exchange factor domains. *Proc. Natl. Acad. Sci. U. S. A* 93, 5466-5471.

Dejana, E. (2004). Endothelial cell-cell junctions: happy together. *Nat. Rev. Mol. Cell Biol*. 5, 261-270.

Di Lorenzo, A., Lin, M. I., Murata, T., Landskroner-Eiger, S., Schleicher, M., Kothiya, M., Iwakiri, Y., Yu, J., Huang, P. L. and Sessa, W. C. (2013). eNOS derived nitric oxide regulates endothelial barrier function via VE cadherin and Rho GTPases. *Journal of Cell Science*.

Djinovic-Carugo, K., Gautel, M., Yl+ñnne, J. and Young, P. (2002). The spectrin repeat: a structural platform for cytoskeletal protein assemblies. *FEBS Letters* 513, 119-123.

Gavard, J. and Gutkind, J. S. (2006a). VEGF controls endothelial-cell permeability by promoting the beta-arrestin-dependent endocytosis of VE-cadherin. *Nat. Cell Biol*. 8, 1223-1234.

Helwani, F. M. (2004). Cortactin is necessary for E-cadherin-mediated contact formation and actin reorganization.

Hoelzle, M. K. and Svitkina, T. (2012). The cytoskeletal mechanisms of cellGÇôcell junction formation in endothelial cells. *Molecular Biology of the Cell* 23, 310-323.

Hordijk, P. L., ten Klooster, J. P., van der Kammen, R. A., Michiels, F., Oomen, L. C. and Collard, J. G. (1997). Inhibition of invasion of epithelial cells by Tiam1-Rac signaling. *Science* 278, 1464-1466.

Hultin, S. (2014). AmotL2 links VE-cadherin to contractile actin fibres necessary for aortic lumen expansion.

Huveneers, S. (2012). Vinculin associates with endothelial VE-cadherin junctions to control force-dependent remodeling.

Huveneers, S. and de Rooij, J. (2013). Mechanosensitive systems at the cadherinGÇôF-actin interface. *Journal of Cell Science* 126, 403-413.

Huveneers, S., Oldenburg, J., Spanjaard, E., van der Krogt, G., Grigoriev, I., Akhmanova, A., Rehmann, H. and de Rooij, J. (2012). Vinculin associates with endothelial VE-cadherin junctions to control force-dependent remodeling. *The Journal of Cell Biology* 196, 641-652.

Ivanov, A. I. (2005). Differential roles for actin polymerization and a myosin II motor in assembly of the epithelial apical junctional complex.

**Kashef, J.** (2009). Cadherin-11 regulates protrusive activity in Xenopus cranial neural crest

cells upstream of Trio and the small GTPases.

Knezevic, I. I., Predescu, S. A., Neamu, R. F., Gorovoy, M. S., Knezevic, N. M., Easington, C., Malik, A. B. and Predescu, D. N. (2009). Tiam1 and Rac1 are required for platelet-activating factor-induced endothelial junctional disassembly and increase in vascular permeability. *J. Biol. Chem.* 284, 5381-5394.

Kobielak, A. (2004). Mammalian formin-1 participates in adherens junctions and polymerization of linear actin cables.

Kovacs, E. M. (2002). Cadherin-directed actin assembly: E-cadherin physically associates with the Arp2/3 complex to direct actin assembly in nascent adhesive contacts.

Kovacs, E. M., Goodwin, M., Ali, R. G., Paterson, A. D. and Yap, A. S. (2002). Cadherin-directed actin assembly: E-cadherin physically associates with the Arp2/3 complex to direct actin assembly in nascent adhesive contacts. *Curr Biol* 12, 379-382.

Kroon, J., Daniel, A. E., Hoogenboezem, M. and Van Buul, J. D. (2014). Real-time Imaging of Endothelial Cell-cell Junctions During Neutrophil Transmigration Under Physiological Flow. e51766.

Lambert, J. M., Lambert, Q. T., Reuther, G. W., Malliri, A., Siderovski, D. P., Sondek, J., Collard, J. G. and Der, C. J. (2002). Tiam1 mediates Ras activation of Rac by a PI(3)K-independent mechanism. *Nat. Cell Biol.* 4, 621-625.

Lampugnani, M. G. (1992). A novel endothelial-specific membrane protein is a marker of cell-cell contacts.

Lampugnani, M. G., Zanetti, A., Breviario, F., Balconi, G., Orsenigo, F., Corada, M., Spagnuolo, R., Betson, M., Braga, V. and Dejana, E. (2002). VE-cadherin regulates endothelial actin activating Rac and increasing membrane association of Tiam. *Mol. Biol. Cell* 13, 1175-1189.

Li, Y. (2011). HOXC8-Dependent Cadherin 11 Expression Facilitates Breast Cancer Cell Migration through Trio and Rac.

Naikawadi, R. P., Cheng, N., Vogel, S. M., Qian, F., Wu, D., Malik, A. B. and Ye, R. D. (2012). A Critical Role for P-Rex1 in Endothelial Junction Disruption and Vascular Hyper-Permeability. *Circ. Res.*

Navarro, P. (1995). Catenin-dependent and -independent functions of vascular endothelial cadherin.

Navarro, P., Ruco, L. and Dejana, E. (1998). Differential localization of VE- and N-cadherins in human endothelial cells: VE-cadherin competes with N-cadherin for junctional localization. *J. Cell Biol.* 140, 1475-1484.

Ngok, S. P., Geyer, R., Liu, M., Kourtidis, A., Agrawal, S., Wu, C., Seerapu, H. R., Lewis-Tuffin, L. J., Moodie, K. L., Huveldt, D. et al. (2012). VEGF and Angiopoietin-1 exert opposing effects on cell junctions by regulating the Rho GEF Syx. *J. Cell Biol.* 199, 1103-1115.

Ngok, S. P., Geyer, R., Kourtidis, A., Mitin, N., Feathers, R., Der, C. and Anastasiadis, P. Z. (2013). TEM4 is a junctional RhoGEF required for cell-cell adhesion, monolayer integrity, and barrier function. *Journal of Cell Science.*

Noda, K. (2010). Vascular endothelial-cadherin stabilizes at cell-cell junctions by anchoring to circumferential actin bundles through alpha- and beta-catenins in cyclic AMP-Epac-Rap1 signal-activated endothelial cells.

Noda, K., Zhang, J., Fukuhara, S., Kunimoto, S., Yoshimura, M. and Mochizuki, N. (2010). Vascular Endothelial-Cadherin Stabilizes at CellGÇôCell Junctions by Anchoring to Circumferential Actin Bundles through +¦- and +¦-Catenins in Cyclic AMP-Epac-Rap1 Signal-activated Endothelial Cells. *Molecular Biology of the Cell* 21, 584-596.

Oldenburg, J. (2014). Mechanical control of the endothelial barrier.

Oldenburg, J. and Rooij, J. (2014). Mechanical control of the endothelial barrier. *Cell Tissue Res*, 1-11.

Onesto, C., Shutes, A., Picard, V., Schweighoffer, F. and Der, C. J. (2008). Characterization of EHT 1864, a novel small molecule inhibitor of Rac family small GTPases. *Methods Enzymol.* 439, 111-129.

Phng, L. K., Gebala, V., Bentley, K., Philippides, A., Wacker, A., Mathivet, T., Sauteur, L., Stanchi, F., Belting, H. G., Affolter, M. et al. (2015). Formin-mediated actin polymerization at endothelial junctions is required for vessel lumen formation and stabilization. *Dev. Cell* 32, 123-132.

Price, L. S., Langeslag, M., ten Klooster, J. P., Hordijk, P. L., Jalink, K. and Collard, J. G. (2003). Calcium signaling regulates translocation and activation of Rac. *J. Biol. Chem.* 278, 39413-39421.

Rossman, K. L., Der, C. J. and Sondek, J. (2005). GEF means go: turning on RHO GTPases with guanine nucleotide-exchange factors. *Nat. Rev. Mol. Cell Biol.* 6, 167-180.

Sauteur, L., Krudewig, A., Herwig, L., Ehrenfeuchter, N., Lenard, A., Affolter, M. and

Belting, H. G. (2014). Cdh5/VE-cadherin promotes endothelial cell interface elongation via cortical actin polymerization during angiogenic sprouting. *Cell Rep.* 9, 504-513.

Schulte, D. (2011). Stabilizing the VE-cadherin-catenin complex blocks leukocyte extravasation and vascular permeability.

Spindler, V., Schlegel, N. and Waschke, J. (2010). Role of GTPases in control of microvascular permeability. *Cardiovasc. Res.* 87, 243-253.

Timmerman, I., Hoogenboezem, M., Bennett, A. M., Geerts, D., Hordijk, P. L. and van Buul, J. D. (2012). The tyrosine phosphatase SHP2 regulates recovery of endothelial adherens junctions through control of beta-catenin phosphorylation. *Mol. Biol. Cell* 23, 4212-4225.

van Buul, J. D., Allingham, M. J., Samson, T., Meller, J., Boulter, E., Garcia-Mata, R. and Burridge, K. (2007). RhoG regulates endothelial apical cup assembly downstream from ICAM1 engagement and is involved in leukocyte trans-endothelial migration. *J. Cell Biol.* 178, 1279-1293.

van Buul, J. D., Anthony, E. C., Fernandez-Borja, M., Burridge, K. and Hordijk, P. L. (2005). Proline-rich tyrosine kinase 2 (Pyk2) mediates vascular endothelial-cadherin-based cell-cell adhesion by regulating beta-catenin tyrosine phosphorylation. *J Biol. Chem* 280, 21129-21136.

van Hinsbergh, V. W. (2002). Intracellular signalling involved in modulating human endothelial barrier function.

van Rijssel J., Hoogenboezem, M., Wester, L., Hordijk, P. L. and van Buul, J. D. (2012a). The N-terminal DH-PH domain of Trio induces cell spreading and migration by regulating lamellipodia dynamics in a Rac1-dependent fashion. *PLoS. ONE.* 7, e29912.

van Rijssel J., Kroon, J., Hoogenboezem, M., van Alphen, F. P., de Jong, R. J., Kostadinova, E., Geerts, D., Hordijk, P. L. and van Buul, J. D. (2012b). The Rho-GEF Trio controls leukocyte transendothelial migration by promoting docking structure formation. *Mol. Biol. Cell.*

Van Rijssel, J., Timmerman, I., Van Alphen, F. P. J., Hoogenboezem, M., Korchynskyi, O., Geerts, D., Geissler, J., Reedquist, K. A., Niessen, H. W. M. and Van Buul, J. D. (2013). The Rho-GEF Trio regulates a novel pro-inflammatory pathway through the transcription factor Ets2. *Biology Open* 2, 569-579.

van Wetering, S., van Buul, J. D., Quik, S., Mul, F. P., Anthony, E. C., ten Klooster, J. P., Collard, J. G. and Hordijk, P. L. (2002). Reactive oxygen species mediate Rac-induced loss of cell-cell adhesion in primary human endothelial cells. *J Cell Sci.* 115, 1837-1846.

Verma, S. (2004). Arp2/3 activity is necessary for efficient formation of E-cadherin adhesive contacts.

Vestweber, D., Winderlich, M., Cagna, G. and Nottebaum, A. F. (2009). Cell adhesion dynamics at endothelial junctions: VE-cadherin as a major player. *Trends in Cell Biology* 19, 8-15.

Wilson, C. W., Parker, L. H., Hall, C. J., Smyczek, T., Mak, J., Crow, A., Posthuma, G., De Mazi+¿re, A., Sagolla, M., Chalouni, C. et al. (2013). Rasip1 regulates vertebrate vascular endothelial junction stability through Epac1-Rap1 signaling. *Blood* 122, 3678-3690.

Wittchen, E. S. and Burridge, K. (2008). Analysis of low molecular weight GTPase activity in endothelial cell cultures. *Methods Enzymol.* 443, 285-298.

Yamada, S. and Nelson, W. J. (2007). Localized zones of Rho and Rac activities drive initiation and expansion of epithelial cell-cell adhesion. *J. Cell Biol.* 178, 517-527.

Yamazaki, D., Oikawa, T. and Takenawa, T. (2007). Rac-WAVE-mediated actin reorganization is required for organization and maintenance of cell-cell adhesion. *J. Cell Sci.* 120, 86-100.

Yano, T. (2011). Tara up-regulates E-cadherin transcription by binding to the Trio RhoGEF and inhibiting Rac signaling.

Yap, A. S. (2003). Direct cadherin-activated cell signaling: a view from the plasma membrane.

Zhang, J., Betson, M., Erasmus, J., Zeikos, K., Bailly, M., Cramer, L. P. and Braga, V. M. (2005). Actin at cell-cell junctions is composed of two dynamic and functional populations. *J. Cell Sci.* 118, 5549-5562.

5

Figure S1. *Trio controls endothelial barrier function.* **(A)** TagRFP-shTrio constructs were expressed in ECs. Western blot shows efficient Trio knockdown in TagRFP-expressing ECs. **(B)** ECs, transiently transfected with VE-cadherin-GFP and treated with shCTRL or shTrio, are analyzed for FAJ length. Red line represents FAJ length and white line represents linear junction. When VE-cadherin staining showed zigzag pattern, it was quantified as FAJ. Graph on the right shows quantification of ratio between FAJ length and total junction length. Experiment is carried out three times independently from each other and 25 cells per experiment are analyzed. Data are mean±SEM. **(C)** Permeability was measured by culturing HUVECs on FN-coated Transwell filters and fluorescently-labeled Dextran was allowed to diffuse through the monolayer for four hours. Both dextran 3K and 10K showed increased permeability across Trio-deficient ECs. This experiment is carried out three times in duplicate. Data are mean±SD. *$p<0.05$. **(D)** ECs were cultured on FN-coated ECIS arrays and treated with ITX3 (100μM) or DMSO. Resistance was determined after 10h treatment and showed decreased resistance. Experiment is carried out three times independently from each other. Data are mean±SEM. *$p<0.01$. **(E)** Western blot analysis on the left shows efficient overexpression of GFP, GFP-TrioN and GFP-TrioC in endothelial cells. Blots on the right show expression of GFP-TrioN or GFP only in Trio-deficient endothelial cells. Actin is shown as loading control. **(F)** Intercellular gaps are quantified based on DIC images. shCTRL or shTrio-HUVECs were transfected with VE-Cadherin-GFP and 1U/mL Thrombin was administered for time periods (minutes) indicated in left lower corner. Stills show the gap size, illustrated with the white line. Bar: 10 μm. **(G)** ECs were cultured on FN-coated glass covers, transfected as indicated, stained. The constitutively active mutant of RhoG (Q61L), GFP-CAAX or GFP do not co-localize with VE-cadherin (red), whereas constitutively active Rac1 (Q61L) does co-localize with VE-cadherin. Bar: 20 μm. **(H)** Western blot confirms efficient VE-cadherin knock down. For the experiment, 1:50 dilution was used. The same blot was re-probed for ß-catenin . Actin is used as loading control. **(I)** Trio-GEF1 activity is not required for its interaction with the VE-cadherin complex. DMSO- or ITX3-treated HUVECs were lysed and subjected to an IP for Trio. **(J)** ECs were cultured on FN-coated glass covers, transfected as indicated, stained. The N-terminal GEF1 domain of Trio (GEF1) as well as the C-terminal GEF domain of Trio (GEF2) do not show clear co-localization with VE-cadherin (red). Bar: 20 μm.
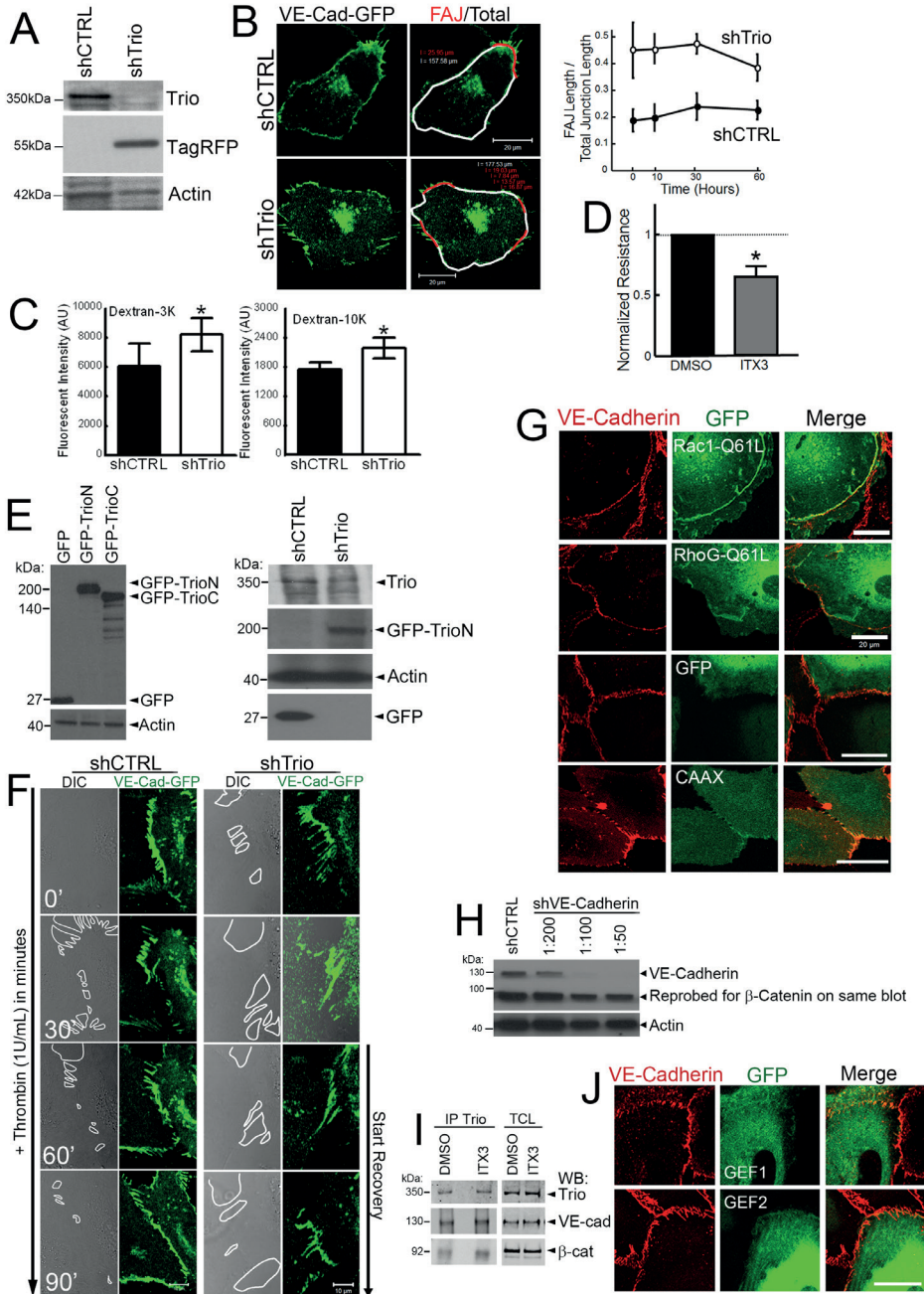
Figure S1.

Figure S2. *Trio interacts with VE-cadherin.* **(A)** GST-spectrin-repeats 1-4 and 5-8 and GST alone were incubated with VE #2 or scrambled peptide as indicated. Western blot analysis shows that spectrin-repeats 5-8 bound to the VE and not to the scrambled peptide. **(B)** Western blot shows the input of the GST proteins as indicated for pull down experiments in Figure 4G and S2A. **(C)** Trio-deficient (shTrio) or control (shCTRL) ECs were treated with 4mM EGTA as indicated to chelate calcium and calcium (1mM $CaCl_2$) was added back for 30-60 min. Cells were stained as indicated. Bar: 20 μm. **(D)** ECs were grown to confluence and stimulated with 50ng/mL VEGF for 30 min. Cells were lysed and subjected to Trio IP. Association of VE-cadherin and ß-catenin to Trio was determined by Western blotting. Quantification of three independent experiments is shown in lower panel. Data are mean±SEM. *$p<0.05$. **(E)** ECs were transduced with control or Trio shRNA, grown to confluency and lysed. Expression levels of several junction markers were determined by Western Blotting. Quantification of three independent experiments is shown in lower panel. **(F)** ECs were transduced with control or Trio shRNA, grown to confluency, lysed and an immunoprecipitation (IP) for VE-cadherin was performed. Blot shows that binding of catenins to VE-cadherin is not altered in Trio-depleted cells. Quantification of three independent experiments is shown in lower panel.

Figure S2.
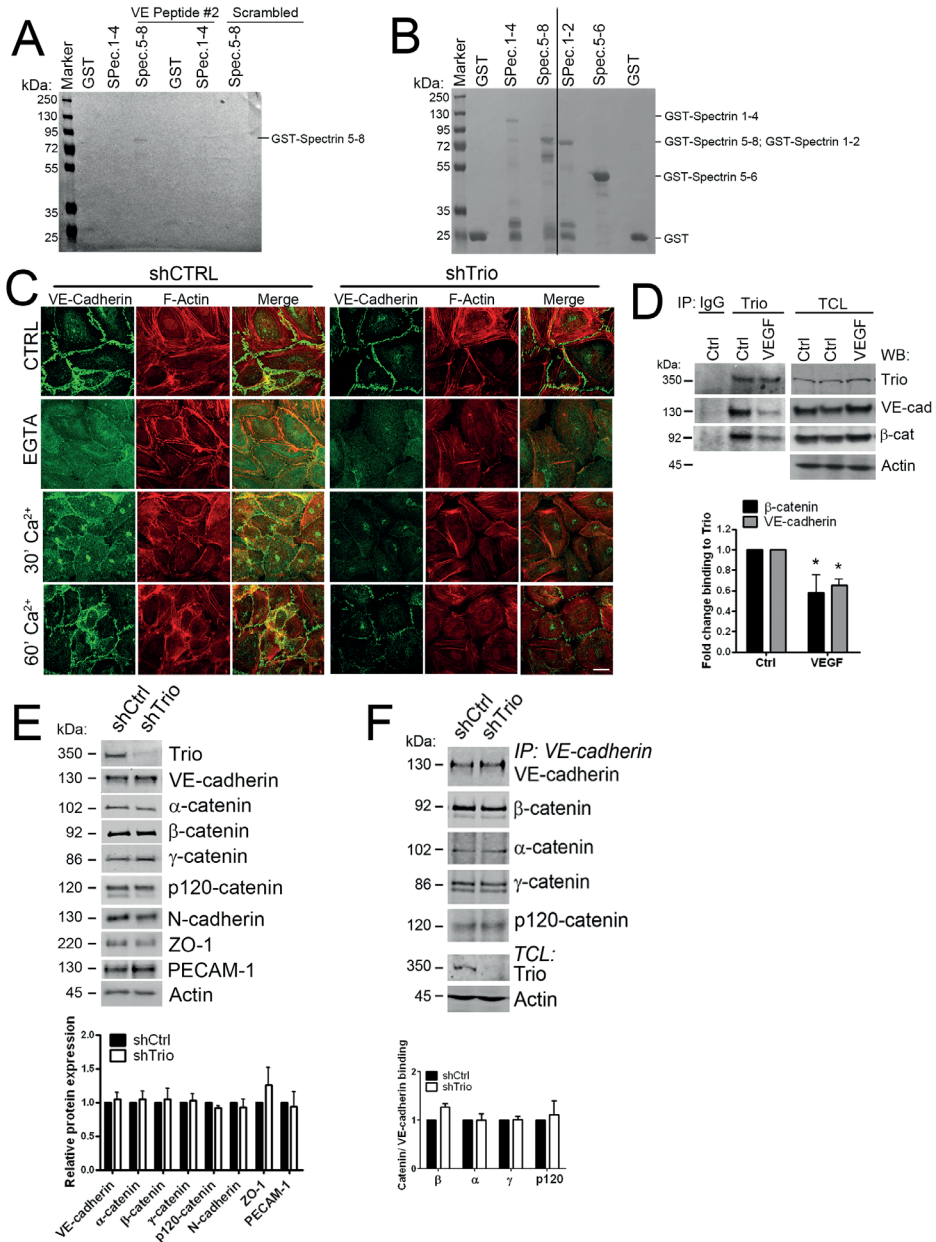
Figure S3. *Trio promotes linear F-actin-rich cell-cell junctions and Rac1 activation.* **(A)** ECs were cultured on FN-coated glass covers, transfected with GFP-TrioN and stained as indicated. Region of interest (ROI) shows increase in F-actin at cell-cell junctions. Bar: 20 µm. **(B)** VE-cadherin-ectodomain-Fc- or Fc-coated magnetic dyna-beads were added to an EC monolayer to induce VE-cadherin ligation. ECs were lysed and adhered beads were isolated using a magnetic holder. Binding of endogenous VE-cadherin and β-catenin to the beads was determined by Western blotting. **(C)** VE-cadherin ligation does not increase RhoG activation, as analyzed using a GST-ELMO pull-down assay. **(D)** RhoA activation was analyzed using a G-LISA kit and showed a significant decrease in RhoA activation upon VE-cadherin ligation. Experiment is carried out three times. Data are mean±SEM. $p < 0.05$. **(E)** HUVECs were transduced with control or Trio shRNA #1 and incubated with VE-cadherin-ectodomain-Fc-coated magnetic beads to induce VE-cadherin ligation. Right panels show quantification, including Western blot control for Trio knockdown. Data are mean±SEM. $p < 0.05$. **(F)** HEK293 cells were transfected with GFP, GFP-TrioN-wt or GFP-TrioN-1406A/D1407A and Rac1 and RhoG activity was measured as described in the Method section. The catalytic-dead mutant N1406A/D1407A of TrioN showed no increase in Rac1 activation. Upper panel shows GTPase activity after pull down and panels below show total cell lysates and protein loading. Experiment is carried out three times independently from each other. (G) HUVECs were cultured to confluency and RhoG was silenced using shRNA as indicated. GFP-TrioN was overexpressed and localized to cell-cell junctions. Cells were fixed, permeabilized and stained for VE-cadherin in red, F-actin in blue. Merge shows co-localization between GFP-Trio, VE-cadherin and F-actin. RhoG depletion did not affect TrioN-induced linearization of cell-cell junctions. Western blot analysis showed efficient RhoG knock down (shRhoG) in HUVECs. Actin is shown as loading control. Previous work from our group showed that this shRNA did not affect Rac1 levels (Van Rijssel et al., MBoC 2012).

Figure S3.
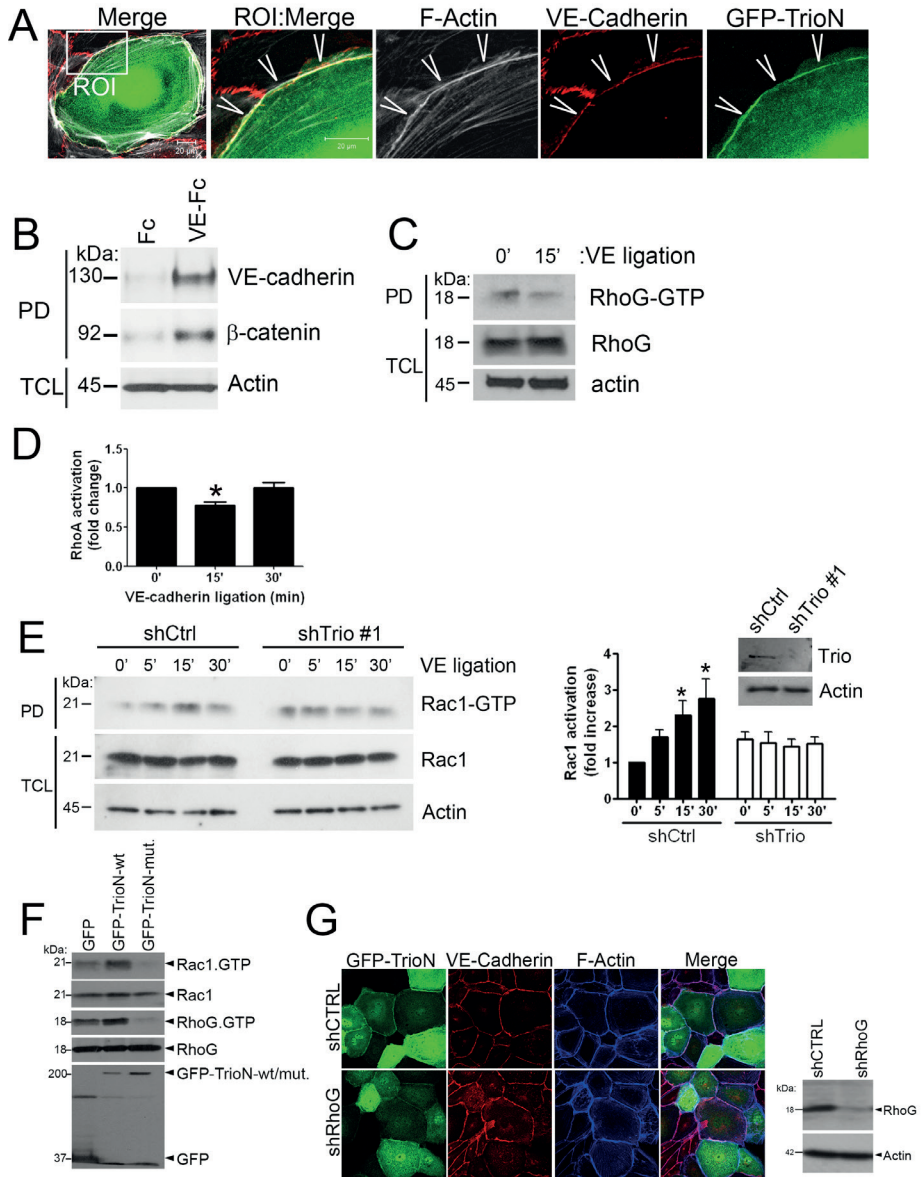
Figure S4. *Quantification of DORA Rac1 sensor.* **(A)** Schematic drawing of the Rac1 single-chain DORA sensor. Rac1-wt and the Pak-binding domain (PBD) are both located at the outside of the sensor. Cerulean3 and Venus are used to generate FRET when Rac1 and PBD are in close proximity. Both parts are linked through the ribosome linker protein L9, ensuring low off-rate FRET. **(B)** Stills from Movie 5 (left) showing spontaneous protrusions of Rac1 DORA sensor transfected ECs with spatial and temporal Rac1 activation at protrusions. Heat map (LUT) on the right shows FRET ratio. Warm colors indicate FRET. **(C)** HeLa cells were transfected with the Rac1 sensor and stimulated with EGF (concentration; arrow/asterisk) for indicated time points. Rac1 activity, as result of FRET, was shown in warm colors according to the heat map and showed transient activation upon EGF treatment. Right graph shows normalized intensity of Cerulean (blue) and Venus (yellow) and red line indicates transient increased FRET (YFP/CFP) ratio upon EGF (asterisk). Second most right graph shows average of three independent experiments of FRET ratio upon EGF treatment. **(D)** Western blot analysis of Rac1 activity upon EGF reflects FRET data presented under C. **(E)** ECs transfected with DORA Rac1 sensor were stimulated with thrombin (1U/mL; arrow/asterisk). Rapid decrease in FRET signals was detected, followed by a local increase in FRET signal during the recovery phase. Warm colors indicate increased FRET. Graph on the right shows FRET ratio. **(F)** Quantitative imaging of active and wt Rac1 biosensor by fluorescence lifetime imaging (FLIM). Reduced FLIM of the constitutively active Rac1 (Q61L) sensor mutant compared to the Rac1-wt sensor was measured, indicating efficient FRET. **(G)** Dominant negative DORA Rac1-PAK-mutant sensor shows no increase in FRET, indicating low background sensor signals. Also the graphs on the right show no change in fluorescent intensity for Cerulean, Venus or FRET ratio. **(H)** Trio-deficient ECs (marked by TagRFP-shTrio) show high FRET signals, reflecting Rac1 activity at the front of a protrusion (white arrow). However, upon initial cell-cell contact, marked by VE-cad-647 (red arrow), no increase in FRET is measured (green arrow). LUT: heat map on right shows warm colors as high FRET.

Figure S4.

A DORA Rac1 sensor

B Venus/Cer3 FRET

C Venus/Cer3 FRET

D hEGF

E Venus/Cer3 FRET: Thrombin stimulus

F Donor Intensity · Fluorescence Lifetime · Lifetime histogram

G DORA Rac1-PAK-mutant sensor

H
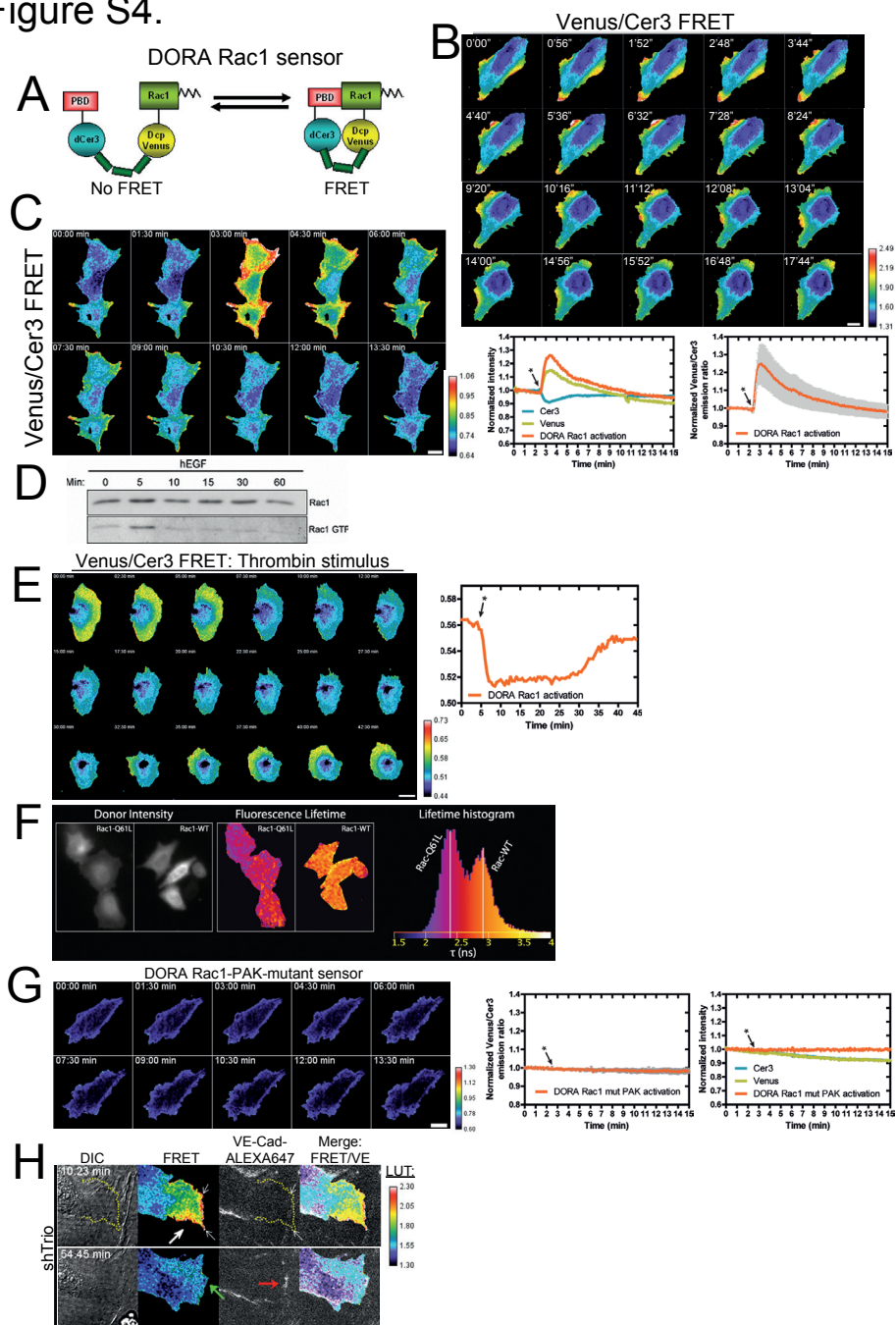
6

Specific regulation of permeability during leukocyte TEM by RhoGEFs and GAPs.

Niels Heemskerk[1], Lilian Schimmel[1], Jaap D. van Buul[1,*]
[1]Department of Molecular Cell Biology, Sanquin Research and Landsteiner Laboratory, Academic Medical Centre, University of Amsterdam, 1066CX, the Netherlands.

[*] Corresponding author:
Jaap D. van Buul; Sanquin Research and Landsteiner Laboratory; Academic Medical Centre; University of Amsterdam; Address: Plesmanlaan 125, 1066 CX, Amsterdam, the Netherlands. Phone: +31-20-5121219; Fax: +31-20-5123310; E-mail j.vanbuul@sanquin.nl

Abstract

The role of several GTPases including RhoA, Rac1 and Cdc42 in the regulation of the endothelial barrier has been extensively investigated, however which Rho GTPase-activating proteins (GAPs) and Guanine nucleotide exchange factors (GEFs) regulate local GTPase cycling at endothelial junctions during neutrophil diapedesis is poorly understood. Using a screen of short hairpin RNAs targeting 25 distinct endothelial Rho GEFs or GAPs, we identified two Cdc42-specific Rho GEFs, Tuba and FGD5 and two Rho GAPs, breakpoint cluster region (Bcr) and ARHGAP11a that control permeability during leukocyte diapedesis. Additionally, we report on eight potential Rho GEFs and GAPs that are involved in regulating basal endothelial junction integrity. In conclusion, we found that different Rho GEFs/GAPs specifically control local Rho GTPase signals that are involved in either leukocyte diapedesis or basal endothelial junction integrity.

INTRODUCTION

During inflammation leukocyte diapedesis and extravasation of plasma proteins require the opening of endothelial cell (EC) junctions. At the molecular level the opening of cell-cell junctions is differentially regulated for leukocytes compared to permeability inducing agents such as histamine (Vestweber, Wessel, and Nottebaum 2014; Wessel et al. 2014). A study that used VE-cadherin Y731F and Y685F mutant knock in mice unraveled the source of this selective junctional opening. It was demonstrated that dephosphorylation of Y731 is required to unlock VE-cadherin-based endothelial cell-cell contacts allowing leukocyte extravasation, while vascular permeability-inducing agents strongly enhance the phosphorylation of Y685, allowing proper induction of vascular permeability *in vivo* (Wessel et al. 2014). This recent work is in agreement with earlier *in vivo* studies showing that under inflammatory conditions, sites of plasma protein leakage were often distinct from those of leukocyte adhesion or transmigration. Although sites of plasma protein leakage and leukocyte diapedesis do overlap, in general plasma leakage occurs upstream of sites of leukocyte adhesion and transmigration (P Baluk et al. 1998; Peter Baluk et al. 1995; Gawlowski, Benoit, and Granger 1993; McDonald, Thurston, and Baluk 1999; McDonald 1994; Rosengren, Ley, and Arfors 1989). Moreover, several studies have shown that elevated vascular permeability precedes leukocyte influx, demonstrating that leukocyte adhesion and transmigration are not well correlated with the evoked permeability change during acute inflammation (Kim, Curry, and Simon 2009; Lewis and Granger 1988; Lewis, Miller, and Granger 1989; Valeski and Baldwin 1999). Maintaining a tight and intact EC barrier during neutrophil recruitment to inflammatory sites is crucial for human health. For example, neutrophil diapedesis in thrombocytopenia patients provokes spontaneous organ hemorrhages. The physical movement of inflammatory cells through the endothelial cell-cell junctions has been found to be responsible for the bleeding defect (Hillgruber et al. 2015). Interestingly, mutating Y731 in the cytoplasmic tail of VE-cadherin reduced neutrophil diapedesis and the associated organ bleeding (Hillgruber et al. 2015). We recently showed how the endothelium limits vascular permeability during inflammation. By generating F-actin-rich contractile endothelial pores that require local RhoA activation, the endothelial barrier function during leukocyte diapedesis is maintained (Heemskerk et al. 2016). However, RhoA activation has also been recognized to induce large endothelial gaps by generating acto-myosin tension (Amerongen et al. 2000). Next to that, local Rac1 activation is required to maintain stable endothelial cell-cell junctions (Timmerman, Heemskerk, Kroon,

Schaefer, van Rijssel, et al. 2015). Thus, these GTPases are in need of local and specific regulation to execute their functional task in each of these distinct cellular processes. However, which GEFs and GAPs control local GTPase cycling during leukocyte diapedesis or basal junctional integrity is not completely clear.

Here we identified the Cdc42-specific Rho-GEFs, Tuba and FGD5 and 2 Rho-GAPs, Bcr and ARHGAP11a that control permeability during leukocyte diapedesis. Moreover, we describe in detail a method to examine the involvement of RhoGAP and GEF activity in limiting of plasma protein leakage during leukocyte diapedesis.

Materials and Methods

Generation of lentiviral particles containing shRNAs that target distinct Rho GEFs

HEK-293T were maintained in Dulbecco's Modified Eagle Medium (DMEM) (Invitrogen, Breda, The Netherlands) containing 10% (v/v) heat-inactivated fetal calf serum (Invitrogen, Breda, The Netherlands), 300 mg/ml L-glutamine, 100 U/ml penicillin and streptomycin and 1x sodium pyruvate (Invitrogen, Breda, The Netherlands).

Cells were cultured at 37°C and 5% CO_2. Cells were transfected with the expression vectors according to the manufacturer's protocol with Trans IT-LT1 (Myrus, Madison, WI, USA).

Lentiviral constructs were packaged into lentivirus in Human embryonic kidney (HEK)-293T cells by means of third generation lentiviral packaging plasmids (Dull et al., 1998; Hope et al 1990).

Lentivirus containing supernatant was harvested on day 2 and 3 after transfection. Lentivirus was concentrated by Lenti-X concentrator (Clontech, Cat# 631232).

Transduced target cells were used for assays after 72 hours.

Human Umbilical Vein Endothelial Cells

Culture pooled Human Umbilical Vein endothelial Cells (HUVECs) purchased from Lonza (P938, Cat # C2519A), on fibronectin (FN)-coated dishes (10 μg/ml dissolved in water) in Endothelial Basal Medium, supplemented with Endothelial Growth Medium (EGM-2) singlequots (Lonza, Verviers, Belgium). Culture cells at 37°C and 5% CO_2.

Day 1: Coat two six well plates with 500 μl of fibronectin (10 μg/ml in PBS) for at least 1 hour at 37°C and 5% CO_2. Plate 150,000 HUVECs in every single well and let growth overnight in an incubator at 37°C and 5% CO_2.

Day 2: Transduce cells that are 60-70 % confluent with lentiviral particles containing shRNAs targeting particular Rho GEFs.

Day 3: Coat the required 24 well cell culture inserts (Corning FluoroBlok, Falcon, 3.0 µm pore size # 351151) with FN at least 1 hour before plating., wash HUVECs with RT phosphate buffer saline (PBS) before adding Trypsin that dissociates the ECs from the culture dish and plate 200,000 HUVECs in every single culture insert. Centrifuge at 1200 rmp and plate 200,000 cells in every insert. The Top compartment fits 300-500 µl media and the lower compartment 800 µl.

Day 4: Refresh EGM-2 media in the morning and stimulate HUVEC with 10 ng/ml recombinant Tumor-Necrosis-Factor (TNF)-α (PeproTech, Rocky Hill, NJ) overnight. TNF-α stimulation induces transcription of inflammatory mediators such as adhesion molecule ICAM-1.

Day 5: Refresh EGM-2 media in the morning and start neutrophil isolation.

NEUTROPHIL ISOLATION

Prepare N-2-hydroxyethylpiperazine-N'-2-ethanesulfonic acid (HEPES)-buffer: dilute 7.72 g NaCl (132 mM), 4.76 g HEPES (20 mM), 0.45 g KCl (6 mM), 0.25 g MgSO4 · 7H2O (1 mM), K2HPO4 · 3H2O (1.2 mM) in 1 L of demineralized water and adjust to pH 7.4 (this stock can be stored at 4 °C for months).

Prepare 10% trisodium citrate (TNC) solution in PBS, pH 7.4

Prepare erythrocyte lysis (155 mM NH_4CL, 10 mM $KHCO_3$, 0.1 mM EDTA, pH7.4 in Milli-Q (Millipore)

Prepare HEPES ++ by adding 100 µl 1 M CaCl2 (1 mM), 2.5 ml human albumin from a 200 g/L stock concentration (0.5% v/v) and 0.1 g glucose to 100 ml (0.1% w/v) HEPES-buffer.

Acquire 20 ml of whole blood in sodium heparine derived from healthy donors. Dilute whole blood (1:1) with 5% (v/v) TNC in PBS. Pipette diluted blood on 12.5 ml Percoll (room temperature) 1.076 g/ml. Spin the tubes in a centrifuge (Rotanta 96R) at 2000 rpm, slow start, low brake for 20 minutes. Remove percoll and the ring fraction and lyse the erythrocytes in an ice-cold isotonic lysis buffer (155 mM NH_4CL, 10 mM $KHCO_3$, 0.1 mM EDTA, pH7.4 in Milli-Q (Millipore). Incubate the tube on ice until the suspension turns dark red or transparent, continue the process by centrifugation at 1500 rpm for five minutes at 4°C. Remove supernatant and leave neutrophils in erythrocyte lysis buffer for five minutes on ice, centrifuge again at 1500 rpm for five minutes at 4°C, wash once with PBS, and centrifuge again at 1500 rpm for five minutes at 4°C and resuspend neutrophils in HEPES medium.

Determine neutrophil counts using a cell counter (Casey) and resuspend cells at 5 x 10^6 cells/ml.

LABELLING OF NEUTROPHILS WITH CALCEIN-RED ORANGE

Prepare calcein red-orange by adding 12.5 µl DMSO to 50 µg calcein red-orange AM (Molecular probes C34851). Solution can be stored at -20 °C for several months.

Add 2µl calcein red-orange to 2 ml neutrophils 5*10^6/ml and shake cells for 30 minutes in a 37°C water bath.

Wash calcein red-orange labelled cells with 10 ml HEPES ++ buffer and spin at 1500 rpm for five minutes at RT.

Resuspend cells in 1 ml HEPES ++ buffer and leave at 37°C until further usage.

FITC-DEXTRAN PERMEABILITY ASSAY

Pre-warm thermo pad (Harvard apparatus) at 37°C.

Prepare 3 ml FITC-dextran solution 5mg/ml (Sigma) in HEPES++ medium.

Prepare 10ml of 0.1 nM C5a (Sigma C-5788) in HEPES.

Create a method on the Infinite F200 pro plate reader (TECAN) using the manufacture manual that measures the two fluorescent colors leaking through Fluorblok inserts over a period of 30 minutes. Use the following settings; temperature must be set to 37 °C. EX BP 485/9 and EM BP 535/20 are used to measure FITC-dextran kinetics. EX BP 535/9 and EM BP 595/20 are used to measure neutrophil (calcein red-orange) transmigration kinetics.

Place the 24 well plate containing the Fluorblok inserts on the pre-warmed thermo pad to prevent the plate from cooling down. Remove EGM-2 medium from the upper and lower compartment and fill the lower compartment with 800 µl C5a and the upper compartment with 300 µl FITC-dextran solution.

Add 500,000 calcein red-orange labelled neutrophil in the designated inserts.

Treat HUVECs with 1U/ml thrombin (Sigma-Aldrich, St. Louis, USA) 10 seconds before starting the measurement.

Place the 24 well plate in the plate reader and start the predefined method to acquire dextran and neutrophil extravasation.

Results

To investigate vascular permeability during leukocyte diapedesis, we simultaneously measured neutrophil diapedesis kinetics and FITC-dextran extravasation across TNFα stimulated endothelial cells (ECs) towards a C5a gradient (Fig. 1a). ECs are cultured on Transwells equipped with a three μm-pore size filter that blocks all the fluorescence from the dyes in the upper compartment, ensuring a good signal-to-noise ratio. Once calcein red-orange labelled neutrophils or FITC-dextran enters the lower compartment, the plate-reader detects the signal at four distinct locations to acquire the kinetics of permeability and extravasation of FITC-dextran and labelled neutrophils, respectively, over time. Some variations in starting values between wells were observed, these differences may be caused by distinct scattering of individual wells and positions in each well. Because of the variable starting values we decided to work with the average of the four positions and normalize the data to a baseline; the average of the first five data points. To test whether changes in endothelial barrier could be measured using this setup, we treated ECs with thrombin, a vascular permeability-inducing agent, and examined FITC-dextran leakage over a period of 30 min. Thrombin provoked opening of cell-cell junctions and consequently diffusion of FITC-dextran into the lower compartment (Fig. 1b). To test whether extravasated neutrophils could be detected over time, we added 500.000 neutrophils to each Transwell (EC/PMN ratio of 1:2) and followed neutrophil diapedesis towards a C5a gradient over time. Transmigrated neutrophils were detected after 5 minutes of addition and increased up to 7-10 fold within 30 minutes (Fig. 1c). To investigate vascular permeability during leukocyte diapedesis, we simultaneously measured neutrophil diapedesis kinetics and FITC-dextran leakage across TNFα-stimulated ECs and found that under these conditions neutrophil diapedesis across TNF-α-treated ECs was associated with minimal FITC-dextran leakage (Fig. 1d). Note that in this particular experiment the fold increase of transmigrated neutrophils is lower than in Figure 1c. To investigate the source of this variation we checked if neutrophil labelling caused these differences. Labelling of neutrophils with calcein red-orange does not show significant differences between donors (Fig. 1e). Therefore we assume that donor variation, the intrinsic ability of neutrophils to migrate across the endothelium, is the source of this variation. Thus, endothelial cells are equipped with mechanisms to maintain a tight EC barrier during neutrophil diapedesis.
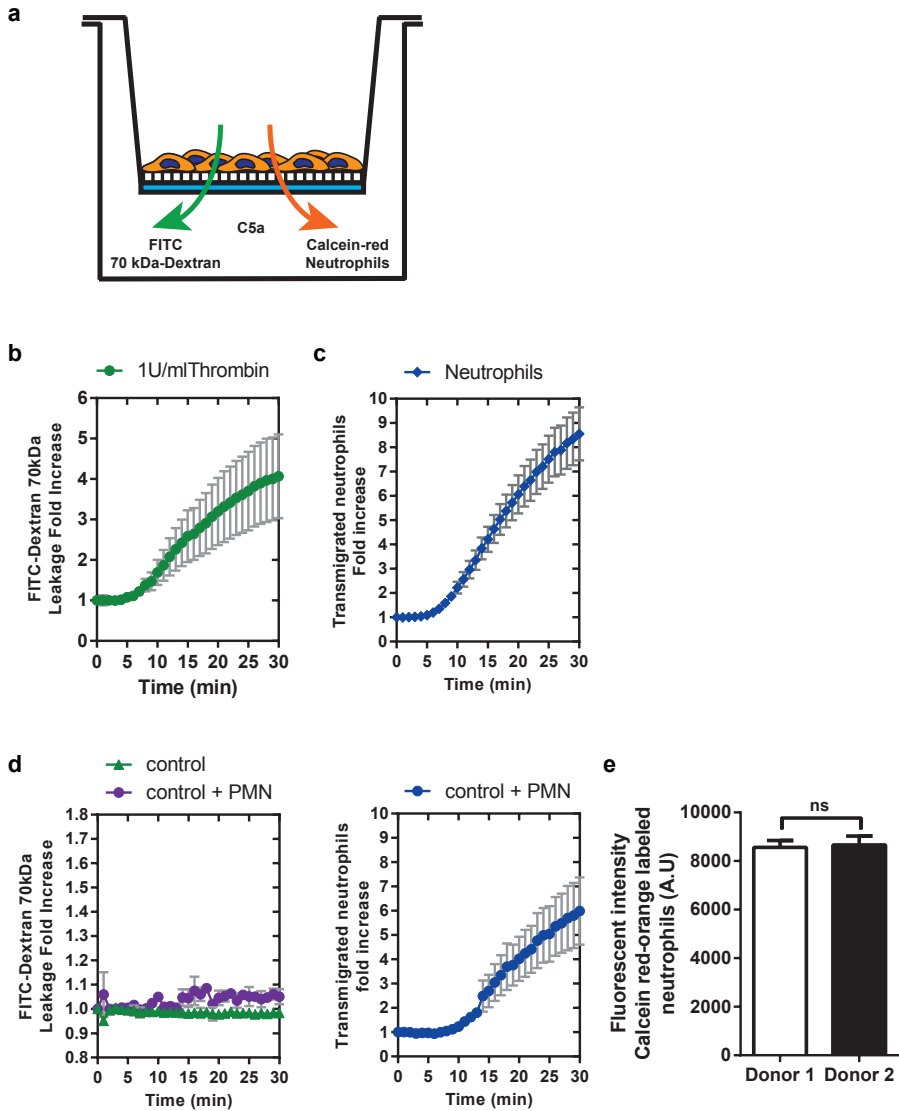
Figure 1 Endothelial cells maintain barrier function during leukocyte diapedesis. (**a**) Schematic illustration of a transwell fluoroblok cell culture insert. ECs were cultured on cultured on 3μm pore permeable filters. 70kDa FITC-dextran was added to the top compartment and a C5a chemotactic gradient was created through C5a addition to the lower compartment. (**b**) Kinetics of FITC-dextran leakage through ECs after thrombin stimulation. (**c**) Neutrophil transmigration kinetics towards a C5a chemotactic gradient. (**d**) Extravasation kinetics of FITC-dextran and calcein-red labelled neutrophils through TNF-α treated (overnight) HUVECs. Neutrophils transmigrated towards a C5a chemotactic gradient (**e**) Quantification of fluorescent calcein red-orange labelled neutrophil from different donors.

Tuba, FGD5, Ect2, LARG, Bcr and ARHGAP11a regulate vascular permeability during neutrophil diapedesis

Endothelial barrier function during leukocyte diapedesis is regulated through the generation of endothelial F-actin-rich contractile rings that require local RhoA activation (Heemskerk et al. 2016). Moreover, Rac1 controls the basal resistance of endothelial monolayers. However, which guanine-nucleotide exchange factors (GEFs) or GTPase activating proteins (GAPs) regulate local and specific GTPase activity during leukocyte diapedesis is not completely clear. To investigate this, we performed a screen of shRNA's targeting 25 endothelial Rho GEFs and GAPs and examined dextran leakage under basal but also during neutrophil extravasation using the above described experimental set-up (Fig. 1a). Since antibodies for each individual GEF or GAP were not available, ECs were grown in the presence of puromycin, an antibiotic used for selection in order to increase knockdown efficiency. To organize the GEF/GAP screen we divided the knockdown results into three distinct categories: 1. the regulation of basal monolayer resistance; 2. limiting permeability during diapedesis, and 3. neutrophil diapedesis efficiency.

Four Rho-GEFs and 2 Rho-GAPs were found to be involved in limiting endothelial leakage during neutrophil extravasation. Endothelial Tuba depletion did not alter basal endothelial barrier function or efficient neutrophil TEM (Fig. 2a). However, permeability gradually increased when neutrophil TEM occurred, indicating that Tuba is involved in limiting leakage during neutrophil TEM (Fig. 2a). In addition to Tuba, we found the Rho GEFs FGD5, Ect2, LARG and Bcr as potential regulators of endothelial pore formation (Fig. 2b). Among the Rho-GAPs we found ARHGAP11a and potentially the GAP domain of Bcr to be involved in the regulation of endothelial leakage during neutrophil diapedesis (Fig. 2b). Thus, several Rho-GEFs and Rho-GAPs that are recognized for their specificity towards RhoA and Cdc42 may potentially be involved in controlling vascular leakage during leukocyte TEM.

TRIO, Vav2, β-pix, Nm23-H1, PLEKH1, CdGAP, DLC1 and ARAP3 regulate basal endothelial junction integrity

From our screen, we found 5 Rho-GEFs and 3 Rho-GAPs to be involved in the regulation of basal endothelial barrier function. Our recent work demonstrates that TRIO-deficient ECs show instable VE-cadherin-based cell-cell junctions (Timmerman, Heemskerk, Kroon, Schaefer, Rijssel, et al. 2015). In agreement with this study, TRIO-deficient ECs showed impaired endothelial barrier under basal conditions and consequently diffusion of FITC-dextran into the lower compartment of the Transwell (Fig. 3a). In addition to TRIO, we found the Rho-GEFs VAV2, ARHGEF7, NME1 and

6
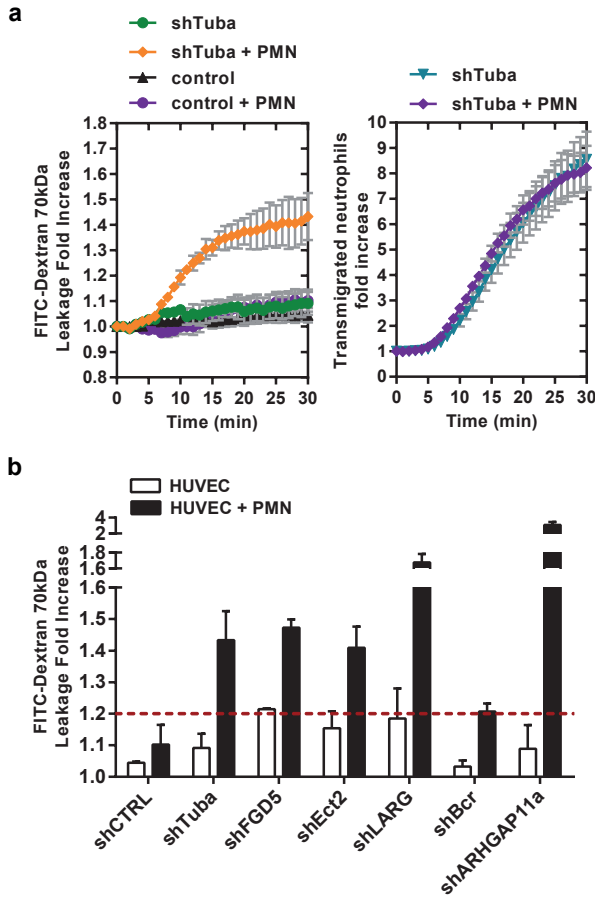
Figure 2 A set of Rho GEFs and GAPs that limits vascular leakage during leukocyte diapedesis. (**a**) Extravasation kinetics of FITC-dextran and calcein-red labelled neutrophils through TNF-α treated Tuba deficient ECs. (**b**) Rho GEFs and Rho GAPs involved in endothelial pore formation.

PLEKHG1 and the Rho-GAPs ARHGAP31, Deleted in Liver Cancer 1 (DLC1) and ARAP3 as potential candidates that regulate basal endothelial barrier function (Fig. 3b). Thus, we identified Rho GEFs and GAPs that all function in regulating the endothelial barrier maintenance, either in resting conditions or during leukocyte TEM events.

DISCUSSION

Endothelial barrier function during leukocyte diapedesis is regulated through the generation of F-actin rich contractile endothelial pores that require local RhoA activation (Heemskerk et al. 2016). Additionally, it
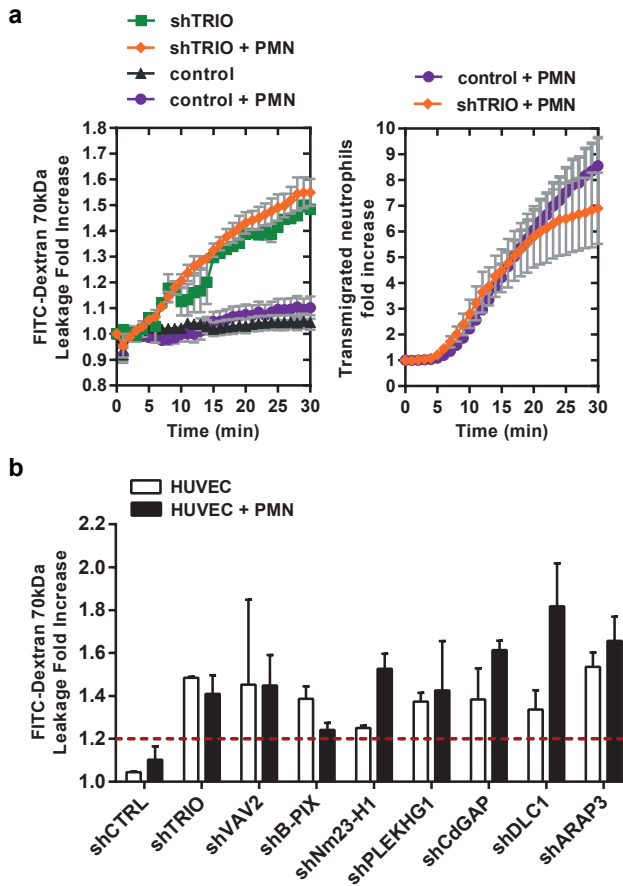
Figure 3 Potential Rho GEFs and GAPs involved in the stabilization of EC junctions. (**a**) Extravasation kinetics of calcein red-orange labelled neutrophils and FITC dextran through TRIO deficient ECs stimulated with TNF-α overnight. (**b**) Rho GEFs and Rho GAPs involved in endothelial barrier function.

is also well established that RhoA is involved in contraction-mediated opening of endothelial cell-cell junctions, for instance upon thrombin or histamine treatment (Amerongen et al. 2000; Mikelis et al. 2015). Also the small GTPase Rac1 is recognized for its role not only in stabilizing endothelial cell-cell junctions but also during the recovery phase after junction disruption (Daneshjou et al. 2015; Timmerman, Heemskerk, Kroon, Schaefer, Rijssel, et al. 2015). However, when and where these GTPases are activated and inactivated by GEFs and GAPs is not well understood. These proteins are recognized for their local GTPase activity regulation. To understand which GEFs and/or GAPs are controlling this, we performed a screen of short hairpin RNAs targeting 25 distinct endothelial Rho GEFs or GAPs to identify candidates that regulate permeability of

endothelial cells during diapedesis or under resting conditions. Note that this method does not exclude GEFs or GAPs but was solely intended to identify new candidates involved in endothelial pore regulation which should be additionally validated. We found six Rho-GEFs and/or GAPs with activity towards RhoA and Cdc42 that are involved in the regulation of permeability during leukocyte diapedesis and discovered eight Rho GEFs and/or GAPs with enzymatic activity towards Rac1 that are involved in the regulation of basal endothelial junction integrity (Table 1 and 2).

We showed that endothelial permeability during neutrophil diapedesis is limited by the formation of an F-actin-rich endothelial pore that surrounds extravasating neutrophils. Mechanistically it has been shown that ICAM-1 clustering and exerted force on ICAM-1 recruits the Rho-GEFs LARG, known to control RhoA activity (Lessey-Morillon et al. 2014). These signals result in endothelial pore confinement and consequently limit vascular permeability during a neutrophil breaching event (Heemskerk et al. 2016; Lessey-Morillon et al. 2014). In line with these studies, we found the Rho-GEFs Ect2 and LARG to be involved in prevention of vascular leakage during neutrophil diapedesis. The Rho-GEF LARG contains a regulator of G-protein signaling (RGS) homology (RH) domain located at the N-terminus that binds to activated heterotrimeric G protein α12/13 (Suzuki et al. 2003). In line, it would be interesting to investigate the role of G protein activation in the endothelial pore regulation, in particular because intracellular vesicles including chemokines are locally released into pore guiding directional transmigration of neutrophils (Shulman et al. 2011). This may open up a regulatory mechanism for additional Rho-GEFs, like the ones we identified here.

In addition to a role for RhoA-specific GEFs, we found the Cdc42-specific Rho GEFs Tuba and FGD5 as potential regulators of limiting vascular

Table 1. Rho GEFs and GAPs regulating endothelial pore formation

Gene name	Rho GTPase target	Activity
Tuba	Cdc42	GEF
FGD5	Cdc42	GEF
Ect2	RhoA, Rac1, Cdc42	GEF
LARG	RhoA, RhoC	GEF
Bcr	RhoA (GEF), Rac1(GAP), Cdc42	GEF/GAP
ARHGAP11a	RhoA, RhoB, RhoC	GAP

Table 2. Rho GEFs and GAPs regulating basal endothelial barrier

Gene name	Rho GTPase target	Activity
TRIO	Rac1, RhoG, RhoA	GEF
VAV2	Rac1, RhoG, RhoA, Cdc42	GEF
B-PIX	Rac1, Cdc42	GEF
Nm23-H1	Rac1 (Tiam1), Cdc42 (Dbl) Arf6	GEF
PLEKHG1	RhoA, RhoB, RhoC, Cdc42	GEF
CdGAP	Rac1, Cdc42	GAP
DLC1	RhoA, RhoB, RhoC, Cdc42	GAP
ARAP3	RhoA, Arf6	GAP

leakage during TEM. The properties of Tuba have been linked to both Rho-GTPase signaling and F-actin assembly. The N-terminal domain of Tuba binds dynamin through its Src homology-3 (SH-3) domains, whereas similar SH-3 domains in the C-terminus provide the binding site for a variety of actin-regulatory proteins, including N-WASP and Ena/VASP proteins. Interestingly, N-WASP was detected in the so-called docking structures, endothelial apical membrane protrusions that surround transmigrating leukocytes (Mooren et al. 2014). In addition, N-WASP and Ena/VASP have been identified as key effectors of Listeria entry into cells (Bierne et al. 2005). Potentially, (part of) this signaling mechanism may also be used by endothelial cells during leukocyte diapedesis. Moreover, Tuba may control endothelial membrane curvature during leukocyte crossing, since Tuba contains a Bin/amphiphysin/Rvs (BAR) domain instead of a classical plekstrin-homology (PH) domain. These BAR domains are lipid binding domains that are recruited to curved membranes (Salazar et al. 2003). Although the mechanisms of Tuba recruitment to diapedesis sites are not understood, we speculate that Tuba is recruited to endothelial membrane curvatures that are induced by probing neutrophils and consequently act as a scaffold protein to support local GTPase signaling and F-actin assembly.

In epithelial cells, Tuba controls the linearity of cell-cell junctions through local activation of Cdc42 that creates junctional surface tension and, supported by the cortical actin cytoskeleton, causes the linear morphology of apical endothelial junctions (Otani et al. 2006). Moreover, Tricellulin, a protein located at tricellular contacts regulates junctional

6

tension of epithelial cells through Tuba (Oda et al. 2014). This might be of particular interest because it has been suggested that neutrophils may prefer crossing the endothelium at tricellular contacts (Burns et al. 1997; Rabodzey et al. 2008).

In addition to Tuba, we found the Rho-GEF FGD5 as a potential regulator of vascular leakage limitation during TEM. This is in agreement with a recent study showed that Rap1 potentiate EC junctions through activation of FGD5. Mechanistically, FGD5 strengthens EC junctions by formation of circumferential actin bundles that are induced through activation of Cdc42, MRCK and myosin-II (Ando et al. 2013). From these data, we speculate that the borders of paracellular endothelial pores require stabilization of cell-cell junctions to ensure endothelial pore integrity, FGD5 may play a role in the potentiation of EC junctions at the endothelial pores margins. Among Rho-GAP involvement, we found potential roles for the Rho-GAPs Bcr and ARHGAP11a to be involvement in endothelial pore regulation. The enzyme activity of Bcr is intriguing since is contains a centrally located GEF domain that has been shown to activate RhoA (Dubash et al. 2013; Sahay et al. 2008) and a c-terminal GAP domain important for Rac1 inactivation (Kweon et al. 2008). Although the mechanisms of junctional destabilization prior to leukocyte diapedesis are not completely clear we may speculate that junctional opening underneath adherent leukocytes requires local inactivation of Rac1.

ARHGAP11a depletion induced a massive increase in vascular permeability during leukocyte diapedesis. However, nothing is known about the functional role of ARHGAP11a in endothelial cells. In epithelial cells, ARHGAP11a has been shown to be involved in cell-cycle arrest and apoptosis (Xu et al. 2013). On the contrary in some cancers increased expression of ARHGAP11a is involved in RhoA inhibition and thereby increasing cancer cell motility and invasiveness (Kagawa et al. 2013). Future research on ARHGAP11a in ECs is needed to elucidate its functional role in endothelial barrier protection during neutrophil diapedesis.

The role of several GTPases including RhoA, Rac1 and Cdc42 in the regulation of basal endothelial barrier have been extensively investigated, however which GAPs and GEFs regulate local GTPase cycling at endothelial junctions is poorly understood. Previously we found that the GEF TRIO regulates EC junctions through local activation of Rac1 (Timmerman, Heemskerk, Kroon, Schaefer, Rijssel, et al. 2015). Our screen underscores these findings. In addition we found the GEF VAV2 to be involved in basal endothelial barrier regulation. In line with this, Vav-2 and Rac1 activation have both been described to strengthen endothelial junctions (Schlegel and Waschke 2013). In contrast, Vav-2 has also been shown to be involved in the internalization of VE-cadherin after VEGF stimulation causing

increased vascular permeability (Gavard and Gutkind 2006). Because Vav2 is very promiscuous, activating Rac1, RhoA, Cdc42 and RhoG it is not surprising Vav2 is found to be involved in several signaling routes involving junctional regulation. In our screen depletion of endothelial β-pix, a Rho GEF for Rac1 and Cdc42, resulted in increased basal permeability but no effect on leukocyte TEM. In contrast to our findings of β-pix involvement in regulation of basal EC barrier integrity, β-pix has been shown to play a pivotal role in LPS-mediated induction of vascular permeability *in vivo* (Stockton et al. 2007). Again this could be explained by the promiscuous nature of GEFs. In contrast to the study of Stockton et al, Tiam1 and β-pix have also been implicated in strengthening of the endothelial barrier in response to OxPAP-C (Birukova et al. 2007). This is in line with our finding that β-pix plays a role in the junctional stabilization. Moreover, β-pix has been shown to play a pivotal role in junctional stabilization of cerebral vessels during zebrafish development (Liu et al. 2007). These findings indicate that a similar exchange factor can have other functions in different tissues or during different stages of development. Moreover basal endothelial integrity was impaired upon depletion of Nm23-H1, a nucleoside diphosphate kinase, highly expressed in HUVEC that functions as a scaffold protein for the Rho GEFs Dbl and Tiam1 (Van Buul, Geerts, and Huveneers 2014).

Recently, EMMPRIN-deficient mice show impaired recruitment of Nm23-H1 to endothelial junctions resulting in altered VE-cadherin localization and increased vascular permeability (Moreno et al. 2014). In agreement with these findings, we found that the permeability in Nm23-H1-deficient ECs was increased. In epithelial cells, Nm23-H1 recruitment by ADP-ribosylation factor 6 (ARF-6) controls clathrin-dependent endocytosis of E-cadherin-based junctions regulating junctional disassembly (Palacios et al. 2002). Moreover, Nm23-H1 recruitment to cell-cell contacts inhibits Rac1 activity through inactivation of the Rho GEF Tiam1, which is thought to play a critical role in contact inhibition (Tanaka, Kuriyama, and Aiba 2012). Thus, Nm23-H1 may control endothelial permeability through altered VE-cadherin endocytosis or recycling (Wessel et al. 2014).

Another Rho-GTPase regulator that associates with the small GTPase ARF6 is the Rho-GAP ARAP3. ARAP3-deficient mice and zebrafish are embryonically lethal due to defects in angiogenesis during embryonic development (Gambardella et al. 2010; Kartopawiro et al. 2014). Our data, showing increased endothelial permeability in ARAP3 deficient ECs, underscores the role of ARAP3 in vascular integrity also after embryonic development. Depletion of the Rho-GAP DLC1 promotes endothelial permeability. In line with our findings, in HEK 293 cells DLC-1 interacts with α-catenin, resulting in stabilization of adherens junctions through

local inhibition of Rho-GTPase activity (Tripathi, Popescu, and Zimonjic 2012). Finally, we found that depletion of PLEKH1 a Rho-GEF for RhoA-C and Cdc42 and CdGAP a Rho GAP for Rac1 and Cdc42 (Lamarche-Vane and Hall 1998) reduced endothelial barrier function. Future research on PLEKH1 and CdGAP in endothelial junction regulation is interesting since the function of PLEKH1 and CdGAP in ECs is unknown.

In conclusion, we discovered several Rho GEFs and GAPs involved in the regulation of the endothelial barrier under basal conditions or during leukocyte diapedesis. GEFs and GAPs provide specificity to broadly involved GTPase cycles triggered in many distinct cellular signaling pathways. Exactly this feature makes GEFs and GAPs an important subject for future research.

ACKNOWLEDGEMENTS

COMPETING FINANCIAL INTEREST

The authors declare that they have no competing financial interest

References

Amerongen, G. P. v. N. et al. 2000. "Activation of RhoA by Thrombin in Endothelial Hyperpermeability : Role of Rho Kinase and Protein Tyrosine Kinases." *Circulation Research* 87(4): 335–40. https://caehbj4r4lz7cfmrugl7nq2pkk.sec.amc.nl/content/87/4/335.full (January 5, 2015).

Ando, Koji et al. 2013. "Rap1 Potentiates Endothelial Cell Junctions by Spatially Controlling Myosin I Activity and Actin Organization." *Journal of Cell Biology* 202(6): 901–16.

Baluk, P et al. 1998. "Endothelial Gaps and Adherent Leukocytes in Allergen-Induced Early- and Late-Phase Plasma Leakage in Rat Airways." *The American journal of pathology* 152(6): 1463–76. /pmc/articles/PMC1858452/?report=abstract (February 3, 2015).

Baluk, Peter et al. 1995. "NK1 Receptors Mediate Leukocyte Adhesion in Neurogenic Inflammation in the Rat Trachea." *The American journal of physiology* 268(31): L263–69.

Bierne, Hélène et al. 2005. "WASP-Related Proteins, Abi1 and Ena/VASP Are Required for Listeria Invasion Induced by the Met Receptor." *Journal of cell science* 118(Pt 7): 1537–47. http://jcs.biologists.org/content/118/7/1537 (January 22, 2016).

Birukova, Anna A et al. 2007. "Tiam1 and betaPIX Mediate Rac-Dependent Endothelial Barrier Protective Response to Oxidized Phospholipids." *Journal of cellular physiology* 211(3): 608–17. https://cz2pflinceb6odvtcsam5w6cke.sec.amc.nl/doi/10.1002/jcp.20966/full (August 12, 2015).

Burns, a R et al. 1997. "Neutrophil Transendothelial Migration Is Independent of Tight Junctions and Occurs Preferentially at Tricellular Corners." *Journal of immunology (Baltimore, Md. : 1950)* 159: 2893–2903.

Van Buul, Jaap D., Dirk Geerts, and Stephan Huveneers. 2014. "Rho GAPs and GEFs: Controling Switches in Endothelial Cell Adhesion." *Cell Adhesion and Migration* 8(2): 108–24.

Daneshjou, N. et al. 2015. "Rac1 Functions as a Reversible Tension Modulator to Stabilize VE-Cadherin Trans-Interaction." *The Journal of Cell Biology* 208(1): 23–32. http://www.jcb.org/cgi/doi/10.1083/jcb.201409108.

Dubash, Adi D. et al. 2013. "The GEF Bcr Activates RhoA/MAL Signaling to Promote Keratinocyte Differentiation via Desmoglein-1." *Journal of Cell Biology* 202: 653–66.

Gambardella, Laure et al. 2010. "PI3K Signaling through the Dual GTPase-Activating Protein ARAP3 Is Essential for Developmental Angiogenesis." *Science signaling* 3(145): ra76.

Gavard, Julie, and J Silvio Gutkind. 2006. "VEGF Controls Endothelial-Cell Permeability by Promoting the Beta-Arrestin-Dependent Endocytosis of VE-Cadherin." *Nature cell biology* 8(11): 1223–34.

Gawlowski, D M, J N Benoit, and H J Granger. 1993. "Microvascular Pressure and Albumin Extravasation after Leukocyte Activation in Hamster Cheek Pouch." *The American journal of physiology* 264(2 Pt 2): H541–46. http://www.ncbi.nlm.nih.gov/pubmed/7680539 (December 19, 2014).

Heemskerk, Niels et al. 2016. "F-Actin-Rich Contractile Endothelial Pores Prevent Vascular Leakage during Leukocyte Diapedesis through Local RhoA Signalling." *Nature Communications* 7: 10493. http://www.nature.com/doifinder/10.1038/ncomms10493.

Hillgruber, C. et al. 2015. "Blocking Neutrophil Diapedesis Prevents Hemorrhage during Thrombocytopenia." *Journal of Experimental Medicine.* http://www.jem.org/cgi/doi/10.1084/jem.20142076.

Kagawa, Yoshinori et al. 2013. "Cell Cycle-Dependent Rho GTPase Activity Dynamically Regulates Cancer Cell Motility and Invasion in Vivo." *PLoS ONE* 8(12).

Kartopawiro, Joëlle et al. 2014. "Arap3 Is Dysregulated in a Mouse Model of Hypotrichosis-Lymphedema-Telangiectasia and Regulates Lymphatic Vascular Development." *Human Molecular Genetics* 23(5): 1286–97.

Kim, Min-Ho, Fitz-Roy E Curry, and Scott I Simon. 2009. "Dynamics of Neutrophil Extravasation and Vascular Permeability Are Uncoupled during Aseptic Cutaneous Wounding." *American journal of physiology. Cell physiology* 296(4): C848–56. http://www.pubmedcentral.nih.gov/articlerender.fcgi?artid=2670654&tool=pmcentrez&rendertype=abstract (December 18, 2014).

6

Kweon, Soo Mi et al. 2008. "Activity of the Bcr GTPase-Activating Domain Is Regulated through Direct Protein/protein Interaction with the Rho Guanine Nucleotide Dissociation Inhibitor." *Journal of Biological Chemistry* 283(6): 3023–30.

Lamarche-Vane, Nathalie, and Alan Hall. 1998. "CdGAP, a Novel Proline-Rich GTPase-Activating Protein for Cdc42 and Rac." *Journal of Biological Chemistry* 273(44): 29172–77.

Lessey-Morillon, Elizabeth C et al. 2014. "The RhoA Guanine Nucleotide Exchange Factor, LARG, Mediates ICAM-1-Dependent Mechanotransduction in Endothelial Cells to Stimulate Transendothelial Migration." *Journal of immunology (Baltimore, Md. : 1950)* 192: 3390–98. http://www.ncbi.nlm.nih.gov/pubmed/24585879.

Lewis, R E, and H J Granger. 1988. "Diapedesis and the Permeability of Venous Microvessels to Protein Macromolecules: The Impact of Leukotriene B4 (LTB4)." *Microvascular research* 35: 27–47.

Lewis, R.E., R.A. Miller, and H.J. Granger. 1989. "Acute Microvascular Effects of the Chemotactic Peptide N-Formyl-Methionyl-Leucyl-Phenylalanine: Comparisons with Leukotriene B4." *Microvascular Research* 37(1): 53–69. http://www.sciencedirect.com/science/article/pii/0026286289900721 (February 26, 2015).

Liu, Jing et al. 2007. "A betaPix Pak2a Signaling Pathway Regulates Cerebral Vascular Stability in Zebrafish." *Proceedings of the National Academy of Sciences of the United States of America* 104: 13990–95.

McDonald, D M. 1994. "Endothelial Gaps and Permeability of Venules in Rat Tracheas Exposed to Inflammatory Stimuli." *The American journal of physiology* 266: L61–83.

McDonald, D M, G Thurston, and P Baluk. 1999. "Endothelial Gaps as Sites for Plasma Leakage in Inflammation." *Microcirculation (New York, N.Y. : 1994)* 6: 7–22.

Mikelis, Constantinos M et al. 2015. "RhoA and ROCK Mediate Histamine-Induced Vascular Leakage and Anaphylactic Shock." *Nature communications* 6: 6725. http://www.ncbi.nlm.nih.gov/pubmed/25857352 (April 13, 2015).

Mooren, Olivia L, Jinmei Li, Julie Nawas, and John A Cooper. 2014. "Endothelial Cells Use Dynamic Actin to Facilitate Lymphocyte Transendothelial Migration and Maintain the Monolayer Barrier." *Molecular biology of the cell* 25(25): 4115–29. http://www.ncbi.nlm.nih.gov/pubmed/25355948 (December 19, 2014).

Moreno, Vanessa et al. 2014. "An EMMPRIN/γ-catenin/Nm23 Complex Drives ATP Production and Actomyosin Contractility at Endothelial Junctions." *Journal of cell science* 23: 3768–81. http://www.ncbi.nlm.nih.gov/pubmed/24994937.

Oda, Y., T. Otani, J. Ikenouchi, and M. Furuse. 2014. "Tricellulin Regulates Junctional Tension of Epithelial Cells at Tricellular Contacts through Cdc42." *Journal of Cell Science* 127: 4201–12. http://jcs.biologists.org/cgi/doi/10.1242/jcs.150607.

Otani, Tetsuhisa, Tetsuo Ichii, Shinya Aono, and Masatoshi Takeichi. 2006. "Cdc42 GEF Tuba Regulates the Junctional Configuration of Simple Epithelial Cells." *Journal of Cell Biology* 175(1): 135–46.

Palacios, Felipe, Jill K Schweitzer, Rita L Boshans, and Crislyn D'Souza-Schorey. 2002. "ARF6-GTP Recruits Nm23-H1 to Facilitate Dynamin-Mediated Endocytosis during Adherens Junctions Disassembly." *Nature cell biology* 4(December): 929–36.

Rabodzey, Aleksandr, Pilar Alcaide, Francis W Luscinskas, and Benoit Ladoux. 2008. "Mechanical Forces Induced by the Transendothelial Migration of Human Neutrophils." *Biophysical journal* 95(August): 1428–38.

Rosengren, S, K Ley, and K E Arfors. 1989. "Dextran Sulfate Prevents LTB4-Induced Permeability Increase, but Not Neutrophil Emigration, in the Hamster Cheek Pouch." *Microvascular research* 38: 243–54.

Sahay, S et al. 2008. "The RhoGEF Domain of p210 Bcr-Abl Activates RhoA and Is Required for Transformation." *Oncogene* 27: 2064–71.

Salazar, Marco a. et al. 2003. "Tuba, a Novel Protein Containing bin/amphiphysin/Rvs and Dbl Homology Domains, Links Dynamin to Regulation of the Actin Cytoskeleton." *The Journal of biological chemistry* 278(49): 49031–43.

Schlegel, Nicolas, and Jens Waschke. 2013. "cAMP with Other Signaling Cues Converges on Rac1 to Stabilize the Endothelial Barrier- a Signaling Pathway Compromised in Inflammation." *Cell and Tissue Research*: 1–10.

Shulman, Ziv et al. 2011. "Transendothelial Migration of Lymphocytes Mediated by Intraendothelial Vesicle Stores rather than by Extracellular Chemokine Depots." *Nature Immunology* 13(1): 67–76.

Stockton, Rebecca et al. 2007. "Induction of Vascular Permeability: Beta PIX and GIT1 Scaffold the Activation of Extracellular Signal-Regulated Kinase by PAK." *Molecular biology of the cell* 18(6): 2346–55. https://cz2xow-mme5clog-oh2phe.sec.amc.nl/content/18/6/2346.full (August 12, 2015).

Suzuki, Nobuchika, Susumu Nakamura, Hiroyuki Mano, and Tohru Kozasa. 2003. "G Alpha 12 Activates Rho GTPase through Tyrosine- Phosphorylated Leukemia-Associated RhoGEF." *Pnas* 100(2).

Tanaka, M., S. Kuriyama, and N. Aiba. 2012. "Nm23-H1 Regulates Contact Inhibition of Locomotion Which Is Affected by Ephrin-B1." *Journal of Cell Science*.

Timmerman, Ilse, Niels Heemskerk, Jeffrey Kroon, Antje Schaefer, Jos Van Rijssel, et al. 2015. "A Local VE-Cadherin / Trio-Based Signaling Complex Stabilizes Endothelial Junctions through Rac1 Journal of Cell Science Accepted Manuscript." (June).

Timmerman, Ilse, Niels Heemskerk, Jeffrey Kroon, Antje Schaefer, Jos van Rijssel, et al. 2015. "A Local VE-Cadherin and Trio-Based Signaling Complex Stabilizes Endothelial Junctions through Rac1." *Journal of cell science* 128(16): 3041–54. http://www.ncbi.nlm.nih.gov/pubmed/26116572 (December 8, 2015).

Tripathi, V., N. C. Popescu, and D. B. Zimonjic. 2012. "DLC1 Interaction with -Catenin Stabilizes Adherens Junctions and Enhances DLC1 Antioncogenic Activity." *Molecular and Cellular Biology* 32(11): 2145–59.

Valeski, J E, and a L Baldwin. 1999. "Effect of Early Transient Adherent Leukocytes on Venular Permeability and Endothelial Actin Cytoskeleton." *The American journal of physiology* 277: H569–75.

Vestweber, Dietmar, Florian Wessel, and Astrid Fee Nottebaum. 2014. "Similarities and Differences in the Regulation of Leukocyte Extravasation and Vascular Permeability." *Seminars in Immunopathology* 36: 177–92.

Wessel, Florian et al. 2014. "Leukocyte Extravasation and Vascular Permeability Are Each Controlled in Vivo by Different Tyrosine Residues of VE-Cadherin." *Nature immunology* 15(3): 223–30. http://www.ncbi.nlm.nih.gov/pubmed/24487320.

Xu, Jie et al. 2013. "RhoGAPs Attenuate Cell Proliferation by Direct Interaction with p53 Tetramerization Domain." *Cell Reports* 3: 1526–38.

6

7

SUMMARY AND CONCLUDING REMARKS

Summary and concluding remarks

Dynamic remodeling of endothelial cell (EC) junctions is essential for proper function of the vascular system. Disruptive stressors such as thrombin, histamine, adherent and transmigrating leukocytes, and effects of blood pressure or temperature, daily impact the integrity of EC. The constant cycle of endothelial junctional disassembly and assembly enables EC to cope with this dynamic vascular environment. In this thesis, we aimed to examine which endothelial proteins orchestrate junctional remodeling in response to common endothelial activators such as thrombin or transmigrating leukocytes.

Trio-mediated Rac1 activity locally restores junctional stability

The regulation of the F-actin cytoskeleton by RhoGTPases is indispensable for proper junctional dynamics. However, little is known about which GEFs and GAPs regulate local RhoGTPase cycling to mediate transient remodeling of EC junctions. In **chapter 5** we show that TRIO, a GEF for Rac1, regulates stabilization of VE-cadherin-based junctions through its first GEF domain [1]. Cell-cell junctions between Trio-deficient EC were unstable and showed continuous dis- and re-assembly. Mechanistically, we show that homophilic ligation of VE-cadherin in nascent junctions recruits Trio to VE-cadherin. Next, Trio can activate Rac1 in close proximity of the VE-cadherin-catenin complex enabling the formation of cortical actin bundles along the junction at the expense of radial actin bundles perpendicular to the junction. The subsequent connection of the VE-cadherin-catenin complex to these cortical actin bundles increases junctional stability and endothelial monolayer resistance (Fig. 1). In contrast to our model, Rac1 cycling has also been described to be required for VE-cadherin endocytosis and the formation of reactive oxygen species (ROS), which both mediate junctional instability [2-4]. These contradictory roles for Rac1 in EC are not in conflict with each other since its spatiotemporal activity is tightly regulated by numerous pathway-specific GEFs and GAPs. For instance, Trio deficiency did not prevent Rac1-induced membrane protrusive activity during formation of initial cell-cell contact. Thus, prior to stabilization of the nascent cell-cell contact induced by local signaling through the VE-cadherin-Trio-Rac1 axis, other Rac-GEFs likely contribute to promote initial cell-cell contact formation for example by junction-associated lamellipodia (JAILs) [5]. Still, many details of the mechanisms driving spatiotemporal Rac1 activation at distinct stages of junction formation remain to be uncovered. The recently published DORA Rac1 biosensor [1] will be a good tool to dissect the consecutive involvement of distinct GEFs in Rac1-mediated junctional stabilization.
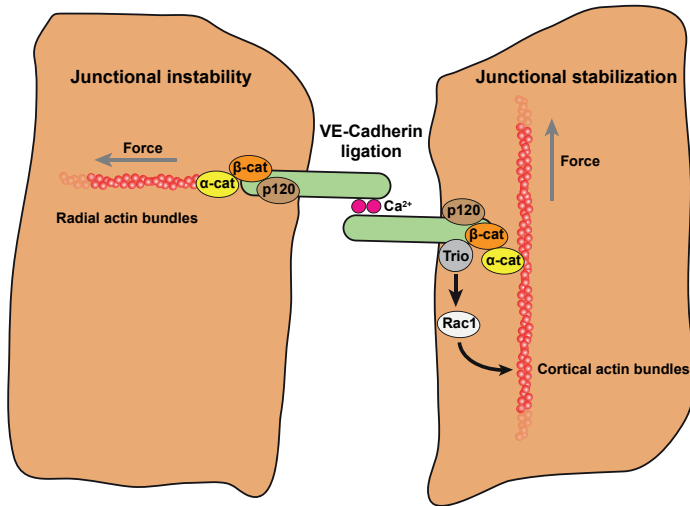
Figure 1. Trio-mediated Rac1 activation stabilizes VE-cadherin based cell-cell contacts. The process of adherens junctions (AJ) formation can be segmented into three phases: first, membrane protrusions limit the gap between two cells to mediate initial contact; second, VE-cadherin molecules engage in homophilic interactions and form clusters; and third, VE-cadherin clusters trigger the transition from radial to cortical actin bundles along the junction. Subsequent connection of the VE-cadherin-catenin complex to cortical actin bundles increases junctional stability and endothelial monolayer resistance. Trio-mediated rac1 activity plays a crucial role during the third stage of the AJ formation process.

ANNEXIN A2 CONTROLS NEUTROPHIL TRANSENDOTHELIAL MIGRATION BY REGULATING THE SPATIAL ORGANIZATION OF ICAM-1 INTO CAVEOLAE

The endothelial β2-integrin ligand ICAM-1 facilitates effective neutrophil trafficking in and out of the vasculature. Being involved in rolling, arrest, crawling and transmigration of neutrophils in vivo [6-11], ICAM-1 has been postulated to reside in various membrane complexes with different protein content, spatial organization and subcellular localization, to regulate leukocyte behavior in each distinctive step [12-14]. However, little is known about how the spatial organization of endothelial ICAM-1 affects ICAM-1-mediated leukocyte adhesion and how the cell surface distribution of ICAM-1 between various membrane domains is regulated. In **Chapter 3** we report on annexin A2, an ICAM-1-binding protein that regulates the spatial distribution of ICAM-1 at the plasma membrane during the adhesion phase of leukocyte TEM [15]. We established that clustered ICAM-1 translocates from ezrin-rich membrane domains to caveolin-1-rich membrane domains, a step mediated by annexin A2 (Fig. 2). Endothelial annexin A2 depletion increased neutrophil adhesion and transmigration, whereas neutrophil crawling distance and velocity was reduced. These findings suggest that the redistribution of ICAM-1 into caveolae has a

limiting effect on ICAM-1-mediated leukocyte adhesion, likely by limiting the number of accessible ICAM-1 molecules at the endothelial surface. ICAM-1 in caveolae has also been reported to be rapidly transported to the basolateral surface of ECs by a process named transcytosis [12]. The amount of apically exposed ICAM-1 and ICAM-1 transcytosis events have been proposed to be part of a mechanism for transcellular migration, but not paracellular migration of T cells and neutrophils [12,16,17]. Future studies investigating the role of endothelial signaling in leukocyte TEM should include biosensors to investigate at what stage a particular protein is participating in the process. Notably, addressing spatial and temporal differences of ICAM-1-adaptor-GTPase-effector complexes would be an interesting line of future research. Important questions to study are: when does ICAM-1 clustering occur? And for which particular step would this be required; do neutrophils induce clustering during the crawling phase? The generation of an ICAM-1 FRET-based biosensor to allow imaging of spatial and temporal ICAM-1 clustering in real-time during TEM of leukocytes may help to address this intriguing topic.

7
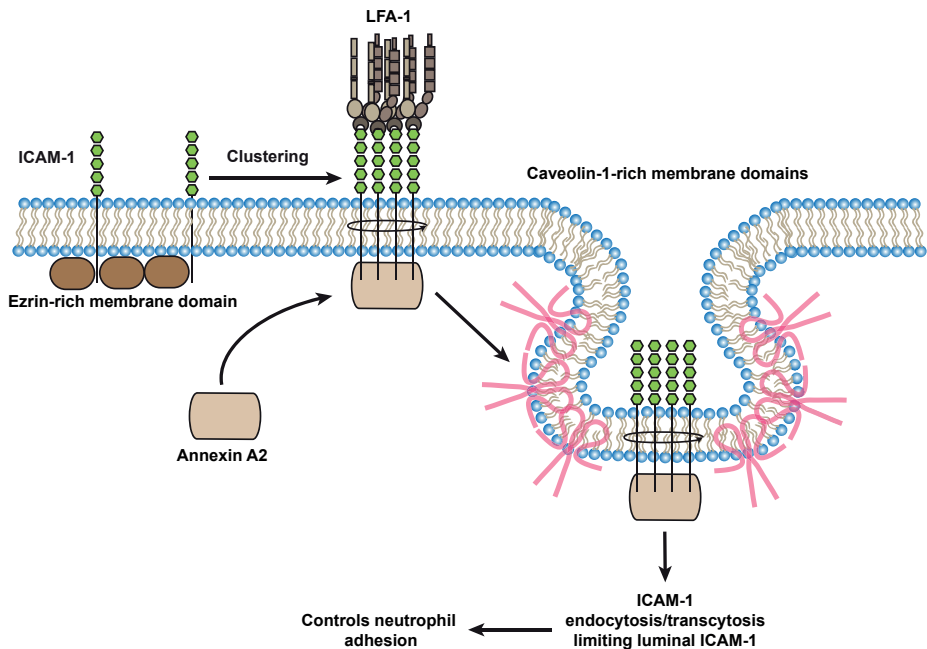
Figure 2. A model of annexin A2 controlling ICAM-1-mediated neutrophil transendothelial migration. In endothelial cells unengaged ICAM-1 resides in ezrin-rich membrane domains. Upon LFA-1 induced ICAM-1 clustering, ICAM-1 is redistributed to caveolin-1-rich membrane domains in an annexin A2 dependent manner. Subsequent ICAM-1 endocytosis or transcytosis limits the number of free accessible ICAM-1 molecules at the endothelial surface, thereby negatively regulating ICAM-1-mediated neutrophil adhesion.

A RhoA MEDIATED CONTRACTILE RING PREVENTS PLASMA LEAKAGE DURING LEUKOCYTE DIAPEDESIS

Every day, billions of leukocytes cross the endothelial barrier to fulfill protective immune functions against pathogens, cancerous cells and foreign material. Despite numerous crossings, immune cell traffic seems to have minor impact on endothelial integrity and permeability [18-22]. Already in 1988, researchers showed that intimate contact between neutrophils and ECs was maintained during the entire TEM process. This intimate contact could explain transmigration of leukocytes without vascular damage [23]. However, a mechanism was lacking. In **chapter 4** we show that local RhoA-mediated F-actin rings contribute to endothelial pore confinement which maintains endothelial barrier integrity during leukocyte diapedesis [24]. Neutrophil diapedesis initiates the clustering of ICAM-1 which in turn recruits the RhoA GEFs LARG and Ect2. RhoA activation by LARG and Ect2 results in local Rock2b-mediated Myosin II activation near the endothelial pore. Subsequent tightening of F-actin-rich membrane around transmigrating neutrophils creates intimate neutrophil-endothelial contact that prevents plasma leakage during the entire TEM process (Fig. 3a, b). Our study has been focused particularly on the diapedesis of neutrophils and monocytes during inflammation-driven leukocyte recruitment. Perhaps, endothelial pore confinement could also maintain endothelial integrity during immune surveillance or adaptive immune responses. For example during TEM of B cells, T-lymphocytes or dendritic cells through high endothelial venules in lymph nodes. However, endothelial pore confinement is not the only mechanism used by endothelial cells to cope with the mechanical disruptive strains induced by transmigrating leukocytes. Some studies showed that ECs reseal their endothelial barrier prior to or during neutrophil penetration of the basal lamina by the formation of endothelial dome structures or ventral lamellipodia [25-27]. Our data indicates that these alternative pathways are likely relevant downstream of endothelial pore confinement (Fig. 3a).

Exploring RhoA cycling dynamics using a RhoA FRET sensor led to an unexpected finding; RhoA was not activated during the opening of endothelial junctions upon leukocyte breaching, despite the fact that this has been proposed for years due to fact that thrombin-mediated RhoA activation results in contraction-mediated opening of endothelial cell-cell junctions [28,29]. We detected RhoA activation after junctional opening, i.e. during the mid-diapedesis step, when a leukocyte was already half way through. This suggests that ECs are equipped with mechanisms that initiate the opening of endothelial junctions independently of RhoA signalling. Moreover, we found that many F-actin-rich contractile rings comprise apical membrane protrusions. These Rac1-mediated

projections, also known as 'docking structures' or 'transmigratory cups' [30-32], have been suggested to mediate apical projection-guidance. Which means the guidance of leukocytes along adhesion molecule-enriched apical membrane protrusions on the endothelial apical surface. [12,31,33-36]. Two common principles are emerging; apical projections give directional guidance to leukocytes whereas the basolateral F-actin ring prevents vascular leakage during leukocyte crossing.
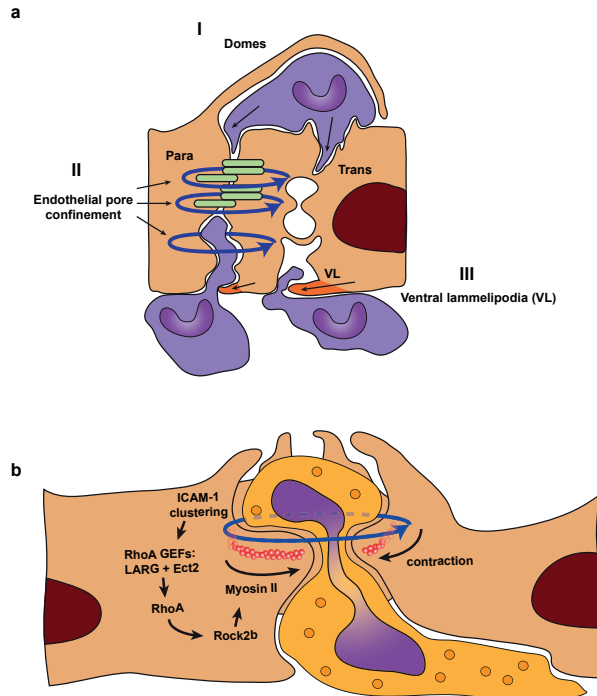
Figure 3. Mechanisms that prevent vascular leakage during leukocyte diapedesis. (**a**) Electron microscopy studies in the late 80's showed that leukocytes and endothelial cells maintain intimate contact during the entire diapedesis process. Transmigration occurred without vascular damage or leakage. In the years that followed several research groups searched for a mechanism that could explain this remarkable observation. Vascular leakage during leukocyte diapedesis is prevented by; **I** domes, that fully encapsulate migrating leukocytes, **II** RhoA-mediated endothelial pore confinement, contractile F-actin rings in the endothelium that form a natural crimp ring preventing plasma leakage into the underlying tissue. **III** Ventral lammelipodia (VL), Rac1-mediated F-actin-rich membrane protrusions at the basal surface of the endothelium that seal and restore the endothelial monolayer after leukocyte breeching. VE-cadherin complex (green), EC (brown) leukocytes (purple). (**b**) Mechanistically endothelial pore confinement is triggered by ICAM-1 clustering that activates RhoA through the RhoA GEFs LARG and Ect2. RhoA activation occurs during the mid-phase of diapedesis i.e. when the neutrophil partly breeched the endothelium. RhoA-mediated Myosin II activation through the kinase Rock2b induces contraction of F-actin-rich membrane around transmigrating neutrophils forcing tight neutrophil-endothelial contact that prevents plasma leakage during TEM. F-actin (red), neutrophil (yellow), EC (brown).

Concluding remarks and future perspectives

Could some of the findings in this thesis be translated into new treatments for patients that suffer from spontaneous leukocyte induce hemorrhages or endothelial barrier dysfunction in general?

Under some conditions such as disturbed flow and prolonged endothelial injury, the adherence of neutrophils to activated platelets could lead to a chain reaction. Ros produced by leukocyte-platelet aggregates could inflict more vascular damage, extracellular matrix exposure platelet activation and prolonged inflammation. Such an destructive feed forward loop may accelerate disease progression in for instance, thrombo-embolism or in a chronically expanding atherosclerotic lesion [37,38] where a blood clot or stenosis obstructs the blood flow to a tissue inflicting hypoxia, ischemia, infarction and tissue death. Interestingly, platelet-matrix interactions require an increase in microvascular permeability [39]. Therefore, prevention of vascular leakage by directly targeting the endothelial junctions may be a successful manner of intervention to prevent prolonged vascular permeability and tissue damage during acute inflammation. Several potential targets could be further explored for this specific type of intervention. For instance Y685 on VE-cadherin that specifically blocks vascular permeability [20] or endothelial specific GEFs such as Trio or EPAC, that are involved in stabilizing the endothelial barrier [40,41]. In addition, we show that leukocyte diapedesis and vascular permeability are each regulated by different unique exchange factors (**chapter 6**). Once their specific involvement in junctional regulation is validated, each of these proteins might be interesting as a therapeutic target to accompany the family of barrier strengthening agents. Moreover, several clinical trials aim to specifically inhibit vascular leakage by targeting Rho/ROCK signaling (www.clinicaltrials.gov). Fasudil is a FDA-approved Rho-kinase inhibitor showing protection against anaphylaxis in a murine sepsis model. However, as an unwanted side-effect, blocking Rho-kinase may additionally promote permeability under TEM conditions. Therefore, blocking both events separately at the same time is likely to increase therapy efficiency.

In other diseases such as immune thrombocytopenia, it is the lack of platelets that causes serious tissue damage and spontaneous hemorrhages [42]. Blocking neutrophil diapedesis by mutating Y731 in the cytoplasmic tail of VE-cadherin attenuates these spontaneous organ hemorrhages. Therefore, specifically targeting Y731 may present a novel therapeutic target to prevent spontaneous bleedings in these patients. Alternatively, some of these patients may benefit from drugs that are designed to strengthening endothelial junctions around transmigrating leukocytes.

We anticipate that future research and validation of the GEFs and GAPs involved in endothelial pore strengthening and confinement (**chapter 6**) may open therapeutic options for this type of drug development. Recently, a genetic study unravels that ECs express a distinctive gene profile encoding for an unique combination of transcription factors, chemokines, adhesion receptors and angiocrine growth factors [43]. Understanding what molecules regulate tissue-specific transmigration of each immune cell subtype would have a great impact on for example cancer immunotherapy. The key principles of leukocyte diapedesis, the path of least resistance, chemotaxis, durotaxis, haptotaxis and shear stress are evidently involved in the modulation of diapedesis into distinct tissues. These principles together with the unique tissue-specific gene profile may open a whole new avenue for cancer drug development. Although our findings do not have a direct benefit for patients, the advances made in this thesis greatly improves our general understanding about transendothelial migration and vascular integrity as a whole and increase the potential to find useful drugs that benefit cardiovascular diseases, cancer, acute inflammation and chronic inflammation.

In conclusion, this body of work shows that the endothelium has several mechanisms to cope with disruptive strains that challenge its barrier during inflammation and leukocyte diapedesis. ICAM-1 regulates both leukocyte adhesion and endothelial barrier strengthening during inflammation-driven leukocyte diapedesis. Increasing evidence points out that dynamic remodeling of EC junctions to increase vascular permeability or inflammation-driven leukocyte recruitment are independent processes that are likely occur in parallel. EC barrier maintenance during inflammation and leukocyte diapedesis require unique exchange factors which can be further explored to investigate where these closely associated pathways uncouple.

7

REFERENCES

1. Timmerman, I. *et al.* A local VE-cadherin / Trio-based signaling complex stabilizes endothelial junctions through Rac1 Journal of Cell Science Accepted manuscript. (2015).
2. Gavard, J. & Gutkind, J. S. VEGF controls endothelial-cell permeability by promoting the beta-arrestin-dependent endocytosis of VE-cadherin. *Nat. Cell Biol.* **8,** 1223–1234 (2006).
3. Spindler, V., Schlegel, N. & Waschke, J. Role of GTPases in control of microvascular permeability. *Cardiovasc. Res.* **87,** 243–253 (2010).
4. van Wetering, S. *et al.* Reactive oxygen species mediate Rac-induced loss of cell-cell adhesion in primary human endothelial cells. *J.Cell Sci.* **115,** 1837–1846 (2002).
5. Abu Taha, A., Taha, M., Seebach, J. & Schnittler, H.-J. ARP2/3-mediated junction-associated lamellipodia control VE-cadherin-based cell junction dynamics and maintain monolayer integrity. *Mol. Biol. Cell* **25,** 245–56 (2014).
6. Bourdillon, M. *et al.* Fed a Fat or a Chow Diet. *Arterioscler. Thromb.* 2630–2635 (2000).
7. Bullard, D. C. *et al.* P-selectin/ICAM-1 double mutant mice: Acute emigration of neutrophils into the peritoneum is completely absent but is normal into pulmonary alveoli. *J. Clin. Invest.* **95,** 1782–1788 (1995).
8. Gorina, R., Lyck, R., Vestweber, D. & Engelhardt, B.   2 Integrin-Mediated Crawling on Endothelial ICAM-1 and ICAM-2 Is a Prerequisite for Transcellular Neutrophil Diapedesis across the Inflamed Blood-Brain Barrier. *J. Immunol.* **192,** 324–337 (2013).
9. Kadono, T., Venturi, G. M., Steeber, D. a & Tedder, T. F. Leukocyte rolling velocities and migration are optimized by cooperative L-selectin and intercellular adhesion molecule-1 functions. *J. Immunol.* **169,** 4542–4550 (2002).
10. Phillipson, M. *et al.* Intraluminal crawling of neutrophils to emigration sites: a molecularly distinct process from adhesion in the recruitment cascade. *J. Exp. Med.* **203,** 2569–2575 (2006).
11. Sligh, J. E. *et al.* Inflammatory and immune responses are impaired in mice deficient in intercellular adhesion molecule 1. *Proc. Natl. Acad. Sci. U. S. A.* **90,** 8529–8533 (1993).
12. Millán, J. *et al.* Lymphocyte transcellular migration occurs through recruitment of endothelial ICAM-1 to caveola- and F-actin-rich domains. *Nat. Cell Biol.* **8,** 113–123 (2006).
13. Schaefer, A. *et al.* Actin-binding proteins differentially regulate endothelial cell stiffness, ICAM-1 function and neutrophil transmigration. *J. Cell Sci.* 4470–4482 (2014). doi:10.1242/jcs.154708
14. Barreiro, O. *et al.* Endothelial adhesion receptors are recruited to adherent leukocytes by inclusion in preformed tetraspanin nanoplatforms. *J. Cell Biol.* **183,** 527–542 (2008).
15. Heemskerk, N., Asimuddin, M., Oort, C., van Rijssel, J. & van Buul, J. D. Annexin A2 Limits Neutrophil Transendothelial Migration by Organizing the Spatial Distribution of ICAM-1. *J. Immunol.* **196,** 2767–2778 (2016).
16. Abadier, M. *et al.* Cell surface levels of endothelial ICAM-1 influence the transcellular or paracellular T-cell diapedesis across the blood-brain barrier. *Eur. J. Immunol.* **45,** 1043–58 (2015).
17. Yang, L. *et al.* ICAM-1 regulates neutrophil adhesion and transcellular migration of TNF- □ – activated vascular endothelium under flow. **106,** 584–593 (2005).
18. Baluk, P., Bolton, P., Hirata, A., Thurston, G. & McDonald, D. M. Endothelial gaps and adherent leukocytes in allergen-induced early- and late-phase plasma leakage in rat airways. *Am. J. Pathol.* **152,** 1463–76 (1998).
19. McDonald, D. M. Endothelial gaps and permeability of venules in rat tracheas exposed to inflammatory stimuli. *Am. J. Physiol.* **266,** L61–L83 (1994).
20. Wessel, F. *et al.* Leukocyte extravasation and vascular permeability are each controlled in vivo by different tyrosine residues of VE-cadherin. *Nat. Immunol.* **15,** 223–30 (2014).
21. Herzog, B. H. *et al.* Podoplanin maintains high endothelial venule integrity by interacting with platelet CLEC-2. *Nature* **502,** 105–9 (2013).
22. Kim, M.-H., Curry, F.-R. E. & Simon, S. I. Dynamics of neutrophil extravasation and vascular permeability are uncoupled during aseptic cutaneous wounding. *Am. J. Physiol. Cell Physiol.* **296,** C848-56 (2009).
23. Lewis, R. E. & Granger, H. J. Diapedesis and the permeability of venous microvessels to protein macromolecules: the impact of leukotriene B4 (LTB4). *Microvasc. Res.* **35,** 27–47 (1988).
24. Heemskerk, N. *et al.* F-actin-rich contractile endothelial pores prevent vascular leakage during leukocyte diapedesis through local RhoA signalling. *Nat. Commun.* **7,** 10493 (2016).
25. Kaur, J. *et al.* Endothelial LSP1 is involved in endothelial dome formation , minimizing vascular permeability changes during neutrophil transmigration in vivo. **117,** 942–953 (2014).

26. Phillipson, M., Kaur, J., Colarusso, P., Ballantyne, C. M. & Kubes, P. Endothelial domes encapsulate adherent neutrophils and minimize increases in vascular permeability in paracellular and transcellular emigration. *PLoS One* **3,** e1649 (2008).
27. Martinelli, R. *et al.* Release of cellular tension signals self-restorative ventral lamellipodia to heal barrier micro-wounds. *J. Cell Biol.* **201,** 449–65 (2013).
28. Amerongen, G. P. v. N., Delft, S. v., Vermeer, M. A., Collard, J. G. & van Hinsbergh, V. W. M. Activation of RhoA by Thrombin in Endothelial Hyperpermeability : Role of Rho Kinase and Protein Tyrosine Kinases. *Circ. Res.* **87,** 335–340 (2000).
29. Mikelis, C. M. *et al.* RhoA and ROCK mediate histamine-induced vascular leakage and anaphylactic shock. *Nat. Commun.* **6,** 6725 (2015).
30. Carman, C. V, Jun, C.-D., Salas, A. & Springer, T. a. Endothelial cells proactively form microvilli-like membrane projections upon intercellular adhesion molecule 1 engagement of leukocyte LFA-1. *J. Immunol.* **171,** 6135–6144 (2003).
31. Carman, C. V. & Springer, T. A. A transmigratory cup in leukocyte diapedesis both through individual vascular endothelial cells and between them. *J. Cell Biol.* **167,** 377–388 (2004).
32. van Rijssel, J. *et al.* The Rho-guanine nucleotide exchange factor Trio controls leukocyte transendothelial migration by promoting docking structure formation. *Mol. Biol. Cell* **23,** 2831–2844 (2012).
33. Barreiro, O. *et al.* Dynamic interaction of VCAM-1 and ICAM-1 with moesin and ezrin in a novel endothelial docking structure for adherent leukocytes. *J. Cell Biol.* **157,** 1233–1245 (2002).
34. Van Buul, J. D. *et al.* RhoG regulates endothelial apical cup assembly downstream from ICAM1 engagement and is involved in leukocyte trans-endothelial migration. *J. Cell Biol.* **178,** 1279–1293 (2007).
35. Vestweber, D., Zeuschner, D., Rottner, K. & Schnoor, M. and ICAM-1 clustering in endothelium Implications for the formation of docking structures. 1–5 (2013).
36. Sandig, M., Negrou, E. & Rogers, K. A. Changes in the distribution of LFA-1, catenins, and F-actin during transendothelial migration of monocytes in culture. *J. Cell Sci.* **110 (Pt 2,** 2807–2818 (1997).
37. Kapoor, J. R. Platelet activation and atherothrombosis. *N. Engl. J. Med.* **358,** 1638; author reply 1638-1639 (2008).
38. Langer, H. F. & Gawaz, M. Platelet-vessel wall interactions in atherosclerotic disease. *Thromb. Haemost.* **99,** 480–6 (2008).
39. He, P., Zhang, H., Zhu, L., Jiang, Y. & Zhou, X. Leukocyte-platelet aggregate adhesion and vascular permeability in intact microvessels: role of activated endothelial cells. *Am. J. Physiol. Heart Circ. Physiol.* **291,** H591–H599 (2006).
40. Schlegel, N. & Waschke, J. cAMP with other signaling cues converges on Rac1 to stabilize the endothelial barrier- a signaling pathway compromised in inflammation. *Cell Tissue Res.* 1–10 (2013). doi:10.1007/s00441-013-1755-y
41. Post, A. *et al.* Rasip1 mediates Rap1 regulation of Rho in endothelial barrier function through ArhGAP29. *Proc. Natl. Acad. Sci. U. S. A.* **110,** 11427–32 (2013).
42. Hillgruber, C. *et al.* Blocking neutrophil diapedesis prevents hemorrhage during thrombocytopenia. *J. Exp. Med.* (2015). doi:10.1084/jem.20142076
43. Nolan, D. J. *et al.* Molecular signatures of tissue-specific microvascular endothelial cell heterogeneity in organ maintenance and regeneration. *Dev. Cell* **26,** 204–19 (2013).

7

&

APPENDICES

Nederlandse samenvatting

Het vatenstelsel in ons lichaam wordt gevormd door talrijk aan elkaar gekoppelde bloedvaten die zich verspreiden door heel het menselijk lichaam. Als je al het omliggende weefsel zou verwijderen en enkel alleen naar de bloedvaten zou kunnen kijken, zie je een beeld dat de contouren van ons lichaam compleet weerspiegeld. Dit geeft aan hoe groot de dichtheid van onze bloedvaten in onze weefsels en organen is. Sterker nog, als je alle bloedvaten achter elkaar legt kom je tot een lengte van wel 100.000 km! Een goede werking van onze bloedvaten is essentieel voor onze gezondheid. De bloedstroom voorziet het lichaam van voedingstoffen, zuurstof en hormonen en het reguleert andere belangrijke functies zoals onze temperatuur, pH en het afvoeren van afvalstoffen. Naast deze belangrijke functies begeleidt het vasculaire systeem immune cellen naar specifieke plekken binnen het menselijk lichaam en ondersteunt hiermee het afweersysteem dat ons lichaam beschermt tegen ziekteverwekkers zoals virussen, bacteriën en parasieten. Daarnaast wordt het immuunsysteem ook gebruikt om afvalstoffen en zieke of uitgeputte lichaamscellen zoals kanker op te ruimen. Het vasculaire systeem kan echter uit balans raken, met een verscheidenheid aan bloedvat-gerelateerde ziekten tot gevolg. Zoals: atherosclerose, het dichtslibben van de aderen; embolie, een kleine massa rondzwervend puin dat de bloedbaan kan blokkeren; ontsteking, ontsteking van de bloedvaten kan verschillende oorzaken hebben die kunnen leiden tot vaatvernauwing en vaatverstopping; trauma, schade aan de bloedvaten kan leiden tot ontsteking of infectie. De verstoring van de balans gaat vaak geleidelijk en wordt daarom pas vaak in een laat stadium ontdekt. Het is daarom belangrijk om meer inzicht te krijgen in hoe een gezond vatenstelsel werkt en wanneer de balans zoek is. Om hier een goed antwoord op te krijgen is basaal onderzoek nodig.

In dit proefschrift hebben wij verschillende mechanismen onderzocht die ervoor zorgdragen dat de integriteit van de naden van onze bloedvaten, genaamd juncties, gehandhaafd blijven zodat ze niet langdurig open staan en gaan lekken. Verder hebben we onderzocht waarom de juncties niet lekken in specifieke gevallen zoals tijdens het uitreden van immune cellen uit de bloedbaan, leukocyt transmigratie genaamd. Daarnaast hebben wij onderzoek gedaan naar een molecuul, bekend als ICAM-1, dat zowel de aanhechting van immune cellen aan de vaatwand als het voorkomen van vaatlekkage reguleert. De transmigratie van leukocyten verloopt volgens een aantal stappen: de leukocyten beginnen met het rollen over de binnenkant van de vaatwand; vervolgens gaat dat over in kruipen; en uiteindelijk transmigreren de cellen door de vaatwand heen. ICAM-1 ondersteunt de adhesie van leukocyten aan de bloedwand tijdens

&

al deze stappen. Er wordt gedacht dat verschillende eiwit complexen aan het oppervlak van het cel membraan de overgangen tussen deze verschillende stappen reguleert. Het is echter onduidelijk hoe ICAM-1 zich tussen deze complexen verplaatst en welke eiwitten de lokale en tijdelijke organisatie van ICAM-1, met betrekking tot tijd en plaats, reguleren. In **hoofdstuk 3** introduceren wij het eiwit annexin A2 als een nieuwe interactie partner voor ICAM-1. Onze bevindingen duiden erop dat annexin A2 de ruimtelijke distributie van ICAM-1 op het celoppervlak kan reguleren. Endotheel cellen zonder annexin A2 hebben een verstoorde ICAM-1 distributie wat leidt tot een verhoogde adhesie van leukocyten onder ontstekingscondities. Verder onderzoek moet uitwijzen of de verhoging van het aantal transmigrerende leukocyten schadelijk is of juist gebruikt kan worden om de transmigratie onder bepaalde omstandigheden te verhogen op bepaalde plekken in ons lichaam.

Het lekken van de vaten word vaak geassocieerd met een onbalans van onze vaten. Echter, vasculaire permeabiliteit is niet altijd schadelijk, een beetje lekkage ondersteunt diverse inflammatoire functies zoals activatie van bloedstolling, het complement systeem en het aantrekken van leukocyten die deel uitmaken van ons afweer systeem. Een opeenstapeling van bevindingen wijst er echter op dat het uitreden van leukocyten uit de bloedbaan gepaard gaat zonder lekkage of schade aan de bloedwand. Deze paradox laat zien dat de vasculaire permeabiliteit in deze twee processen onafhankelijk van elkaar wordt gereguleerd. In **hoofdstuk 4** hebben wij onderzocht waarom bloedvaten niet lekken tijdens het uitreden van leukocyten uit de bloedbaan. Deze studie laat zien dat de endotheel cellen, de cellen die de binnenkant van de bloedwand bekleden, een natuurlijke knelring vormen die de ruimte tussen de uittredende leukocyte en de vaatwand afknelt, waarmee lekkage van de naden tijdens dit proces voorkomen wordt. De knelring is flexibel, hierdoor is de leukocyt toch instaat om zich door de bloedwand heen te bewegen. Wij hebben gevonden dat dit ingenieuze mechanisme wordt gereguleerd door verschillende signaal moleculen zoals ICAM-1, LARG en Ect2, RhoA, ROCK, Myosin-II en actine filamenten. ICAM-1 is een receptor die zich bevindt op het celoppervlak van endotheel cellen. ICAM-1 neemt waar wanneer een leukocyt door de bloedwand heen kruipt. Als dit het geval is initieert ICAM-1 een signaal dat ervoor zorgt dat de omliggende endotheel cellen beginnen met het aanmaken van de knelring. Het natuurlijke bouwmateriaal voor de knelring bestaat uit actine. Actine kan worden opgebouwd in filamenten die talrijke structuren kunnen vormen waarmee de vorm en omvang van lichaamscellen wordt gereguleerd. Het door ICAM-1 geïnitieerde signaal wordt binnenin de endotheel cel doorgegeven door Ect2, LARG, RhoA en ROCK. Deze cascade aan eiwitten

activeert een mechanische motor genaamd Myosin-II. Myosin-II verbind de actine filamenten en oefent kracht uit op de actine filamenten waardoor de knelring verkleind wordt en vaatlekkage tijdens de transmigratie van leukocyten wordt tegengegaan.

In de naden van onze bloedvaten bevindt zich een dynamisch eiwit complex dat instaat is om de naden even open te zetten en daarna meteen weer te sluiten. Deze dynamiek is belangrijk omdat de endotheel cellen die met elkaar in contact staan los van elkaar moeten kunnen bewegen om processen zoals leukocyt transmigratie of het groeien van nieuwe bloedvaten mogelijk te maken. Het meest beschreven eiwit in dit complex is VE-cadherin. VE-cadherin verbindt twee endotheel cellen doormiddel van een homo-typische interactie. Om de integriteit van bloedvaten te behouden wordt VE-cadherin in juncties doorlopend vernieuwd. De integriteit van onze bloedvaten wordt strikt gereguleerd. Een van de eiwitten die betrokken is bij het behouden van de integriteit van de naden, of met een moeilijke term "endotheliale juncties" is het signaal molecuul Rac1. Maar Rac1 is ook beschreven in processen die cel-cel contacten kunnen verbreken, zoals Rac-1-gemedieerde endocytose of reactieve zuurstof radicaal productie. Dit impliceert dat de activiteit van Rac1 in tijd en plaats gereguleerd is. In **hoofdstuk 5** hebben wij onderzocht welke eiwitten lokale Rac1 activiteit reguleren tijdens junctie homeostase. Deze studie laat zien dat de guanine nucleotide echange factor TRIO lokale Rac1 reguleert wat ervoor zorgt dat pasgevormde instabiele naden of "juncties" zich stabiliseren tot sterke integere naden.

Tot slot, in **hoofdstuk 6** zijn wij op zoek gegaan naar andere exchange factoren die mogelijk bijdragen aan het herstel van endotheel naden nadat deze verbroken zijn, bijvoorbeeld na intrinsieke VE-cadherin vernieuwing binnen de endotheel monolaag of tijdens de transmigratie van leukocyten. In totaal hebben we zes RhoA-, Rac1- en Cdc42-specifieke Rho-GEFs en GAPs gevonden die betrokken zijn bij de stabilisatie van cel-cel naden tijdens de transmigratie van leukocyten en acht RhoA-, Rac1-, Cdc42- en ARF6-specifieke Rho-GEFs en GAPs gevonden die junctie integriteit reguleren onder basale condities. De potentiële targets zijn samengevat in table 1 en 2 van hoofstuk 6.

&

PhD portfolio Niels Heemskerk

PhD period	september 2011 - september 2015
Promotor	prof.dr P.L. Hordijk
Copromotor	dr. J.D. van Buul

Courses	Year
Cytoskeleton in control of cell migration, NKI, Amsterdam the Netherlands	2013
Zooming in on plasma membrane dynamics with advanced microscopy, SILS (Uva), Amsterdam, the Netherlands	2012
Art. 9 course 'proefdierkunde', AMC, Amsterdam, the Netherlands	2012
FRET/FLIM workshop, Nikon and Lambert instruments, Amsterdam, the Netherlands	2012
Advanced immunology course, Sanquin, Amsterdam, the Netherlands	2012

Seminars, workshops and masterclasses	Type of presentation	Year
Department meetings	12x Oral	2011-2015
Journal Club	3x Oral	2011-2015
Masterclass Bill Muller	Oral	2016
Masterclass Rafael García-Mata	Oral	2015
Masterclass Richard Cheney	Oral	2014
Masterclass José A. Lopez	Oral	2014
Masterclass Miguel A. del Pozo	Oral	2013
Masterclass Jose Javier Bravo Cordero	Oral	2013
Masterclass Jaime Millan	Oral	2013
Masterclass Emmanual Lemichez	Oral	2012
Masterclass Sussan Nourshargh	Oral	2012
Masterclass Dietmar Vestweber	Oral	2015
Atherosclerosis meeting with the AMC, Amsterdam (2x)	Attended	2012-2013

Tutoring, mentoring and supervising	year
Master student: Bram Teunissen (6 months)	2015
HLO student: Chantal Oort (9 months)	2013-2014

(International) conferences	Type of presentation	Year
The Society for Leukocyte Biology's 49th Annual Meeting/Neutrophil 2016, Verona, Italy	Oral	2016
Maastricht Inflammation in the Metabolic Syndrome and Atherosclerosis (MIMSA), Maastricht, the Netherlands. Organization: Dr. K. Wouters and Dr. M. Donners.	Oral	2015
Sanquin Science Day, Nemo, Amsterdam, The Netherlands	Poster	2014
Sanquin, Staff meeting, Amsterdam, The Netherlands	Oral	2014
5th Rembrandt Symposium, Noordwijkerhout, The Netherlands	Poster	2014

Dutch Endothelial Biology Society (DEBS) Fall meeting, Biezenmortel, The Netherlands	Oral	2014
4th Trippenhuis meeting: Vesicles on the move: The cytoskeletal connection, Amsterdam, The Netherlands	Attended	2014
Gordon Research Conference (GRC). Signaling by adhesion receptors. Bates College, Lewiston, ME, USA. Chair: M. J. Humphries, Vice Chair: A. S. Yap	Oral and Poster	2014
Vascular Research meeting VUMC, Amsterdam, the Netherlands Organization: G. P. van Nieuw Amerongen	Oral	2014
4th Cardiovascular Conference (CVC), Noordwijkerhout, The Netherlands	Attended	2014
4th Rembrandt Symposium, Noordwijkerhout	Attended	2013
3rd Trippenhuis meeting: From Stem Cells to Aging, Amsterdam, The Netherlands	Attended	2013
3rd Cardiovascular Conference (CVC), Noordwijkerhout, The Netherlands	Poster	2013
Sanquin Science Day, Nemo, Amsterdam, The Netherlands	Poster	2012
Dutch Endothelial Biology Society (DEBS) Fall meeting, Joint meeting DEBS MiVaB, dr. Chris V. Carman (Harvard, USA), Biezenmortel, The Netherlands	Poster	2012
3rd Rembrandt Symposium, Noordwijkerhout, The Netherlands	Poster	2012
2nd Trippenhuis meeting: Dynamic interactions in Cell Biology, Amsterdam, The Netherlands	Attended	2012
Sanquin, Staff meeting, Amsterdam, The Netherlands	Oral	2012
Cell Adhesion and Cell Polarity in Development and Disease. Ghent, Belgium	Poster	2012
NIN symposium, Sanquin, Amsterdam, The Netherlands	Oral	2012
2rd Cardiovascular Conference (CVC), Noordwijkerhout, The Netherlands	Poster	2012
Sanquin, Staff meeting, Amsterdam, The Netherlands	Oral	2012
1st Trippenhuis meeting: Vascular and Cell Biology in Health and Disease, Amsterdam, The Netherlands	Attended	2011

Awards and prizes	Year
SLB 1st place Junior Faculty Presidential Award (Verona, Italy)	2016
Runner-up at the Sanquin in house Seminars, Amsterdam, The Netherlands	2015
Opportunity to present at the Gordon Research Conference (GRC), Bates College, Lewiston, ME, USA.	2014
Poster presentation award at Dutch Endothelial Biology Meeting (DEBS), Biezenmortel, The Netherlands	2012

&

Curriculum vitae

Niels Heemskerk was born in Haarlem, the Netherlands on the 9th of February 1987. After finishing High School in 2005, he studied Biomedical Sciences at the VU University in Amsterdam. And obtained his MSc degree in Biomolecular sciences in 2011. As part of this program he performed an internship at the department of Molecular Cell Biology at the Netherlands Cancer institute in Amsterdam. After obtaining his MSc degree, he started working as a PhD student within the department of Molecular Cell Biology at Sanquin Research in Amsterdam, under the supervision of dr. J.D. van Buul. Since September 2015 he is working as a Postdoc within the department of Molecular Cell Biology and Immunology at the VU University medical center in the group of prof.dr. M. van Egmond.

LIST OF PUBLICATIONS

Lilian Schimmel, **Niels Heemskerk**, Jaap D. van Buul. Leukocyte transendothelial migration: A local affair.
Small GTPases. 2016 Aug 15:1-15.

Niels Heemskerk, Mohammed Asimuddin, Chantal Oort, Jos van Rijssel, and Jaap D. van Buul. Annexin A2 Limits Neutrophil Transendothelial Migration by Organizing the Spatial Distribution of ICAM-1.
J Immunol. 2016 Mar 15;196(6):2767-78.

Niels Heemskerk, Lilian Schimmel, Chantal Oort, Jos van Rijssel, Taofei Yin, Bin Ma, Jakobus van Unen, Bettina Pitter, Stephan Huveneers, Joachim Goedhart, YiWu, Eloi Montanez, Abigail Woodfin & Jaap D. van Buul. F-actin-rich contractile endothelial pores prevent vascular leakage during leukocyte diapedesis through local RhoA signalling.
Nat. Commun. 7, 10493 (2016).

Timmerman I, **Heemskerk N**, Kroon J, Schaefer A, van Rijssel J, Hoogenboezem M, van Unen J, Goedhart J, Gadella TW Jr, Yin T, Wu Y, Huveneers S, van Buul JD. A local VE-cadherin and Trio-based signaling complex stabilizes endothelial junctions through Rac1.
J. Cell Sci. 128, 3041–54 (2015).

Marinković G, **Heemskerk N**, van Buul JD, de Waard V. The Ins and Outs of Small GTPase Rac1 in the Vasculature.
J Pharmacol Exp Ther. 2015 Aug;354(2):91-102.

Heemskerk N, van Rijssel J, van Buul JD. Rho-GTPase signaling in leukocyte extravasation: an endothelial point of view.
Cell Adh Migr. 2014;8(2):67-75.

&

DANKWOORD

Het zijn 4 fantastische jaren geweest waarin er veel ruimte was mezelf te ontwikkelen en waar ik met veel plezier op terugkijk. Ik ben trots op datgene wat we met z'n allen hebben bereikt, want onderzoek doe je nooit alleen.

Jaap: als mijn copromotor wil ik je bedanken voor je steun. Wat jou kenmerkt is Bruce Springsteen, je uitbundige enthousiasme, doorzettingsvermogen, presentatie skills en het vermogen mensen bij elkaar te brengen. Het zijn eigenschappen waarvan wij als groep, maar vooral ikzelf veel van heb geleerd. Als mijn proef was mislukt wist je me altijd op een goede manier te motiveren om door te gaan. Ik denk dat deze manier van werken en de vele woensdagochtend besprekingen, waarin de emoties soms hoog opliepen, hebben geleid tot dit eindresultaat. Ik wil je bedanken voor alle zaadjes die je, misschien soms onbewust, in mijn hoofd hebt weten te planten. Bedankt voor de geweldige tijd, de samenwerking, inspiratie en dat je me altijd met beide benen op de grond hebt gehouden. Onderzoek is je hart volgen, hard werken, omgaan met tegenslagen, en berust voor een groot deel op toeval.

Peter: als mijn promotor wil ik je bedanken voor je relativeringsvermogen. Op de achtergrond hield je de grote lijnen, de haalbaarheid en de planning in de gaten. Hierdoor heeft het enthousiasme van Jaap en mij nooit de overhand gekregen en is het helemaal goed gekomen. Ik heb veel respect voor de manier waarop je gedurende mijn promotietraject structuur hebt gegeven aan mijn project. Het is fijn dat je bij je medewerkers het gevoel weet te scheppen dat alles mogelijk is. Zijn er toch restricties dan ben je daarin zeer duidelijk, wat ik altijd erg heb kunnen waarderen. Bedankt voor je begeleiding.

Leden van de promotiecommissie: Prof. Dr. Theodorus W.J. Gadella, Prof. Dr. Arnoud Sonnenberg, Prof. Dr. Kees Jalink, Prof. Dr. Carlie J.M. de Vries, Dr. Johan de Rooij. Hartelijk dank voor het lezen en beoordelen van mijn proefschrift.

Jeffrey en **Ilse**: de paranimfen. Het geeft me een goed gevoel dat we nog één keer als team mogen opereren. Ilse, jouw nuchtere kijk op de wetenschap heeft me altijd geïnspireerd. Toen ik aan mijn PhD begon was jij toe aan je laatste jaar en daarmee naar de afwerking van je proefschrift aan het toewerken. Dit heeft mij het inzicht gegeven hoe belangrijk het is om een goede planning te maken om je PhD op tijd af te ronden. Ook

wil ik je bedanken voor de mogelijkheid mee te publiceren met jouw ''levenswerk'' wat uiteindelijk ook is opgenomen in hoofdstuk 5 van dit proefschrift. Mark, Jeffrey en ik waren vaak erg aanwezig, primitief, en druk, zeker in het begin. In die tijd heb jij de ''moeder rol'' op je genomen en had je als Timmermama een flinke taak om bold statements af te zwakken en ons in het gareel te houden. Bedankt voor deze heropvoeding ;). Jef: als ik terug denk aan toen, krijg ik een grijns op mijn gezicht, gezellig dat was het. De vrijdagmiddagkamerborrel, de kunstborrel, einde van de maand borrel, vinyl plaatjes draaien, zwemmen in het IJsselmeer, Hoorn, zeilen met de PhD dag, de houthaven, congres centrum Noordwijkerhout, een orchidee... Gent, cover bandjes kijken, Biezenmortel, Gent aan de Schinkel, BCR borrel, promotieborrel, tuinfeest, parkbarbecues. Bedankt voor deze gezellige ''borreltijd''.

Stephan: bedankt voor alle inspirerende, motiverende en inzichtelijke gesprekken. Het was prettig om jou als persoon en collega gedurende mijn promotietraject in de buurt te hebben. Ik weet nog dat we op de Gordon Research Conference, Signaling by adhesion receptors 2014, na de borrel tot in de late uurtjes zijn bezig geweest om mijn presentatie te finetunen. Het gebruik van Lifeact, jouw opvattingen over tension en junctions zijn onmiskenbaar van invloed geweest op dit proefschrift, bedankt daarvoor.

Lilian: bedankt voor je hulp bij het afronden van het Nature Communications paper. Het was leuk om samen met jou aan de GEF/GAP screen te werken. Hopelijk heb je veel aan deze pilotstudie gehad. Heel veel succes met het afronden van je PhD.

Jos: tijdens mijn stageperiode bij Jaap kon ik met vragen altijd bij je terecht. We waren het misschien niet altijd eens over de juiste hypothese of proefopzet maar juist dat hield me scherp. Bedankt!

Erik: ik wil je bedanken voor jouw enthousiasme voor fancy, high-end equipment en drang naar innovatie. Hierdoor was er op het gebied van microscopie veel mogelijk zoals een FRET opstelling met twee ORCA-R2 camera's, een uitzonderlijke investering. Het was leuk om met jou te brainstormen over proeven, lasers, fluorescentie en het aankopen van nieuwe microscopen. Ik heb erg genoten van de Leica demo in Rotterdam, ons enthousiasme werd ons op de terugreis bijna fataal. Even opletten, en vervolgens weer gewoon doorpraten over HyD's en White light lasers. Heel veel plezier en succes met de faciliteit. Wie weet kom ik nog een keer langs om een aantal metingen te doen.

&

Floris: tijdens mijn MCB stageperiode hebben wij samen met Jeffrey en Mark gewerkt aan het opzetten van het ibidi flow systeem. Alle transmigratie experimenten werden vanaf dat moment onder flow gedaan. De experimenten werden daardoor sophisticated maar ook tien keer moeilijker. Bedankt voor alle ondersteuning en je hulp bij de microscopen. Hilarisch was ook jouw sabotage van het door Mark en Jeffrey vervaardigde flow-tube-water-straal-apparaat die onopgemerkt boven het plafond van kamer U264c liep om vervolgens iemand nat te spuiten. Briljant!

Anna: bedankt voor de fijne tijd in Y3 en U264c en het nalopen van mijn manuscripten. Het was fijn om jou als internationale kamergenoot in onze groep te hebben. Jouw aanwezigheid heeft zeker bijgedragen aan het verbeteren van mijn taalgevoel.

Nathalie: hé FRET buddy! Het was keer op keer een verassing welke compound je nu weer op de endotheel cellen gegooid had, spectaculaire beelden! Bedankt voor de fijne tijd.

Mar: bedankt voor je input tijdens de werkbesprekingen in B108, en de gezellig tijd.

Coert: bedankt voor je input en het kritisch lezen van het Nature Communications manuscript.

Chantal: bedankt voor je ongekende inzet en overgave waarmee je tijdens je stageperiode experimenten hebt verricht. Het was fijn je te mogen begeleiden tijdens je stage bij ons op het lab.

Bram: het was leuk om samen met jou met de Rac1 sensor te experimenteren. Heel veel succes met je nieuwe job als technici bij Synvolux.

Mohammed: Asim, thanks for helping identifying the interaction between annexin A2 and ICAM-1. I hope you are doing well in India.

Antje Schaefer: thanks for all the stimulating discussions.

Eloise en **Anne-Marieke**: bedankt voor het organiseren van het lab. De systematiek in het antilichamen systeem, het organiseren van de plasmidenlijsten en het uitzoeken van de cell biology tools is slechts een kleine greep uit de verbeteringen die jullie hebben doorgevoerd in het lab. Bedankt daarvoor, het heeft onderzoek doen erg vergemakkelijkt.

Corry en **Johanna**: bedankt voor alle hulp bij het bestellen van goederen, en het bijvullen van disposables. Corry, bedankt voor je gezellige aanwezigheid en het delen van het laatste nieuws. Op het tuinfeest moesten de bouwvakkers van je afgeslagen worden om jou aandacht te krijgen, de aanhouder wint, uiteindelijk heb je toch met me gedanst ;).

Simon: bedankt voor je hulp bij het opzetten van de membraan fractionering. Ik heb goeie herinneringen aan onze gesprekken over Lynyrd Skynyrd tijdens de overnachting in de houthaven.

Mark: bedankt voor je input, enthousiasme en hulp bij de imaging, MacGyver.

Martin: veel succes met je PhD!

Marion, **Wanda** en **Gerty**: bedankt voor alle ondersteuning bij het administratieve gedeelte van mijn PhD periode.

Igor, **Timo**, **Yvonne**, **Tsveta**, **Kalim**, **Daphne**, **Michel**, **Bart-Jan**, **Micha**, **Daniel**, **Younes**, **Emily**, en **Dion**: bedankt voor jullie gezelligheid, input en leuke tijd bij MCB!

Yi and **Taofei**: I want to thank you for sharing the DORA Rho biosensors. I am very grateful for it. It was really nice to meet you in person during your visit to Sanquin.

Abigail and **Bin**: thank you for a nice and successful collaboration. I really appreciate the effort you both put in doing many *in vivo* experiments. Thanks!

Eloi and **Bettina**: thanks a lot for sharing data from your Lifeact-GFP mice. **Dirk**: bedankt voor alle shRNA constructen!

Rafael: thanks for the great evening in de Haven van Texel and doing the 40+ FRET experiments together.

Beste collega's van BCR, ik heb mij altijd zeer op mijn gemak gevoeld binnen jullie groep, bedankt voor jullie gastvrijheid. **Paul**: bedankt voor de gezellige tijd in het VMT en virus lab. **Anton**: zonder jouw hulp, reagentia en expertise was hoofdstuk 4 van dit proefschrift nooit afgekomen.

Michel: bedankt voor de gezelligheid en het bijvullen van de HEPES en de Percoll.

&

Jakobus: jouw enthousiasme voor wetenschap is zeer inspirerend. Ruim vijf jaar geleden gingen we beiden de uitdaging van een PhD aan. Jij op het SILS en ik op Sanquin. Bedankt voor je hulp tijdens de 6 maanden dat ik bij jullie te gast was. Succes met je kleine en veel plezier bij Olivier Pertz.

Joachim: bedankt voor alle hulp en ondersteuning. Ik ben je erg dankbaar voor het feit dat je de tijd hebt genomen om me gedurende 6 maanden de fijne kneepjes van FRET en microscopie bij te brengen. Deze 'stage' aan het begin van mijn PhD heeft onmiskenbaar de toon gezet voor de rest van mijn PhD en heeft mede bijgedragen aan een mooi proefschrift.

Mijn nieuwe **collega's bij MCBI**: **Marjolein**, bedankt voor de kans en het vertrouwen deel uit te mogen maken van jouw groep. Ik ben blij dat ik mag werken binnen het veld van de tumor immunologie, waarbij ik met mijn vertrouwde microscopie helemaal los mag gaan. Verder wil ik al mijn nieuwe collega's bedanken voor het feit dat jullie me zo snel thuis hebben laten voelen.

Vivian and **Goran**: thanks a lot for the opportunity to co-publish on your excellent review about the ins and outs of small GTPase Rac1 in the vasculature.

Mijn mede-bandleden van **Southern Train** 2011-2016: Hoorn 2011, ons eerste optreden in Swaf, met je versterker in de plee. Meteen hard, super strak en een geweldige chemie. Inmiddels hebben we elkaar na 100 optredens de hand geschud en zijn we allemaal onze eigen weg gegaan. Ik wil jullie allen bedanken voor deze mooie tijd. Een tijd waarvan ik erg genoten heb, op muzikaal gebied, maar vooral onze tijd samen, als vrienden, en de gesprekken in de band bus. Het is een understatement als ik zeg dat we veel hebben meegemaakt. Remmert, Edgar, Sytse, Merlijn, bedankt! Dude: bedankt voor al het zware roadie werk. Het is echt waar! Kanker cellen hebben pootjes. En omdat we toch nog even willen laten zien dat we een intelligente band zijn tellen we nog 1 keer tot 4. Een, twee, drie... tot hier tot daar tot Free Bird.

Katka, Niels en **Olivia**: bedankt voor alle kopjes koffie bij het Terrasmus, de etentjes, lekkere gehakt ballen en heerlijke barbecues.

Boukje: Bedankt voor alle gezellige avonden, eten, uiteten, oud en nieuw aan de Singel. Hanke en ik vinden het heel erg fijn dat je af en toe op Linde wilt passen zodat wij een avondje uit kunnen ☺.

Frank en **Juke**: bedankt voor het warme onthaal dat jullie me keer op keer geven als we bij jullie in Dordt zijn. Frank, als ik naar jouw verhalen luister dan merk ik dat er nog zoveel te leren valt, je hebt een unieke geest en kijk op de wereld waar ik veel bewondering voor heb. In het bijzonder de kunst van het zorgvuldig formuleren. Frank en Juke we blijven genieten, dan komt alles goed.

Jelka en **Rein**: Bedankt voor alle gastvrije momenten in zeeland, het is fijn om bij jullie langs te komen. Het is heerlijk het stadse leven bij jullie eventjes te kunnen ontvluchten.

Rick en **Mark**: Mannen, bedankt voor alle gezellige borrels, etentjes, avonden in de Hoek en dat jullie altijd voor me klaar staan.

Marieke: Lieve zus, het is grappig dat we beiden werken met lenzen en licht. We proberen allebei een onderwerp zo mooi mogelijk in beeld te brengen. Verlies nooit dat enthousiasme dan komt alles goed.

Merlijn: Muziek is iets wat als een rode draad door ons leven loopt. Het is de Southern rock en blues die ons verbind. Ik wil je bedanken voor je steun. Je bent een echte simple man.

Pap en **mam**: De koffie op de Pleiadenstraat blijft lekker. Bedankt dat jullie er altijd voor me zijn.

Lieve **Hanke**, bij jou voel ik me altijd op mijn gemak. Bedankt voor je geduld, ondersteuning, hulp bij planning en alle wetenschappelijke ideeën die je stiekem in mijn hoofd hebt geplant. Ik kijk er naar uit om samen met jou onze lieve dochter Linde groot te zien worden.
Niels

&